Investigating lipidomic determinants of cognitive impairment in mouse models of Alzheimer's disease

Matthew Granger

A thesis submitted to the

Faculty of Graduate and Postdoctoral Studies

In partial fulfillment of the requirements for the

PhD degree in Neuroscience

Department of Cellular and Molecular Medicine

Faculty of Medicine

University of Ottawa

Abstract

Alzheimer's disease is an insidious neurodegenerative disease that affects millions of people worldwide. Currently, there are no determinants that can accurately predict the onset cognitive decline in AD. This thesis investigates and defines changes in the lipidome that are linked to symptomatic onset and cognitive impairment in mouse models of AD. Using a targeted lipidomic approach employing high performance liquid chromatography electrospray ionization tandom mass spectrometry, direct biochemical assessments, and behavioural evaluation, I was able to (a) profile and quantify cortical and hippocampal glycerophosphocholine and glycerophosphoethanolamine metabolites and signaling molecules in the AβPP^{Swe}/PS1^{dE9} and the N5 TgCRND8 murine models of AD and (b) associate changes in lipid metabolism with learning and memory impairment. I demonstrate that glycerophosphocholine metabolism in the cortex but not the hippocampus is altered at symptomatic onset in both mouse models. These same metabolic changes were seen in younger animals exposed to chronic intermittent hypoxia, an environmental risk factor that accelerates their phenoconversion. In fully impaired transgenic mice, I defined metabolic changes associated with disease progression. To further assess the impact of sex, another risk factor of Alzheimer's disease cognitive decline, I characterized an AD model of sex-specific cognitive resistance. I demonstrated that transgenic males but not females exhibit behavioural indices of cognitive reserve when tested in the Morris Water Maze. Using this mouse line, I then investigated how measures of learning and memory associated with glycerophosphocholine and

glycerophosphoethanolamine metabolism. I identified increases in critical glycerophosphoethanolamine metabolites linked to spatial learning and memory impairment in the cortex of N5 TgCNRD8 mice and demonstrated that these changes could be predicted by profiling the plasma glycerophosphoethanolamine lipidome. Taken together, this thesis links glycerophospholipid metabolism to the onset and progression of learning and memory impairment in experimental models of AD and provides the first evidence that changes in cortical lipid metabolism can be predicted by changes in the plasma lipidome.

Acknowledgements

This is definitely one of the most difficult sections of my thesis to write. How does one appropriately encapsulate the feelings of gratitude and appreciation that arise when they look back on the multitude of years, effort and training that brought them to this stage? Many influences have nurtured and contributed to my love of neuroscience which has ultimately resulted in the development of this thesis.

It has been my observation that everyone has a unique experience in graduate school. Much of this variance can be attributed to the influence of the supervisor. I have been truly blessed to have Steffany Bennett as my supervisor. She has played an integral role in developing and refining my scientific skillset and critical thinking abilities. By allowing me to pursue my own hypotheses while still instilling a rigorous attention to detail, she has cultivated and encouraged me to greater achievements than I thought I would be capable of. It has been a true pleasure and honour to work with and learn from her.

In addition to all the help and guidance I have received from Dr. Bennett, I would be remiss if I did not acknowledge my lovable, positive, intelligent colleagues from the Bennett lab that I have worked so closely with over the years. Caitlin Fowler, Matthew Taylor, Sam Sherman, Dr. Alexandre Blanchard, and Bettina Franko have contributed their work to this thesis and I am grateful to their contributions. Dr. Hongbin Xu is a lipid God that was essential in the development of the mass spectrometry methodologies used in this thesis and I am grateful for all his help and guidance. Additionally, I'd like to thank Mark Akins, Dr. Steph Fowler, Graeme Taylor, and Ashleigh Snell for their years of support as well as

their contributions and criticisms that brought this thesis full term and to those that have kindly agreed to evaluate it.

Last, but definitely not least, I would like to extend a heartfelt thank you to my family. My parents and brother have always been unconditionally supportive of my love of neuroscience despite not always fully understanding everything I might tell them. Ultimately though, a man is only as strong as the partner he has by his side. This thesis is as much my wife's as it is mine. She has supported me and kept me going throughout all the years of this degree. From all the sacrificed weekends and gruelling hours of behavioural experiments and lipid extractions, to the stresses of thesis writing, she has been the backbone that has given me the strength to persevere and produce this piece of work. Thank you all for your incredible patience and support.

Table of Contents

Abbreviations

AA	arachidonic acid
AAG	alkyl-acyl glycerol
Aβ	amyloid-beta
ABCA1	ATP-binding cassette transporter 1
AβPP	amyloid precursor protein
ACN	acetonitrile
AD	Alzheimer's disease
ADP	adenosine diphosphate
ADRDA	Alzheimer's Disease and Related Disorders Association
AICD	amyloid precursor protein intracellular domain
Akt	protein kinase B
aMCI	amnestic mild cognitive impairment
ANOVA	analysis of variance
APOE	apolipoprotein E
ATP	adenosine triphosphate
aMCI	amnestic mild cognitive impairment
BACE1	beta-secretase 1
BUME	butanol/methanol
CCT	CTP:phosphocholine cytidylyltransferase
CDP	cytidine diphosphate
CERAD	Consortium to Establish A Registry for Alzheimer's Disease
CID	collision-induced dissociation
CK	choline kinase
CMP	cytidine monophosphate
CNS	central nervous system
CoA	coenzyme A
COV	compensation voltage
cPLA$_2$	cytosolic phospholipase A_2
CPT	cholinephosphotransferase
CSF	cerebrospinal fluid
CTF	C-terminal fragment
CTP	cytidine triphosphate
CTPNL	Canadian Institute of Health Research Training Program in Neurodegenerative Lipidomics
DAG	diacyl glycerol
DC	direct current
DHA	docosahexanoic acid
DMS	differential mobility spectroscopy
DTT	dithiotreitol
ECT	CTP:phosphoethanolamine cytidylyltransferase
EDTA	ethylenediaminetetraacetic acid
EK	ethanolamine kinase
EOAD	early onset Alzheimer's disease
EPI	enhanced product ion

EPT	ethanolamine phosphotransferase
ERK	extracellular signal-regulated kinase
ESI	electrospray ionization
FITC	fluorescein isothiocyanate
FDG-PET	fluorodeoxyglucose-positron emission tomography
FDR	false discovery rate
fMRI	functional magnetic resonance imaging
G	group (denoting PLA_2 nomenclature)
GPA	glycerophosphatidylglycerol
GPC	glycerophosphocholine
GPCR	G protein-coupled receptor
GPE	gylcerophosphoethanolamine
GPG	glycerophosphatidylglycerol
GPI	glycerophosphoinositol
GPS	glycerophosphoserine
hAβPP	human amyloid precursor protein
HDL	high-density lipoprotein
HPLC	high performance liquid chromatography
HRP	horseradish peroxidase
IDA	information dependent acquisition
IPA	isopropanol
$iPLA_2$	Ca^{2+}-independent phospholipase A_2
LA	linoleic acid
LDLR	low-density lipoprotein receptor
LOAD	late onset Alzheimer's disease
LPA	lysophosphatidic acid
LPAR	lysophosphatidic acid receptor
LPC	monoacylglycerophosphocholine
LPC(O)	monoalkylglycerophosphocholine
LPC(P)	monoalkenylglycerophosphocholine
LPCAT	lysophosphocholine acyltransferase
LPE	monoacylglycerophosphoethanolamine
LPE(O)	monoalkylglycerophosphoethanolamine
LPE(P)	monoalkenylglycerophosphoethanolamine
LPEAT	lysophosphoethanolamine acyltransferase
$LPLA_2$	lysosomal phospholipase A_2
LPLD	lysophospholipase D
LPLAT	lysophospholipid acyl transferase
LRP	low-density lipoprotein receptor-related protein
LTP	long-term potentiation
m/z	mass to charge ratio
MCI	mild cognitive impairment
MRI	magnetic resonance imaging
MRM	multiple reaction monitoring
MS	mass spectrometry
MS/MS	tandem mass spectrometry

MTBE	methyl tert-butyl ether
MWM	Morris Water Maze
naMCI	non-amnestic mild cognitive impairment
NIA	National Institute of Aging
NINCDS	National Institute of Neurological and Communicative Disorders and Stroke
NLS	neutral loss scan
NMDA	N-methyl D-aspartic acid
NonTg	Non-transgenic
HPLC	high performance liquid chromatography
OA	oleic acid
PAF	platelet activating factor
PAFAH	platelet activating factor acetyl hydrolase
PAFR	platelet activating factor receptor
PBS-T	phosphate buffered saline with tween
PC	diacylglycerophosphocholine
PC(O)	1-alkyl,2-acylglycerophosphocholine
PC(P)	1-alkenyl,2-acylglycerophosphocholine
Pde6b	phosphodiesterase 6B
PE	diacylglycerophosphoethanolamine
PE(O)	1-alkyl,2-acylglycerophosphoethanolamine
PE(P)	1-alkenyl,2-acylglycerophosphoethanolamine
PED	plamenylethanolamine desaturase
PEMT	phosphatidylethanolamine methyltransferase
PEN2	presenilin enhancer 2
PET	positron emission tomography
PIS	precursor ion scan
PLA_2	phospholipase A_2
PLS-DA	partial least squares-discriminant analysis
PNS	peripheral nervous system
PPi	pyrophosphate
ProIS	product ion scan
PS	presenilin
PUFA	polyunsaturated fatty acid
Q	quadrupole
RF	radio frequency
RIPA	radioimmunoprecipitation assay
ROS	reactive oxygen species
RT-STaR	Retention Time Standardization and Registration
SLAG	slow angled descent forepaw grasping test
$sPLA_2$	secreted phospholipase A_2
SRM	selected reaction monitoring
sAPPα	soluble amyloid precursor protein-alpha
sAPPβ	soluble amyloid precursor protein-beta
SLAG	slow angled descent forepaw grasping
sn	stereospecific number

TBS-T	tris buffered saline with tween
Tg	transgenic
TM	transmembrane domain
VaLID	Visualization and Phospholipid Identification
VIP	variable importance projection
WT	wild-type
ZT	zeitgeiber time

List of Figures

List of Tables

Chapter 1: General Introduction

1.1 Glycerophospholipids

Lipids are an incredibly diverse and exciting class of organic molecules comprising 50% of human brain dry weight (Sastry, 1985). The most lipid-rich organ in the human body is the brain (Xiang et al., 2015). Brains also have the most diverse molecular lipid composition than any other organ (Bozek et al., 2015; Lauwers et al., 2016). An appreciation of the importance of lipids at the molecular level has only recently emerged. Early canonical perspectives identified glycerophospholipids, the primary structural units of all cell membranes, as ubiquitous masses of identical species distinguished only by hydrophilic head groups and two hydrophobic hydrocarbon chains. Accordingly, the plethora of glycerophospholipid classes, subclasses, and species were considered to be simply packaged as a membranous bilayer with the sole purpose of supporting transmembrane and integral proteins. This underappreciation of the significance of lipid diversity did not acknowledge the structural complexity of various lipid species, or how essential lipids are in signalling and metabolic pathways. In part, this was due to the lack of available technologies capable of identifying and quantifying such diverse yet structurally similar molecules. Fifty year ago, renowned biochemist Albert Lehninger commented on the untapped resource of what would be known as lipidomics when he argued that "*Although considerable information is available on the electrical behavior of the neuronal membrane, very little is yet known of its molecular composition and structure because of the severe difficulties in separating lipid species…. Developments in the study of natural membranes promises to open the door to a molecular biology of neuronal transmission"* (Lehninger, 1968). This remark was

predicated on answering two seemingly simple questions: How many lipid species are there? What effect does lipid diversity have on cellular function?

1.1.1 Structure and nomenclature

There are eight overarching lipid classes: fatty acyls, glycerolipids, glycerophospholipids, sphingolipids, sterol lipids, prenol lipids, saccarolipids, and polyketides (Fahy et al., 2005; Fahy et al., 2009). Neural membranes are enriched in glycerophospholipids, sphingolipids, and cholesterols (sterol lipids) (Frisardi et al., 2011). Glycerophospholipids are the most common lipid class found in the neural membrane (Frisardi et al., 2011). They account for 20-25% of the entire brain dry weight, thus comprising half of the brain lipidome (Farooqui et al., 2000). When structural membrane glycerophospholipids are metabolized through a variety of enzymatic and non-enzymatic pathways (reviewed below), hydrolysis alters membrane curvature (reviewed in (Bennett et al., 2013)) and produces bioactive metabolites and lipid second messengers capable of signal transduction (Bennett et al., 2013; Frisardi et al., 2011; Lauwers et al., 2016; Ryan et al., 2009). These processes are specific to the structural composition of each glycerophospholipid thus requiring illustrative nomenclature to accurately represent these molecules.

Glycerophospholipids are characterized by three components: (1) a glycerol backbone, (2) a phosphate-linked head group at the stereospecific number-3 position (*sn*-3), and (3) one or two hydrocarbon chains at the *sn*-1 and/or *sn*-2 carbon positions of the glycerol backbone (Fig. 1.1A). Glycerophospholipids are divided into 20 different classes defined by differential phospho-head groups (Fahy et al., 2005; Fahy et al., 2009). The

Figure 1.1 – Glycerophospholipid structure and nomenclature. (A) Left panel schematic depicts glycerophospholipid structure with *sn-1* hydrocarbons of various lengths (R', blue) and *sn*-2 hydrocarbons (R'', green) linked to the glycerol backbone (black) with a phospho-head group (red) at the *sn*-3 position. X denotes the phospho-head group molecule that defines the glycerophospholipid class. Right panel indicates the two head group molecules found at the X position (focus of this thesis): choline and ethanolamine. (B) Schematic of acyl, alkyl, and alkenyl linkages of the hydrocarbon chains at either the *sn-1* or *sn-2* positions. In the event that one of the hydrocarbon chains is hydrolyzed, the residual *sn-1* or *sn-2* positions are hydroxylated thus making a *lyso*-glycerophospholipid. (C) Nomenclature of six main subclasses of the metabolites and second messengers that are the focus of this thesis. (D) An example of the molecular structure of a PC(O) denoting the nomenclature. PC(O-16:1/2:0) defines a molecular species belonging to the glycerophosphocholine class of lipids with a polar phosphocholine head group (PC) at the *sn*-3 position of the glyceride backbone, a hydrocarbon chain of 16 carbons with 1 double bond at the *sn*-1 position via an alkyl (ether) linkage (O-), and a saturated fatty acyl chain of 2 carbons at the *sn*-2 position via an ester linkage.

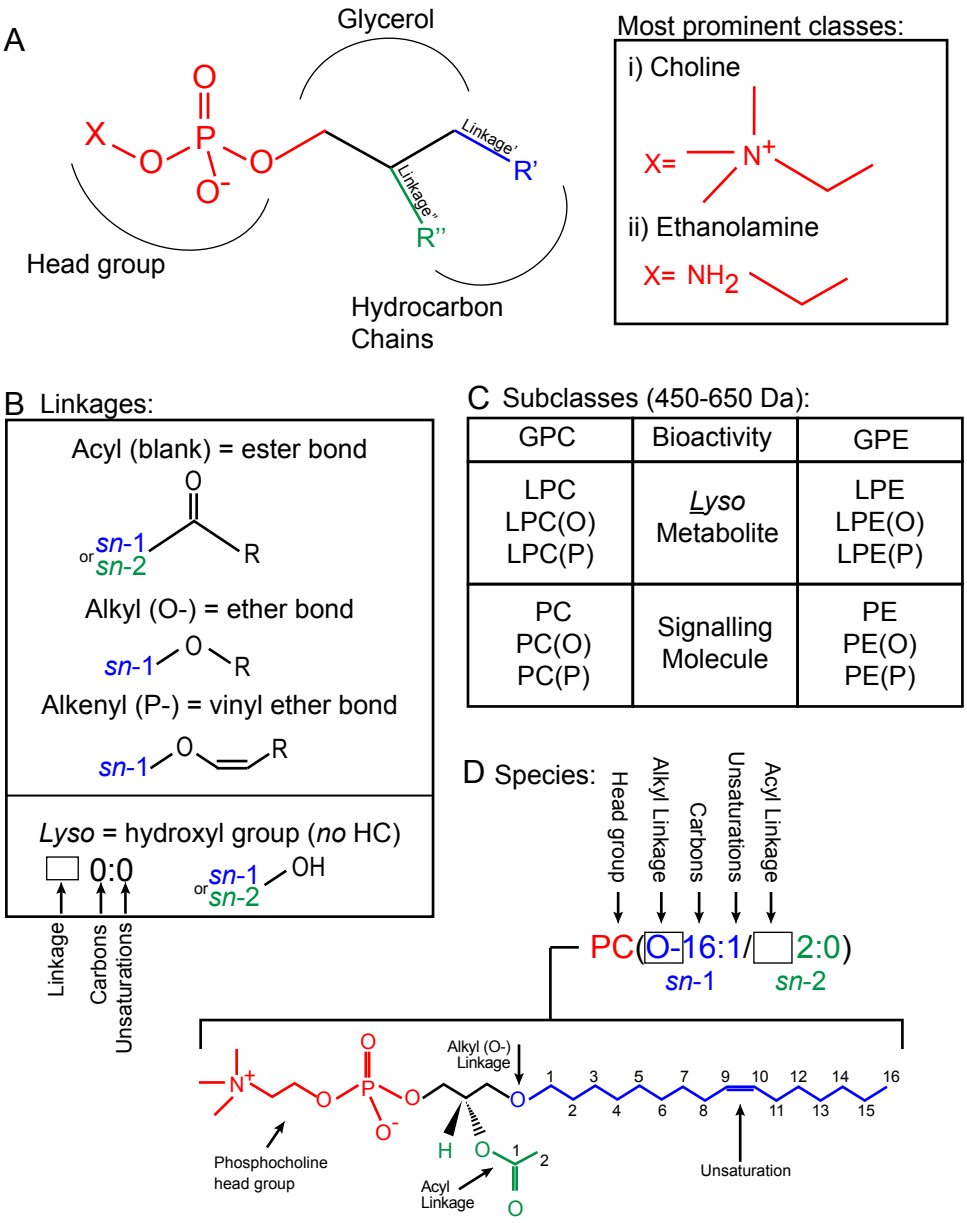
A
Glycerol
Head group
Hydrocarbon Chains
Linkage'
Linkage''
R'
R''
Most prominent classes:
i) Choline
X=
ii) Ethanolamine
X= NH2
B Linkages:
Acyl (blank) = ester bond
or sn-1 sn-2
Alkyl (O-) = ether bond
sn-1
Alkenyl (P-) = vinyl ether bond
sn-1
Lyso = hydroxyl group (no HC)
0:0
or sn-1 sn-2
OH
Linkage
Carbons
Unsaturations
C Subclasses (450-650 Da):
GPC
Bioactivity
GPE
LPC
LPC(O)
LPC(P)
Lyso Metabolite
LPE
LPE(O)
LPE(P)
PC
PC(O)
PC(P)
Signalling Molecule
PE
PE(O)
PE(P)
D Species:
Head group
Alkyl Linkage
Carbons
Unsaturations
Acyl Linkage
PC(O-16:1/2:0)
sn-1
sn-2
Alkyl (O-) Linkage
Phosphocholine head group
Acyl Linkage
Unsaturation

Figure 1.1

most abundant phospho-moieties contain either a choline or ethanolamine which identify the lipid classes of glycerophosphocholine (GPC) and glycerophosphoethanolamine (GPE) respectively (Fig. 1.1A). The hydrocarbon chains found at either the *sn*-1 or *sn*-2 glycerol carbons are conjugated to the glycerol back bone by: (a) an acyl linkage denoted by an ester bond, (b) an alkyl linkage denoted by an ether bond (O-), or (c) an alkenyl linkage denoted by a vinyl ether bond (P-) (Fig. 1.1B). If the hydrocarbon chain is replaced by a hydroxyl moiety at either the *sn*-1 or *sn*-2 positon, the molecule is designated as a *lyso*-glycerophospholipid. These linkages dictate, in part, the signalling and metabolic properties of GPCs and GPEs. Therefore, these linkage-specific subclasses each have their own hierarchical subclassifications. In GPCs, for example, when a hydrocarbon chain is present at both the *sn*-1 and *sn*-2 positions, individual species are first defined as diacylglycerophosphocholines (PC); 1-alkyl,2-acylglycerophosphocholines (PC(O)); or 1-alkenyl,2-acylglycerophosphocholine (PC(P)) wherein the hydrocarbon chain at the *sn*-1 position is linked by acyl, alkyl, or alkenyl bond, respectively, and the hydrocarbon chain at the *sn*-2 position is linked by an acyl linkage. While consideration has been given to alkyl and alkenyl-linked hydrocarbon chains at the *sn*-2 position, dialkylglycerophosphocholines are exceedingly rare (Pugh et al., 1977; Witzke and Bittman, 1986) and to our knowledge, dialkenylglycerophosphocholines have not been identified in mammals. Thus, these two latter subclasses will not be discussed in this thesis. While the majority of PC, PC(O) and PC(P) molecules make up the inherent structure of the glycerophospholipid bilayers that compartmentalize membranes and are, therefore, structural in nature, there are bioactive subgroups of PC, PC(O)s, and PC(P)s denoted by shorter hydrocarbon chains at the *sn-2* position that can act as signalling

molecules (discussed below). These molecules are smaller in nature (~450-650 Da) and for the purposes of this thesis, only PC, PC(O) and PC(P) signalling molecules (and GPE counterparts) will be discussed (Fig. 1.1C). Both signaling and structural membrane glycerophospholipids can be further metabolized into monoacylglycerophosphocholines (LPC), monoalkylglycerophosphocholines (LPC(O)), or monoalkenylglycerophosphocholines (LPC(P)) by hydrolysis of either the *sn*-1 or *sn*-2 hydrocarbons (Fig 1.1C). GPEs are metabolized in a similar manner albeit using different enzymes (reviewed below) and will be similarly examined in this thesis.

These structural differences are fully represented by recently standardized lipid nomenclature (Fahy et al., 2009). As an example (Fig. 1.1D), the PC(O-16:1/2:0) molecule is defined by the presence of a phosphocholine headgroup (PC) at the *sn*-3 position of the glycerol backbone, a hydrocarbon chain composed of 16 carbons with one unsaturation (i.e., one double bond, 16:1) linked to the *sn*-1 position of the glycerol backbone by an alkyl linkage (O-16:1), and an acyl-linked (no prefix) fully saturated two-carbon acetyl group (2:0) at the *sn*-2 position. This precision allows the diversity in lipid structure to be easily described.

1.1.2 Alkyl and alkenyl glycerophospholipid signalling molecules

PC(O) lipids with short *sn*-2 hydrocarbon chains represent a group of particularly bioactive molecules called platelet-activating factors (PAFs). The most potent species are defined as having the alkyl linkage at the *sn-1* position and an acetyl group at the *sn-2* position (Liu et al., 2016). This subclass also includes PAF-like molecules, characterized by a longer hydrocarbon chain at the *sn-2* (between 4-10 carbons), that

can result from the oxidation of longer *sn*-2 hydrocarbons (Marathe et al., 2002). Activity is, in part, dictated by binding to a single G-protein coupled PAF receptor (PAFR), primarily implicated in regulating pro-inflammatory processes (Ryan et al., 2008; Smiley et al., 1991). PAFR can also bind to 1-alkyl,2-acylglycerophosphoethanolamines (PE(O)s) with a similar response albeit with lower binding affinity (O'Flaherty et al., 1994). PAFR-dependent pathways are involved in platelet aggregation, leukocyte activation, chemotaxis and reactive oxygen species (ROS) generation as well as inducing the expression of proinflammatory molecules such as IL-6 and iNOS (reviewed in (Liu et al., 2016)). PAFs can also operate through PAFR-independent pathways and will activate differential mechanisms based on the length of the *sn-1* hydrocarbon chain which our lab has shown mediates chain-specific pro- or anti-apoptotic effects (Ryan et al., 2008). *Lyso*-PAFs, (i.e. LPC(O)s), are usually considered the inactive metabolite of PAF but may also modulate PAF signalling cascades, particularly by reducing the production of superoxides and inhibiting platelet aggregation (Welch et al., 2009). In the brain, PAFs play a dual role. As in the circulation, they act as inflammatory mediators and are involved in inflammation, ischemic injury, and stroke (Bozlu et al., 2007; Hostettler and Carlson, 2002; Row et al., 2004). However, they have also been linked to cognition, likely through modulation of long-term potentiation (LTP) via actions as retrograde neurotransmitters released by the post-synaptic cell in response to glutaminergic stimulation that activate pre-synaptic PAFR to potentiate further glutamate release (Kato et al., 1994). When PAF analogs are injected into the hippocampus, entorhinal cortex, amygdala or striatum, memory retention is enhanced in avoidance and spatial habituation tasks corresponding with a lower escape latency in the Morris Water Maze (MWM) (Izquierdo et al., 1995;

Packard et al., 1996). Interestingly, in PAFR-/- mice, there is an amelioration of hypoxic impairment suggesting that PAFR signalling can mediate the cognitive response to hypoxic exposure (Row et al., 2004).

Alkenyl-linked glycerophospholipids are also known as plasmalogens. These species are considered antioxidants due to the cis-double bond defining the vinyl ether (alkenyl) group at the *sn*-1 position. This double bond makes plasmalogens more susceptible to oxidative attacks by ROS therefore protecting cells from the deleterious effects of ROS on the cell (Braverman and Moser, 2012; Broniec et al., 2011). This could be in part why plasmalogens are thought to be anti-apoptotic in the central nervous system (CNS) (Hossain et al., 2013; Hossain et al., 2016). Plasmalogens may also be involved through the activation of the protein kinase B (Akt) and extracellular signal-regulated kinase (ERK) pathways (Hossain et al., 2013). Similar to alkyl-linked glycerophospholipids, these pathways may be activated through the actions of plasmanyl-specific G protein-coupled receptors (GPCRs). Five neuron-specific GPCRs with previously unknown functions demonstrate enhance plasmanyl-dependent phosphorylation of ERK and Akt when overexpressed. Furthermore, this effect can be inhibited when these GPCRs are knocked down (Hossain et al., 2016).

1.1.3 Synthesis, remodeling, and oxidation

PC(O)s, PCs, PE(O)s, and diacylglycerophosphoethanolamines (PEs) can be synthesized via the Kennedy (*de novo*) pathway. Subsequent desaturation of PE(O) to PE(P) or conversion of 1-alkenyl,2-acylglycerophosphoethanolamine (PE(P)) to PC(P) generates the plasmalogens (Fig 1.2.A). All subclasses can be remodelled via the Lands'

Figure 1.2 – Pathways of GPC and GPE synthesis and remodeling. (A) The Kennedy pathway of *de novo* GPE and GPC synthesis. (B) The Lands' cycle of enzymatic remodeling of GPCs and GPEs into bioactive metabolites and second messengers. (C) Non-enzymatic oxidation of glycerophospholipids into GPC and GPE with truncated carbon chains. Abbreviations: ATP – adenosine triphosphate; ADP – adenosine diphosphate; CK – choline kinase; EK – ethanolamine kinase; CTP – cytidine triphosphate; PPi – pyrophosphate; CCT – CTP:phosphocholine cytidylyltransferase; ECT – CTP:phosphoethanolamine cytidylyltransferase; CDP – cytidine diphosphate; DAG – diacyl glycerol – AAG – alkyl-acyl glycerol; CMP – cytidine monophosphate; CPT – cholinephosphotransferase; EPT – ethanolamine phosphotransferase; PEMT – phosphatidylethanolamine methyltransferase; PED – plasmenylethanolamine desaturase. $sPLA_2$ – secreted phospholipase A_2; $cPLA_2$ – cytosolic phospholipase A_2; $iPLA_2$ – Ca^{2+}-independent phospholipase A_2; PAFAH – platelet-activating factor acetyl hydrolase; $LPLA_2$ – lysosomal PLA_2; LPCAT – lysophosphocholine acyltransferase; LPEAT – lysophosphoethanolamine acyltransferase; ROS – reactive oxygen species.

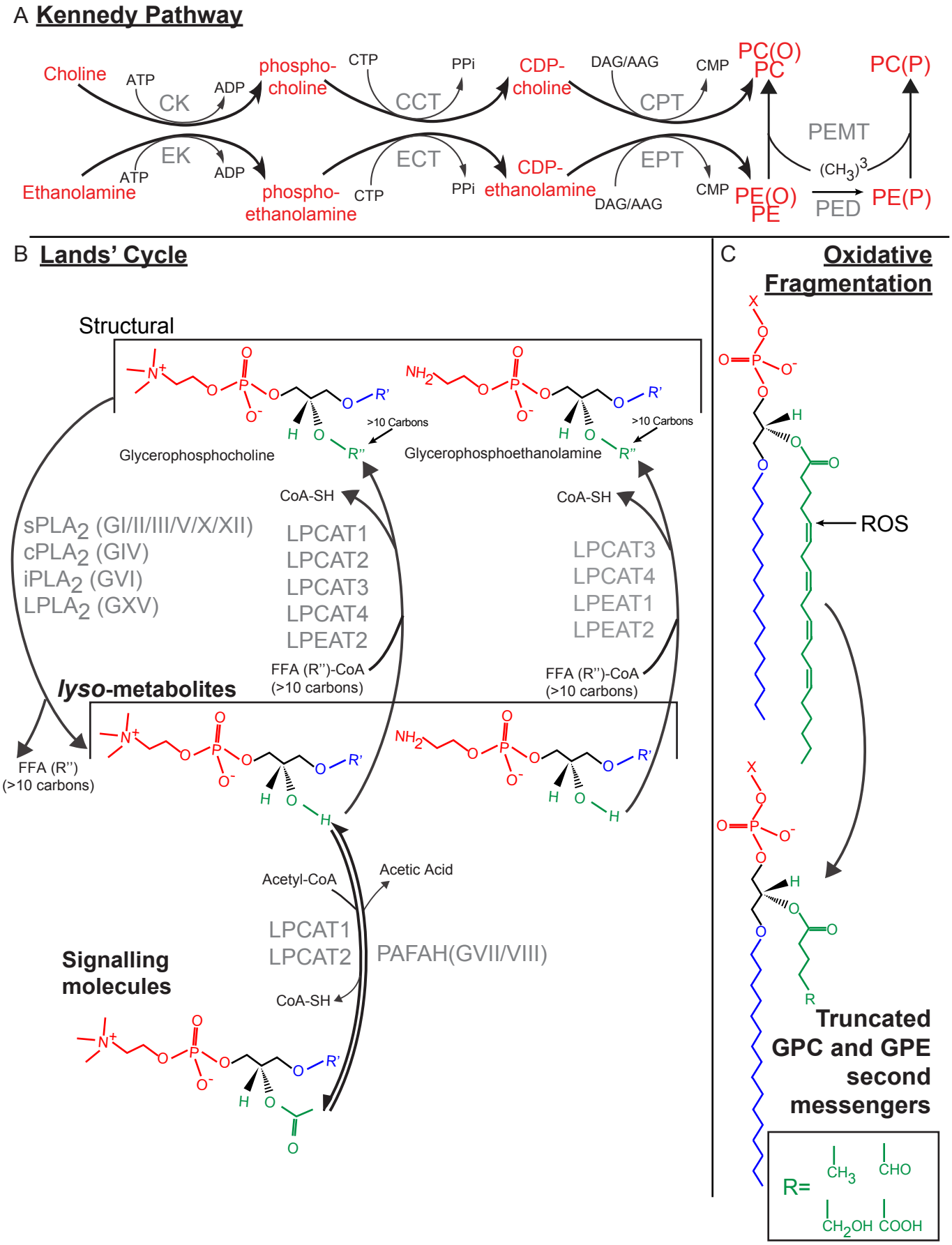
A Kennedy Pathway
Choline
ATP
CK
ADP
phospho-choline
CTP
CCT
PPi
CDP-choline
DAG/AAG
CPT
CMP
PC(O)
PC
PC(P)
PEMT
(CH3)3
Ethanolamine
ATP
EK
ADP
phospho-ethanolamine
CTP
ECT
PPi
CDP-ethanolamine
DAG/AAG
EPT
CMP
PE(O)
PE
PED
PE(P)
B Lands' Cycle
Structural
Glycerophosphocholine
Glycerophosphoethanolamine
>10 Carbons
>10 Carbons
CoA-SH
CoA-SH
sPLA2 (GI/II/III/V/X/XII)
cPLA2 (GIV)
iPLA2 (GVI)
LPLA2 (GXV)
LPCAT1
LPCAT2
LPCAT3
LPCAT4
LPEAT2
LPCAT3
LPCAT4
LPEAT1
LPEAT2
FFA (R'')-CoA
(>10 carbons)
FFA (R'')-CoA
(>10 carbons)
lyso-metabolites
FFA (R'')
(>10 carbons)
Acetyl-CoA
Acetic Acid
LPCAT1
LPCAT2
PAFAH(GVII/VIII)
Signalling molecules
CoA-SH
C Oxidative Fragmentation
ROS
Truncated GPC and GPE second messengers
R=
CH3
CHO
CH2OH
COOH

Figure 1.2

cycle remodelling pathway (Gibellini and Smith, 2010; Kennedy and Weiss, 1956; Moessinger et al., 2014; Shindou et al., 2009) (Fig. 1.2). The initiating reaction in the Kennedy pathway is the phosphorylation of a choline or ethanolamine molecule by choline or ethanolamine kinase (CK or EK) respectively (Gibellini and Smith, 2010) however some CKs can also phosphorylate ethanolamine (Kent, 1995). In the rate-limiting second step, cytidine triphosphate (CTP):phosphocholine cytidylyltransferase (CCT) or the phosphoethanolamine equivalent (ECT) will use CTP to form cytidine diphosphate (CDP)-choline or CDP-ethanolamine, releasing a pyrophosphate (Gibellini and Smith, 2010). In the final step of GPC *de novo* synthesis, cholinephosphotransferase (CPT) transfers CDP-choline to either diacylglycerol (DAG) or alkyl-acylglycerol (AAG) to form a GPC molecule releasing cytidine monophosphate (CMP). The final step in GPE synthesis is equivalent with the ethanolamine-specific enzyme (EPT) (Gibellini and Smith, 2010). Additionally, GPEs can be transformed into GPCs via the action of phosphatidylethanolamine methyltransferase (PEMT) that methylates the amine of the ethanolamine headgroup to convert it to a choline (Guan et al., 1999b). Once PE(O)s are formed, the proximal carbon of the *sn*-1 moiety can be desaturated by plasmenylethanolamine desaturase (PED) to form PE(P). Since there is no plasmenylcholine desaturase to form PC(P)s (Braverman and Moser, 2012), PE(P) must be converted to PC(P) either by methylation through PEMT or through the actions of phospholipase C which will cleave the PE(P) head group, allowing CPT to transfer a PC as the *sn*-3 moiety, thus forming PC(P) (Braverman and Moser, 2012).

The Lands' cycle reversibly remodels GPCs and GPEs from structural membrane components to (and from) bioactive metabolites and signalling molecules (Fig. 1.2B).

GPCs and GPEs with hydrocarbon chains between 12 and 30 carbons at both the *sn*-1 and *sn*-2 positions are defined as structural glycerophospholipids commonly found as the central component of the membrane. These molecules can be hydrolyzed at the *sn-2* position through the actions of phospholipase A_2 (PLA_2) enzymes to yield *lyso*-GPCs and *lyso*-GPEs and a free fatty acid (Burke and Dennis, 2009; Richmond and Smith, 2011). There are also phospholipase A_1 enzymes that hydrolyze hydrocarbons at the *sn*-1 position of glycerophospholipids not directly related to the Lands' cycle pathway (Imae et al., 2010; Richmond and Smith, 2011).

The PLA_2 superfamily is composed of five specific categories of enzymes subdivided into 15 groups and multiple subgroups (Fig 1.2B). This hierarchy is defined, in part, by their molecular weights, Ca^{2+} activity dependency, and hydrocarbon chain affinity (reviewed in (Burke and Dennis, 2009; Schaloske and Dennis, 2006)). The five categories of the PLA_2 superfamily are: i) secreted PLA_2, ii) cytosolic PLA_2 ($cPLA_2$), iii) Ca^{2+}-independent PLA_2 ($iPLA_2$), iv) PAF acetylhydrolase (PAFAH), and v) lysosomal PLA_2 ($LPLA_2$) (Burke and Dennis, 2009; Schaloske and Dennis, 2006). $sPLA_2$s are primarily distinguished by their low molecular weight (13-18 kDa), although there has recently been a 55 kDa $sPLA_2$ found in humans (Valentin et al., 2000). Humans express group (G) I, II, III,V, X and XII $sPLA_2$, though more isoforms of $sPLA_2$ be found in other organisms (Schaloske and Dennis, 2006; Valentin and Lambeau, 2000). Individual groups of $sPLA_2$s show preferential cleavage of specific hydrocarbon chains from the *sn*-2 position (Murakami et al., 2015; Pruzanski et al., 2005). For example, GV has a low preference for polyunsaturated fatty acid (PUFA)-linked *sn-2* chains but GX does show preference, particularly for linoleic acid (LA, 18:2) and arachidonic acid (AA, 20:4)

(Pruzanski et al., 2005). AA can form a group of lipids called eicosanoids involved in pro-inflammatory pathways but can also be β-oxidized and converted to ROS (Rapoport, 2014; Schaloske and Dennis, 2006).

While some subgroups of $cPLA_2$ also exhibit preferential cleavage for AA, the $cPLA_2$ family of proteins are larger, ranging from 61-114 kDa defining GIV of PLA_2 isoforms (Burke and Dennis, 2009). Of this group, there are six subgroups (GIVA-F) which have differing affinities for *sn*-2 moieties (Burke and Dennis, 2009). All of these subgroups are Ca^{2+}-dependent except for GIVC however its homology with other GIV PLA_2s phylogenetically justified its inclusion as a GIV phospholipase (Burke and Dennis, 2009; Underwood et al., 1998). The primary subgroup related to cleavage of AA is group IVA (Clark et al., 1991). Group IVD has a specificity for LA (18:2). GIVB and GIVC have no specificity. GIVE and GIVF have specificity for both AA and LA (Burke and Dennis, 2009; Ohto et al., 2005). Interestingly, GIVF also shows substrate specificity for glycerophospholipid headgroups, preferring GPEs to GPCs. (Ohto et al., 2005).

Similar to $cPLA_2$s, $iPLA_2$ are larger (28-146 kDa) and are comprised of six subgroups encompassing GVI PLA_2s (Burke and Dennis, 2009). It was originally believed that unlike other PLA_2 categories, $iPLA_2$s have no known fatty acyl specificity (Schaloske and Dennis, 2006). However, recent discoveries suggest this untrue. iPLA2 exhibits both head group and hydrocarbon chain composition specificity. It has a mild preference for GPEs and prefers LA substrate binding (Mouchlis et al., 2018).

PAFAHs are PLA_2 enzymes that specifically hydrolyze the acetyl group from PAF molecules to produce *lyso*-PAFs (i.e. LPC(O)) (Schaloske and Dennis, 2006). They range from 26-46 kDa and include GVII and GVIII PLA_2s. Both GVII and GVIII PAFAHs

incorporate two subgroups (A and B) respectively. GVIIA PAFAHs are a secreted form of the enzyme released into circulation whereas GVIIB, GVIIIA and GVIIIB all are intracellular. GVIIIA and GVIIIB PLA_2s each have a catalytic subunit (α1 and α2 respectively) and a regulatory subunit (β). The catalytic subunits dimerize to affect substrate specificity of PAFAH activity. For instance, α2/α2 homodimer shows higher specificity for PC(O) and PE(O) molecules whereas α1/α2 and α1/α1 dimers prefer glycerophosphatidic acids (GPAs) (Manya et al., 1999; Schaloske and Dennis, 2006).

The final PLA_2, $LPLA_2$s, encompass GXV PLA_2s with both PLA_2 activity and transacylase activity. They are responsible for acylating the hydroxyl groups on ceramides (the building block of sphingolipids) and hydrolyze the *sn*-2 fatty acyl groups from glycerophospholipids to use as donors (Abe and Shayman, 1998). There is only one known isoform (45 kDa) currently known of (Schaloske and Dennis, 2006). The complexity in substrate specificity in the hydrolysis of *sn-2* hydrocarbon chains coupled with the advanced nomenclature of PLA_2 enzymes is a prime example of the diversity and depth of lipid metabolism.

Once PLA_2 enzymes act on GPCs and GPEs, they produce *lyso*-GPCs such as LPCs, LPC(O)s, LPC(P)s, as well as *lyso*-GPEs including monoacylglycerophosphoethanolamines (LPEs), monoalkylglycerophosphoethanolamines (LPE(O)s), and monoalkenylglycerophosphoethanolamines (LPE(P)s) (Fig. 1.2B). These metabolites can either be remodeled back into their respective structural precursors via the actions of lysophospholipid acyl transferases (LPLATs) or further modified into bioactive second messengers. In order for LPLATs to operate, fatty acids are first conjugated to coenzyme

A (CoA). LPLATs will bind the fatty acyl-CoA and transfer it to the hydroxyl-bound *sn*-1 or *sn*-2 position of the *lyso*-glycerophoshopholipid (Shindou et al., 2009). There are at least 15 known LPLAT isoforms with various specificities for the type of hydrocarbon chain, the linkages, and the headgroup of its *lyso* lipid substrate (Hishikawa et al., 2008; Shindou et al., 2009). There are five LPLATs with LPC specificity: lysophosphocholine acyltransferase 1 (LPCAT1), LPCAT2, LPCAT3, LPCAT4 and lysophosphoethanolamine acyltransferase 2 (LPEAT2). Evidenced by LPC-active LPEAT2, there is cross-reactivity with LPEs as well. LPLATs active with LPEs are LPCAT3, LPCAT4, LPEAT1 and LPEAT2 (Shindou et al., 2009). LPLATs also have selectivity for specific hydrocarbon chains (Shindou et al., 2009). LPCAT1 and LPCAT2 have PAF acetyl transferase activity and will preferentially bind an acetyl group to PAF (Harayama et al., 2008). However, LPCAT1 also has affinity for saturated hydrocarbon chains ranging from 6-16 carbons (Chen et al., 2006; Nakanishi et al., 2006). This is very different than LPCAT2 which will also transfer an arachidonyl group (20:4) (Shindou et al., 2009). LPCAT3, LPCAT4, LPEAT1 and LPEAT2 all will preferentially transfer an oleoyl group (18:1) (Hishikawa et al., 2008). LPCAT3 will also selectively transfer linoleoyl and arachidonyl groups while LPEAT2 selects for arachidonyl, palmitoyl (16:0) and stearoyl (18:0) groups (Cao et al., 2008; Hishikawa et al., 2008).

Finally, as summarized in Fig 1.2C, enzymatic pathways are not the only process involved in the remodelling of glycerophospholipids. In the presence of oxidative stress, unsaturated hydrocarbon chains become targets for ROS and will be oxidatively fragmented at the site of their double bond (Bochkov et al., 2010; Chen et al., 2008; Solis-Calero et al., 2015). This makes PUFA-linked GPCs and GPEs more susceptible to

oxidative fragmentation. The result of this fragmentation can be the production of bioactive PAF-like molecules (McIntyre, 2012). Oxidative fragmentation can also occur at 1-alkenyl and 1-acyl-linkages to glycerophospholipid backbone (Reis and Spickett, 2012; Wynalda and Murphy, 2010). The remaining truncated glycerophospholipid hydrocarbon chain is composed of a methyl, aldehyde, hydroxyl, or carboxylic acid group (Reis and Spickett, 2012; Spickett and Pitt, 2015) (Fig. 1.2C).

1.2 Methodologies in neurolipidomics

Recent advances in high performance liquid chromatography (HPLC), electrospray ionization (ESI), and mass spectrometry (MS), coupled with new membrane separation and extraction methodologies, have provided us with the means to quantify the diversity of lipid species (Bou Khalil et al., 2010; Brown and Murphy, 2009; Piomelli et al., 2007; Xu et al., 2013). This new “omics” field, lipidomics, considered a sub-field of metabolomics, is defined by the comprehensive and quantitative analysis of specific lipid categories, classes, and species present in different cell organelles, cells, tissues, and organisms. Neurolipidomics, in particular, focuses on the lipid composition of the CNS and peripheral nervous systems (PNS). This focus encompasses not only the profiling and quantification of lipid composition but also the exploration of the regulatory enzymes altering lipid metabolism, the protein effectors of lipid signalling, and the impact of lipid composition on the function of membrane proteins.

1.2.1 – Technical considerations when isolating glycerophospholipids for lipidomic analysis

The diversity of glycerophospholipids reviewed above is also reflected in their abundance; concentrations of different species are estimated to range between amol to nmol/mg protein, a 10^9-fold difference (Yang and Han, 2016). Thus, as with all 'omic' technologies, sample preparation is crucial, as it dictates which lipid classes, subclasses and species will be enriched for in a given extract. Not surprisingly, individual classes and subclasses are extracted with different degrees of efficiency depending on the protocol employed. There are four primary methods of lipid extraction, each with different lipid-specific extraction efficiencies: (1) the methyl tert-butyl ether (MTBE) method, (2) the butanol/methanol (BUME) method, (3) the Folch method, and (4) the Bligh and Dyer method. In the case of neurolipidomics, each method begins with dissection, flash-freezing, and subsequent homogenization of different brain regions in extraction solvents along with necessary standards. Internal standards allow for the accurate quantification of lipid abundances by considering sample-to-sample variations in extraction efficiency. Each class of lipid under investigation must be normalized to an internal standard of the same class with the inherent assumption of an identical MS response.

The MTBE method uses a mixture of MTBE, methanol and water that separates the MTBE organic phase as the top layer after phase separation. While this method allows for rapid automated sampling from the upper phase, it is also considered somewhat "dirty" as considerable aqueous contaminants are retained in the MTBE phase (Yang and Han, 2016). The BUME method solves some of these problems combining BUME (3:1, butanol:methanol) with an aqueous solution followed by the addition of heptane/ethyl

acetate (3:1) with acetic acid for phase separation (Lofgren et al., 2016; Yang and Han, 2016). This method specifically recovers sterols, glycerolipids, sphingolipids, and glycerophospholipids (Lofgren et al., 2016). Of the glycerophospholipids, it is particularly efficient at recovering glycerophosphoserines (GPSs), GPAs, glycerophosphatidylglycerols (GPGs) and glycerophospholinsositals (GPIs) but not GPCs or GPEs (Lofgren et al., 2016). Present adaptations of classic lipid extraction methods include the modified Folch method (Folch et al., 1957) and the modified Bligh and Dyer method (Bligh and Dyer, 1959). Both include chloroform as the organic phase used to isolate lipids. Technical considerations for these widely-used methods are the chloroform toxicity and the challenge of recovering the solvent extract from the bottom phase. Both use a combination of chloroform/methanol/aqueous solution that only vary in ratio (Yang and Han, 2016). They are ideal for small tissue samples such as specific anatomical regions in the rodent brain. The modified Folch method is optimal for 100 mg of tissue while the modified Bligh and Dyer methods are used for even smaller tissue samples under 50 mg tissue weight (Yang and Han, 2016). Additionally, the modified Bligh and Dyer method, particularly using acidified conditions, is more efficient in the recovery of GPCs and GPEs, particularly LPC metabolites and signalling molecules, than either the Folch or MTBE methods (Reis et al., 2013). Our laboratory has shown that adding acetic acid to the methanol phase at time of homogenization both improves recovery of acidic glycerophospholipids without compromising extraction of neutral phospholipids and indeed enriches extracted GPCs for species with labile alkyl (PC(O)) and alkenyl (PC(P)) linkages (Xu et al., 2013).

In any type of lipid extraction, there are certain experimental caveats that must be considered to avoid contaminating results. As mentioned above, glycerophospholipids are susceptible to oxidation (Furse et al., 2015). Thus, care must be taken to limit exposure to oxygen during an extraction. Even once lipids are extracted, they should be stored in an environment to reduce any oxidative reactions. One way to accomplish this is by replacing the air in the storage vials with pure nitrogen gas. Another consideration is to avoid exposure to ultraviolet light which can form acylating agents that will target nucleophilic groups such as the GPE headgroup (Cone et al., 1982; Furse et al., 2015). Therefore samples must be stored in the dark, preferably opaque storage vials that reduce light exposure during transport and use. A final consideration in lipid extractions often overlooked by many teams, is the degradation of plastics by organic solvents that extracts are stored in. Organic solvents even as weak as ethanol cause degradation of plastics such as polypropylene found in the common Eppendorf tube which will contaminate biological extracts (McDonald et al., 2008). Our laboratory has unpublished data indicating that the extraction of cerebrospinal fluid (CSF) in plastic Eppendorf tube or glass kimble tubes yields vastly different profiles with additional contaminants found in the Eppendorf extraction that were absent from the kimble extraction. Indeed, in a recent Keystone Symposia presentation, Dr. Walt Shaw, the chief scientific officer of Avanti Polar Lipids, the leader in synthesis of MS-grade lipid standards, emphasized requirement to extract in acid-washed glass and store samples in SCHOTT FIOLAX® glass vials (Shaw et al., 2017). While a seemingly inconsequential decision, it is suggested that the attention paid to extraction procedures will fundamentally dictate results and inter-lab reproducibility.

1.2.2 – Direct infusion and HPLC-ESI-MS

Profiling the lipidome primarily relies on MS technologies that are capable of distinguishing between species based on subtle structural differences. There are two main ESI-MS based approaches used to profile glycerophospholipids: (1) direct-infusion MS (also known as shotgun lipidomics) and (2) HPLC-ESI-MS. Shotgun lipidomics directly infuses samples into the mass spectrometer without prior LC separation. It is a high throughput method that requires minimal sample manipulation. This approach enables rapid simultaneous analysis of all glycerophospholipids with bias for the most abundant species, yet is unable to separate molecular species with equivalent mass (isobaric species). For example, PC(18:0/0:0) and PC(O-16:0/2:0) have the same exact mass (523.3638 Da) but with considerably different signalling and metabolic properties (Gazos-Lopes et al., 2014). These species will not be separated by direct-infusion methods and are therefore unable to be appropriately quantified.

The most common technique for the separation of isobaric species is the use of specific liquid chromatography methods prior to MS analysis. HPLC is a highly accurate, reproducible and sensitive method of species separation, particularly for glycerophospholipids and sphingolipids (Sethi and Brietzke, 2017). It is ideal for the detection of lower abundant species such as metabolites and signalling molecules (Han, 2016). Normal-phase and reverse-phase HPLC are the two commonly used LC in lipidomics research (Kofeler et al., 2012). In normal-phase HPLC, lipids are separated by their differences in hydrophilicity that is primarily determined by the polar head groups, thus allowing lipid classes to be separated. In contrast, reverse-phase HPLC separates molecules based on hydrophobicity (Fig. 1.3A). For glycerophospholipids, hydrophobicity

is mainly determined by the length and degree of unsaturation of the hydrophobic hydrocarbon chains at the *sn*-1 and/or *sn*-2 positions. Thus, reverse-phase HPLC allows for the separation of glycerophospholipid molecular species including most isobaric species (Sethi and Brietzke, 2017; Zhao et al., 2015). Isobaric species with the same exact mass (e.g. PC(O-16:0/2:0) and PC(18:0/0:0)), but different hydrophobicities (e.g. differing hydrocarbon chain lengths), will be separated (Fig. 1.3A). Due to this separation, these molecules will elute from the column at different times, this is known as “elution time” or “retention time” (Sethi and Brietzke, 2017; Zhao et al., 2015). Thus, separated isobaric species will be injected into the mass spectrometer at different times.

Once sample molecules are separated by reverse phase HPLC, they flow through a capillary to be injected into the mass spectrometer (now in order of hydrophobicity). Two requirements to remember when injecting lipids into a mass spectrometer are a) analytes must be detected in gaseous form and b) MS will only detect charged analytes, thus analytes must be detected as a mass-to-charge (m/z) ratio (Dass, 2000). In order to accomplish both of these criteria using a lipid extraction solubilized in liquid solvent, lipids must be desolvated and ionized before entering the spectrometer. However, lipids are relatively labile and they tend to undergo unwanted fragmentation in the ionization source using conventional ionization techniques (Banerjee and Mazumdar, 2012). The introduction of the “soft ionization” techniques such as ESI has greatly facilitated lipidomics research by minimizing intrasource fragmentation. ESI is particularly sensitive in processing GPCs and GPEs, thus making it one of the most used soft ionization techniques in lipidomics (Li et al., 2014; Tian et al., 2013). In ESI, a strong electric field is

Figure 1.3 – HPLC-ESI-MS/MS methodologies on a triple quadrupole mass spectrometer. (A) A schematic of reverse-phase HPLC wherein lipid molecules are separated by hydrophobicity prior to ESI. Coloured dots indicate lipid molecules of varying hydrophobicities separated along the HPLC column (red is the most hydrophobic and violet the least hydrophobic). (B) A schematic of ESI as lipid molecules are transferred from the capillary to the mass spectrometer. Adapted from (Banerjee and Mazumdar, 2012). (C) A list of detection and quantification methods used with triple quadrupole mass spectrometers using tandem mass spectrometry (MS/MS). The top panel represents the flow-through of each quadrupole while the bottom table differentiates between different detection methods. ProIS, NLS and PIS are used to scan across a range of m/z values before and/or after fragmentation in Q2 for detection of all analytes within that range. SRM/MRM select for specific values within those ranges to enhance resolution of detection. Adapted from (Lam and Shui, 2013).

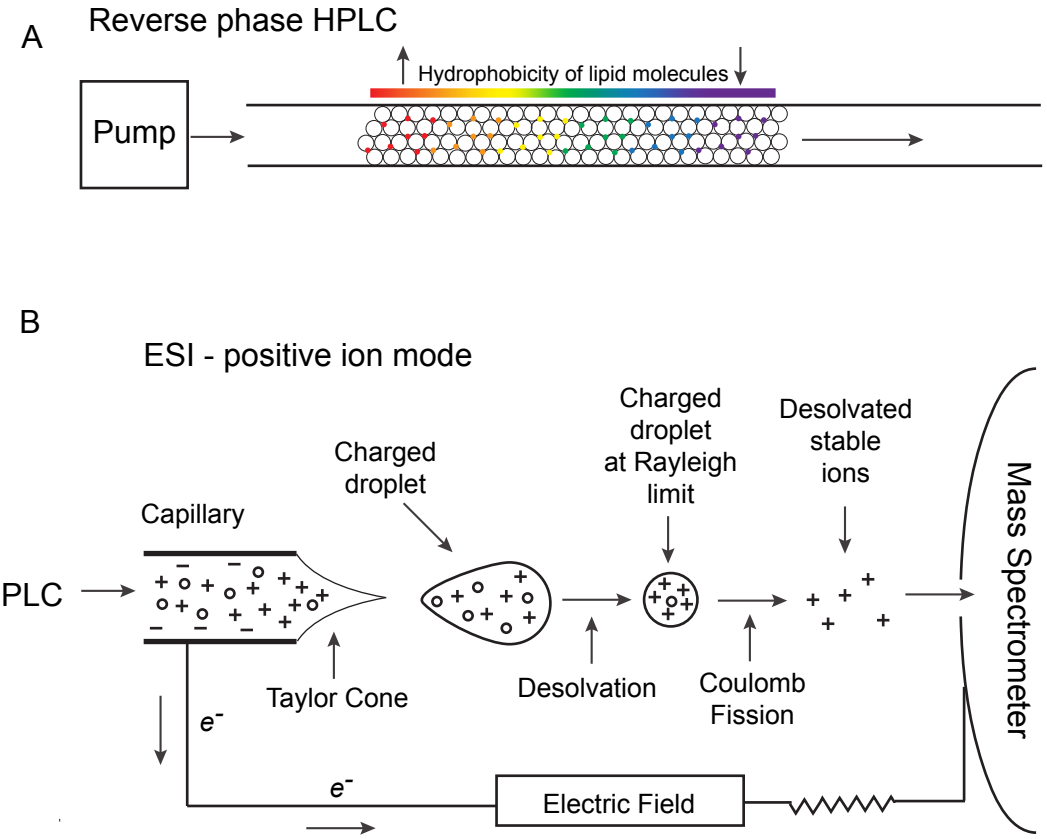

Scan Mode	Q1	Q2	Q3
ProIS	Selects	Fragments	Scans
NLS	Scans	Fragments	Scans (difference of Q1 m/z and neutral product)
PIS	Scans	Fragments	Selects
SRM/MRM	Selects	Fragments	Selects

Figure 1.3

produced at the ion source by the application of high voltages. Heated gas is also applied once lipid extract is sprayed from capillary to facilitate evaporation. Ionized molecules generated in the liquid solvent (with either a positive or negative charge) will be concentrated near the capillary tip by the electric field. These molecules will then be sprayed from the capillary tip in the form of liquid droplets. In positive ion mode (Fig. 1.3B, adapted from (Banerjee and Mazumdar, 2012)), the high voltage applies a net positive charge to solvated lipid droplets as they spray from the tip of the capillary. The spray is the result of an accumulation of positive charges at the end of the capillary that emerge from the capillary tip in the form of an inverted cone. This phenomenon is called a “Taylor cone” and immediately initiates the spraying of a fine mist composed of lipid-containing liquid droplets with a net positive charge from the tip (Banerjee and Mazumdar, 2012). As the liquid droplets are sprayed, there is a progressive evaporation of liquid solvent enhanced by the application of heated gas which concentrates the charge in the droplet. As the like charges become more concentrated, the electrostatic repulsion forces (Coulomb’s forces) in the droplet grows until the charge exceeds the surface tension of the droplet (Rayleigh limit). Once this occurs, there is an explosive dissociation (Coulomb fission) of the droplet, completely desolvating the lipid ions. This creates a steady spray of gaseous lipid ions into the mass spectrometer while maintaining their structural integrity (Fig. 1.3B) (Banerjee and Mazumdar, 2012; Bruins, 1998; Ho et al., 2003; Yang and Han, 2016).

Desolvated lipid ions entering the mass spectrometer are filtered by a mass analyzer. A very common mass analyzer utilized in lipidomics is the quadrupole (Kofeler et al., 2012). Quadrupole mass analyzers are an essential tool when directing lipidomic

profiling to a specific class of lipids. A quadrupole mass analyzer is composed of four parallel metal rods. A direct current (DC) is applied to two opposing rods and alternating radio frequency (RF) to the other two rods. These regulate the flight of ions between the four rods. Specific DC and RF dictate which ions are allowed to pass through based on m/z (Di Girolamo et al., 2013). This permits experimenters to mass-select for specific analytes or to profile across a broad mass range of analytes thus allowing for the specific profiling of a myriad of lipid molecules of varying sizes.

One of the most utilized mass spectrometers in lipidomics is a triple quadrupole mass spectrometer (Kofeler et al., 2012). Triple quadrupoles offer specific methods for detection of lipid classes, subclasses and species. They possess three sequential quadrupoles (Q1, Q2, Q3) that analytes must pass through to be detected. Q1 and Q3 are true mass analyzers while Q2 is a collision cell responsible for fragmenting analytes by bombarding them with inert gas molecules. Q1 can be programmed to scan for “precursor” ions found in the sample. Once the desired precursor ions enter Q2, they undergo collision-induced dissociation (CID) and are fragmented into product fragments. Q3 then scans for “product” fragment ions created by the fragmentation of the precursor ions. The fragment ions allowed through Q3 are then detected by a detector. Through these basic concepts, triple quadrupole mass spectrometers enable researchers to profile, detect and quantify both targeted and non-targeted lipid profiles.

In lipidomics, there are three main scans performed on a triple quadrupole for directed detection of lipid molecules: product ion scans (ProISs), precursor ion scan (PISs), and neutral loss scans (NLSs) (Fig. 1.3C, adapted from (Lam and Shui, 2013)). ProISs are used for directed analyses to determine the specific molecular structure of a

precursor ion (Lam and Shui, 2013). In ProIS mode, Q1 is programmed to filter through the m/z of the precursor ion of interest. The precursor ion enters Q2 to undergo CID, and the resulting product ions will be scanned in Q3 and all ion current recorded. The information collected from the detected m/z of the product ions is indicative of the structural and molecular composition of the precursor ion. In PIS, a specific product ion is selected in Q3 and the precursor ions are scanned across a range in Q1. This method is selective for ions with a common functional group. For example, GPCs all have a common phosphocholine head group. Q1 is programmed to scan a m/z range of precursor ions (e.g. 450-650 m/z for metabolites and signalling molecules), after CID in Q2, fragment ions at 184.1 m/z corresponding to the phosphocholine head group from the precursor ions are scanned in Q3. This provides a viable method where only lipid species that possess a phosphocholine molecule will be detected by the mass spectrometer. However, not all glycerophospholipid head groups will be charged when fragmented and are therefore undetectable by the mass spectrometer. GPEs are an example of a lipid class that upon fragmentation, lose a common neutral fragment (i.e. the phosphoethanolamine head group). This makes NLSs essential in lipidomics. In a NLS, both Q1 and Q3 scan across a m/z range but with a constant mass offset. This will lead to the selective detection of all ions that, when fragmented, will lose a common neutral fragment (e.g. the phosphoethanolamine head group). This allows for the detection of glycerophospholipids with neutral head groups. Both PIS and NLS allow the experimenter to detect and profile all specific lipid molecules within a set range. Though powerful in profiling, these types of scan modes waste time scanning in m/z regions where there are no analytes present. Selected or multiple reaction monitoring systems (SRM

and MRM respectively) is the method of choice for selective and sensitive quantification. In these methods, neither Q1 nor Q3 scan across a m/z range but instead are programmed for known precursor and product ions. Based on the discovery of specific precursors found in a sample through PIS or NLS, a precursor transition list of m/z values representing all the detected precursor ions in a sample is generated. Q1 is programmed to exclusively select for the m/z of one or multiple precursor ions. Q3 will be similarly set to select for either a single common product ion fragment or multiple product ion fragments. This allows the mass spectrometer to focus specifically on the selected m/z values of the transition lists which provides better resolution by reducing baseline noise and allowing for more accurate and sensitive detection of specific lipid molecules. These reaction monitoring systems drastically improve the accuracy and reproducibility of lipidomic quantification (Lam and Shui, 2013). Applying these technologies to biomarker discovery and the search for therapeutic targets in neurological diseases offers a new neurolipidomic perspective on the effects that changes in glycerophospholipids have on the brain and how these impact cognition.

1.3 – Applying a neurolipidomic approach to provide new insight into Alzheimer's disease (AD) cognitive decline

Of all neurodegenerative diseases, AD is the most prevalent and results in impaired cognition and dementia with defined pathological criteria (Ferri et al., 2005; Plassman et al., 2007; Qiu et al., 2009; Reitz et al., 2011). Cognitive decline in AD is an insidious process which current biomarkers are currently unable to predict with confidence. Furthermore, treatment options are limited and are not curative nor disease-

altering. In this thesis I demonstrate that using tools such as HPLC-ESI-MS/MS, neurolipidomics offers a critical avenue of investigation to determine metabolic changes indicative of cognitive decline and to provide earlier detection and prevention of cognitive impairment in AD.

1.3.1 – The characteristics of AD pathology

In the original discovery of AD pathology by Dr. Alzheimer in 1907, two primary AD pathologies were described. Both of these pathologies are still used in diagnosis today (Alzheimer et al., 1995; Hippius and Neundorfer, 2003). They are (1) the accumulation and deposition of amyloid-beta (Aβ) peptides in the form of extracellular plaques, and (2) the intraneuronal aggregation of hyperphosphorylated tau into neurofibrillary tangles (Kang et al., 2017).

Aβ is processed from amyloid precursor protein (AβPP), a type I transmembrane protein (Matsui et al., 2007). AβPP is transcribed from the *APP* gene on chromosome 21 and is composed of 18 exons; Aβ is processed from exon 16 and 17 (Rademakers et al., 2003; Tanzi et al., 1987). There are three principal isoforms of AβPP in the human CNS. AβPP 770 and 751 are found in glia, whereas the much more predominant AβPP 695 is localized to neurons (Matsui et al., 2007). AβPP 770 is the longest form of the protein; AβPP 751 and 695 are formed through alternative splicing of exons 7 and 8 (Panegyres, 1997). Post-translational AβPP processing is dependent on a family of secretases and is divided into non-amyloidogenic and amyloidogenic pathways (Haass et al., 2012; Wilkins and Swerdlow, 2016; Zhang et al., 2011) (Fig. 1.4A). The non-amyloidogenic pathway involves sequential cleavage by α-, and γ-secretase. The α-secretase cleavage site is

Figure 1.4 – Production of neuropathological Aβ peptides from AβPP. (A) Processing of AβPP through the non-amyloidogenic (left) pathway via the actions of α- and γ-secretases and the amyloidogenic (right) pathway via β- and γ-secretase activity generating Aβ peptides. Adapted from (Pajak et al., 2016). (B) The specific amino acid sequence of the Aβ peptide identifying specific cleavage sites of α- and β-secretase along with the multiple cleavage sites recognized by the γ-secretase complex that generate Aβ peptides of different sizes. Mutations in AβPP (Swedish and Indiana) that promote the amyloidogenic pathway are identified. Adapted from (Benilova et al., 2012). (C) After β-secretase cleavage, the presenilin subunit of γ-secretase cleaves Aβ from AICD. The most common AD-promoting mutation is found in this subunit with the deletion of exon 9 (dE9) that promotes cleavage at the neuropathological $A\beta_{42}$ site. Adapted from (Erez et al., 2009).

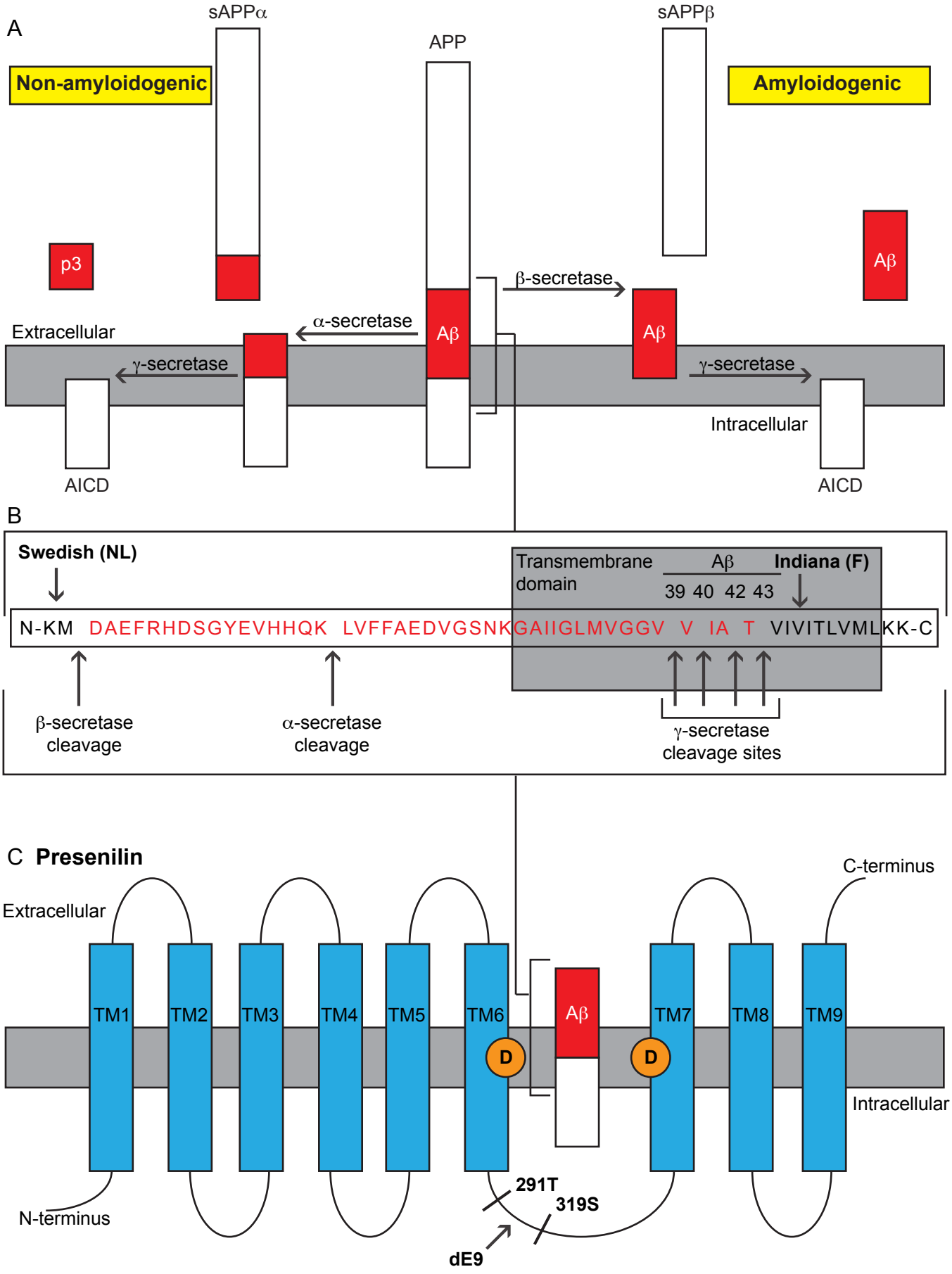
A
sAPPα
APP
sAPPβ
Non-amyloidogenic
Amyloidogenic
p3
Aβ
β-secretase
α-secretase
Aβ
Aβ
Extracellular
γ-secretase
γ-secretase
Intracellular
AICD
AICD
B
Swedish (NL)
Transmembrane domain
Aβ
Indiana (F)
39 40 42 43
N-KM DAEFRHDSGYEVHHQK LVFFAEDVGSNKGAIIGLMVGGV V IA T VIVITLVMLKK-C
β-secretase cleavage
α-secretase cleavage
γ-secretase cleavage sites
C Presenilin
C-terminus
Extracellular
TM1
TM2
TM3
TM4
TM5
TM6
Aβ
TM7
TM8
TM9
D
D
Intracellular
N-terminus
291T
319S
dE9

Figure 1.4

found in the middle of the Aβ peptide. Cleavage by α- and γ-secretase results in soluble APPα (sAPPα), a short peptide (p3), and the AβPP intracellular domain (AICD). In the pathological amyloidogenic pathway, AβPP is cleaved by β-, then γ-secretase; this produces sAPPβ, AICD and Aβ (Fig. 1.4A). The γ secretase complex is composed of four subunits: (a) the catalytic subunit--a presenilin (PS) heterodimer composed of PS1 and PS2 proteins, (b) nicastrin, (c) anterior pharynx defective 1, and (d) PS enhancer 2 (PEN-2). The PS subunit is an aspartic protease with diverse substrate binding that promotes non-specific cleavage by γ–secretase along transmembrane proteins such as AβPP (Nalivaeva and Turner, 2013; Zhang et al., 2014). Due to this diverse binding, the size of Aβ fragments can range anywhere from 39-43 amino acids (Qiu et al., 2015) (Fig. 1.4B). The most common lengths are $A\beta_{40}$ and $A\beta_{42}$ (Qiu et al., 2015). $A\beta_{42}$ is the more toxic isoform and is the main component of dense core amyloid plaques found in AD patients. $A\beta_{40}$ is also a contributor to AD pathology in that its aggregates are found in cerebral amyloid angiopathy, a prominent characteristic of AD (Qiu et al., 2015).

Tau is a microtubule-associated protein found primarily in the axons of neurons and is responsible for microtubule stability and neurite growth. There are six main isoforms of tau in the human brain with over 40 phosphorylation sites collectively (Duan et al., 2012; Gong and Iqbal, 2008). Hyperphosphorylation of tau occurs when the ratio of phosphorylated/dephosphorylated sites exceeds homeostasis (i.e. 1/1), thus leading to the aberrant detachment of tau from microtubules, particularly when Ser262, Thr231 and Ser235 are phosphorylated (Duan et al., 2012; Sengupta et al., 1998). Furthermore, the phosphorylation of Thr231 along with Ser396 and Ser422 has been shown to promote the aggregation of tau into paired helical filaments and subsequently the neurofibrillary

tangles that define AD pathology (Gong and Iqbal, 2008). Both amyloid plaque aggregation and neurofibrillary tangles must exceed clinical standards for an individual to be diagnosed with AD.

1.3.2 – Early- and late-onset AD

The diagnosis of AD is subdivided into two specific groups based on the age of onset (± 65 years): early-onset (EOAD) and late-onset (LOAD) (Bateman et al., 2012; Koedam et al., 2010). In both cases, AD pathophysiology must be present post-mortem to confirm an antemortem AD diagnosis and include clinical diagnosis of cognitive decline and dementia (McKhann et al., 2011). EOAD is a familial form of the disease manifested by inherited autosomal dominant mutations in genes involved in Aβ processing (Puzzo et al., 2015; Selkoe and Hardy, 2016). In EOAD, familial mutations in the *APP* gene promoting the amyloidogenic pathway all occur at exons 16 and 17, the site of amyloidogenic cleavage (Tanzi et al., 1987). Other autosomal dominant mutations are found in genes *PSEN1* and *PSEN2* that encode for the PS1 and PS2 proteins of the PS heterodimer, the catalytic subunit of γ-secretase (Haass et al., 2012; Wilkins and Swerdlow, 2016; Zhang et al., 2011). Many of these genetic mutations are used to produce transgenic mouse models of AD (reviewed in (Webster et al., 2014)). Specific to this thesis, Swedish (KM670/671NL) and Indiana (V717F) point mutations in the *APP* gene along with the deletion of exon 9 (291T-319S) in the *PSEN1* gene are used in many murine models of AD (Fig. 1.4B,C). Mutations promoting the amyloidgenic pathway accelerate dementia onset in AD whereby patients will experience symptoms before the 65 years of age. However, not all mutations promote the amyloidogenic pathway; some

mutations can be protective. Individuals with a mutation at the β-secretase cleavage site (A673T) in the AβPP gene renders the protein resistant to hydrolysis by β-secretase, thus decreasing Aβ formation and conferring resistance to AD (Jonsson et al., 2012).

The discovery of causative amyloidogenic mutations involved in EOAD led to the development of the amyloid cascade hypothesis (Bateman et al., 2012; Herrup, 2010). Here, increased levels of Aβ in the brain resulting from aberrant AβPP processing is proposed to lead to a cascade of events that lead to synaptic dysfunction and neuronal loss, culminating in cognitive impairment (Hardy and Selkoe, 2002; Herrup, 2010).

The amyloid cascade hypothesis was originally applied to describe cognitive decline in LOAD as well. In LOAD specifically, it is suggested that increased amyloid deposition in the brain is the result of an impaired balance between Aβ production and clearance in the brain that is increasingly impaired with age. (Hardy and Selkoe, 2002; Herrup, 2010). While compelling in that this hypothesis links the defining AD neuropathology to AD symptoms, a disconnect exists between levels of Aβ deposition and the manifestation (and severity) of cognitive decline in LOAD (Katzman et al., 1988; Morris et al., 1996; Snowdon and Nun, 2003). Moreover, Aβ pathologies detected post-mortem at levels that meet the Consortium to Establish A Registry for Alzheimer's Disease (CERAD) criteria for AD in persons of advanced age at time of death have been found in individuals that were devoid of any antemortem dementia symptoms (Delaere et al., 1993; Katzman et al., 1988; Morris et al., 1996; Snowdon and Nun, 2003). Thus, while Aβ plaque deposition is a unique neuropathological feature of AD and likely increases the risk of developing cognitive impairment (Dubois et al., 2016; Nelson et al., 2009), biogenesis does not necessarily equate to the onset or progression of clinical

symptoms. This has led to a “reimagining” of the amyloid cascade hypothesis whereby in the presence of amyloid pathology, additional triggers or insults are required that initiate a “change-of-state” in the physiology of the brain, thus promoting degeneration at the expense of resiliency (Herrup, 2010). This altered physiology is hypothesized to be necessary to initiate the onset and progression of cognitive decline in the face of pre-existing Aβ accumulation in LOAD (Herrup, 2010).

1.3.3 – Preclinical to clinical AD: from an asymptomatic diagnosis to progressive cognitive decline

As a result of this “reimagining” of the amyloid cascade hypothesis, cognitive decline in AD is subdivided into two phases: (1) a “preclinical” stage defined by the presence of specific biomarkers indicative of AD neuropathology but a lack of any behavioural symptoms; and (2) a “clinical” stage defined as the presence of behavioural symptoms in persons with the AD pathological hallmarks (Dubois et al., 2016). A preclinical AD diagnosis is dependent on longitudinal *in vivo* assessments of AD pathology. *In vivo* biomarkers of amyloid pathology measure amyloidosis in two ways: lower levels of $A\beta_{42}$ in the cerebrospinal fluid (CSF), and advanced amyloid positron emission tomography (PET) imaging (Dubois et al., 2016; Jack et al., 2013; Jack et al., 2010). These techniques measure two different aspects of amyloid processing. Decreased Aβ42 levels in the CSF reflect a depression in Aβ42 clearance from brain and is associated with a pathological accumulation of Aβ42 in brain parenchyma. Amyloid PET directly visualizes and localizes amyloid plaque deposition in the brain. Both of these biomarkers are valid for preclinical AD diagnosis, but must also be paired with a biomarker

of tau pathology (Dubois et al., 2016).

Tau pathology can similarly be monitored *in vivo* through both CSF quantification and neuroimaging. In the CSF, increased levels of phosphorylated and total tau are indicative of neurofibrillary tangles and cortical neuronal loss, respectively. However, tau pathology in the CSF is not specific to AD and thus cannot be used to diagnose preclinical AD (Dubois et al., 2016; Jack et al., 2013; Jack et al., 2010; van Harten et al., 2011). However, spatial progression of tau pathology in the brain *is* specific to AD and *in vivo* imaging is used to elicit the differences between preclinical AD and normal aging. In normal aging, there is evidence of tau pathology in the medial temporal lobe (Scholl et al., 2016). However, in AD, the propagation of neurofibrillary tangles extends laterally and then dorsally. This progression has been classified into six stages described by Braak and Braak (Braak et al., 2006; Braak and Braak, 1991, 1995). Although Braak staging is performed post-mortem, PET imaging of tau pathology *in vivo* emulates this staging of tau progression in living AD patients (Scholl et al., 2016), which allows clinicians to use the in vivo progression of tau pathology as a preclinical AD-specific biomarker. It is important to note that a diagnosis of preclinical AD is predicated exclusively on the combined positivity of amyloid and tau pathologies in the absence of cognitive decline. There are currently no biomarkers that can be used to predict when (or if) a person with pre-existing AD pathology will undergo cognitive decline.

An antemortem diagnosis of clinical AD requires evidence of cognitive decline, which includes both prodromal and dementia stages of AD (Dubois et al., 2016; McKhann et al., 1984; McKhann et al., 2011). The progression of clinical decline in AD can begin with an initial diagnosis of mild cognitive impairment (MCI). MCI has been considered a

prodromal form of various clinical dementias including AD (Petersen, 2004; Petersen et al., 2013). There are two types of MCI: amnestic MCI (aMCI) and non-amnestic MCI (naMCI). Advancement to dementia in clinical AD is more associated with aMCI (Petersen et al., 2013). The diagnostic criteria for aMCI requires evidence of objective memory impairment, although the individual maintains general cognitive function (Petersen, 2004). AD pathology is not a requirement in an aMCI diagnosis. In fact, only 57% of individuals diagnosed with aMCI present with amyloid pathology, suggesting that not all aMCI patients are at risk of AD dementia (Petersen et al., 2013). In fact, MCI is reversible, meaning that some patients are able to revert back to a healthy cognitive state. Other resistant patients will remain static in aMCI and not progress to AD dementia, remaining in a cognitively functional, albeit impaired, state (Petersen et al., 2013). However, aMCI still infers risk of progressive cognitive decline. Rate of conversion from aMCI to AD dementia can rise to over 50% within five years following an aMCI diagnosis (Petersen et al., 2010a; Rountree et al., 2007; Ward et al., 2013). Taken together, these data suggest that evidence of AD pathology and/or evidence of cognitive decline are, in and of themselves, not sufficient to predict conversion to AD dementia.

What is AD dementia? Dementia is a more advanced form of cognitive impairment than MCI (McKhann et al., 2011; Petersen, 2004; Petersen et al., 2013). It is classified as an impairment that causes significant interference in the ability of an individual to function on a daily basis (McKhann et al., 1984; McKhann et al., 2011). Clinical diagnosis of AD dementia was first defined by a joint effort of the National Institute of Neurological and Communicative Disorders and Stroke (NINCDS) and the Alzheimer's Disease and Related Disorders Association (ADRDA) in 1984 (McKhann et al., 1984), and has been

updated since its inception (McKhann et al., 2011). Currently, AD dementia diagnoses are subdivided into three classifications: 1) probable AD dementia, 2) possible AD dementia, and 3) probable/possible AD dementia with evidence of AD pathology (McKhann et al., 2011).

Both probable and possible AD dementia diagnoses require an initial diagnosis of general (i.e. “all cause”) dementia (McKhann et al., 2011). This is an umbrella term that includes declining cognitive impairment not attributed to any other neuropsychiatric disorder that is acknowledged by both the subjective observations of the patient or caregiver and the objective results of a professional cognitive assessment (McKhann et al., 2011). Two of five clinical symptoms must be present on neuropsychological testing: (i) impaired acquisition and retention of information, (ii) impaired reasoning and poor judgement, (iii) impaired visuospatial abilities, (iv) impaired language functions, and (v) changes in behaviour and personality (McKhann et al., 2011).

For a diagnosis of probable AD dementia, symptomatic onset must be gradual and occur over months to years. Initial presentation can include both amnestic and non-amnestic qualities, but the most distinguishing criteria is that patients must be lacking features of other neurologically-determined dementias, including concomitant cerebrovascular disease, Dementia with Lewy Bodies, frontotemporal dementia, primary progressive aphasia, or any other neurological co-morbidities that may impact on cognition (McKhann et al., 1984; McKhann et al., 2011).

Conversely, a possible AD dementia diagnosis requires the consideration of comorbid and aberrant processes that may accompany AD dementia. For instance, individuals with a less gradual onset of cognitive symptoms or with comorbidities

implicating other dementias or neurological diseases are diagnosed with possible AD dementia (McKhann et al., 2011). Note that neither probable nor possible AD dementia take AD pathological biomarkers into consideration.

A separate diagnosis, however, of either probable or possible AD dementia with evidence of AD pathology can be given to individuals with AD-specific biomarkers that represent three pathological features of AD: amyloid deposition, neurofibrillary tangles, and brain atrophy (Jack et al., 2011; McKhann et al., 2011). These biomarkers increase the confidence that an *in vivo* diagnosis of AD dementia (whether probable or possible) is, in fact, AD because of the presence of AD-specific pathological processes (Jack et al., 2011; McKhann et al., 2011).

1.3.4 – Alternative biomarkers are required to predict the onset of cognitive decline in preclinical AD patients

Current biomarkers of AD pathology are not yet predictive of cognitive impairment. In addition to measures of amyloid and tau pathology (Jack et al., 2013; Jack et al., 2010), imaging methods including hypometabolism in fluorodeoxyglucose-PET (FDG-PET) scans and decreased brain volume in structural magnetic resonance imaging (MRI) are also potential AD biomarkers, specifically used to measure brain atrophy (Jack et al., 2013; Jack et al., 2010). While biomarkers indicative of amyloid deposition, tau phosphorylation, and brain atrophy are certainly of use in monitoring the pathophysiology of AD, they are not accurately representative or predictive of the onset or severity of AD cognitive impairment (Davis et al., 1999; Jack et al., 2011; Jack et al., 2013; Jack et al., 2010; Knopman et al., 2003; Price and Morris, 1999). All of these biomarkers are found

to *precede* the definitive cognitive decline of clinical AD but are not directly associated with the prognosis or severity of clinical AD onset and progression. (Jack et al., 2013; Jack et al., 2010; Snowdon and Nun, 2003). In healthy aging, approximately 30% of cognitively intact individuals present with these pathological hallmarks and should be diagnosed with preclinical AD (Jack et al., 2011; Knopman et al., 2003; Price and Morris, 1999). The preclinical AD stage can last up to decades with no evidence of cognitive impairment. It is inherently believed that individuals diagnosed with preclinical AD will eventually experience the onset of cognitive symptoms, although some are more resistant than others. Many patients expire before ever showing any signs of cognitive impairment (Fiandaca et al., 2014; Pietrzak et al., 2015; Snowdon and Nun, 2003; Sperling et al., 2011).

The variable latency between preclinical and clinical AD indicates that current diagnostic biomarkers of AD pathophysiology are not efficient prognostic biomarkers of cognitive decline (Fiandaca et al., 2014; Sperling et al., 2011). In fact, there is so much temporal discrepancy between AD cognitive decline and the progression of AD pathology, they have been deemed separate entities by the National Institute of Aging (NIA) and the Alzheimer's Association (Jack et al., 2011). There is a critical window between preclinical and clinical AD for therapeutic strategies but biomarkers are needed to predict the onset of cognitive symptoms so treatment can be provided to at-risk populations.

1.3.5 – Current therapeutic options in AD are ineffective a halting the progression of cognitive decline

Presently there are only four main therapeutic drugs offered to AD patients. None of these treatment options are curative or disease-altering, but each temporarily reduces symptomatic burden. All four drugs target neurotransmitter disturbances that accompany AD pathology. Three of these medications, donepezil, rivastigmine, and galantamine, were developed based on AD-specific changes in the cholinergic system, particularly in the basal forebrain, associated with cognitive decline (Bartus et al., 1982). In AD brains, there is evidence of reduced activity in choline acetyltransferase, an enzyme involved in acetylcholine synthesis, as well as a loss of cholinergic neurons (Bartus et al., 1982). These three drugs inhibit acetylcholinesterase, the enzyme responsible for the degradation of acetylcholine at the synaptic cleft; inhibition of acetylcholinesterase increases the half-life and reuptake of acetylcholine at the synapse (Bartus et al., 1982). Typically these drugs are the most effective when given early in cognitive decline (Farlow et al., 2000; Yiannopoulou and Papageorgiou, 2013). Unfortunately, they improve cognitive status for only a limited time, do not alter the pathological progression of AD, and are only effective for 30-40% of AD patients (Douchamps and Mathis, 2017).

The fourth drug available to treat AD symptoms, memantine, is an N-methyl-D-aspartic acid (NMDA) antagonist. It targets NMDA receptors that contribute to excitotoxicity during AD by reducing sustained activation of the receptor. When there is sustained activation of the NMDA receptor, there is continual influx if Ca^{2+} into the neuron, thus leading to neurotoxicity. Memantine inhibits the sustained activation of NMDA receptors, thus having no impact on glutamate transmission but reducing sustained Ca^{2+}

influx (Lipton, 2005; Rogawski and Wenk, 2003). Neither memantine nor the acetylcholinesterase inhibitors affect any change on encroaching AD pathology, and they only mask cognitive decline in AD (if they are effective at all). Therefore it is necessary to employ new avenues of investigation in the search for curative, disease-altering drugs in AD that will target the “change-of-state” hypothesized to be upstream of phenoconversion in AD (Herrup, 2010).

1.3.6 – AD risk is age-dependent and sexually dimorphic

Between 2011 and 2012, reports estimated that the global prevalence of AD was approximately 24 million (Mayeux and Stern, 2012; Reitz et al., 2011). By 2017, AD prevalence had increased to a staggering 40 million individuals worldwide (Selkoe and Hardy, 2016) and is expected to further double every 20 years (Reitz et al., 2011). North America has the highest prevalence and progressively increasing incidence rates worldwide with an overall prevalence of 6.5% and incidence rate of 1% (Reitz and Mayeux, 2014). These statistics increase if one exclusively considers only persons over the age of 65 (Ferri et al., 2005; Reitz et al., 2011; Reitz and Mayeux, 2014). Between the ages of 65 and 85, the incidence rate of AD increases by over 12-fold and prevalence rates increase by 15-fold (Evans et al., 1989; Mayeux and Stern, 2012; Reitz et al., 2011). Taken together, these results indicate that age is the greatest risk factor for AD.

Women are more susceptible to the onset of AD dementia than men (Brundtland, 2002; Rizzi et al., 2014). Two-thirds of AD patients are women (Lin and Doraiswamy, 2014; Mielke et al., 2014). In persons 65 and over, the risk of being diagnosed with AD dementia in men is 6.3%, while in women it is 12% (Seshadri et al., 1997). It is

hypothesized that since onset of AD is age-dependent, that these differences may be due to lifespan in that women live longer than men (Luy and Minagawa, 2014). Yet even with an AD diagnosis, women still survive 1.5 years longer than men (Larson et al., 2004) demonstrating that sex differences in longevity are present in AD patients regardless of onset. Interestingly, while more females have AD dementia, there is a higher prevalence of MCI in North American males (Petersen, 2011; Petersen et al., 2010b). This suggests that men are more resistant to the advancement of cognitive decline in AD which is supported by the observation that women are more cognitively susceptible to AD pathology than men (Barnes et al., 2005). Women are therefore more likely to experience cognitive decline, lose their independence more rapidly, and become unable to care for themselves faster than men in the presence of AD pathology (Sinforiani et al., 2010).

Slower cognitive decline in men has been attributed to a higher "reserve" (Okonkwo and Vemuri, 2017; Stern, 2012). Reserve in AD is subdivided into two main models: brain reserve and cognitive reserve (Stern, 2012). For the purposes of this thesis, brain reserve is defined as differences in brain structure and/or synaptic density that enable individuals to compensate for the progressive "change-of-state" that renders persons susceptible to Aβ toxicity (Jicha and Rentz, 2013; Stern, 2002, 2006, 2012). Brain reserve is the passive model of reserve based on the assumption that more pathological insults are needed to provoke cognitive decline in persons with greater brain volume or synaptic number (Sole-Padulles et al., 2009; Stern, 2002). It can be measured *in vivo* via imaging methods designed to quantitatively assess brain structure and volume.

Cognitive reserve is the active model of reserve, defined as the ability to cognitively adapt to progressive neuropathology by using alternative networks and strategies to

accomplish a task (Jicha and Rentz, 2013; Sole-Padulles et al., 2009; Stern, 2002, 2006, 2012). Often associate with enriched life experiences, it is argued that higher education levels and higher occupational attainment predispose cognitive networks to be more flexible when challenged with neuropathology, therefore enhancing cognitive reserve (Mielke et al., 2014; Stern, 2006, 2012). Indeed, cognitive reserve could contribute to the disconnect between AD pathology and cognitive decline. Individuals with higher cognitive reserve will have a longer preclinical AD stage because they are able to adopt alternative cognitive strategies to cope with advancing pathology (Fig. 1.5, adapted from (Stern, 2012)) (Stern, 2006, 2012). Metabolic correlates of cognitive reserve have only begun to be identified (Bauckneht et al., 2018) and are a focus of this thesis.

Interestingly, it has been postulated that brain and cognitive reserve are contributing factors to the sex differences in AD cognitive decline. Men are theorized to have greater brain and cognitive reserve than women (Laws et al., 2016; Mielke et al., 2014). In fact, it is one of the most accepted theories explaining why the prevalence for MCI is higher in men than women. Men are more resistant to further cognitive impairments associated with progressive dementia while women will more rapidly progress to AD dementia, possibly due to greater reserve in men (Mielke et al., 2014; Petersen et al., 2010b). Imaging studies have shown that in men and women at the same stage of AD, men require more brain atrophy than women to achieve the same level of clinical severity (Perneczky et al., 2007). Likewise, when brain atrophy is equivalent, women experience greater cognitive impairment than men (Bai et al., 2009). This supports the idea that men have a higher brain reserve and must experience greater deterioration to achieve comparable cognitive decline to women. Additionally, an increase in AD pathology in the

Figure 1.5 – Symptomatic onset in AD is prolonged by high reserve. Individuals with higher reserve (blue line) exhibit greater AD pathology than individuals with lower reserve (red line) before transitioning to clinical AD. Adapted from (Stern, 2012).

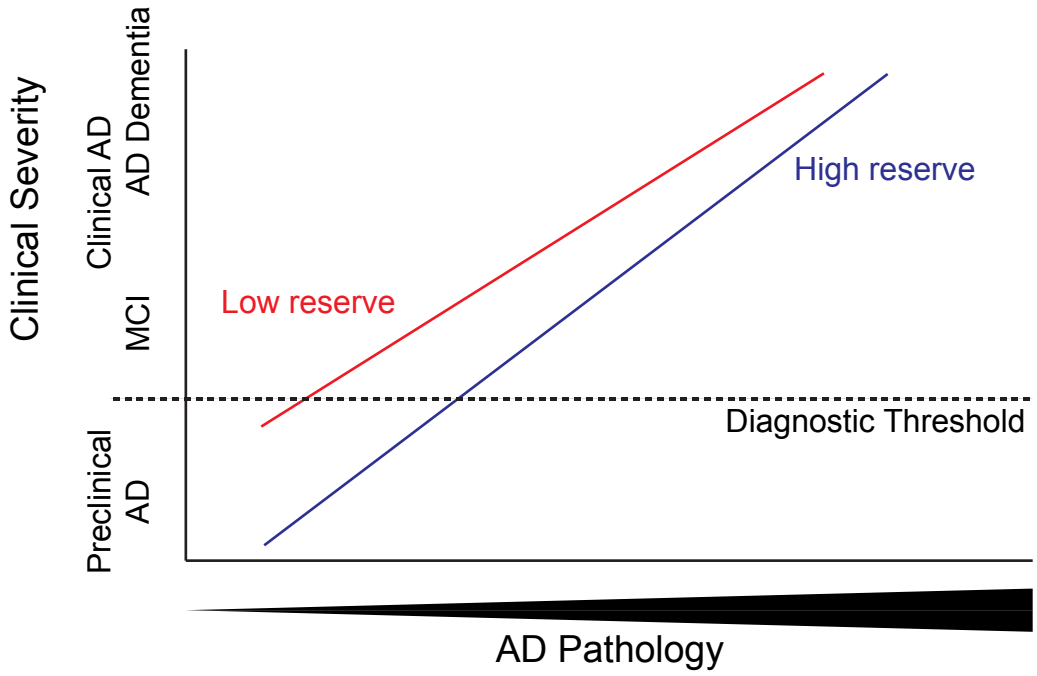
Clinical Severity
Clinical AD
AD Dementia
MCI
Preclinical
AD
Low reserve
High reserve
Diagnostic Threshold
AD Pathology

Figure 1.5

female brain increases the odds of clinical AD by 20-fold, whereas in men there is only a 3-fold risk increase (Barnes et al., 2005). This demonstrates that men are more cognitively resistant and thus more able to withstand AD pathology compared to women.

Currently there is no sexually dimorphic AD model that recapitulates cognitive reserve in males when both sexes are challenged with comparable AD pathology. Is it possible that males have a metabolic shift corresponding with enhanced resistance to AD cognitive decline? Perhaps males and females have different physiological responses to amyloid pathology which associate with a susceptibility or resistance to cognitive impairment. Therapeutic interventions to effect these "change in states" would be valuable in preventing the transition from preclinical to clinical AD.

1.3.7 – Genetic alterations in lipid metabolism affect risk of AD

Interestingly, lipid transport and lipid metabolism are affected in AD, suggesting that these metabolic defects may be part of the "change in state" that precipitates cognitive decline in preclinical AD patients. The most associated genetic risk factor for LOAD is the apolipoprotein E (*APOE)* gene, specifically the APOE4 variant (Andrews et al., 2017; Apostolova, 2017; Giri et al., 2016). The *APOE* gene is found on chromosome 19 and has three possible alleles of different frequencies: APOE2 (5-10%), APOE3 (65-70%), and APOE4 (15-20%). These alleles give rise to three homozygous and three heterozygous phenotypes that confer differing AD cognitive decline risk. Individuals carrying APOE2 are more resistant to AD cognitive decline, whereas carrying the APOE4 allele enhances risk (Liu et al., 2013). Homozygous APOE3 is the most common genotype and has no impact on AD risk. Approximately 40% of patients with AD are

carriers of the APOE4 allele (Farrer et al., 1997; Liu et al., 2013). Carriers of APOE4 show a reduced age of symptomatic onset in AD (Corder et al., 1993; Davidson et al., 2007). In APOE4 homozygotes, mean age of onset is 68 years of age, while in heterozygous (APOE3/4) individuals it is 76 years of age. In comparison, the mean age of onset for non-carriers is 84 years of age (Corder et al., 1993).

The *APOE* gene codes for the protein apoE. This protein is involved in the transport of lipids, particularly cholesterol, glycerophospholipids, and triglycerides, in the plasma and brain. Lipids associated with apoE can be internalized into cells through interactions with endocytic lipoprotein receptors such as low density lipoprotein receptors (LDLRs) and LDLR-related proteins (LRPs) (Hauser et al., 2011; Huang and Mahley, 2014; Lane-Donovan et al., 2014). In the brain, apoE is associated with high-density lipoprotein (HDL)-like lipoprotein particles containing cholesterol and glycerophospholipids.

Structurally, apoE is 299 amino acids long and is composed of two major functional regions: a lipid-binding domain and a receptor-binding domain. The lipid-binding domain links apoE to lipoproteins and lipid molecules, while the receptor-binding domain bind to LDLRs and LRPs to internalization of apoE into the cell. ApoE is mostly synthesized by astrocytes but also by microglia. This protein maintains lipid homeostasis by binding to lipid molecules and transporting cholesterol and glycerophospholipids between glia and neurons (Kim et al., 2014; Lane-Donovan et al., 2014). The lipid-binding affinities of apoE are determined by three isoforms: apoE2, apoE3, and apoE4. Lipidation of apoE is modulated through the actions of ATP-binding cassette A1 (ABCA1), found in astrocytes (Wahrle et al., 2004). Polymorphisms in ABCA1 are also linked to a higher risk of AD (Rodriguez-Rodriguez et al., 2007). Structural differences in apoE4 limit lipid-binding

affinities to larger lipid molecules while apoE2 and apoE3 are able to bind lipids of various sizes (Bu, 2009). The limited lipid-binding affinity of apoE4 can affect the internalization of specific lipid molecules which contributes to irregular glycerophospholipid homeostasis (Bu, 2009; Zhu et al., 2015). In fact, LDLR binding requires specific interactions between apoE and glycerophospholipids for proper function and maintenance of a homeostatic lipid environment (Huang and Mahley, 2014; Igbavboa et al., 2002; Lomnitski et al., 1999).

Altered lipid regulation and metabolism also affects susceptibility to cognitive impairment when exposed to risk factors of AD. *APOE*$^{-/-}$ mice are susceptible to cognitive decline when exposed to AD risk factors. Hypoxia is a known risk factor of AD (Nalivaevaa et al., 2004). While exposure to hypoxia will also induce cognitive decline in wildtype mice, *APOE*$^{-/-}$ mice experience a significantly greater impairment in learning and memory (Kheirandish et al., 2005). In humans, APOE4 carriers are particularly susceptible to hypoxic conditions such as sleep apnea (Gottlieb et al., 2004). When APOE4 carriers are exposed to such hypoxic insults, they are more vulnerable to cognitive impairment (Cosentino et al., 2008). This indicates that when lipid homeostasis is compromised, susceptibility to cognitive decline is enhanced. Conversely, genetic manipulation of lipid signalling can ameliorate the impairing effects of hypoxia. Knocking out PAFR in mice reduces cognitive impairments brought on by hypoxic conditions (Row et al., 2004), thus demonstrating that cognitive resistance to an AD risk factor can also be modulated through lipid homeostasis and signalling.

1.3.8 – Altered glycerophospholipid metabolism is associated with cognitive decline in AD

Direct analysis of glycerophospholipids in the brain and biofluids of AD patients have also found several significant changes linking AD with lipidomics. In the brain of fully symptomatic AD patients, increases in glycerophospholipid metabolites such as *lyso*-glycerophospholipids are linked with cognitive impairment in patients with LOAD (Klein, 2000; Wood, 2012). Increases in *lyso*-glycerophospholipids indicate increases in PLA_2 during AD cognitive decline. Indeed, increases in PLA_2 activity and expression are found in the brains of AD patients (Frisardi et al., 2011). This is indicative of a breakdown in the phospholipid bilayers of neurons and glia, a potential sign of neurodegeneration. These findings correspond with decreased levels of PCs, PEs, PC(P)s, and PE(P)s in AD brains (Ginsberg et al., 1995; Guan et al., 1999a; Igarashi et al., 2011; Nitsch et al., 1992). PE(P) levels have actually been found reduced by 40% in white matter at early stages of AD, yet remain constant during disease progression. In the grey matter, PE(P) levels also decrease but gradually with disease progression. This indicates regionally specific changes that may not only be indicative of clinical AD onset, but also of progression of cognitive impairment (Han et al., 2001).

At the molecular level, specific oleic acid (OA, 18:1)-containing, AA-containing, and docosahexanoic acid (DHA, 22:6)-containing PCs and PEs were reduced in the AD brain (Guan et al., 1999b; Igarashi et al., 2011). However, total brain lipids were not altered in AD brain, demonstrating the necessity of profiling lipids at the subclass and species level (Igarashi et al., 2011). In fact, our lab has identified changes in species-specific PC(O) metabolism in both post-mortem AD brain and the TgCRND8 mouse model of Aβ

accumulation using a targeted lipidomic approach (Ryan et al., 2009). We have found that the levels of a specific PAF, PC(O-16:0/2:0), is elevated in human and murine temporal cortex. Further, we found that these changes are mediated by Aβ accumulation and mechanistically signal an endoplasmic reticulum stress response leading to activation of cyclin-dependent kinase5 that phosphorylates tau on AD epitopes linking lipid signalling to AD pathology (Ryan et al., 2009). These are very interesting changes occurring in the brain, but quantifying brain levels of glycerophospholipids *in vivo* is not feasible. Researchers must look to biofluids such as CSF and blood to identify biomarkers of cognitive impairment onset and progression.

In the CSF, changes in GPCs appear to occur early in cognitive decline. GPCs are unaltered in AD dementia patients when compared with undemented controls with memory complaints (Mulder et al., 2003). However, there is an overall increase in CSF GPCs when comparing AD patients with cognitively intact controls (Walter et al., 2004). Therefore, any changes in CSF GPC levels must correspond with the onset of mild cognitive symtoms prior to an official diagnosis. Interestingly, a decrease in the LPC/GPC ratio was also found in the CSF of AD patients. Closer analysis indicated a decrease in LPC levels, particularly in species containing AA and LA (Mulder et al., 2003). This contrasts with findings in the brain, suggesting accumulation of LPCs in the brain may be the result of unbalanced/unregulated remodelling or clearance into the CSF.

In the plasma of AD patients, there is a significant decrease in many GPE and GPC species (Yamashita et al., 2016). There are progressive decreases PUFA-containing GPCs (PC(16:0/20:5), PC(16:0/22:6), and PC(18:0/22:6)), and GPEs (PE(P-16:0/22:6) and PE(P-18:0/22:6)) indicating a potential role for oxidative fragmentation at

the *sn-2* moiety as PUFAs are a notable target of ROS (Whiley et al., 2014; Wood et al., 2016) but also an increase in PLA_2 activity. The progressive nature of these decreases corresponds with declining levels of cognition in age-matched cognitively intact, MCI and AD patients (Whiley et al., 2014; Wood et al., 2016). These findings have been further supported with by reductions in other PUFA-linked GPC species in the serum of AD patients (Oresic et al., 2011). These data raise two main questions: i) is the decline in circulating glycerophospholipid levels indicative of an increase in abundances of smaller, bioactive signalling molecules and metabolites of glycerophospholipid metabolism? ii) Do these changes associate with impaired glycerpphospholipid metabolism in the CNS? What is missing in lipidomic research in the context of neurological disease is a direct link between the circulating and central lipidomes as they associate with cognition.

1.4 – Rationale, Hypotheses, and Specific Aims

In AD, the long latency between the presence of AD neuropathology (preclinical AD) and the onset of cognitive decline (clinical AD) suggests that other metabolic processes are likely required to trigger symptomatic onset. Converging genetic and biochemical evidence implicating lipid metabolism in AD risk suggests that one of these metabolic defects may be dysregulation of glycerophospholipid homeostasis. The overarching **objective** of this thesis is to address whether quantifiable changes in glycerophospholipid metabolism associates with risk of or resistance to phenoconversion in experimental models of preclinical AD. Specifically, I **hypothesize** that: (1) changes in GPC and/or GPE metabolism manifest when AβPP mouse models first exhibit behavioural indices of learning and memory impairment; (2) this aberrant metabolism is

accelerated by environmental risk factors associated with earlier symptomatic onset; (3) sexually dimorphic propensity to phenoconversion can be modelled in AβPP transgenics; (4) transgenic mice that exhibit behavioural indices of cognitive reserve can be distinguished from symptomatic mice by their central and circulating lipidomes. To test these hypotheses, I proposed three specific aims.

AIMS

I. Identify changes in glycerophosphocholine metabolism in AβPP transgenic mice that associate with phenoconversion and determine whether environmental insults (hypoxia) that accelerate symptomatic conversion also accelerate aberrant GPC metabolism

II. Identify and characterize an AβPP mouse model of AD capable of modelling sexually dimorphic cognitive reserve.

III. Identify the changes in circulating and brain-specific metabolism of GPCs and GPEs that discriminate between AβPP transgenic mice exhibiting behavioural indices of cognitive reserve and those susceptible to behavioural impairment.

Chapter 2: Distinct disruptions in Land's cycle remodeling of glycerophosphocholines in murine cortex mark symptomatic onset and progression in two AD mouse models

Matthew W. Granger[a], Hui Liu[b], Caitlin F. Fowler[a], Alexandre P. Blanchard[a], Matthew Taylor[a], Samantha P.M. Sherman[a], Hongbin Xu[a]*, Weidong Le[b]*, Steffany A.L. Bennett[a]*

[a]Neural Regeneration Laboratory, Ottawa Institute of Systems Biology, University of Ottawa Brain and Mind Research Institute, Centre for Catalysis Research and Innovation, Department of Biochemistry, Microbiology, and Immunology, University of Ottawa, Ottawa, ON, Canada, [b]Institute of Neurology, Ruijin Hospital, Shanghai Jiao Tong University School of Medicine, Shanghai, PR China.

Key words: Hypoxia, Alzheimer's disease, glycerophosphocholine, phospholipids, lipidomics, platelet activating factor, AβPP^{Swe}/PS1^{dE9} mice, TgCRND8 mice, phospholipase A2, platelet activating factor acetylhydrolase

Chapter 2: Distinct disruptions in Land's cycle remodeling of glycerophosphocholines in murine cortex mark symptomatic onset and progression in two AD mouse models

2.1 Objective of study

The objective of this chapter was to investigate how external risk factors of AD impact glycerophosphocholine metabolism in the brain of a mouse model of AD. Lipids were identified and quantified in two brain regions using HPLC-ESI-MS/MS and compared using a network analysis.

2.2 Author contributions

MWG and SALB conceived and designed the experiments. Under the supervision of WL, HL administered hypoxic treatments and dissected brain tissue. Glycerophosphocholines were extracted and HPLC-ESI-MS/MS analysis of the $A\beta PP^{Swe}/PSI^{dE9}$ mouse model were performed by MWG and SPMS. HPLC-ESI-MS/MS analysis of the N5 TgCRND8 mouse model were performed by APB and HX. All HPLC-ESI-MS/MS methods were developed by HX. Data was analyzed by CFF and MWG. PLA_2 activity assays were performed by MT and PAFAH Western blots were performed by APB. MWG and SALB wrote the paper.

This chapter was under second review at the Journal of Neurochemistry at the time of thesis submission: **Granger MW**, Liu H, Fowler CF, Blanchard AP, Taylor MW, Sherman SPM, Xu H, Le W, Bennett SAL (2018). Distinct disruptions in Land's cycle remodeling of glycerophosphocholines in murine cortex mark symptomatic onset and

progression in two AD mouse models. Journal of Neurochemistry, submitted.

2.3 Abstract

Changes in glycerophosphocholine metabolism are observed in AD; however, it is not known whether critical metabolic disruptions are linked to AD cognitive decline. Here, using an unbiased lipidomic approach, we profiled the Land's cycle glycerophosphocholine metabolome in the hippocampus, frontal cortex, and temporal-parietal-entorhinal cortex of pre-symptomatic, symptomatic, and fully impaired human AβPP (hAβPP) overexpressing mice. We identified opposing changes in glycerophosphocholine metabolism initiated at symptomatic onset followed by metabolic changes that associated with progressive behavioural decline. When $A\beta PP^{Swe}/PSI^{dE9}$ and N5 TgCRND8 mice first show learning and memory impairment in the MWM, calcium-sensitive $cPLA_2$ activity declines in cortices but not hippocampus. LPC and LPC(O) levels decrease. Critical metabolic indicators of phenoconversion are decreases in LPC(18:0/0:0), LPC(16:0/0:0), LPC(24:6/0:0), LPC(25:6/0:0), LPC(O-18:0/0:0), and PC(O-22:6/2:0). These same depletions are triggered in younger animals when $A\beta PP^{Swe}/PSI^{dE9}$ mice are challenged by chronic intermittent hypoxia, an environmental risk factor that accelerates onset of learning and memory deficits. Conversely, in fully impaired animals, $cPLA_2$ activity rises; LPC and LPC(O) levels increase; PC(O-18:1/2:0) PAF accumulate in cortex but not hippocampus. An age-dependent shift in the expression of the PAFAH1b α_1 and α_2 catalytic subunits reduces the rate of PAF hydrolysis further favouring PAF accumulation in the presence of these rising LPC(O) substrate levels. Together, these data identify two defining disruptions in Land's cycle glycerophosphocholine metabolism that discriminate pre-symptomatic, from symptomatic, from fully impaired human AβPP overexpressing mice.

2.4 Introduction

Aberrant processing of the AβPP to toxic Aβ fragments and intraneuronal accumulation of neurofibrillary tangles composed of hyperphosphorylated tau are primary AD pathologies (Bierer et al., 1995; Haass and Selkoe, 2007). Their presence can be detected *in vivo* using amyloid positron emission tomography imaging or tracked by monitoring cerebrospinal fluid levels of $A\beta_{42}$, total tau, and phospho-tau (Bateman et al., 2012; Buchhave et al., 2012; Fagan et al., 2014). Longitudinal changes in these biomarkers indicate that AD neuropathology manifests decades before either autosomal-dominant or sporadic AD patients exhibit any signs of dementia (Bateman et al., 2012; Buchhave et al., 2012; Dubois et al., 2016; Fagan et al., 2014). This long latency, dubbed preclinical AD, suggests that additional metabolic dysfunctions are likely required to trigger symptomatic onset in patients with pre-existing AD pathology (Dubois et al., 2016; Herrup, 2010). Identifying and targeting these critical metabolic changes (and their environmental causes) represents a novel, potentially transformative, means of reducing AD risk.

Previous lipidomic studies have reported that circulating glycerophosphocholine levels decline at symptomatic AD onset (Mapstone et al., 2014; Proitsi et al., 2017; Toledo et al., 2017). Metabolic determinants are unclear. Glycerophosphocholine metabolism is, in part, regulated by the Land's cycle. Enzymatic remodelling by the PLA_2 superfamily and LPCATs coordinate the hydrolysis and re-acylation of both structural membrane glycerophosphocholines and bioactive second messengers. At least 35 distinct PLA_2 isoforms are capable of cleaving the *sn*-2 fatty acyl chain from the glycerophosphocholine backbone (Burke and Dennis, 2009). Cleavage generates free fatty acids and *lyso*-GPCs

defined by their *sn*-1 ester, ether (O), or vinyl ether (P) linked hydrocarbon chains (Supplemental Fig. 2.1). LPC, LPC(O) (lyso-PAFs), and LPC(P) metabolites can be subsequently remodeled by LPCATs. Using acyl-CoA, LPCAT1-4 transfers a long-chain hydrocarbon to the *sn*-2 position of LPC, LPC(O), and LPC(P) regenerating structural diacylglycerophosphocholines, 1-alkyl,2-acylglycerophosphocholines, and 1-alkenyl,2-acylglycerophosphocholines respectively (Shindou and Shimizu, 2009) (Supplemental Fig. 2.1). Using acetyl-CoA, LPCAT 1 and 2 transfers an acetyl group to LPC(O) producing pro-inflammatory PC(O)s (PAFs) (Shindou and Shimizu, 2009). LPCATs are also able to transfer short acyl- and acetyl-CoAs to LPCs and LPC(P)s to form PAF-like molecules with either an alkenyl (PC(P)) or acyl (PC) *sn*-1 linkage (Nakanishi et al., 2006) (Supplemental Fig. 2.1). PC(O)s can also be remodelled back to LPC(O) by three different PAFAH isoforms (Prescott et al., 2000). Thus, each glycerophosphocholine is both a product and precursor in the Land's cycle.

Enzymatic dysregulation alters the GPC landscape over the course of AD. However, both increases (Chalbot et al., 2009; Doody et al., 2015; Farooqui and Horrocks, 2006) and decreases (Gattaz et al., 2004; Ross et al., 1998; Smesny et al., 2008) in total PLA_2 activity are reported in CSF, platelets, and post-mortem brain of AD patients (reviewed in (Bennett et al., 2013). While LPC(O) levels are lower in patients diagnosed with "probable" AD compared to cognitively normal controls (Mulder et al., 2003); LPC levels are higher in superior temporal and inferior parietal cortices of AD patients with severe end-state cognitive impairment and psychosis (Sweet et al., 2002). Total LPCAT activity is also elevated in post-mortem human AD brain (Ross et al., 1998) with a shift in substrate preference of LPCAT2 from acyl- to acetyl-CoA upon exposure

to $A\beta_{42}$ (Ryan et al., 2009). These changes effectively increase the remodelling of LPC(O*)* to PC(O) *in vitro* with intraneuronal accumulation of PC(O) shown to activate cyclin-dependent kinase 5 resulting in the hyperphosphorylation of tau on AD-associated epitopes (Ryan et al., 2009). Taken together, these data implicate changes in GPC metabolism in AD etiology. It is not, however, clear whether distinct metabolic disruptions mark different stages of AD cognitive decline.

To address this question, we used an unbiased lipidomic approach and direct biochemical assessment of protein expression and enzymatic activity to profile GPC metabolism in the hippocampus, frontal cortex, and temporal-parietal-entorhinal cortex in two AD mouse models over the course of behavioural decline. We show that GIV $cPLA_2$ activity decreases reducing levels of LPC and LPC(O) in cortices when $A\beta PP^{Swe}/PSI^{dE9}$ and N5 TgCRND8 mice first exhibit learning and memory impairments. Moreover, we show that chronic intermittent hypoxia, an environmental risk factor that accelerates the appearance of learning and memory deficits in $A\beta PP^{Swe}/PSI^{dE9}$ mice (Liu et al., 2016), triggers these same changes in younger mice. We next asked whether deficits were maintained in fully impaired animals. Surprisingly, we find that metabolic differences are reversed over the course of symptomatic progression. Group IVa $cPLA_2$ activity is elevated, LPC and LPC(O) levels rise, and remodelling of LPC(O) to PC(O) increases in the cortex of impaired N5 TgCRND8 mice. Changes are accompanied by an age-dependent shift in the expression of PAFAH1b α_1 and α_2 catalytic subunits predicted to reduce further the hydrolysis of PC(O). Taken together, these data identify two defining disruptions in Land's cycle GPC metabolism in murine cortex linked to symptomatic onset and memory impairment in hAβPP mice.

2.5 Materials and Methods

2.5.1 Animals

AβPP^{Swe}/PSI^{dE9} mice (Jackson Laboratories 004462, RRID:SCR_000708) on a F2 C57BL/6J X C3H/HeJ background were bred to C57BL/6J (Jackson Laboratories 000664, RRID:SCR_000708) mice in the Le laboratory. A flow-chart of our experimental paradigm is presented in Fig. 2.1. A total of n=120 littermates (60 males and 60 females) were randomly assigned to control (normoxic) or hypoxic treatment at three months of age using a random number generator. Because one of our prerequisites before randomization was that our experimental groups contained equal numbers of animals, this randomization process is referred to as pseudo-randomization. Full treatment details and all of the behavioural results for the mice profiled in this study (n=22 of n=120) can be found in (Liu et al., 2016). Briefly, AβPP^{Swe}/PSI^{dE9} and wild-type (WT) littermates were placed in a hypobaric chamber and exposed to either hypoxic or normoxic conditions for six hours/day for 30 consecutive days at three months of age. Experimenters were blinded as to the genotype of the animals over the course of treatment. In the hypoxic group, oxygen levels were reduced to 11.1% to simulate a high-altitude hypoxia of approximately 5000 meters high. In the normoxic group, animals were handled and exposed to the same chambers for equivalent periods of time under normobaric conditions. Water and food (Xietong Medical Biological Engineering, 1010009) were available *ad libitum.* Following a one-month schedule of chronic intermittent hypoxia or sham (normoxic) treatment, mice were divided into three cohorts using the same pseudo-randomization methodology described above (n=10/genotype/normoxic or hypoxic

Figure 2.1 – Flow-chart of our experimental paradigm. (A) In this study, AβPP^{Swe}/PS1^{dE9} mice and WT littermate controls bred at the Institute of Neurology in the Shanghai Jiao Tong University of Medicine, were subjected to either hypoxic or normoxic (sham) treatment in a hypobaric chamber for six hours/day for 30 days between three and four months of age at the Institute of Neurology in the Shanghai Jiao Tong University of Medicine. Separate cohorts of mice subsequently underwent MWM testing for learning and memory at either 4 months or 6-9 months of age. Their performance in this test has been published in (Liu et al., 2016). Mice were sacrificed after MWM testing, frontal cortices and hippocampi were dissected and transferred to the Neural Regeneration Laboratory at the University of Ottawa for glycerophospholipid extraction and lipidomic analyses. (B) N5 TgCRND8 mice, bred in the Neural Regeneration Laboratory at the University of Ottawa were sacrificed at 2, 4, and 6-8 months of age whereupon temporal/parietal/entorhinal cortices were dissected and underwent the same glycerophospholipid and lipidomic analysis of glycerophosphocholine second messengers and metabolites as AβPP^{Swe}/PS1^{dE9} mice.

A

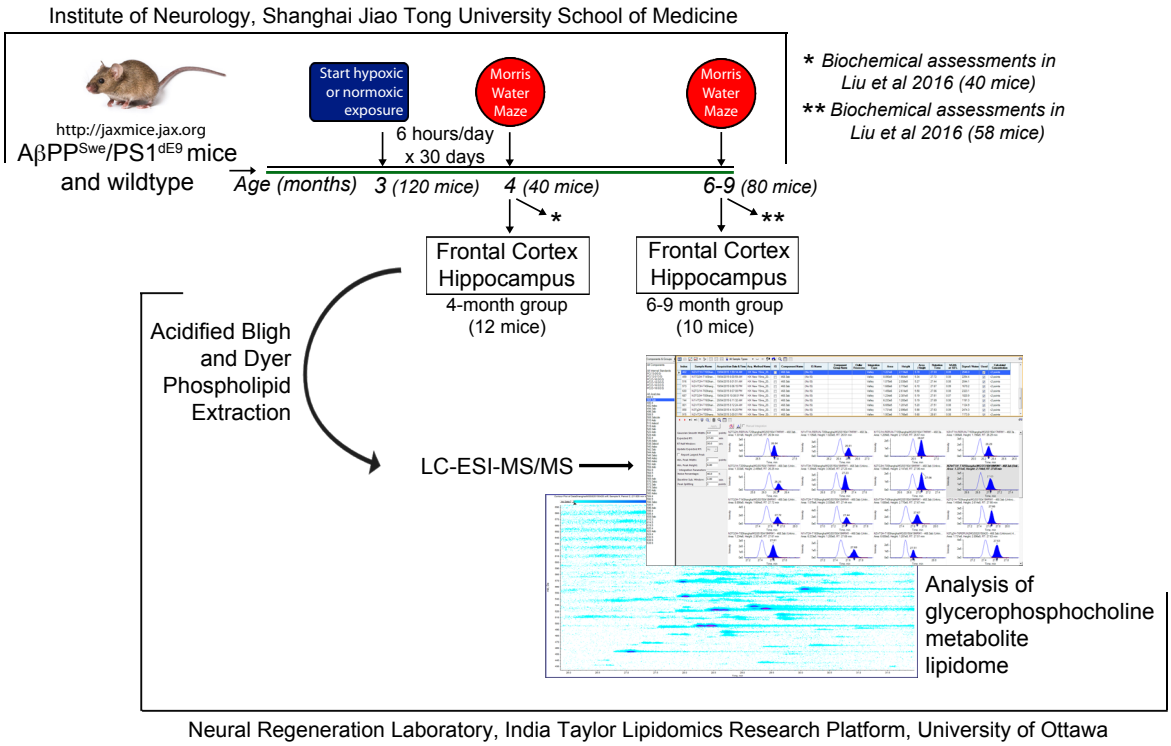
Institute of Neurology, Shanghai Jiao Tong University School of Medicine
http://jaxmice.jax.org
AβPP^Swe/PS1^dE9 mice
and wildtype
Start hypoxic or normoxic exposure
6 hours/day
x 30 days
Morris Water Maze
Morris Water Maze
* Biochemical assessments in Liu et al 2016 (40 mice)
** Biochemical assessments in Liu et al 2016 (58 mice)
Age (months) 3 (120 mice) 4 (40 mice) 6-9 (80 mice)
*
**
Frontal Cortex Hippocampus
4-month group
(12 mice)
Frontal Cortex Hippocampus
6-9 month group
(10 mice)
Acidified Bligh and Dyer Phospholipid Extraction
LC-ESI-MS/MS
Analysis of glycerophosphocholine metabolite lipidome
Neural Regeneration Laboratory, India Taylor Lipidomics Research Platform, University of Ottawa

B

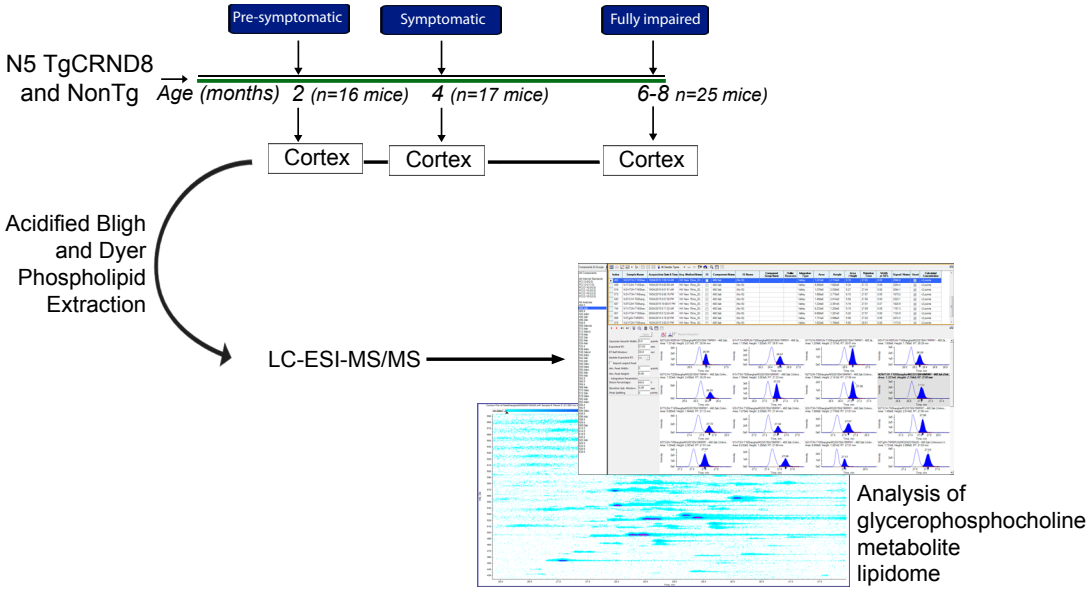
Pre-symptomatic
Symptomatic
Fully impaired
N5 TgCRND8
and NonTg
Age (months) 2 (n=16 mice) 4 (n=17 mice) 6-8 n=25 mice)
Cortex
Cortex
Cortex
Acidified Bligh and Dyer Phospholipid Extraction
LC-ESI-MS/MS
Analysis of glycerophosphocholine metabolite lipidome
Neural Regeneration Laboratory, India Taylor Lipidomics Research Platform, University of Ottawa

Figure 2.1

conditions). Mice were tested MWM at 4, 6, and 9 months of age by an experimenter blinded as to the genotype and treatment of each mouse. Animals were sacrificed within 3 days of testing. At time of sacrifice, mice were again pseudo-randomly assigned using a random number generator for the biochemical assessments (n=98) reported in (Liu et al., 2016) or the lipidomic assessments described here (n=22). A total of twelve 4-month old mice (n=3/genotype/normoxic or hypoxic condition) and ten 6 to 9-month old mice (n=5/genotype/normoxic manipulation only) were analyzed. All lipidomic analyses were performed by an experimenter blinded to the genotype and performance of each mouse on the MWM. Hippocampi and frontal cortices were dissected bilaterally, weighed, flash-frozen in liquid nitrogen at time of sacrifice, and maintained at -80°C until lipid extraction in the Bennett laboratory. Sample sizes indicate biological replicates (number of mice) of each brain region analyzed. All protocols were performed according to Laboratory Animal Care Guidelines and sanctioned by the Animal Committee of Shanghai Jiao Tong University School of Medicine. We had no pre-determined inclusion or exclusion criteria for the behavioural experiments; all animals tested were included.

A total of 58 female N5 transgenic (Tg)CRND8 and non-transgenic (Non-Tg) littermates were randomly assigned using a random number generator at time of weaning for assessment at 2 (n=9 Tg; n=7 NonTg), 4 (n=10 Tg; n=7 NonTg), 6 (n=9 Tg; n=7 NonTg), and 8 (n=6 Tg; n=3 NonTg) months of age. Water and food (Harlan Laboratories, 2018 Teklad Global 18% Protein Rodent Diet) were available *ad libitum.* N5 TgCRND8 (RRID:SCR_000708) mice are a sub-line of the C57BL/6J X C3H/HeJ TgCRND8 mouse model (Chishti et al., 2001) back-crossed in the Bennett laboratory for 5 generations (N5) to a C57BL/6NCrL lineage and maintained by sibling crosses (Granger et al., 2016). This

line does not carry the parental *Pde6b*^{rd1} retinal degeneration mutation that renders homozygotes blind (Chang et al., 2002) or the *Nnt*$^{C57BL/6J}$ allele responsible for diminished insulin secretion and impaired glucose tolerance (Toye et al., 2005). We have previously shown that female N5 Tg mice are pre-symptomatic at 2 months of age, start to show behavioural impairments in the MWM at 4 months of age, and are maximally impaired at 6 months of age (Granger et al., 2016; Wang et al., 2013). Learning and memory deficits are observed for at least 12 months of age (Granger et al., 2016; Wang et al., 2013). Temporal/parietal/entorhinal cortices were dissected bilaterally, weighed, flash-frozen in liquid nitrogen at time of sacrifice, and maintained at -80°C until extraction. Quantification of lipid abundances was performed by experimenters blinded as to the genotype and age of the mice. All procedures were approved by the Animal Care Committee of the University of Ottawa and performed in strict accordance with the ethical guidelines for experimentation of the Canadian Council for Animal Care. These studies were not pre-registered.

2.5.2 Phospholipid Extractions

Dissected brain tissues were extracted using modified Bligh and Dyer protocol (Bligh and Dyer, 1959) previously described (Xu et al., 2013). Briefly, tissues were homogenized using a tissue tearer (BioSpec 985370) in 4 mL acidified methanol (Fisher A412P-4, RRID:SCR_003374) containing 2% acetic acid (Fisher 351271-212, RRID:SCR_003374). MS grade lipid standards, PC(13:0/0:0) [90.7 ng Avanti LM-1600] and PC(12:0/13:0) [100 ng, Avanti LM-1000], were added to the homogenate at time of extraction. Chloroform (Fisher C298-500, RRID:SCR_003374) and 0.1 M sodium acetate

(Sigma S-2889, RRID:SCR_008988) were added to each sample at a final ratio of acidified methanol/chloroform/sodium acetate of 2:1.9:1.6. Samples were vortexed and centrifuged at 600 x *g* for 10 min at 4°C. The organic phase was retained and the aqueous phase successively back-extracted three times using chloroform three times. The four organic extracts were combined and evaporated at room temperature under a constant stream of nitrogen gas. Final extracts were solubilized in 300 µl of anhydrous ethanol (Commercial Alcohols P016EAAN) and stored under nitrogen gas at -80°C in amber vials (BioLynx C779100AW).

2.5.3 High-performance liquid chromatography electrospray ionization tandem mass spectrometry

HPLC was performed using an Agilent 1100 system with an autosampler maintained at 4°C. Samples were prepared for LC injection by mixing 5 µl of lipid extract with 2.5 µl of an internal standard mixture consisting of PC(O-16:0-d_4/0:0) [2.5 ng, Cayman 360906, RRID:SCR_008945], PC(O-18:0-d_4/0:0) [2.5 ng, Cayman 10010228, RRID:SCR_008945], PC(O-16:0-d_4/2:0) [1.25 ng, Cayman 360900, RRID:SCR_008945] and PC(O-18:0-d_4/2:0) [1.25 ng Cayman, 10010229, RRID:SCR_008945] in EtOH, and 16 µL of Solvent A (see below). Chromatography was performed on a 12 cm x 75 µm (I.D.) column packed with ReproSil-Pur 120 C4 (particle size of 5 µm and pore size of 120 Å, Dr. A. Maisch, Ammerbruch, Germany #r15.4e) with a binary solvent gradient of water with 0.1% formic acid and 10 mM ammonium acetate (Solvent A) and acetonitrile/ isopropanol (5:2 v/v) with 0.1% formic acid and 10 mM ammonium acetate (Solvent B). Solvents were pumped at a main flow of 20 µl/min and a split flow configuration was used

to achieve submicroliter/minute flow rate. The gradient started at 5% B, held for 15 min, was then increased to 100% B over 5 min, and was maintained for 25 min for column re-equilibration. The solvent composition was brought back to 5% B within 1 min and maintained for 15 min. Each sample injection was followed by a blank run to ensure no significant carryover. MS acquisition was carried out using a QTRAP 5500 system equipped with a NanoSpray III ion source (SCIEX) with the following optimized instrument parameters: curtain gas was set to 20 µL/min; ion spray voltage to 2500 V, and source gas to 10 µL/min. LC-MS protocols were optimized as follows to ensure sensitivity in the quantification of low abundant lipid metabolites and second messengers.

The complete GPC-containing metabolome (450-650 m/z) in the frontal cortex, temporal/parietal/entorhinal cortex, and hippocampus was profiled using PIS in positive ion mode monitoring the diagnostic product ion of the GPC headgroup at m/z 184.1. To differentiate *lyso*-sphingomyelins and sphingomyelins from GPCs with the same headgroup, we used differential mobility spectroscopy (DMS)-based experiments on a QTRAP 5500 mass spectrometer equipped with SelexION DMS technology (SCIEX) and a Turbo V ion source (SCIEX). Operating conditions were optimized using a lipid standard mixture containing 1 µM PC(12:0/13:0) (LM-1000, Avanti Polar Lipids, Inc,) and porcine brain SM (860062, Avanti Polar Lipids, Inc) with 1-propanol as the DMS chemical modifier. The lipid standards were T-infused with an integrated syringe pump set at 5 µl/min into the flow of 10 µl/min of 100% Solvent B (ACN/IPA at 5:2 v/v ratio containing 0.1% formic acid and 10 mM ammonium acetate) delivered by an Agilent Infinity II system (Agilent, RRID:SCR_013575). The optimized DMS conditions were as follows: separation voltage = 3900 V, DMS cell temperature = 150°C (Low), modifier

concentration= 1.5 % v/v in the transport gas (Low), DMS resolution enhancement = 18 psi (Low), and DMS offset = - 3.0 V. The compensation voltage (COV) values were then optimized for each lipid class by ramping the COV at increments of 0.1 V and the optimal COV values for GPCs and sphingomyelins were determined to be -4.5 V and 1.5 V, respectively. For the flow injection-DMS experiments, the species within each lipid class were monitored using (+) Prec184 for GPCs and sphingomyelins with the predetermined optimal COV values.

Quantitative analysis of validated GPC metabolites and second messengers detected in our profiles was achieved in SRM mode monitoring the transition from the protonated molecular ion of each of the lipid species detected to the headgroup specific product ion of m/z 184.1. Collision gas was set to 10 µL/min with an entrance potential of 10 eV, a declustering potential of 100 eV, and a collision cell exit potential of 9 eV. Collision energy was 47 eV. PIS and SRM spectra were analyzed using Analyst 1.6.2 and MultiQuant 3.0.8664.0 (SCIEX), respectively. Analysis output was converted to .csv format for further bioinformatic processing. Spectra were aligned using RT-STAR (v1.0), an in-house algorithm that standardizes retention times to align lipid species across lipidomes. Molecular identities were assigned using VaLID v3.0 (Blanchard et al., 2013) and the LIPID MAPS Structural Database (RRID:SCR_003817) (Sud et al., 2007). Molecular identities were confirmed in a single HPLC-selected reaction monitoring (SRM)- information dependent acquisition (IDA)- enhanced product ion (EPI) experiment in which SRM was used as a survey scan to identify target analytes and an IDA of EPI spectra were acquired in the linear ion trap. After acquisition, the EPI spectra were examined for structural determination. For quantification, raw peak areas were corrected

for extraction efficiency and instrument response by normalization to internal standards, PC(12:0/13:0) and PC(13:0/0:0), added at time of extraction. Lipid abundances were expressed as pmol equivalent of internal standard per mg of tissue wet weight ($pmol/mg_{tissue}$) or as log_2 fold change of these abundances relative to control.

2.5.4 Lipid nomenclature

We used the standard lipid nomenclature described by Fahy et al., to identify individual lipids (Fahy et al., 2011). For example, PC(O-18:1/2:0) defines a molecular species belonging to the GPC class of lipids with a polar phosphocholine head group (PC) at the *sn*-3 position of the glycerol backbone, a hydrocarbon chain of 18 carbons with 1 double bonds at the *sn*-1 position via an alkyl (ether) linkage (O-), and a saturated fatty acyl chain of 2 carbons at the *sn*-2 position via an ester linkage. For other subclasses, the nomenclature P- refers to an alkenyl (vinyl ether) linkage at the *sn*-1 position. Lack of linkage indicators refers to an acyl (ester) linkage. PC(O) second messengers were defined by their acetyl group at the *sn*-2 position. PAF-like lipids were defined as having an *sn*-1 acyl-group (PC) or alkenyl-group (PC(P)) and up to 2-6 carbons at the *sn*-2 position. We profiled LPC, LPC(O), and LPC(P) as well as PC(O) and PAF-like PC and PC(P) metabolites and second messengers (Supplemental Fig. 2.1).

2.5.5 Western analyses

Cortices were homogenized in Urea-Tris (8 M Urea, 50 mM Tris pH 8.2, 65 mM dithiothreitol (DTT) [#U5128, #T1503, and #43815, Sigma-Aldrich]) supplemented with ethylenediaminetetraacetic acid (EDTA)-free protease inhibitor and phosphatase inhibitor

cocktail tablets [#04693124001 and #04906837001, Roche]) and sonicated (#Sonicator3000, QSonica) three times at 12 W for 20 s. The samples were passed through a 26-gauge needle (#309625, BD Biosciences, ON, Canada) eight times and centrifuged at 22,000 g for 15 min. Protein concentrations were assessed using the Bio-Rad DC protein assay kit (#500-0112, Bio-Rad). Protein was denaturated using the NuPAGE LDS sample buffer and reducing agent (#NP0007, and #NP0009, Life Technologies) in accordance to the manufacturer's guidelines. Thirty µg of protein per well were resolved on NuPAGE 4–12% SDS–PAGE gels (#NP0335, Life Technologies). Gels were transferred onto nitrocellulose membranes (#66485, Pall Life Sciences) and blocked for 30 min with phosphate buffered saline with tween (PBS-T) (10 mM phosphate pH 7.2, 154 mM NaCl [#SPD307, #SPM306, and #SOD001, BioShop], 0.1 % (v/v) Tween 20 [#P1379, Sigma-Aldrich]) containing 5 % (w/v) non-fat milk (Carnation). Membranes were incubated at 4°C overnight with the primary antibody in PBS-T with 3 % (w/v) non-fat milk. Primary antibodies were anti-PAFAH1B1 (LIS1, 1:1000, RRID: AB 10694968, #AB5413, Millipore), anti-PAFAH1B2 (α_2, 1:700, gift of Dr Arai, University of Tokyo), anti-PAFAH1B3 (α_1, 1:700, gift of Dr Arai), and anti-actin (#CLT9001, Cedarlane). Horseradish peroxidase (HRP)-conjugated anti-mouse (1:2000, #610-1319-0500, 1:2000, Rockland) or anti-rabbit IgG (1:5000, #NA834V, GE Healthcare) secondary antibodies in 3 % (w/v) non-fat milk PBS-T were incubated with the membranes for one hour at room temperature. Reactions were visualized using Immobilon Western Chemiluminescent HRP Substrate (#WBKLS0500, Millipore). Membranes were stripped using 1 X ReBlot plus solution (#2504, Millipore) according to the manufacturer's

guidelines. Relative protein expression was quantified by densitometry using the image processing program Fiji v1.0 (National Institutes of Health).

2.5.6 PLA_2 activity

Total GIV $cPLA_2$ activity was assessed in cortical lysates using a commercial assay kit (#765021, Cayman Chemical) according to manufacturer's guidelines.

2.5.7 Statistics

Statistical analyses were performed using Prism 7.0 (GraphPad Software, RRID:SCR_002798). An alpha values of $p<0.05$ was deemed statistically significant. *Post hoc* power analyses were performed for all significant effects using G*Power 3.1 (RRID:SCR_013726) (Faul et al., 2007) with α set to 0.05. Sample and effect sizes were deemed acceptable maintaining a β value of 0.2 or under. Univariate analyses were unpaired, two-tailed t-tests and one- or two-way ANOVAs as indicated. In the event of multiple t-tests, family-wise error was corrected for by setting the false discovery rate (FDR) to Q=0.05 according to the method of (Benjamini et al., 2006). In ANOVA analyses, Holm-Sidak *post hoc* tests were used to control for family-wise comparisons. Partial Least Squares-Discriminant Analysis (PLS-DA) and variable importance in projection (VIP) scores were calculated using MetaboAnalyst 3.0 (RRID:SCR_015539) (Xia et al., 2015). Average linkage hierarchical clustering using city-block similarity metrics (autoscaled pmol equivalents per mg tissue wet weight) or uncentered correlation metrics (log_2 fold changes) were performed using Cluster 3.0 (RRID:SCR_013505) (de Hoon et

al., 2004). Heatmaps were visualized using Java TreeView 1.1.6 (RRID:SCR_013503) (Saldanha, 2004).

2.6 Results

2.6.1 The cortical and hippocampal GPC metabolite lipidomes are distinct.

We first identified the repertoire of glycerophosphocholine metabolites and second messengers with m/z between 450 and 650 in the frontal cortex and hippocampus of adult 4-9-month old WT mice using HPLC-ESI-MS/MS by PIS in positive ion mode. Because these species are much less abundant than their structural precursors, we developed and optimized a nano-flow HPLC-ESI-MS/MS method using a NanoSpray III ion source for their detection and quantification. Dynamic range of detection was confirmed by serial dilution and abundances of all species reported in this study were within this dynamic range. Our analysis excluded sphingomyelins and *lyso*-sphingomyelins identified by HPLC-DMS-ESI-MS/MS (Supplemental Fig. 2.2). Molecular identities were confirmed in a single HPLC-SRM-IDA-EPI experiment.

A total of 61 lipids were profiled as Land's cycle metabolites and second messengers. Cortical and hippocampal metabolite lipidomes segregated according to lipid composition and species abundance (Fig. 2.2A). Four species were unique to the frontal cortex: one PC lipid, PC(18:1/3:0), two LPC(O), LPC(O-18:0/0:0) and LPC(O-21:6/0:0), and one PC(O), PC(O-17:0/2:0) (Fig. 2.2A,B). Eight species were unique to the hippocampus: two PC, PC(16:0/2:0) and PC(18:1/4:0); four LPCs, LPC(26:6/0:0), LPC(22:6/0:0), LPC(22:4/0:0), and LPC(19:1/0:0); one PC(O), PC(O-17:1/2:0); and one LPC(P), LPC(P-20:0/0:0) (Fig. 2.2A,B). The most abundant glycerophosphocholine

Figure 2.2 – Cortical and hippocampal glycerophosphocholine metabolite lipidomes are distinct. (A) Heatmap depicting separation of the cortical and hippocampal glycerophosphocholine metabolite and second messenger landscapes. Data represent autoscaled metabolite abundances calculated in pmol per mg tissue wet weight) of adult (4-8-month-old, n=8) normoxic-treated WT mice. Z-scores were clustered using average linkage hierarchical clustering according to city-block similarity metrics. (B) Venn diagram summarizing glycerophosphocholine metabolite composition in frontal cortex and hippocampus. (C) Total glycerophosphocholine metabolite and second messenger abundances were comparable across regions. Subclass abundances of LPC(P) and PC(O) were lower in cortex compared to hippocampus. Data represent lipid abundance in pmol per mg tissue wet weight ± standard error (SEM). Total Land's cycle metabolite and second messenger levels were not significantly different (two-tailed unpaired t-test, $t=1.46$, $df=14$, $p=0.167$, n=8/region). Levels of LPC(P) and PC(O)-PAF were significantly lower in cortex compared to hippocampus. LPC(P): two-tailed unpaired $t=2.30$, $df=14$, $p=0.037$; PC(O)-PAF: $t=2.15$, $df=14$, $p=0.049$. *$p<0.05$. (D) Differences in regional metabolite abundance were species-specific. Data depict mean $\log_2$ fold change ± SEM (n=8 animals). Each sample was divided by the average abundance of the same lipid species in the hippocampus. Statistics were two-tailed, unpaired t-tests with an FDR of 5%; *FDR-adjusted $q<0.05$.

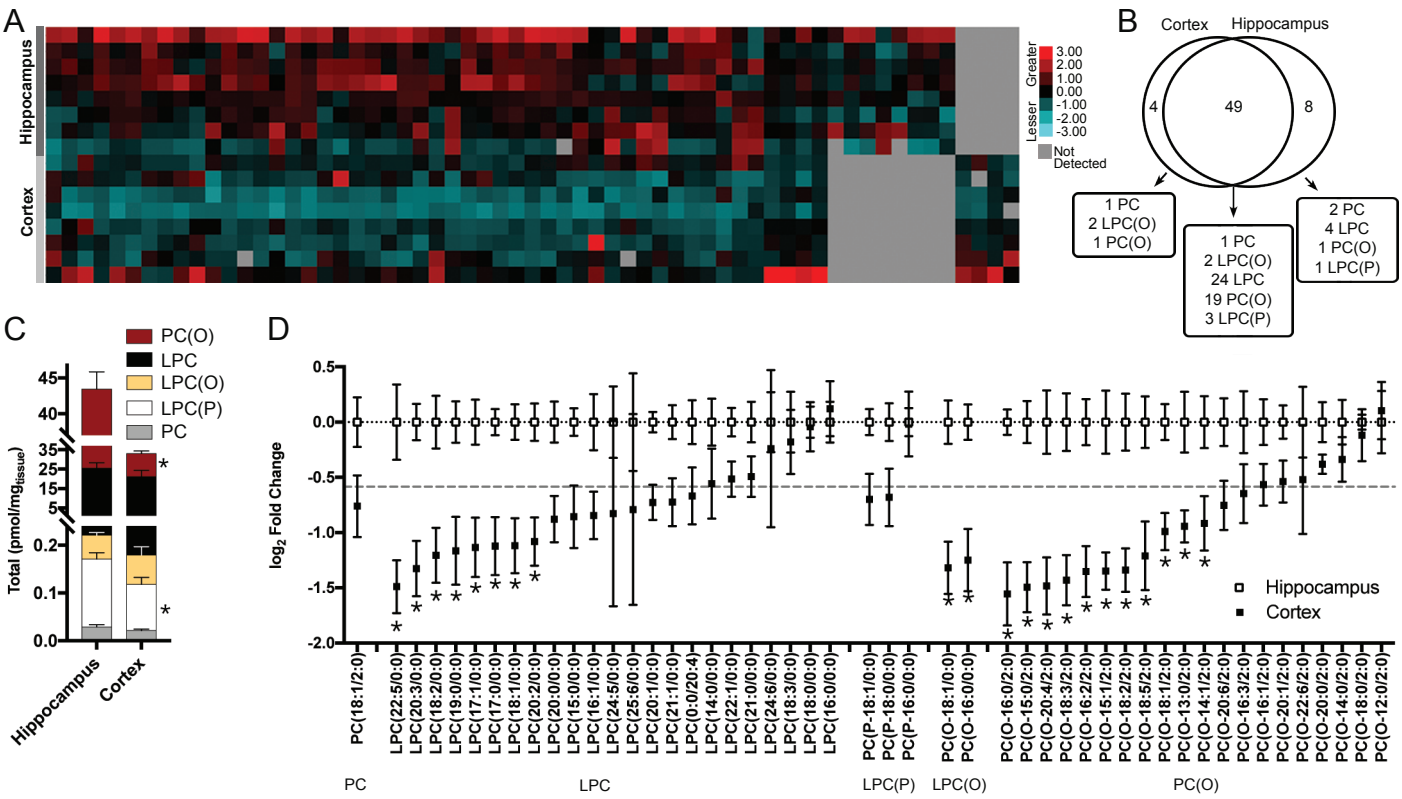
A
Hippocampus
Cortex
Greater
Lesser
3.00
2.00
1.00
0.00
-1.00
-2.00
-3.00
Not Detected
B
Cortex
Hippocampus
4
49
8
1 PC
2 LPC(O)
1 PC(O)
1 PC
2 LPC(O)
24 LPC
19 PC(O)
3 LPC(P)
2 PC
4 LPC
1 PC(O)
1 LPC(P)
C
PC(O)
LPC
LPC(O)
LPC(P)
PC
Total (pmol/mg$_{tissue}$)
Hippocampus
Cortex
D
log$_2$ Fold Change
Hippocampus
Cortex
PC
LPC
LPC(P)
LPC(O)
PC(O)

Figure 2.2

metabolites in both regions were LPC(18:0/0:0) and LPC(16:0/0:0), making up 40 %mol of the total metabolite lipidome. There were no regional differences in the abundances of these species; consequently, there were no statistically significant regional differences in total lipid metabolite content (Fig. 2.2C,D). Overall levels of PC(O) and LPC(P) were, however, lower in cortex compared to hippocampus (Fig. 2.2C). At the molecular level, abundances of 21 LPC, LPC(O), PC(P), and PC(O) species were lower in the frontal cortex compared to the hippocampus (Fig. 2.2D).

2.6.2 GPC metabolism is disrupted in the frontal cortex but not the hippocampus of AβPP^{Swe}/PS1^{dE9} mice when older mice transition from a pre-symptomatic to a symptomatic state.

The AβPP^{Swe}/PS1^{dE9} mice used in this study were a randomly chosen subset of animals previously subjected to normoxic or hypoxic challenge (Liu et al., 2016). All of the behavioural data for these animals are presented in (Liu et al., 2016). In Liu et al., we demonstrated that the performance of normoxic-treated WT animals was comparable in the MWM at 4, 6, and 9 months of age. Animals showed no learning and memory deficits (Liu et al., 2016). Likewise, we found here that their glycerophosphocholine lipidomes were indistinguishable. Glycerophosphocholine metabolism did not change between 4 and 9 months of age (Fig. 2.3A). Next, we interrogated the lipidomes of normoxic AβPP^{Swe}/PS1^{dE9} mice before (pre-symptomatic 4-month old mice) and after (symptomatic 6 to 9-month old mice) onset of learning and memory impairment. We found that total metabolite levels were altered in the frontal cortex but not hippocampus of symptomatic

Figure 2.3 – The cortical but not hippocampal lipidome is altered when AβPP^{Swe}/PS1^{dE9} mice first exhibit learning and memory deficits. (A) No statistically significant age-related changes in glycerophosphocholine metabolite levels were detected in normoxic WT mice at 4-month compared to 6 and 9-month old mice in either the hippocampus or the cortex. (B) Cortical levels of LPCs significantly decreased at symptomatic onset in AβPP^{Swe}/PS1^{dE9} mice under normoxic conditions. No changes in glycerophosphocholine metabolite levels were detected in the hippocampus. Data represent mean lipid abundance (pmol per mg tissue wet weight) ± SEM. Statistics were unpaired, two-tailed, t-tests (4-month: n=3 mice/region; 6-9-months: n=5 mice/region). Cortical LPC: t=2.80, df = 6, p=0.03).

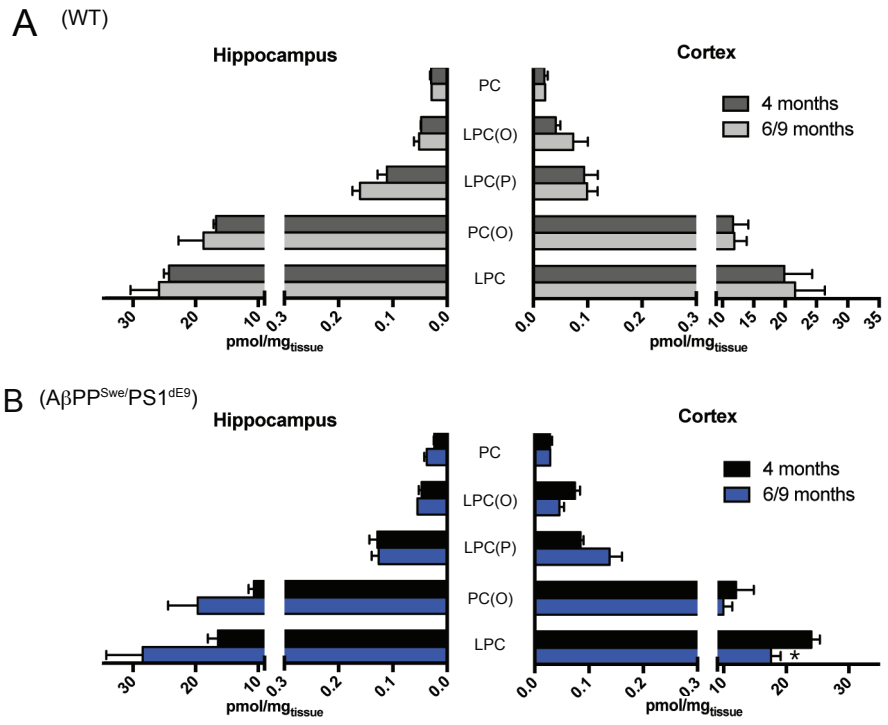
A (WT)
Hippocampus
Cortex
PC
LPC(O)
LPC(P)
PC(O)
LPC
4 months
6/9 months
30 20 10 0.3 0.2 0.1 0.0
0.0 0.1 0.2 0.3 10 15 20 25 30 35
pmol/mg tissue
B (AβPPSwe/PS1dE9)
Hippocampus
Cortex
PC
LPC(O)
LPC(P)
PC(O)
LPC
4 months
6/9 months
*
30 20 10 0.3 0.2 0.1 0.0
0.0 0.1 0.2 0.3 10 20 30
pmol/mg tissue

Figure 2.3

mice (Fig. 2.3B). LPC levels were significantly lower in older symptomatic compared to younger pre-symptomatic AβPP^{Swe}/PS1^{dE9} mice (Fig. 2.3B).

2.6.3 Chronic intermittent hypoxia accelerates changes in cortical GPC metabolism associated with symptomatic onset in AβPP^{Swe}/PS1^{dE9} mice

We used multivariate PLS-DA to determine whether the GPC metabolite lipidome discriminated pre-symptomatic from post-symptomatic AβPP^{Swe}/PS1^{dE9} mice. Pre-symptomatic young mice clearly segregated from symptomatic older mice using the first two principal components in two-dimensional score plots (Fig. 2.4A, left panel). In Liu et al. (2016), we reported that exposure to chronic intermittent hypoxia accelerated AβPP^{Swe}/PS1^{dE9} phenoconversion. The hypoxic AβPP^{Swe}/PS1^{dE9} mice profiled here showed learning and memory deficits by 4-months of age; normoxic AβPP^{Swe}/PS1^{dE9} mice phenoconverted between 6 and 9 months of age (Liu et al., 2016). We found that these pre-symptomatic normoxic 4-month-old AβPP^{Swe}/PS1^{dE9} mice were also clearly discriminated from symptomatic hypoxic 4-month old littermates (Fig. 2.4A, right panel).

We next asked whether age- and hypoxia-induced phenoconversion elicited the same changes in cortical lipid metabolism. Sixty percent of the top ten critical discriminators of age- and hypoxia-induced phenoconversion were identical (Fig. 2.4B). These lipids also showed statistically significant decreases relative to normoxic 4-month old pre-symptomatic mice (Fig. 2.4C). Lipid abundances of five GPC metabolites, LPC(16:0/0:0), LPC(18:0/0:0), LPC(24:6/0:0), LPC(25:6/0:0), LPC(O-18:0/0:0) and PC(O-22:6/2:0) declined significantly in both age-dependent and hypoxia-induced symptomatic AβPP^{Swe}/PS1^{dE9} but not WT mice (Fig. 2.4D, Supplemental Table 2.1).

Figure 2.4 – Chronic hypoxia accelerates glycerophosphocholine metabolic changes associated with the onset of behavioural impairment in the cortex of AβPP^{Swe}/PS1^{dE9} but not WT mice. (A) PLS-DA score plots demonstrating distinct separation of impaired AβPP^{Swe}/PS1^{dE9} 6-9-month normoxic (left panel) and 4-month hypoxic (right panel) mice from pre-symptomatic AβPP^{Swe}/PS1^{dE9} mice. (B) A Venn diagram depicting the top ten critical glycerophosphocholine metabolites identified by PLS-DA analysis with the highest variable projection score (all ≥ 1.4). Of these, six species were common in discriminating phenoconversion of both older normoxic (left ellipse) and younger hypoxic (right ellipse) AβPP^{Swe}/PS1^{dE9} mice. Red font indicates increased abundance in symptomatic mice, green font indicates decreased abundance in symptomatic mice. (C) Levels of these six critical predictors of symptomatic onset were statistically significantly lower following phenoconversion compared to pre-symptomatic mice. Data represent average $\log_2$ fold change relative to pre-symptomatic, 4-month AβPP^{Swe}/PS1^{dE9} mice (n=3/condition). Statistics were one-way ANOVA comparing the abundances of each lipid species across normoxic and hypoxic conditions followed by Holm-Sidak *post-hoc* tests. *p<0.05 for both impaired conditions relative to pre-symptomatic 4-month-old normoxic AβPP^{Swe}/PS1^{dE9} mice. The only other statistically significant change detected was an increase in LPC(21:0/0:0) in older symptomatic but not younger hypoxic AβPP^{Swe}/PS1^{dE9} mice (#p<0.05). (D) Comparison of pmol abundances of the six indicators of glycerophosphocholine metabolic impairment in pre-symptomatic 4-month normoxic A□PP^{Swe}/PS1^{dE9} mice (n=3) and at symptomatic onset in 6-9-month normoxic A□PP^{Swe}/PS1^{dE9} mice (n=5) or 4-month hypoxic AβPP^{Swe}/PS1^{dE9} mice (n=3). Data represent mean species abundance (pmol per mg tissue wet weight) ±

SEM. Statistics were one-way ANOVAs (LPC(16:0/0:0): $F_{(2,8)}$=9.29, df=2, p=0.008; LPC(18:0/0:0): $F_{(2,8)}$=8.98, df=2, p=0.009, LPC(24:6/0:0): $F_{(2,8)}$=0.034, df=2, , LPC(25:6/0:0): $F_{(2,8)}$=6.42, df=2, p=0.02; LPC(O-18:0/0:0): $F_{(2,8)}$=7.81, df=2, p=0.013; and PC(O-22:6/2:0): $F_{(2,8)}$=10.35, df=2, p=0.008) with Holm-Sidak *post-hoc* tests for multiple comparisons (**p<0.01, *p<0.05).

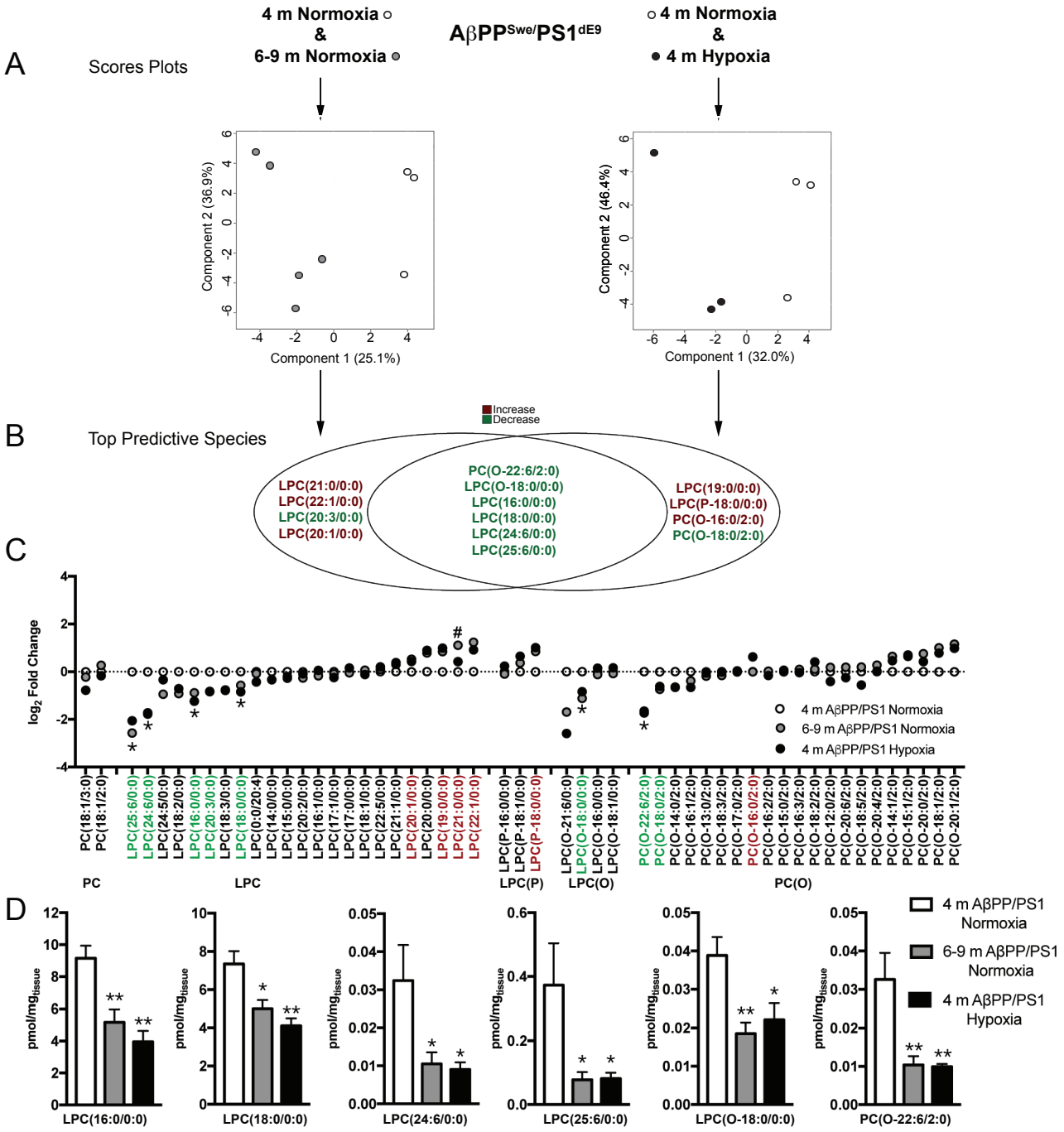
A
Scores Plots
4 m Normoxia ○
&
6-9 m Normoxia ●
AβPPSwe/PS1dE9
○ 4 m Normoxia
&
● 4 m Hypoxia
Component 2 (36.9%)
Component 1 (25.1%)
Component 2 (46.4%)
Component 1 (32.0%)
B
Top Predictive Species
Increase
Decrease
LPC(21:0/0:0)
LPC(22:1/0:0)
LPC(20:3/0:0)
LPC(20:1/0:0)
PC(O-22:6/2:0)
LPC(O-18:0/0:0)
LPC(16:0/0:0)
LPC(18:0/0:0)
LPC(24:6/0:0)
LPC(25:6/0:0)
LPC(19:0/0:0)
LPC(P-18:0/0:0)
PC(O-16:0/2:0)
PC(O-18:0/2:0)
C
log2 Fold Change
4 m AβPP/PS1 Normoxia
6-9 m AβPP/PS1 Normoxia
4 m AβPP/PS1 Hypoxia
PC
LPC
LPC(P)
LPC(O)
PC(O)
D
pmol/mgtissue
LPC(16:0/0:0)
LPC(18:0/0:0)
LPC(24:6/0:0)
LPC(25:6/0:0)
LPC(O-18:0/0:0)
PC(O-22:6/2:0)
4 m AβPP/PS1 Normoxia
6-9 m AβPP/PS1 Normoxia
4 m AβPP/PS1 Hypoxia

Figure 2.4

Hypoxia did not significantly alter the WT lipidome (Supplemental Fig. 2.3). Levels of five of the six critical indicators of AβPP^{Swe}/PS1^{dE9} phenoconversion declined mildly in WT littermates following hypoxic challenge; however, none of these changes were statistically significant (Supplemental Fig. 2.3). Taken together, these data suggested that PLA_2 activity is reduced when AβPP^{Swe}/PS1^{dE9} mice first exhibit either age- or environmental-risk associated learning and memory deficits.

2.6.4 Changes in PLA_2 activity and PAFAH1b subunit protein expression mark symptomatic onset and symptomatic progression in N5 TgCRND8 mice.

To assess enzymatic levels, activity, and lipidomic impact directly, we profiled the Land's cycle GPC metabolome and associated enzyme activities/levels in a second AβPP mouse model. N5 Tg mice (Granger et al., 2016) are a TgCRND8 sub-line, expressing the human AβPP gene with Swedish and Indiana familial AD mutations (KM670/671NL+V717F) under the control of the prion protein promoter (Chishti et al., 2001). N5 Tg females are pre-symptomatic at 2 months of age, phenoconvert in the MWM between 4 and 5 months, and are fully impaired at 6 months of age with deficits tested up to 12 months of age (Granger et al., 2016; Wang et al., 2013). We quantified Land's cycle metabolites and second messengers in the temporal/parietal/entorhinal cortex of 2 (pre-symptomatic), 4 (onset of learning and memory deficits), 6 (fully impaired), and 8 (fully impaired) month-old Tg mice by LC-ESI-MS/MS (Fig. 2.5A). As observed in the frontal cortex of AβPP^{Swe}/PS1^{dE9} mice, overall abundances of LPC metabolites decreased significantly when 4-month old Tg mice first exhibited learning and memory deficits (Fig. 2.5A,B). In addition, significant decreases in LPC(O) metabolites

Figure 2.5 – Decreases and increases in Lands' cycle metabolism differentiate symptomatic onset from symptomatic progression in cortex of N5 TgCRND8 mice. (A) Heat map depicting changes in the glycerophosphocholine metabolic landscape of 2-month (pre-symptomatic, n=4), 4-month (symptomatic onset, n=4), 6-month (fully impaired, n=4) and 8-month (fully impaired, n=3) N5 TgCRND8 mice. Data represent log_2 fold change relative to 2-month pre-symptomatic Tg mice. (B) Total LPC and LPC(O) levels decrease in 4-month old mice when Tg mice become symptomatic; total LPC and LPC(O) levels are restored in fully impaired 6- and 8-month old animals. Data represents mean log_2 fold change ± SEM relative to 2-month pre-symptomatic Tg mice. Statistics were 2-way ANOVA, main effect of age ($F_{(3,19)}$=4.1, df=3, p=0.02) *p<0.05 relative to 2-month N5 Tg mice. (C) Elevations in total PC(O)-PAF levels in fully impaired 6- and 8-month old animals were not statistically significant. Data represents mean log_2 fold change ± SEM relative to 2-month N5 Tg mice. Statistics were a one-way ANOVA ($F_{(3,9)}$=2.26, df=3, p=0.15). (D) Product/Precursor ratios of PC(O-18:1/2:0)/PC(O-18:0/0:0) were performed to assess rate of LPC(O) to PC(O)-PAF remodelling. An increase in remodelling was detected between 6- and 8-month old in Tg but not NonTg mice. Statistics were two-way ANOVA with a significant interaction ($F_{(3,25)}$=3.28, df=3, p=0.037), *p<0.05 relative to 2-month pre-symptomatic Tg mice and #p<0.05 relative to 4-month symptomatic Tg mice. (E) Increases and decreases in $cPLA_2$ activity distinguished symptomatic onset (4-month Tg) from fully impaired (6 and 8-month old) mice. No age-dependent change in $cPLA_2$ activity was observed in NonTg mice. Data represent mean ± SEM nmol/min/mL of $cPLA_2$ activity. Statistics were one-way ANOVA ($F_{(3,8)}$=69.23, df=3, p<0.0001, n=3/age), **p<0.01, *p<0.05 relative to 2-month Tg mice.

(F) PAFAH1b α_1 but not LIS1 or α_2 protein levels increase with age. Data represent western blots (left panel) and densitometry (right panel) of PAFAH protein subunit levels in 2, 4, and 6-month old NonTg and Tg mice. Mean ratio to the actin loading control ± SEM of each subunit are presented. Statistics were two-way ANOVA for each subunit. A significant main effect of age was detected: ($F_{(2,6)}$, df =2, p=0.016, n=2/ages/genotypes), *p<0.05 relative to 2-month old mice. Longer exposures are provided in Supplemental Fig. 4. Blots were probed simultaneously for α_1 and α_2. Blots probed individually are also presented in Supplemental Fig. 2.4.

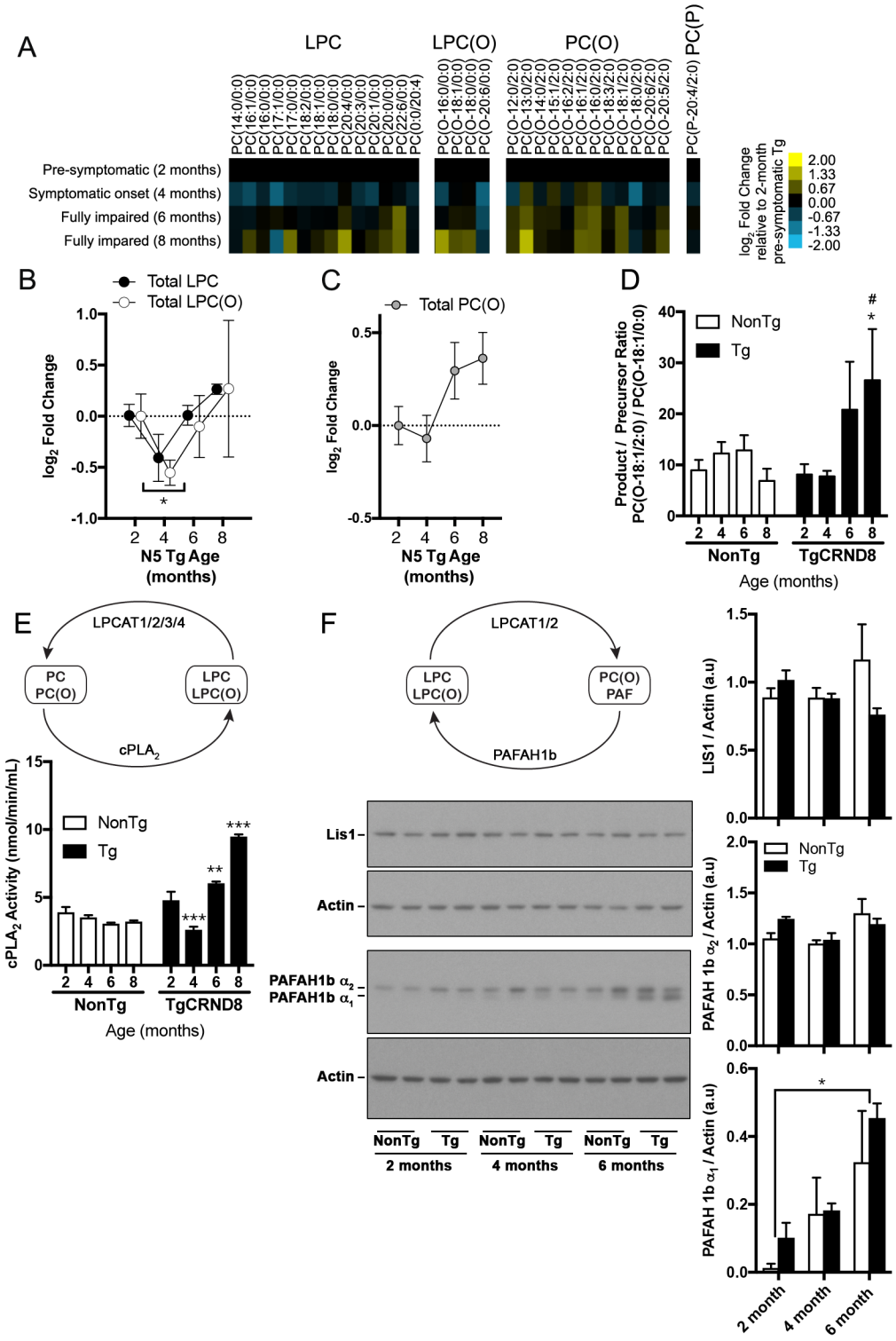
A
LPC
LPC(O)
PC(O)
PC(P)
PC(14:0/0:0)
PC(16:1/0:0)
PC(16:0/0:0)
PC(17:1/0:0)
PC(17:0/0:0)
PC(18:2/0:0)
PC(18:1/0:0)
PC(18:0/0:0)
PC(20:4/0:0)
PC(20:3/0:0)
PC(20:1/0:0)
PC(20:0/0:0)
PC(22:6/0:0)
PC(0:0/20:4)
PC(O-16:0/0:0)
PC(O-18:1/0:0)
PC(O-18:0/0:0)
PC(O-20:6/0:0)
PC(O-12:0/2:0)
PC(O-13:0/2:0)
PC(O-14:0/2:0)
PC(O-15:1/2:0)
PC(O-16:2/2:0)
PC(O-16:1/2:0)
PC(O-16:0/2:0)
PC(O-18:3/2:0)
PC(O-18:1/2:0)
PC(O-18:0/2:0)
PC(O-20:6/2:0)
PC(O-20:5/2:0)
PC(P-20:4/2:0)
Pre-symptomatic (2 months)
Symptomatic onset (4 months)
Fully impaired (6 months)
Fully impared (8 months)
log2 Fold Change relative to 2-month pre-symptomatic Tg
2.00
1.33
0.67
0.00
-0.67
-1.33
-2.00
B
Total LPC
Total LPC(O)
log2 Fold Change
N5 Tg Age (months)
C
Total PC(O)
log2 Fold Change
N5 Tg Age (months)
D
NonTg
Tg
Product / Precursor Ratio PC(O-18:1/2:0) / PC(O-18:1/0:0)
NonTg
TgCRND8
Age (months)
E
LPCAT1/2/3/4
PC PC(O)
LPC LPC(O)
cPLA2
cPLA2 Activity (nmol/min/mL)
NonTg
Tg
NonTg
TgCRND8
Age (months)
F
LPCAT1/2
LPC LPC(O)
PC(O) PAF
PAFAH1b
Lis1
Actin
PAFAH1b α2
PAFAH1b α1
Actin
NonTg
Tg
2 months
4 months
6 months
LIS1 / Actin (a.u)
NonTg
Tg
PAFAH 1b α2 / Actin (a.u)
PAFAH 1b α1 / Actin (a.u)
2 month
4 month
6 month

Figure 2.5

were detected (Fig. 2.5A,B). In older 6 and 8-month old mice, total LPC and LPC(O) levels rebounded (Fig. 2.5A,B) and PC(O) levels rose (Fig. 2.5A,C). We compared product to precursor ratios of PC(O-18:1/2:0) to LPC(O-18:1/0:0) to assess the rate of conversion of *lyso*-PAF to PAFs in both Tg and NonTg littermates (Fig. 2.5D). Remodelling of LPC(O-18:1/0:0) to PC(O-18:1/2:0) increased significantly between 6 to 8 months in symptomatic Tg mice but not in age-matched NonTg littermates (Fig. 2.5D).

We quantified $cPLA_2$ activity directly in temporal/parietal/entorhinal cortex over time (Fig. 2.5E). There was no change in $cPLA_2$ activity in NonTg mice between 2 and 8 months of age (Fig. 2.5E). By contrast, $cPLA_2$ activity decreased significantly in Tg mice at symptomatic onset (4-months of age) and increased significantly in fully impaired 6 and 8-month old mice (Fig. 2.5E). To provide mechanistic insight into why PC(O) levels accumulated in symptomatic Tg mice, we examined neuronal PAFAH1b subunit expression (Fig. 2.5F). The PAFAH1b trimer is composed of two catalytic subunits, α_1 and/ or α_2, and one regulatory subunit, LIS1. α_2 and LIS1 protein levels did not change with age in Tg and NonTg littermates (Fig. 2.5F). PAFAH1b α_1 protein expression significantly increased over time in both Tg and NonTg mice (Fig. 2.5F, Supplemental Fig. 2.4). Because PAFAH α_2/α_2 homodimers have a higher affinity for PC(O) than α_1/α_2 heterodimers or α_1/α_1 homodimers (Bonin et al., 2004; Manya et al., 1999), this shift in catalytic subunit expression is consistent with the accumulation of PC(O-18:1/2:0) over time in fully impaired Tg mice.

2.7 Discussion

In this study, we identify sequential changes in Land's cycle GPC metabolism that discriminate between pre-symptomatic, symptomatic, and fully impaired human AβPP mice. We used two different mouse models to ensure changes were indicative of behavioural indices of learning and memory impairment regardless of how Aβ-deposition was induced. Using an unbiased lipidomic approach and direct biochemical assessments, we show that that the GPC metabolomes of pre-symptomatic $A\beta PP^{Swe}/PS1^{dE9}$ and N5 TgCRND8 mice are indistinguishable from littermate controls lacking human AD AβPP. Upon symptomatic onset, $cPLA_2$ activity is suppressed and LPC and LPC(O) levels are reduced in both the frontal and temporal/parietal/entorhinal cortical regions of $A\beta PP^{Swe}/PS1^{dE9}$ and N5 TgCRND8 mice. Critical metabolic indicators are decreases in abundance of LPC(16:0/0:0), LPC(18:0/0:0), LPC(24:6/0:0), LPC(25:6/0:0), LPC(O-18:0/0:0), and PC(O-22:6/2:0). When human AβPP animals become fully impaired, $cPLA_2$ activity progressively increases. LPC and LPC(O) levels rise. The product to precursor ratio of PC(O-18:1/2:0) to PC(O-18:1/0:0) is progressively elevated indicative of the accumulation of pro-inflammatory PC(O) second messengers. These changes are accompanied by an age-dependent shift in the expression of the PAFAH1b catalytic subunits favouring α_1/α_2 and α_1/α_1 dimerization predicted to further reduce hydrolysis of PC(O) back to LPC(O) thus further promoting accumulation of pro-inflammatory PAFs in Tg cortices.

This study helps to reconcile controversy as to whether PLA_2 activation or inhibition in AD is pathological. Our data indicate that cortical GPC remodelling is suppressed when pre-symptomatic AβPP mice transition to a symptomatic state. This suppression is the

result of decreased $cPLA_2$ activity. We did not assay other PLA_2 isoforms but our findings are consistent with evidence that lower platelet $iPLA_2$ activity predicts risk of conversion from mild cognitive impairment to AD (Gattaz et al., 2014) while lower cortical total PLA_2 activity correlates with earlier AD onset (Gattaz et al., 1996; Ross et al., 1998). We also found that in fully impaired animals, $cPLA_2$ activity rises and LPC levels are elevated. Likewise, levels of arachidonic acid and its metabolites increase in both CSF and brain of mid and late-stage AD patients (Montine et al., 1999). AA is preferentially hydrolyzed from GPCs by $cPLA_2$ (Diez et al., 1992). The rise in LPC levels detected here is also consistent with the increase in glycerophosphocholine metabolite levels in post-mortem AD brain correlating with severity of cognitive decline and psychosis (Sweet et al., 2002). In concert with these increases, we found that downstream PC(O) metabolites accumulate in N5 Tg mice. This accumulation has been seen in network analyses of metabolic changes associated with AD progression in humans (Toledo et al., 2017) wherein higher levels of circulating PC(O) lipids correlate with a faster rate of AD cognitive decline (Toledo et al., 2017). Likewise, PC(O) levels are elevated in the entorhinal cortex of late-stage AD patients post-mortem (Ryan et al., 2009). Taken together, these data provide converging evidence to indicate that the onset and progression of AD are distinguished by distinct changes in Land's cycle metabolism of GPCs. Transient $cPLA_2$ suppression and reductions in *lyso*-metabolites in cortex associates with symptomatic onset while increased $cPLA_2$ activity and accumulation of PC(O)s associate with disease progression.

The biphasic changes observed in $cPLA_2$ activity in this study were both age-independent and required pre-existing Aβ pathology. Both $A\beta PP^{Swe}/PS1^{dE9}$ and N5 Tg

mice exhibited the same decreases in Land's cycle remodelling despite their age differential at symptomatic onset. AβPP^{Swe}/PS1^{dE9} mice first exhibit behavioural impairment between 6 and 9 months of age (Garcia-Alloza et al., 2006; Reiserer et al., 2007; Yang et al., 2015). Tg mice are symptomatic at 4 months of age (Chishti et al., 2001; Granger et al., 2016). Moreover, levels of the same critical indicators of cPLA$_2$ suppression, LPC(16:0/0:0), LPC(18:0/0:0), LPC(24:6/0:0), LPC(25:6/0:0), and LPC(O-18:0/0:0), decline in younger AβPP^{Swe}/PS1^{dE9} mice if symptomatic onset is accelerated by hypoxic insult. Chronic intermittent hypoxia is an environmental risk factor that results in earlier manifestation of learning and memory deficits, enhanced Aβ biogenesis, and exacerbated tau pathologies in human AβPP mouse models (Gao et al., 2013; Li et al., 2009; Liu et al., 2016; Sun et al., 2006; Zhang et al., 2013). This same insult is associated with a higher incidence of AD phenoconversion in humans (Daulatzai, 2013). Interestingly, we show here that decreased GPC metabolite abundances following hypoxic insult depends on pre-existing Aβ pathology. WT littermates subjected to the same chronic hypoxic insult did not show the same degree of lipidomic disruption as AβPP^{Swe}/PS1^{dE9} mice. Together, these data indicate that hypoxia alone does not alter enzymatic activity to the same extent in the absence of Aβ pathology. Moreover, we did not detect any age-associated changes in cortical cPLA$_2$ activity in normoxic mice devoid of human AβPP between 2 and 8 months of age. These data provide converging evidence to indicate that suppression of cPLA$_2$ activity is an indicator of experimental phenoconversion and that hypoxic risk of critical metabolic defects associated with cognitive decline is likely enhanced in preclinical AD patients.

Age, however, remains the primary risk factor for AD (Fjell et al., 2014). Disease incidence increases dramatically after 60 years of age (Kawas et al., 2000). Herrup (2010) has proposed a model in which normal aging, vascular trauma, and chronic neuroinflammation renders the elderly brain vulnerable to the amyloid cascade. Here, any injury that triggers a chronic neuroinflammatory response can precipitate a metabolic 'change in state'. This 'change of state' is envisioned as a convergence of critical metabolic dysfunctions that exacerbate the amyloid cascade and precipitates cognitive decline (Herrup, 2010). We found here that while biphasic changes in $cPLA_2$ activity are likely age-independent, these changes are also accompanied by an age-dependent shift in the relative expression of the catalytic α_1 and α_2 subunits of PAFAH1b in both Tg and NonTg littermates. The PAFAH1b trimer is composed two catalytic subunits, α_1 and/ or α_2 and one regulatory subunit, LIS1. PAFAH1b α_2 homodimers more effectively hydrolyze PC(O) to LPC(O) than PAFAH1b α_2/α_1 heterodimers or α_1/α_1 homodimers (Bonin et al., 2004; Manya et al., 1999). Thus, any shift in protein expression favouring complexes composed of α_2/α_1 and α_1/α_1 is predicted to reduce PC(O) hydrolysis and favour PC(O) accumulation. Our data indicate that younger adult mice predominantly express PAFAH1b α_2 while older mice increasingly express PAFAH1b α_1 at the protein level. These experimental data are supported by evidence that metabolism of PC(O)s is disrupted in AD (de Leeuw et al., 2017; Ryan et al., 2009) with $A\beta_{42}$ promoting remodelling of LPC(O) to PC(O) (McHale-Owen and Bate, 2018; Ryan et al., 2009; Simmons et al., 2014). Elevated cortical PC(O) levels have been linked mechanistically to the progression of other neuroinflammatory-associated dementias (Gelbard et al., 1994;

Kelesidis et al., 2015). Thus, age-dependent reduction in PC(O) hydrolysis likely represents another metabolic correlate of cognitive decline over the course of AD

In summary, we identify in this study two defining disruptions in Land's cycle glycerophosphocholine metabolism that distinguish pre-symptomatic, from symptomatic, from fully impaired human AβPP mice. These data provide the first direct evidence that the cortical glycerophosphocholine metabolome is differentially regulated at symptomatic onset and over the course of symptomatic decline in two mouse models AD.

2.8 Acknowledgements

M.W.G. and S.P.M.S. received Ontario Graduate Scholarships; A.P.B. received an Alzheimer Society of Canada studentship; M.T. received a Natural Science Research Council studentship. This study was funded by a University of Ottawa and Shanghai Jiao Tong University Joint Medical Research Program grant to W.L. and S.A.L.B., Canadian Institute of Health Research (MOP#311838) to S.A.L.B., and Chinese National Sciences Foundation (No.81370470 and No.81430021), National Basic Research Program (No.2011CB510003), and Collaborative Innovation Center for Brain Science to W.L. We thank Louis Dacquay for confirmatory data analysis replicating these analyses performed as part of his participation in our graduate class BCH8110 (University of Ottawa).

Supplemental Figure 2.1 – Lands' cycle metabolism of glycerophosphocholines. We use nano-ESI-LC-MS/MS to profile the repertoire of monoacylglycerophosphocholines (LPC), monoalkylglycerophosphocholines LPC(O), monoalkenylglycerophosphocholines LPC(P) (middle panel), 1-acyl,2-acetylglycerophosphocholines (PC), 1-alkyl,2-aceytlglycerophosphocholines (PC(O)) and 1-alkenyl,2-aceytlglycerophosphocholines (PC(P)) (bottom panel). *Lyso*-GPCs are generated by the hydrolysis of PC, PC(O), or PC(P) membrane precursors (top panel). Hydrolysis is mediated by a superfamily of PLA_2 enzymes, segregated into 16 groups and broadly distinguished by five discrete types. *Lyso*-glycerophosphocholines can be further modified by LPCAT1-4 to either regenerate a structural membrane glycerophosphocholine using acyl-CoA as a substrate (top panel) or produce PAFs, using acetyl-CoA as a substrate (bottom panel). Canonical PAFs have an *sn*-1 alkyl-group and their acetyl group at the *sn*-2 position (PC(O)). PAF-like lipids can have an *sn-1* acyl-group (PC) or alkenyl-group (PC(P)) and up to 2-6 carbons at the *sn-2* position. These second messengers are themselves both the products and the immediate precursors of *lyso*-GPCs in the Lands' cycle as they are remodelled back to their respective *lyso*-metabolites by PAFAHs. Abbreviations: GPC, glycerophosphocholine; $cPLA_2$, cytoplasmic phospholipase A2; $iPLA_2$, calcium-independent phospholipase A_2; $LPLA_2$, lysosomal phospholipase A_2; LPCAT1-4, *lyso*phosphatidylcholine acetyltransferase 1-4; PAF, platelet activating factor; PAFAH, platelet activating factor acetylhydrolase; PLA/AT, the H-RAS-like suppressor enzymes with both PLA_1 and PLA_2 activities as well as O-acyltransferase activities; $sPLA_2$, secretory phospholipase A_2.

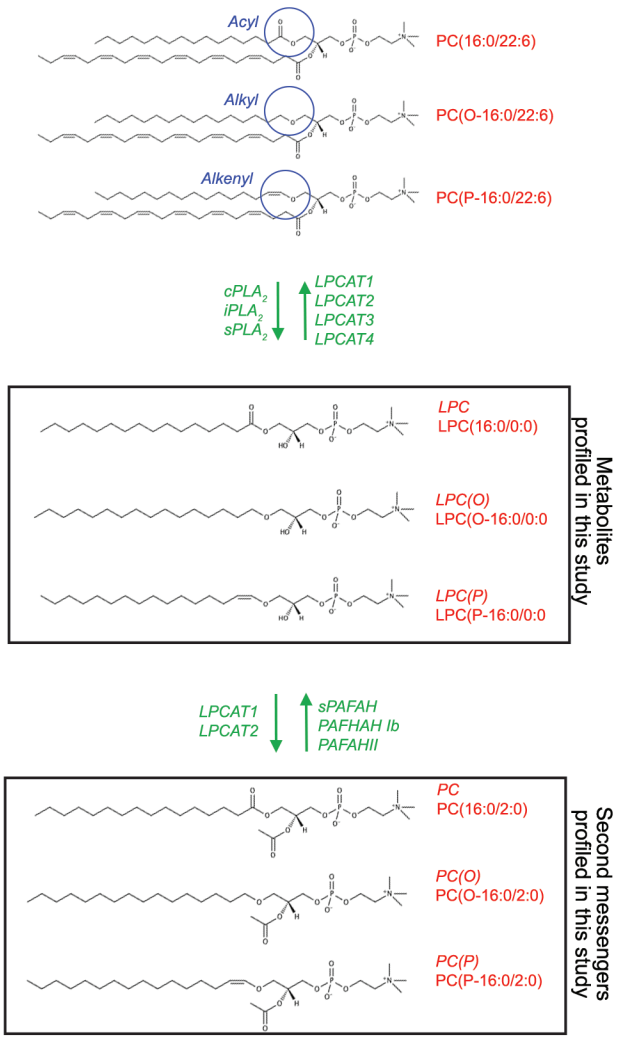
Acyl
PC(16:0/22:6)
Alkyl
PC(O-16:0/22:6)
Alkenyl
PC(P-16:0/22:6)
cPLA2
iPLA2
sPLA2
LPCAT1
LPCAT2
LPCAT3
LPCAT4
LPC
LPC(16:0/0:0)
LPC(O)
LPC(O-16:0/0:0
LPC(P)
LPC(P-16:0/0:0
Metabolites profiled in this study
LPCAT1
LPCAT2
sPAFAH
PAFHAH Ib
PAFAHII
PC
PC(16:0/2:0)
PC(O)
PC(O-16:0/2:0)
PC(P)
PC(P-16:0/2:0)
Second messengers profiled in this study

Supplemental Figure 2.2 – Verification that sphingomyelins are not detected in our glycerophosphocholine metabolite and second messenger LC-ESI-MS/MS profiles. Because sphingomyelins or lyso-sphingomyelins also fragment with a diagnostic m/z 184.1 ion, prior to molecular identification, we verified that all metabolites/second messengers profiled in this study were glycerophosphocholines using differential mobility spectroscopy. All details are as in Materials and Methods. No sphingomyelins or lyso-sphingomyelins were detected in our targeted m/z range of 450-650.

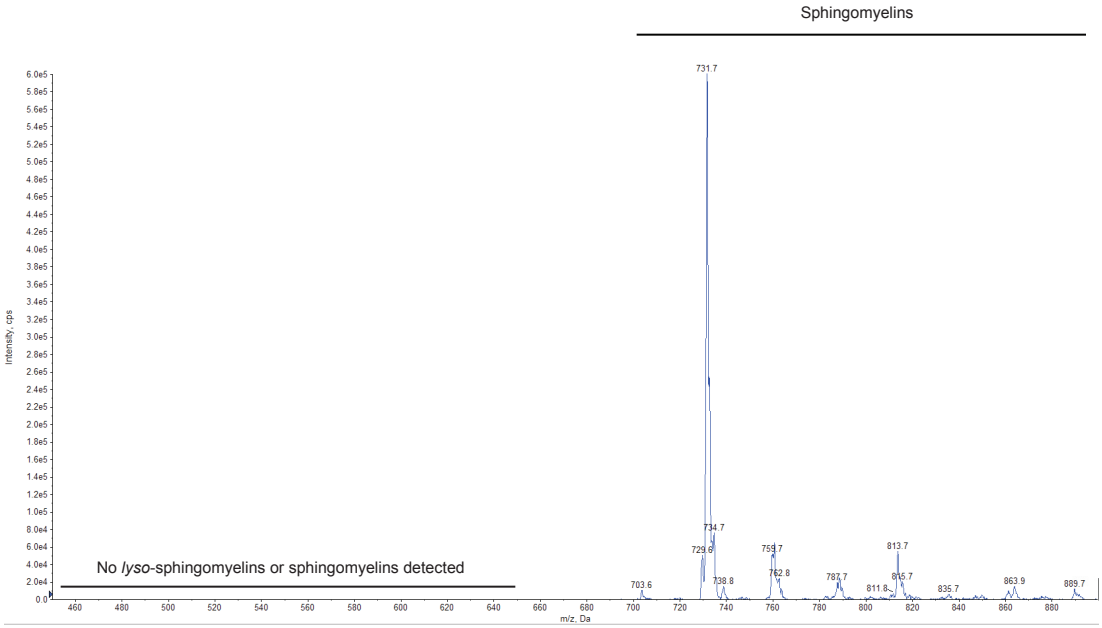
Sphingomyelins
No *lyso*-sphingomyelins or sphingomyelins detected
Intensity, cps
m/z, Da
731.7
734.7
729.6
759.7
762.8
738.8
703.6
787.7
813.7
815.7
811.8
835.7
863.9
889.7

Supplemental Figure 2.3 – Analysis of critical glycerophospholipidome metabolites in 4-month old hypoxic compared to normoxic WT mice. Neither normoxic aging or exposure to hypoxia significantly altered the cortical WT lipidome. Univariate analysis revealed that no species were significantly altered in WT mice challenged with hypoxia or by age. Data represent mean log2 fold change of 6-9-month normoxic WT and 4-month hypoxic WT compared to 4-month normoxic animals. Statistics were one-way ANOVAs. (All ANOVAs: $p>0.05$).

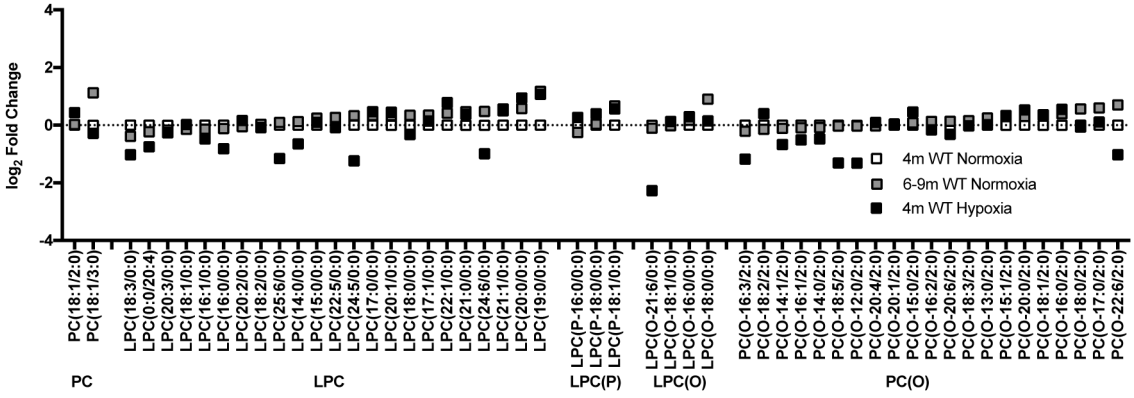
log2 Fold Change
4
2
0
-2
-4
4m WT Normoxia
6-9m WT Normoxia
4m WT Hypoxia
PC(18:1/2:0)
PC(18:1/3:0)
LPC(18:3/0:0)
LPC(0:0/20:4)
LPC(20:3/0:0)
LPC(18:1/0:0)
LPC(16:1/0:0)
LPC(16:0/0:0)
LPC(20:2/0:0)
LPC(18:2/0:0)
LPC(25:6/0:0)
LPC(14:0/0:0)
LPC(15:0/0:0)
LPC(22:5/0:0)
LPC(24:5/0:0)
LPC(17:0/0:0)
LPC(20:1/0:0)
LPC(18:0/0:0)
LPC(17:1/0:0)
LPC(22:1/0:0)
LPC(21:0/0:0)
LPC(24:6/0:0)
LPC(21:1/0:0)
LPC(20:0/0:0)
LPC(19:0/0:0)
LPC(P-16:0/0:0)
LPC(P-18:0/0:0)
LPC(P-18:1/0:0)
LPC(O-21:6/0:0)
LPC(O-18:1/0:0)
LPC(O-16:0/0:0)
LPC(O-18:0/0:0)
PC(O-16:3/2:0)
PC(O-18:2/2:0)
PC(O-14:1/2:0)
PC(O-16:1/2:0)
PC(O-14:0/2:0)
PC(O-18:5/2:0)
PC(O-12:0/2:0)
PC(O-20:4/2:0)
PC(O-20:1/2:0)
PC(O-15:0/2:0)
PC(O-16:2/2:0)
PC(O-20:6/2:0)
PC(O-18:3/2:0)
PC(O-13:0/2:0)
PC(O-15:1/2:0)
PC(O-20:0/2:0)
PC(O-18:1/2:0)
PC(O-16:0/2:0)
PC(O-18:0/2:0)
PC(O-17:0/2:0)
PC(O-22:6/2:0)
PC
LPC
LPC(P)
LPC(O)
PC(O)

Supplemental Figure 2.4. Western analysis of PAFAH α_2 and α_1 catalytic subunits. (A) Higher exposure of immunoblot presented in Fig. 5 demonstrating that the α_1 subunit is detected at low levels in younger mice with protein expression increasing with age. As indicated in Fig 4, blots were probed simultaneously for α_1 and α_2. (B) To confirm these results, the same proteins were run in a replicate immunoblot and probed sequentially for α_2 (top panel), stripped and reprobed for α_1 (middle panel), and stripped and reprobed for the actin loading control (bottom panel). PAFAH α_1 protein levels increased in both NonTg and Tg mice with age. Levels appeared to increase more robustly in older Tg animals compared to NonTg but these genotypic differences were not statistically significant (see densitometry in Fig. 2.5).

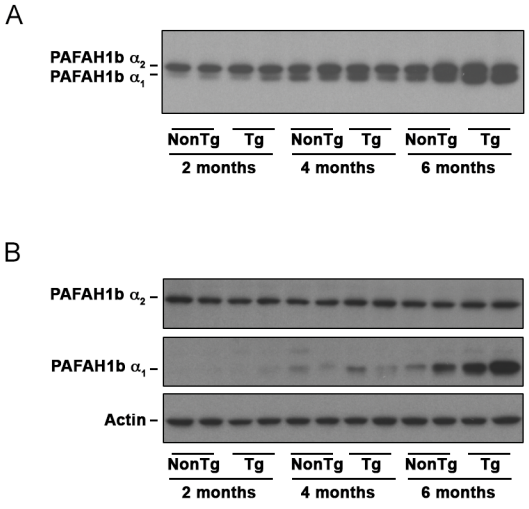
A
PAFAH1b α2
PAFAH1b α1
NonTg
Tg
NonTg
Tg
NonTg
Tg
2 months
4 months
6 months
B
PAFAH1b α2
PAFAH1b α1
Actin
NonTg
Tg
NonTg
Tg
NonTg
Tg
2 months
4 months
6 months

Supplemental Table 2.1. Mean pmol comparisons of frontal cortex GPC metabolites and signaling molecules in WT and AβPP/PS1 mice

	Genotype:	WT							AβPP/PS1						
	Condition:	Normoxia				Hypoxia			Normoxia				Hypoxia		
	Age:	4 months		6-9 months		4 months		ANOVA	4 months		6-9 months		4 months		ANOVA
Subclass	Species	Mean	SEM	Mean	SEM	Mean	SEM	p-value	Mean	SEM	Mean	SEM	Mean	SEM	p-value
PC	PC(18:1/3:0)	0.0056	0.0022	0.0124	0.0044	0.0036	0.0003	0.3430	0.0073	0.0020	0.0060	0.0012	0.0043	0.0015	0.4904
	PC(18:1/2:0)	0.0146	0.0051	0.0147	0.0030	0.0210	0.0082	0.6714	0.0204	0.0046	0.0237	0.0022	0.0180	0.0039	0.4820
LPC	LPC(21:1/0:0)	0.0017	0.0003	0.0026	0.0005	0.0028	0.0013	0.6313	0.0028	0.0003	0.0037	0.0005	0.0036	0.0009	0.6313
	LPC(18:3/0:0)	0.0049	0.0022	0.0034	0.0006	0.0021	0.0005	0.3583	0.0043	0.0015	0.0027	0.0009	0.0023	0.0004	0.4121
	LPC(17:1/0:0)	0.0097	0.0018	0.0134	0.0031	0.0123	0.0050	0.7714	0.0141	0.0034	0.0129	0.0017	0.0120	0.0035	0.8848
	LPC(15:0/0:0)	0.0143	0.0032	0.0188	0.0057	0.0168	0.0064	0.8525	0.0209	0.0055	0.0173	0.0033	0.0176	0.0044	0.8195
	LPC(24:6/0:0)	0.0129	0.0052	0.0437	0.0321	0.0067	0.0027	0.5647	0.0324	0.0094	0.0105*	0.0027	0.0090*	0.0019	0.0340
	LPC(21:0/0:0)	0.0160	0.0034	0.0220	0.0029	0.0247	0.0120	0.6634	0.0163	0.0017	0.0355*	0.0040	0.0229	0.0060	0.0316
	LPC(19:0/0:0)	0.0111	0.0027	0.0257	0.0048	0.0267	0.0121	0.2949	0.0175	0.0029	0.0322	0.0053	0.0345	0.0057	0.1311
	LPC(22:5/0:0)	0.0275	0.0062	0.0354	0.0079	0.0269	0.0067	0.9370	0.0271	0.0071	0.0309	0.0078	0.0310	0.0095	0.9370
	LPC(14:0/0:0)	0.0308	0.0083	0.0365	0.0103	0.0201	0.0072	0.5187	0.0320	0.0098	0.0285	0.0091	0.0245	0.0055	0.8707
	LPC(20:3/0:0)	0.0371	0.0091	0.0342	0.0075	0.0330	0.0103	0.9534	0.0623	0.0155	0.0335	0.0033	0.0359	0.0104	0.1098
	LPC(20:2/0:0)	0.0474	0.0095	0.0479	0.0095	0.0575	0.0189	0.8338	0.0723	0.0120	0.0624	0.0116	0.0703	0.0188	0.8562
	LPC(24:5/0:0)	0.0746	0.0340	0.1188	0.0476	0.0312	0.0147	0.3798	0.0942	0.0352	0.0623	0.0160	0.0617	0.0064	0.5213
	LPC(22:1/0:0)	0.0523	0.0054	0.0725	0.0120	0.1046	0.0432	0.3555	0.0573	0.0145	0.1267	0.0133	0.1073	0.0311	0.0828
	LPC(17:0/0:0)	0.0679	0.0151	0.0923	0.0245	0.1114	0.0527	0.6957	0.1049	0.0125	0.1080	0.0215	0.1216	0.0299	0.8822
	LPC(18:2/0:0)	0.1358	0.0306	0.1461	0.0325	0.1352	0.0394	0.9666	0.2810	0.1560	0.1176	0.0241	0.1296	0.0299	0.3105
	LPC(20:0/0:0)	0.1020	0.0246	0.1497	0.0255	0.2293	0.1105	0.3743	0.1292	0.0239	0.2277	0.0409	0.2455	0.0640	0.2589
	LPC(16:1/0:0)	0.2152	0.0567	0.1969	0.0340	0.1565	0.0430	0.6764	0.1832	0.0351	0.1810	0.0468	0.1907	0.0362	0.9878
	LPC(25:6/0:0)	0.1883	0.1216	0.7429	0.6715	0.0813	0.0497	0.6530	0.3728	0.1316	0.0778*	0.0238	0.0815*	0.0181	0.0217
	LPC(20:1/0:0)	0.2202	0.0288	0.2858	0.0402	0.3164	0.0866	0.5181	0.2746	0.0222	0.4021	0.0437	0.3817	0.0770	0.2469
	LPC(0:0/20:4)	3.7956	1.2575	3.2479	0.6256	2.1360	0.4377	0.4291	2.6946	0.5049	2.6902	0.5210	1.9483	0.1950	0.5376
	LPC(18:1/0:0)	2.2538	0.5572	2.0934	0.4538	2.5393	0.9659	0.8809	3.0168	0.5163	3.1284	0.3720	2.8375	0.6681	0.9148
	LPC(18:0/0:0)	5.1649	1.0693	6.8183	1.4378	3.9312	0.1651	0.3122	7.3510	0.6612	5.0026*	0.4549	4.1094*	0.3880	0.0090
	LPC(16:0/0:0)	7.4005	1.7365	7.3644	1.9419	4.0159	0.4134	0.3957	9.1524	0.7865	5.1759*	0.8128	3.9594*	0.6742	0.0082
LPC(P)	LPC(P-18:1/0:0)	0.0049	0.0016	0.0073	0.0011	0.0089	0.0046	0.5835	0.0063	0.0010	0.0081	0.0009	0.0101	0.0024	0.2636
	LPC(P-16:0/0:0)	0.0148	0.0037	0.0136	0.0038	0.0204	0.0088	0.6558	0.0173	0.0019	0.0167	0.0026	0.0213	0.0052	0.6381
	LPC(P-18:0/0:0)	0.0740	0.0199	0.0780	0.0161	0.1011	0.0351	0.1605	0.0607	0.0039	0.1165	0.0201	0.1293	0.0322	0.1605
LPC(O)	LPC(O-21:6/0:0)	0.0059	0.0022	0.0177	0.0147	0.0012	0.0003	0.6074	0.0106	0.0079	0.0018	0.0005	0.0009	0.0003	0.2074
	LPC(O-18:1/0:0)	0.0080	0.0016	0.0085	0.0020	0.0098	0.0037	0.9053	0.0096	0.0008	0.0102	0.0026	0.0113	0.0030	0.9053
	LPC(O-16:0/0:0)	0.0119	0.0025	0.0152	0.0050	0.0155	0.0053	0.8326	0.0151	0.0014	0.0150	0.0031	0.0177	0.0046	0.8326
	LPC(O-18:0/0:0)	0.0155	0.0031	0.0322	0.0076	0.0182	0.0057	0.2146	0.0389	0.0048	0.0185*	0.0029	0.0222*	0.0042	0.0132
PC(O)	PC(O-17:0/2:0)	0.0023	0.0003	0.0036	0.0006	0.0026	0.0008	0.4012	0.0032	0.0002	0.0038	0.0010	0.0035	0.0009	0.9434
	PC(O-16:3/2:0)	0.0082	0.0021	0.0075	0.0019	0.0034	0.0005	0.2513	0.0051	0.0019	0.0056	0.0014	0.0046	0.0007	0.8796
	PC(O-13:0/2:0)	0.0112	0.0022	0.0132	0.0014	0.0117	0.0028	0.7441	0.0139	0.0045	0.0132	0.0035	0.0126	0.0035	0.9763
	PC(O-15:0/2:0)	0.0091	0.0012	0.0106	0.0025	0.0135	0.0039	0.5929	0.0149	0.0047	0.0150	0.0031	0.0142	0.0039	0.9899
	PC(O-15:1/2:0)	0.0133	0.0017	0.0170	0.0026	0.0175	0.0037	0.5952	0.0111	0.0035	0.0176	0.0042	0.0172	0.0047	0.5603
	PC(O-18:5/2:0)	0.0203	0.0086	0.0195	0.0047	0.0070	0.0008	0.2576	0.0142	0.0042	0.0182	0.0054	0.0090	0.0005	0.4562
	PC(O-20:1/2:0)	0.0182	0.0046	0.0187	0.0032	0.0182	0.0032	0.9927	0.0122	0.0041	0.0307	0.0113	0.0220	0.0062	0.4437
	PC(O-22:6/2:0)	0.0163	0.0064	0.0408	0.0232	0.0074	0.0015	0.4538	0.0326	0.0070	0.0104*	0.0020	0.0099*	0.0007	0.0081
	PC(O-18:2/2:0)	0.0190	0.0026	0.0185	0.0040	0.0291	0.0097	0.4007	0.0240	0.0074	0.0284	0.0086	0.0309	0.0101	0.8891
	PC(O-18:0/2:0)	0.0459	0.0038	0.0749	0.0159	0.0457	0.0099	0.2598	0.0875	0.0091	0.0607	0.0170	0.0588	0.0118	0.4301
	PC(O-12:0/2:0)	0.0933	0.0240	0.0935	0.0203	0.0371	0.0095	0.1673	0.0560	0.0202	0.0615	0.0141	0.0391	0.0096	0.5974
	PC(O-18:3/2:0)	0.0746	0.0161	0.0878	0.0176	0.0801	0.0313	0.8963	0.0865	0.0236	0.0857	0.0230	0.0848	0.0257	0.9990
	PC(O-20:0/2:0)	0.1114	0.0093	0.1377	0.0091	0.1840	0.0731	0.4234	0.1211	0.0236	0.2044	0.0304	0.1723	0.0579	0.3392
	PC(O-20:4/2:0)	0.1631	0.0333	0.1785	0.0436	0.1837	0.0482	0.9533	0.1922	0.0380	0.2335	0.0369	0.2014	0.0581	0.7688
	PC(O-14:1/2:0)	0.2046	0.0717	0.1867	0.0428	0.1232	0.0359	0.6745	0.1160	0.0378	0.1968	0.0567	0.1500	0.0254	0.5387
	PC(O-18:1/2:0)	0.1570	0.0150	0.2087	0.0345	0.2072	0.0361	0.5278	0.1400	0.0385	0.3103	0.0922	0.2396	0.0699	0.3946
	PC(O-16:2/2:0)	0.1746	0.0491	0.1937	0.0359	0.1670	0.0519	0.8997	0.2032	0.0685	0.2077	0.0541	0.1617	0.0377	0.8375
	PC(O-16:0/2:0)	0.1812	0.0514	0.2517	0.0591	0.2801	0.1087	0.6797	0.2214	0.0074	0.2428	0.0527	0.3508	0.0639	0.2794
	PC(O-20:6/2:0)	1.8325	0.5205	2.0051	0.3198	1.5117	0.4624	0.7026	1.7615	0.5458	2.0371	0.4513	1.3571	0.2326	0.5915
	PC(O-14:0/2:0)	4.2494	0.9932	4.1089	0.7725	2.9387	0.3032	0.5171	4.4672	0.9518	2.8455	0.4129	2.6950	0.1313	0.1222
	PC(O-16:1/2:0)	4.2806	0.7748	4.2216	0.8224	3.0984	0.7626	0.5939	4.4108	1.0627	3.3412	0.5423	2.7720	0.6565	0.3779

*** highlighted in green indicates statistically significantly decreases compared to 4 month-old presymptomatic normoxic mice of the same genotype; post-hoc Holm-Sidak tests**
*** highlighted in red indicates statistically significantly increases compared to 4 month-old presymptomatic normoxic mice of the same genotype; post-hoc Holm-Sidak tests**

Chapter 3: A TgCRND8 mouse model of Alzheimer's disease exhibits sexual dimorphisms in behavioural indices of cognitive reserve

Matthew W. Granger[a], Bettina Franko[a], Matthew W. Taylor[a], Claude Messier[b], Peter St George-Hyslop[c], Steffany A.L. Bennett[a]*

[a]Neural Regeneration Laboratory, Ottawa Institute of Systems Biology, Department of Biochemistry, Microbiology, and Immunology, [b]School of Psychology, University of Ottawa, Ottawa, ON, Canada, [c]Department of Clinical Neurosciences, Cambridge Institute for Medical Research, University of Cambridge, Cambridge, UK; Tanz Centre for Research in Neurodegenerative Diseases , University of Toronto, Toronto, ON, Canada.

Keywords

Alzheimer's disease, cognitive reserve, amyloid-β, search strategy, stereotypy, visual acuity, Morris Water Maze, learning, memory, transgenic mouse

Chapter 3: A TgCRND8 mouse model of Alzheimer's disease exhibits sexual dimorphisms in behavioural indices of cognitive reserve

3.1 Objective of Study

In Chapter 2, I demonstrated that changes in glycerophosphocholine metabolism detected at phenoconversion were accelerated in the presence of an external AD risk factor that enhances susceptibility to cognitive decline. This finding led me to hypothesize that differences in glycerophopsholipid metabolism would not only indicate animals susceptible to impairment, but animals that are resistant. Cognitive reserve was determined to be a viable representation of resistance in AD. Metabolic indices of cognitive reserve have yet to be identified. To address whether glycerophospholipid metabolism could discriminate between animals capable of adopting alternative behavioural strategies from impaired animals when challenged with equivalent Aβ pathology, the objective of this chapter was to develop a mouse model of AD that models sex-specific dimorphisms in behavioural indices of cognitive reserve that could be used in Chapter 4 to test these hypotheses.

3.2 Author contributions

MWG and SALB conceived and designed the experiments. MWG analyzed all of the experiments with input from SALB and CM. MWG ran the MWM experiments with assistance from MWT. MWG performed the immunohistochemistry, immunofluorescence, estrous and enzyme-linked immunosorbent assay (ELISA) experiments and assisted in the development of MWM Visual and MWM experimental

paradigms. SALB completed plaque counts and Western blotting. BF executed the SLAG and cued MWM experiments. PSGH provided the parental TgCRND8 line.

This chapter is published in the Journal of Alzheimer's Disease: **Granger MW**, Franko B, Taylor MW, Messier C, St George-Hyslop P, Bennett SAL (2016) A TgCRND8 mouse model of Alzheimer's disease exhibits sexual dimorphisms in behavioural indices of cognitive reserve. Journal of Alzheimer's Disease; 51(3):757-73.

3.3 Abstract

Cognitive decline is sexually dimorphic in AD. Men show higher incidences of amnestic mild cognitive impairment yet women disproportionally phenoconvert to AD. It is hypothesized that men maintain greater cognitive reserve than women under comparable Aβ challenge. One behavioural aspect of cognitive reserve in mice is the capacity to cope with Aβ-associated stereotypies by switching to increasingly effective navigational search strategies in the MWM. To explore inherent sex differences in this paradigm, however, we require an AβPP mouse model wherein behavioural flexibility is impaired earlier in females than males despite equivalent Aβ load. Here, we show that when F1 C57Bl/6 x C3H/HeJ Tg mice are placed on C57Bl/6 background, N5 Tg males and females exhibit equivalent Aβ pathologies at 2, 4, 6, and 8 months of age yet females display learning and memory deficits earlier than males. We further show that this N5 line does not carry the autosomal recessive *pde6b*^{rd1} mutation that impairs visual acuity and that the estrous cycle is not disrupted on this genetic background. At 5.5 months of age, Tg males, but not females compensate for Aβ-associated stereotypic behaviours (i.e., hyperactive tight circling) by alternating navigational search strategies and adopting increasingly productive spatial search strategies. Females fail to overcome amyloid-β-associated stereotypies and do not efficiently switch from systematic to spatial learning strategies. Together, these data identify a novel AβPP mouse model that can be used for preclinical testing of interventions targeting sexual dimorphisms in behavioural indices of cognitive reserve.

3.4 Introduction

Aberrant cleavage of the AβPP into toxic oligomeric Aβ peptides and intraneuronal accumulation of neurofibrillary tangles composed of hyperphosphorylated tau are defining AD pathologies (Benilova et al., 2012; Hardy and Selkoe, 2002; Palop and Mucke, 2010). The amyloid cascade has been modeled in transgenic mice by ectopically expressing human familial mutant AβPP and/or PS1 genes linked to EOAD (Webster et al., 2014; Zahs and Ashe, 2010). AD-associated tauopathies have been further engineered using triple transgenics expressing mutant human tau (Hochgrafe et al., 2013; Oddo et al., 2003; Webster et al., 2014). These models have clearly demonstrated that higher Aβ loads are associated with greater learning and memory impairments in mice. For example, interventions that accelerate Aβ deposition and tau aggregation in 3xTg-AD mice exacerbate learning and memory deficits (Barron et al., 2013). Similarly, memory impairments in $A\beta PP_{Swe}$/PS1 mice increase as soluble Aβ levels and plaque burden rise (Hooijmans et al., 2009; Savonenko et al., 2005; Zhang et al., 2011).

In humans, cognitive decline in AD is sexually dimorphic (Barnes et al., 2005; Fjell et al., 2010; Hua et al., 2010; Mielke et al., 2014; Snowdon, 2003; Vemuri et al., 2012). Two-thirds of AD patients are women (Hebert et al., 2013; Mielke et al., 2014; Thies et al., 2013). Men currently show a higher incidence of amnestic mild cognitive impairment, often with a greater Aβ load than women, yet women disproportionally transition to AD (Barnes et al., 2005; Hua et al., 2010; Mielke et al., 2014; Vemuri et al., 2012). It is hypothesized that men maintain greater brain and cognitive reserves in the face of Aβ challenge (Irvine et al., 2012; Perneczky et al., 2007). Here, brain reserve refers to differences in brain structure or synaptic densities that enable individuals to compensate

for declining neural function resulting from Aβ toxicity (Sperling et al., 2011; Stern, 2012). Cognitive reserve is defined as the capacity to switch between cognitive strategies, using alternative brain networks and cognitive paradigms to cope with progressive Aβ pathologies (Sperling et al., 2011; Stern, 2012). To our knowledge, no AβPP mouse model robustly recapitulates sexual dimorphisms in cognitive reserve given pre-existing sex differences in Aβ biogenesis. While female AβPP transgenics often display more severe learning and memory deficits (Clinton et al., 2007; Gallagher et al., 2013), they also consistently exhibit higher $A\beta_{40}$ and $A\beta_{42}$ levels and greater Aβ plaque loads than males (Callahan et al., 2001; Hirata-Fukae et al., 2008; Schafer et al., 2007; Wang et al., 2003). Accelerated Aβ accumulation in female mice is attributed, in part, to sex-dependent increases in beta-secretase (BACE-1) expression (Gallagher et al., 2013), decreases in insulin-degrading enzyme expression (Gallagher et al., 2013), and enhanced γ-secretase activity (Placanica et al., 2009). Interestingly, mild learning and memory impairments have been reported in 3xTg-AD females at ages when Aβ and tau pathologies begin to diverge (Bories et al., 2012; Clinton et al., 2007). While these data hint at sex differences in Aβ vulnerability, robust sex-specific impairments have only been reported once Aβ load in females exceeds that of males (Carroll et al., 2010; Hirata-Fukae et al., 2008). Identifying an AβPP transgenic model in which females and males exhibit comparable Aβ burden at all ages yet females phenoconvert earlier than males would provide an ideal preclinical model for testing strategies designed to enhance cognitive reserve and would further our understanding of AD sexual dimorphisms.

The TgCRND8 line is an aggressive AβPP mouse model. Tg mice express the human AβPP gene with double KM670/671NL+V717F Swedish and Indiana familial AD

mutations (Chishti et al., 2001). Extracellular $A\beta_{40}$ and $A\beta_{42}$ are detected by one month of age (Chishti et al., 2001). Soluble $A\beta_{42}/A\beta_{40}$ ratios are elevated by two months of age (Chishti et al., 2001). Learning and memory deficits manifest by three months of age (Chishti et al., 2001). Since this line exhibits a high mortality rate, males and females are commonly pooled for behavioural testing (Chishti et al., 2001; Janus, 2004; Lovasic et al., 2005). Sex differences have yet to be evaluated. We have previously shown that backcrossing C57Bl/6 x C3H/HeJ TgCRND8 mice onto a C57Bl/6 lineage for 5 generations (N5) delays the onset of learning and memory impairment in females (Wang et al., 2013). We have yet to characterize males on this genetic background. Here, we asked whether N4 and N5 C57Bl/6 x C3H/HeJ Tg mice display sexual dimorphisms in behavioural indices of cognitive reserve. We show that $A\beta$ load is equivalent between Tg sexes yet Tg males exhibit fewer learning and memory deficits in the MWM. We analyzed the search strategies used by NonTg and Tg mice to navigate the MWM to assess behavioural flexibility associated with cognitive reserve. We find that Tg males can overcome $A\beta$-associated non-productive behaviours (hyperactive repetitive tight circling) by adopting increasingly productive spatial search strategies whereas Tg females cannot ultimately affecting behavioural measures of learning and memory. Together, these data identify the N4/N5 Tg line as a mouse model capable of recapitulating clinically relevant sexually dimorphic differences associated with risk of AD phenoconversion.

3.5 Materials and Methods

3.5.1 Animals

A total of 78 Tg males, 194 Tg females, 61 NonTg males, and 96 NonTg females were used in this study. All mice were derived from F1 TgCRND8 C57Bl/6 x C3H/HeJ hybrid mice (Chishti et al., 2001) generously provided by Dr. Paul Fraser (University of Toronto). Mice were backcrossed for 4 and 5 generations (N4/N5) to wild-type C57Bl/6 mice in our laboratory (Wang et al., 2013) and then maintained by filial breeding of N4 Tg with N4 NonTg females. All mice were genotyped twice for the human AβPP transgene (Wang et al., 2013) and the autosomal recessive retinal degeneration phosphodiesterase 6B (*Pde6b*^{rd1}) mutation (Gimenez and Montoliu, 2001) (Supplemental Table 3.1). At 50 days of age, males and females were single-housed on a 12:12 light:dark cycle with zeitgeiber time (ZT) 0 set to 6:00 AM. Mice were fed a normal chow diet (Harlan Laboratories, 2018 Teklad Global 18% Protein Rodent Diet) *ad libitum*. Natural survival rates were calculated between 50-181 days of age. All experiments were approved by the Animal Care Committee of the University of Ottawa and performed in strict accordance with the ethical guidelines for experimentation of the Canadian Council for Animal Care.

3.5.2 Western blotting

Soluble protein was extracted from the cortex of NonTg and Tg mice at 2, 4, and 6 months of age using RadioImmunoprecipitation Assay (RIPA) buffer (1% Nonidet P40 substitute, 0.5% sodium deoxycholate, 0.1% sodium dodecyl sulfate, 1 mM sodium orthovanadate, 1 mM sodium fluoride, 300 μg/mL aprotinin and 100 μg/mL

phenylmethylsulfonyl fluoride in 10 mM phosphate-buffered saline). Protein samples of 15 μg then were processed as previously described (Wang et al., 2013). Briefly, proteins were incubated at 70ºC in NuPAGE lithium dodecyl sulfate sample buffer, resolved on a NuPAGE 4-12% SDS-PAGE gel (Invitrogen), transferred to nitrocellulose membrane (Pall Life Sciences #66485), and blocked in 5% non-fat milk in Tris buffered saline with tween (TBS-T) (50 mM Tris base, 150 mM NaCl, 0.1% Tween 20). Immunoblotting was performed with overnight probe at 4ºC using an Aβ antibody that recognizes human AβPP, C-terminal fragment β (CTFβ) but not CTFα, and Aβ peptides (6E10 Cedarlane SIG-39320 at 1:2000 dilution). Secondary antibodies were horseradish peroxidase-conjugated anti-mouse IgG (Rockland 610-1319-0500 at 1:10 000 dilution) visualized by chemiluminescence using Immobilon Western substrate (Millipore WBKLS0500).

3.5.3 Aβ plaque counts

Tg males and females were euthanized at 2, 4, 6, and 8 months of age (n=3-6 per genotype/age/sex). Animals were injected with euthanyl (1EUS001, Bimeda-MTC Animal Health Ins) prepared in sterile water to a final concentration of 65 mg/ml and transcardially perfused with 10 mM phosphate buffered saline (PBS; 10 mM sodium phosphate and 154 mM NaCl) followed by either 3.7% paraformaldehyde in 10 mM PBS for serial coronal sectioning or by Lana's fixative (4% paraformaldehyde, 0.2% picric acid in 0.16 M sodium phosphate buffer, pH 7.1) for sagittal sectioning to assess Aβ plaque distribution. Brains were removed, post-fixed for 24 hours in either 3.7% paraformaldehyde in 10 mM PBS or for 1 hour in Lana's fixative, and cryoprotected in 20% sucrose. Lana's fixed sagittal 30 μm serial sections were collected between interaural 0.24 and 1.92 mm using the

coordinates of Franklin and Paxinos (Franklin and Paxinos, 2007) on a Leica CM1900 cryostat (Leica Microsystems). Sagittal sections were processed for immunohistochemistry using mouse anti-4G8 (1/250; SIG-39220, Covance) recognizing human and murine Aβ, biotin-labeled anti-mouse IgG (1/300; B9904, Sigma), extravidin-peroxidase (1/20; E2886, Sigma), and visualized by a reaction with Sigma *FAST* 3,3'-diaminobenzidine (D4418-50SET, Sigma). Sections were dehydrated in an increasing series of ethanol washes (50-100%) and coverslipped in DPX Mountant (44581, Fluka). All antibodies were diluted in antibody buffer (3% bovine serum albumin (A6003, Sigma), 0.3% Triton X-100 (T9284, Sigma), in 10 mM PBS, pH 7.0). For plaque quantification, 10 mM PBS-buffered 3.7% paraformaldehyde-fixed 10 µm serial coronal cryosections between bregma -1.0 to -2.6 using the coordinates of Hof et al. (Hof et al., 2001) were collected. Total plaque number in the dorsal hippocampus and cortex as we have previously described (Pettit et al., 2012) and defined by Fanselow and Dong (Dong et al., 2009), restricted to the dorsal retrosplenial, parietal association, and primary sensory cortices as identified according to Hof et al. (Hof et al., 2001), were quantified on a DMXRA2 epifluorescent microscope (Leica Microsystems) using the Advanced Measurement Module of OpenLab 5.0.2 (Improvision) software. Counting methodologies were as described (Pettit et al., 2012), adapted to assess Aβ plaques. Briefly, a series of coronal sections (10 µm) were incubated overnight at 4˚C with mouse anti-4G8 (1:500). Sections were washed with 10 mM PBS, incubated with fluorescein isothiocyanate (FITC)-labeled anti-mouse IgG (1:1000, 715-095-150, Jackson ImmunoResearch) for 1 hour at room temperature, and washed in 10 mM PBS prior to being coverslipped in 0.05% p-phenylenediamine (w/v, P6001, Sigma) in glycerol (BP229-1, Fisher) adjusted

to pH 8.0 with 0.5 M sodium carbonate/sodium bicarbonate buffer. Plaques were defined as immunoreactive round or annular aggregates with diameters of 5 µm or greater representing the minimum diameter of deposits meeting this morphological criteria detected. The maximum plaque size detected in these animals was 50 µm. Average plaque size was 27.2 $\pm$ 12 µm. An average of five 10 µm sections, serially sampled along the entire anterior-posterior axis of the hippocampus between bregma -1.0 and -2.6, were analyzed per animal. Sections were a minimum of 30 µm apart to ensure the same plaque was not counted twice in adjacent sections. A single investigator blinded to the identity of the sections assessed plaque numbers. Total number of plaques per animal was calculated as the sum of the plaque counts per region in both hemispheres multiplied by the total number of serial sections collected, divided by the number of sections sampled and further divided by three to account for plaque size and thus overlap given assessment in 16 series of 10 µm sections.

3.5.4 Quantification of $A\beta_{40}$ and $A\beta_{42}$ peptides

Tg males and females were euthanized at two or six months of age (n=4-5 per sex) using euthanyl (1EUS001, Bimeda-MTC Animal Health Ins) prepared in sterile water to a final concentration of 65 mg/ml. Brains were extracted and the cerebrum dissected, weighed and flash-frozen in liquid nitrogen. Tissue was prepared as per ELISA kit instructions (human Aβ42: Invitrogen #KHB3442; human Aβ40: Invitrogen #KHB3482). Briefly, tissue was homogenized in a 5 M guanidine hydrochloride, 50 mM Tris hydrochloride solution and then diluted 1:25 in Dulbecco's PBS (0.2 g/L KCl, 0.2 g/L KH_2PO_4, 8 g/L NaCl, 1.15 g/L Na_2HPO_4) with 5% BSA (Fisher, CAS 9048-46-8) and

0.03% Tween (Sigma-Aldrich, P1379) augmented with 1x protease inhibitor cocktail (Calbiochem #539131). Six-month samples were further diluted 1:1000 and two-month samples 1:2 to fall within range of commercial standard curves using age-matched NonTg mice as a negative control. Each sample was run in duplicate. Data are reported as ng Aβ peptide per gram of tissue wet weight.

3.5.5 MWM behavioural testing

Behavioural indices of spatial learning and memory were assessed in the MWM paradigm. Testing began when mice were 158 ± 10 days (5.3 months) of age and ended when mice were 167 ± 10 days (5.6 months) of age. An additional cohort of male mice was tested when mice were 338 ± 50 days (11.27 months) of age and ended when mice were 347 ± 50 days (11.57 months) of age. The apparatus, a circular plastic pool (ENV-594M-B, Med Associates Inc.), measured 134.5 cm in diameter and 53.3 cm deep. The pool was filled with water maintained at 21˚C and made opaque by the addition of white, nontoxic, water-soluble paint (506-BT12801O, Scholar's Choice). The water level was maintained at a depth of 1 cm above the 10 cm diameter circular escape platform. Visual cues included a black "X" and square on the front and left walls respectively. Mice were acclimated to MWM facilities using a white noise generator (70 dB; 2325-0144, San Diego Instruments) with overhead white light of 100 lux for one hour before being placed in the pool. Mice underwent four trials with 20-minute intervals per day for eight test days. Each test day, mice were placed in four equidistant locations around the pool in a random order and navigation was tracked for 60 seconds. If mice did not find the escape platform independently, the experimenter guided the mouse to the platform ensuring the mouse

remained on the platform for 5 seconds before being removed. On day nine, mice were subjected to a probe test whereby the platform was removed and mice were placed in the pool for 60 seconds to evaluate reference memory. Separate cohorts of Tg and NonTg mice were tested in the cued MWM at 5.5 months of age using the same experimental paradigm except that the platform location was made clearly visible with a flag emerging from the center of the hidden escape platform. In all experiments, mice were tracked using a video camera (Bosch, LTC0355/20; Pentax 3.5-8 mm Ins, TS2V314BED) and data collected using either Ethovision XT7 or XT8 (Noldus).

3.5.6 Navigational Search Strategy Analysis

As defined by Janus (Janus, 2004) and Brody and Holtzman, (Brody and Holtzman, 2006), swim patterns were used to assess the cognitive strategies used by mice to acquire the MWM. Swim patterns were classified as one of three overarching search strategies: (1) spatial, (2) non-spatial systematic, or (3) repetitive looping. Spatial strategies were defined by focally specific searches in which there is a clear emphasis on the quadrant where the escape platform is located (Brody and Holtzman, 2006; Janus, 2004; Wolfer and Lipp, 2000). These included swim trajectories in which the mouse navigates directly to the target or concentrates its search in the correct quadrant. Systematic strategies represented a non-spatial navigational approach (Brody and Holtzman, 2006; Janus, 2004; Wolfer and Lipp, 2000). Searches were comprehensive but are not selective for the escape quadrant in that they included random or scanning behaviours in multiple quadrants as well as focused searches of an incorrect quadrant. Looping referred to a primarily repetitive circling approach where mice swim in either

small, tight circles or wider, concentric loops (Brody and Holtzman, 2006; Janus, 2004; Wolfer and Lipp, 2000). Floating was further assessed as a possible confounding phenotype as this behaviour lacks a deliberate trajectory or an intentional navigational search strategy. Floating was defined by a velocity under 6 cm/s (Janus, 2004) and an escape latency of over 50 s for a given trial. A mouse with an average velocity of under 6 cm/s and average escape latency of over 50 s for more than four of the eight test days was considered a floater and was excluded from analysis. Only one N5 NonTg female was identified as a floater and excluded from this study. Search strategies were analyzed by (a) two investigators blinded to the subjects' genotypes and (b) using a fully automated algorithm, MWM Visual, developed in-house. Both the inter-rater agreements and the consensus agreement of the two raters with the software were comparable at 85-90% (κ=0.825 and κ=0.804 respectively). Data reported in this study represent classifications assigned exclusively using the MWM Visual algorithm.

3.5.7 Slow angled descent forepaw grasping test (SLAG)

Two days before cued MWM testing, visual acuity was assessed using the SLAG test (Gil-Pages et al., 2013). The performances of 5 month old N4 NonTg and Tg mice were compared to those of an in-house colony of N15 C57BL/6 as well as to C3H/HeNCrl mice (Charles River). C57BL/6 mice have no visual deficits; C3H/HeNCrl are homozygous for *Pde6b*^{rd1} mutation and exhibit retinal degeneration (Gimenez and Montoliu, 2001). Mice heterozygous for *Pde6b*^{rd1} have normal retinas but increased photosensitivity (Hussain et al., 1992). The F1 TgCRND8 parental line is *Pde6b*$^{rd1/+}$. Our N4 NonTg and Tg either retained one copy of the mutant allele or were wildtype

(*Pde6b*$^{+/+}$). N5 mice were all *Pde6b*$^{+/+}$. Briefly, the behaviour of mice descending to a wire mesh cage lid in either ventral or dorsal orientations was recorded using a Sony High Definition Camcorder (HDR-CX210/R) in the presence of a desk lamp (Illuminada Gooseneck Desk Lamp, 17341-000) that emitted 600-700 lux located on the opposite side of the cage. Mice were subjected to six trials (three in each orientation) separated by five-minute intervals over two test days. Trial videos were scored for the presence (score=1) or absence (score=0) of the SLAG reflex. A SLAG reflex was defined by the following behaviours: (1) persistent extension of the forepaws towards the wire lid, (2) multiple reaches of the forepaws towards the wire lid, (3) forepaw extension with head elevation or hind limb extension in attempt to reach the wire lid, or (4) rotating the body to reach the wire lid. Absence of a SLAG reflex was defined by: (1) no extension of forepaws toward the wire lid, (2) rotation of the body to reach the hind limb or tail and not the wire lid, (3), or extension of the forepaws in the correct direction only when the mouse was less than 4 cm away from the wire lid thus guided by whisker proprioception (Gil-Pages et al., 2013). The percentage of total trials in which an animal exhibited a SLAG reflex was reported. Animals with an incidence of 30% or less were considered severely visually impaired, between 30% and 90% moderately to mildly photosensitive, and greater than 90% were defined as without visual impairment.

3.5.8 Estrous Staging

Vaginal smears were collected from a separate cohort of NonTg (n=7) and Tg (n=7) mice for at least two consecutive cycles and estrous cycle length determined for each mouse and each genotype as we have described (McLean et al., 2012).

3.5.9 Statistical Analyses

GraphPad Prism 6.0 software (GraphPad, San Diego, USA) or IBM SPSS Statistics v22 (IBM, Armonk, USA) was used for all statistical measures. Alpha values of $p<0.05$ were deemed significant for assessment of main and interactions effects. For amyloid load analyses, we performed two group power analyses to estimate effect sizes afforded by the number of subjects assessed at 6 months of age with α set to 0.05 and β set to 0.2. Subject size in this study was sufficient to detect a 1.7 fold-change in $A\beta_{42}$, a 2.1 fold-change in $A\beta_{40}$, and a 2.1 fold-change in plaque number. Groups of two were analyzed by unpaired Student's t-tests. Changes in groups of three or more were assessed by one-way or two-way ANOVA or t-test followed by Holm-Sidak, Tukey, or Dunnett's *post-hoc* tests adjusting the alpha levels for pairwise and multiple comparisons as indicated. Paired or repeated measures analyses were performed where warranted. Reference memory was analyzed using a one-sample t-test. Natural survival of different sexes and genotypes was compared using Mantel-Cox log-rank tests.

3.6 Results

3.6.1 AβPP, CTFβ, Aβ peptide, and Aβ plaque load are comparable in N4 and N5 Tg males and females at 2, 4, 6, and 8 months of age

We first assessed protein levels of soluble 6E10-reactive AβPP and CTFβ protein levels in the cortex of male and female Tg mice at 2, 4, and 6 months of age by Western blotting (Fig. 3.1A). No sex differences in protein levels were detected (Supplemental Fig. 3.1). We next determined the distribution and morphology of 4G8-immunoreactive

Figure 3.1 – Aβ burden is comparable in 2-8 month old Tg male and female mice. (A) No sex-differences in cortical AβPP and CTFβ protein levels are detected at 2, 4, or 6 months of age (n=2 animals/sex/genotype). M-Males; F-Females. Representative immunoblots are depicted. An increase in CTFβ levels is apparent in both sexes at 6 months of age. Note that the CTFβ panel is presented at a higher exposure than the AβPP panel (see Supplemental Figure 1 for the full blot at both exposures). (B,C) Dense-core plaques, with either round or annular morphologies (insets), were enriched in dorsal hippocampus and parietal/temporal cortex of both male and female Tg mice at 6 months of age. Scale bars: 2000 µm; insets, 20 µm. The total number of plaques > 5 µm diameter were quantified stereologically from bregma -1.0 to -2.6 in the (D,E) dorsal hippocampus and (D,F) cortex of male and female Tg mice and in 6 month-old NonTg littermates. No sex differences in plaque number were detected at any age. In both males and females, a significant increase in plaque number was evident at 6 and 8 months of age compared to 2 and 4 month old animals. In cortex but not hippocampus, plaque number was lower in 8 month-old compared to 6 month-old animals. Levels of $A\beta_{42}$ (G) and $A\beta_{40}$ (H) peptides and relative $A\beta_{42}/A\beta_{40}$ ratios (I) were quantified at 2 and 6 months of age by ELISA. Data represent mean ± standard error of measurement (SEM) of n=3-6 mice per group. No sex-differences in Aβ peptide levels were detected. Statistics were two-way ANOVA followed by *post hoc* Tukey's tests. *p<0.05, **p<0.01. (Abbreviations: DH-dorsal hippocampus; M1-primary motor cortex; M2-secondary motor cortex; RSD-retrosplenial dysgranular cortex; RSG-retrosplenial granular cortex; V2-secondary visual cortex)

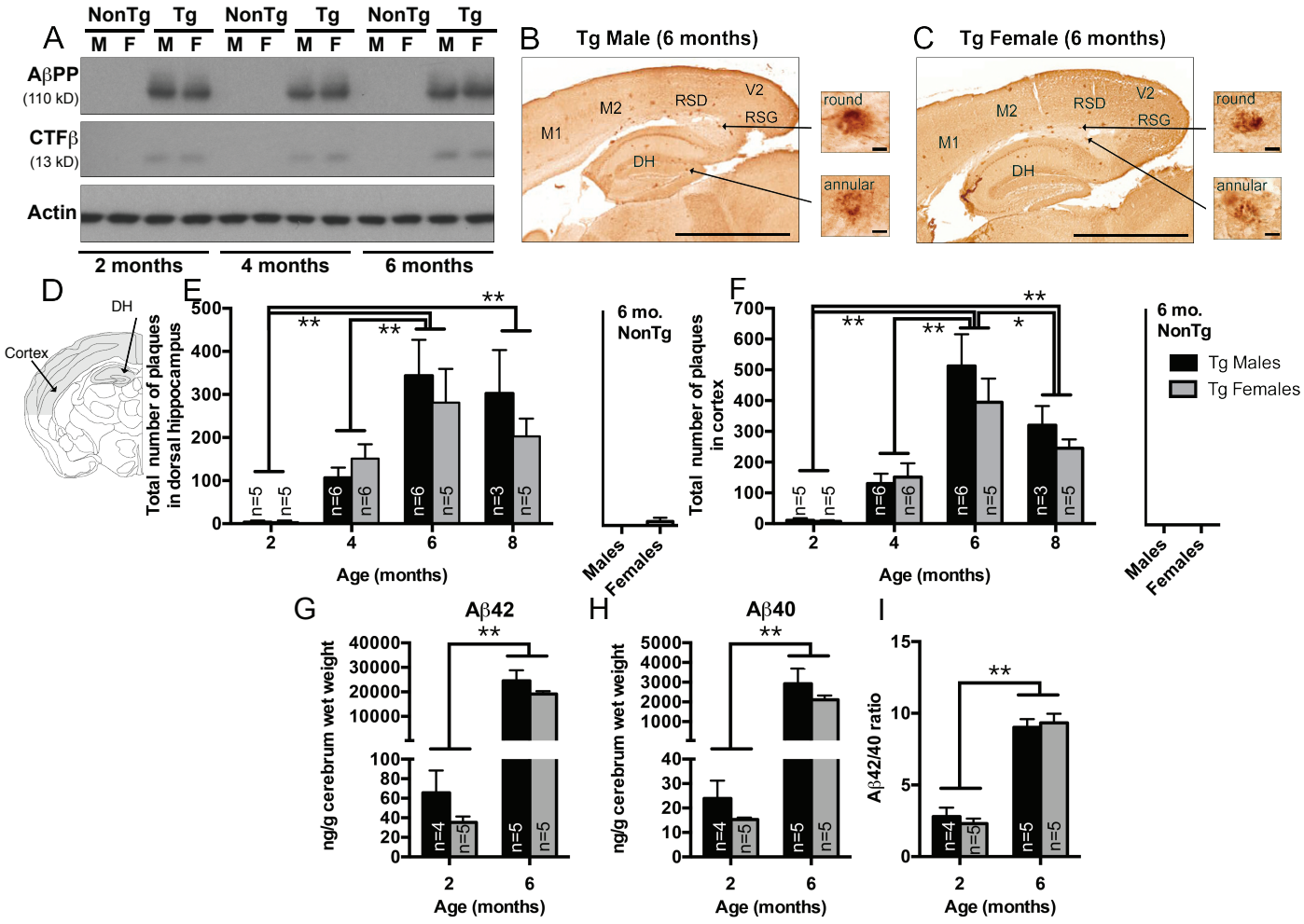
A
NonTg Tg NonTg Tg NonTg Tg
M F M F M F M F M F M F
AβPP
(110 kD)
CTFβ
(13 kD)
Actin
2 months
4 months
6 months
B
Tg Male (6 months)
M1
M2
RSD
V2
RSG
DH
round
annular
C
Tg Female (6 months)
D
DH
Cortex
E
Total number of plaques in dorsal hippocampus
Age (months)
6 mo. NonTg
Males
Females
F
Total number of plaques in cortex
Age (months)
6 mo. NonTg
Tg Males
Tg Females
G
Aβ42
ng/g cerebrum wet weight
Age (months)
H
Aβ40
ng/g cerebrum wet weight
Age (months)
I
Aβ42/40 ratio
Age (months)

Figure 3.1

deposits at 6 months in sagittal sections of Tg males and females (Fig. 3.1B,C). Aβ deposits with dense-core (both round and annular) morphologies were enriched in the cortex (specifically retrosplenial, parietal association, and primary sensory cortices) and hippocampus (Fig. 3.1B,C). We quantified total plaque numbers in serial coronal sections at 2, 4, 6, and 8 months of age in dorsal hippocampus and these cortical regions by stereology (Fig. 3.1D-F). Data were analyzed by two-way ANOVA identifying main effects of age (Hippocampus: $F_{(3,33)}=13.15$, $p<0.001$; Cortex: $F_{(3,33)}=22.14$, $p<0.001$) but not sex (Hippocampus: $F_{(1,33)}=0.590$, $p>0.05$; Cortex: $F_{(1,33)}=1.092$, $p>0.05$). Rare Aβ deposits were detected at 2 months of age in both Tg males and females (Fig. 3.1E,F). Statistically significant increases were evident at 6 and 8 months compared to 2 or 4 months (*post hoc* Tukey's tests Fig. 3.1E,F). Plaque load in hippocampus and cortex was equivalent in males and females at all time points. Few to no 4G8-reactive deposits were detected in NonTg mice (Fig. 3.1E-F). Soluble and insoluble $A\beta_{40}$ and $A\beta_{42}$ peptide levels were quantified in the cerebrum of male and female Tg mice at 2 and 6 months (Fig. 3.1G,H). A significant increase in $A\beta_{40}$ and $A\beta_{42}$ peptide levels was evident between 2 and 6 months of age in both males and females (Fig. 3.1G,H; $A\beta_{42}$: $F_{(1,15)}=85.6$, $p<0.0001$; $A\beta_{40}$: $F_{(1,15)}=33.65$, $p<0.0001$) with a significant increase in the $A\beta_{42}$ / $A\beta_{40}$ ratio evident by 6 months of age (Fig. 3.1I; $F_{(1,15)}=139.1$, $p<0.0001$). No sex differences in peptide levels were detected ($A\beta_{42}$: $F_{(1,15)}=1.319$, $p>0.05$; $A\beta_{40}$: $F_{(1,15)}=0.9201$, $p>0.05$; Ratio: $F_{(1,15)}=0.0241$, $p>0.05$).

3.6.2 Tg males undergo a higher Aβ-associated mortality rate than females.

In cortex but not hippocampus, a statistically significant decline in plaque number was observed at 8 compared to 6 months of age in both sexes (Fig. 3.1D-F). To test whether this decline was due to mortality, we compared the natural survival rates of N4 and N5 Tg mice with the parental F1 C57Bl/6 x C3H/HeJ Tg line over a 6-month observation period. The 75% and 50% survivorship of the F1 TgCRND8 line is 85 days (2.8 months) and 260 days (8.7 months) of age respectively when males and females are considered collectively (Chishti et al., 2001). Our N4 and N5 Tg mice exhibited a comparable collective 75% survivorship (80 days, 2.6 months). Fifty-six percent of N4/N5 Tg mice survived to the end of our observation period (6 months of age) (Chishti et al., 2001). When males and females were analyzed separately (Fig. 3.2), we found that survival was significantly compromised in both sexes (Mantel-Cox: Males χ^2=8.8, df=1, p<0.01; Females χ^2=12.5, df=,1 p<0.01). Mutant AβPP overexpression, however, was less lethal to Tg females than males (Mantel-Cox: χ^2=4.3, df=1, p<0.05). The 50% survivorship for males was 112 days (3.7 months); 60% of females survived to 6 months of age. Thus, while we cannot rule out definitively that the decline in plaque load between 6 and 8 months is not due to mortality of animals with highest Aβ load, these data do suggest that males are more susceptible to AβPP-associated lethality than females despite equivalent Aβ and plaque load.

We further asked whether hormonal status was disrupted in female Tgs by comparing estrous cycles with NonTg littermates. Acyclicity indicates the onset of reproductive senescence, the human equivalent of menopause and associated with increased risk of AD phenoconversion. This could dramatically skew behavioural

Figure 3.2 – Tg females modulate lethality associated with AβPP overexpression better than Tg males. Cumulative survival as a function of sex was tracked between 50-181 days of age (n=21 NonTg males, n=44 Tg males, n=54 NonTg females, n=161 Tg females). Survival of female Tg mice was significantly better than males. Statistics were Mantel-Cox log-rank tests.

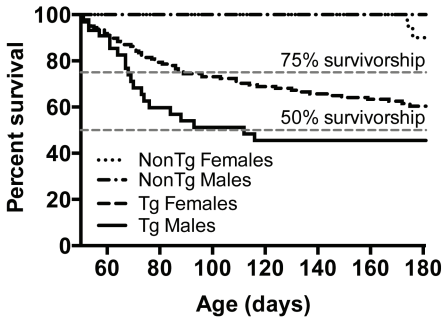
100
80
60
40
20
0
Percent survival
75% survivorship
50% survivorship
NonTg Females
NonTg Males
Tg Females
Tg Males
60
80
100
120
140
160
180
Age (days)

Figure 3.2

outcomes in this model. Tg females exhibited regular estrous cycles (Supplemental Fig. 3.2). There were no differences in the length of cycles between Tg and NonTg females (Supplemental Fig. 3.2).

3.6.3 NonTg males adopt spatial navigational strategies faster than females in the MWM; NonTg females exhibit higher indices of anxiety than males when first exposed to the MWM

To determine whether adult NonTg males and females exhibit inherent sex differences learning and memory in the absence of Aβ pathology, we compared their acquisition of the MWM (Fig. 3.3A). Data were analyzed by two-way repeated measures ANOVA followed by Tukey's *post hoc* for multiple comparisons. As expected, time to find the escape platform progressively decreased with repeated testing in both sexes indicative of learning and memory (main effect of time: $F_{(7,322)}=24.64$, $p<0.001$, Fig. 3.3A). Performance was comparable between sexes (main effect of sex: $F_{(1,46)}=3.25$, $p>0.05$, Fig. 3.3A). After eight days of testing, the escape platform was removed and spatial bias for the correct quadrant was quantified in a probe trial (Supplemental Fig. 3.3A). Both males and females exhibited significant (and comparable) spatial biases for the correct quadrant, indicative of *bona fide* spatial learning and memory (One sample t-test: Males, $t=8.147$; $df=20$, $p<0.0001$; Females $t=5.069$; $df=26$, $p<0.0001$, Supplemental Fig. 3.3A).

Analysis of simple effects of test days suggested that platform acquisition was, however, mildly accelerated in males. Escape latencies differed significantly over the first three days in males compared to their maximal MWM performance (i.e., test day eight, simple effect of days, *post hoc* Tukey's pairwise comparisons, Fig. 3.3A). In females,

Figure 3.3 – NonTg mice do not exhibit sexual dimorphisms in learning and memory in the MWM. (A) Escape latencies of 5.5-month old male and female NonTg mice are comparable across all test days. Data represent average escape latency ± SEM. Statistics were two-way repeated measures ANOVA. *Post-hoc* Tukey's multiple comparisons testing simple effects of the main effect of test day indicated learning was mildly accelerated in males, ††p<0.01, †p<0.05 in NonTg females versus test day eight. ##p<0.01 in NonTg males versus test day eight. (B) MWM search strategy classifications. Time in maze is color-coded as indicated in the time bar. (C) The percentage of spatial strategies ± SEM used by NonTg males was higher on test day one compared females. Statistics were unpaired Student's t-test, *p<0.05. (D) NonTg male mice (top panel) transitioned from primarily systematic to primarily spatial search strategies one day earlier than females (bottom panel). Symbols are defined in (B). Data represent the percentage of search strategies used in the four trials per day over eight test days ± SEM. Statistics were two-way repeated measures ANOVA followed by *post hoc* Tukey's test examining the significant test day x strategy interaction, *p<0.05, **p<0.01 looping or spatial versus systematic. (E) NonTg males independently find the escape platform faster than females. Data represent mean number of trials ± SEM to obtain the escape platform. Statistics were unpaired Student's t-test, *p<0.05. (F) NonTg females display more thigmotaxic behaviors indicative of anxiety on test day one than males. Data represent the percent thigmotaxis ± SEM in n=21 NonTg males and n=27 NonTg females. Statistics were unpaired Student's t-test, *p<0.05.

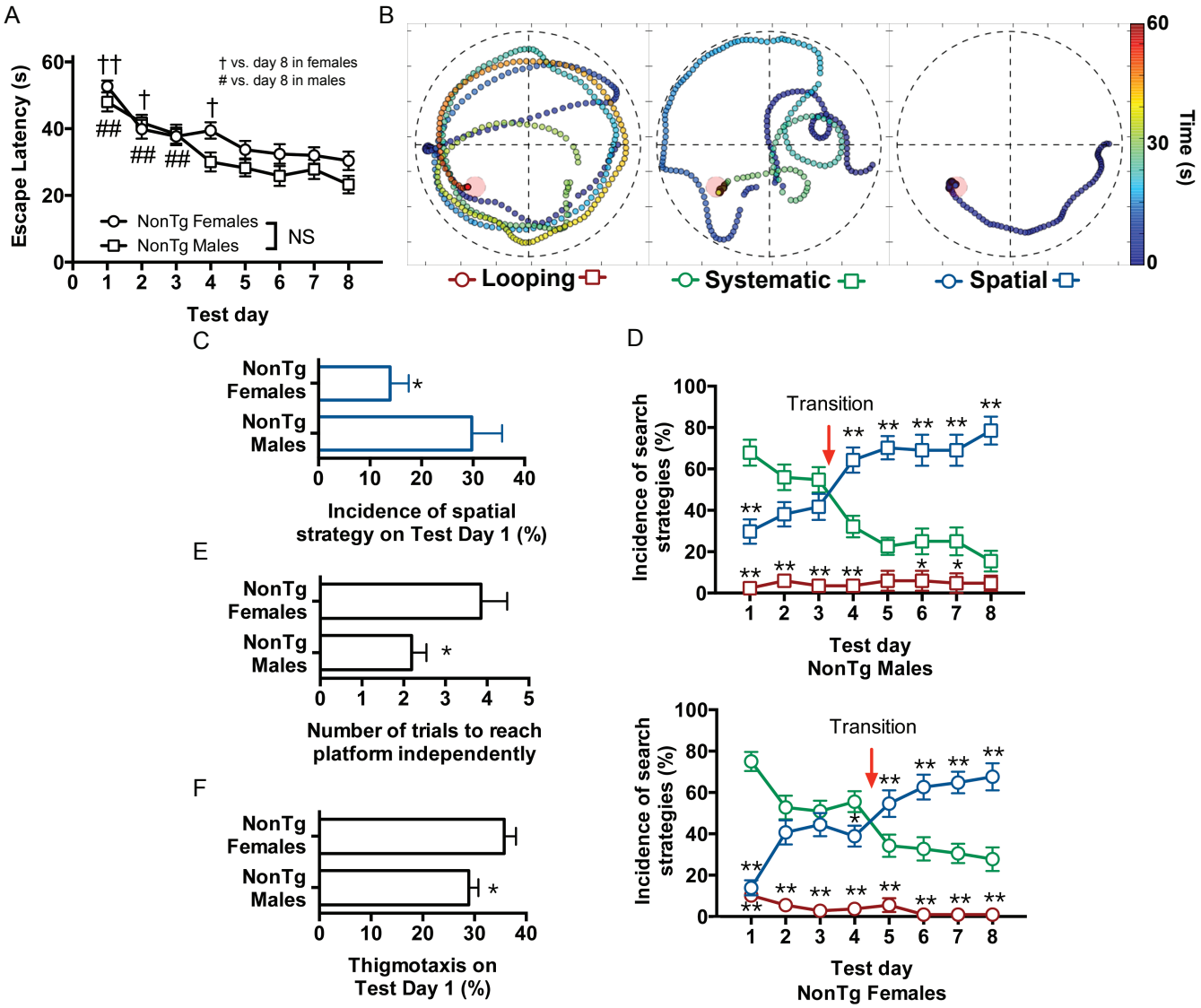
A
Escape Latency (s)
60
40
20
0
0 1 2 3 4 5 6 7 8
Test day
†† † † ## ## ##
† vs. day 8 in females
# vs. day 8 in males
NonTg Females
NonTg Males
NS
B
Looping
Systematic
Spatial
60
30
0
Time (s)
C
NonTg Females
NonTg Males
*
0 10 20 30 40
Incidence of spatial strategy on Test Day 1 (%)
D
Incidence of search strategies (%)
100
80
60
40
20
0
Transition
1 2 3 4 5 6 7 8
Test day
NonTg Males
E
NonTg Females
NonTg Males
*
0 1 2 3 4 5
Number of trials to reach platform independently
F
NonTg Females
NonTg Males
*
0 10 20 30 40
Thigmotaxis on Test Day 1 (%)
Incidence of search strategies (%)
Transition
Test day
NonTg Females

escape latencies were significantly elevated on test day 4 (Fig. 3.3A). To assess whether this subtle difference reflected sexual dimorphisms in behavioural flexibility, we asked whether spatial learning was triggered in males and females at different rates. The murine MWM learning process has been well characterized (Brody and Holtzman, 2006; Janus, 2004; Wolfer and Lipp, 2000). Typically, on first exposure to the pool, mice swim in a looping or chaining fashion in close proximity to pool wall (Wolfer and Lipp, 2000) (Fig. 3.3B, left panel). Mice must exhibit behavioural flexibility to overcome this tendency and randomly deviate into the pool interior to make first contact with the escape platform. This independent discovery of the platform initiates the spatial learning process triggering a systematic maze exploration wherein mice deliberately explore the entire pool in search of the escape platform (Wolfer and Lipp, 2000) (Fig. 3.3B, middle panel). With repeated testing, cognitively intact animals will then transition from predominantly systematic to predominantly spatial search strategies (Brody and Holtzman, 2006; Janus, 2004; Wolfer and Lipp, 2000) (Fig. 3.3B, right panel). Spatial searches require that animals use distal intra- and extra-maze cues to navigate directly to the escape platform (Brody and Holtzman, 2006; Janus, 2004; Wolfer and Lipp, 2000). Once spatial navigation strategies are adopted, escape latencies plateau and animals are considered to have acquired the MWM to their maximal performance (Wolfer and Lipp, 2000). We found that NonTg males adopted spatial search strategies faster than NonTg females (Fig. 3.3C,D). Males exhibited a higher incidence of spatial navigation as early as test day 1 ($t=2.569$, $df=40$, $p<0.05$, Fig. 3.3C). Males also transitioned from a predominantly systematic to spatial strategy one day earlier than females (Two-way repeated measures ANOVA, test day x strategy interaction: Males $F_{(14,420)}=17.05$, $p<0.0001$; Females, $F_{(14,546)}=16.20$, $p<0.0001$,

post hoc Tukey's pairwise comparison, $p<0.05$, Fig. 3.3D). As expected, once both sexes adopted primarily spatial strategies, escape latencies plateaued (test day 3-8 in males, test day 4-8 in females). No further navigational improvements were attained (compare Fig. 3.3A and D).

We next asked why spatial learning is triggered moderately faster in NonTg males compared to females. If female mice do not independently find the platform as fast as males, they will not initiate the spatial learning process as rapidly (Wolfer and Lipp, 2000). To test this hypothesis, we calculated the number of trials needed for both sexes to independently discover the MWM platform (Fig. 3.3E). Males randomly found the escape platform significantly earlier than females ($t=2.130$, $df=46$, $p<0.05$). We next assessed known impediments to behavioural flexibility. Anxiety manifested as thigmotaxis has been shown to delay random exploration of the interior of the MWM (Wolfer and Lipp, 2000). NonTg females exhibited more thigmotaxic swim patterns when first introduced to the MWM on test day 1 than males (Test Day 1, $t=2.242$, $df=46$, $p<0.05$, Fig. 3.3F) yet without significant overall differences in anxiety with repeated MWM exposure when averaged over the entire test period (ANOVA, $F_{(3,76)}=1.823$, $p>0.05$, Supplemental Fig. 3.3B). Elevated thigmotaxis on test day 1 in females was independent of motor impairment. Average distance moved was comparable regardless of sex both on test day 1 (ANOVA, $F_{(3,76)}=21.88$, $p<0.0001$, *post hoc* Holm-Sidak's multiple comparisons NonTg males vs. NonTg females, $p>0.05$, Supplemental Fig. 3.3C) and across the entire test period (ANOVA $F_{(3,76)}=27.67$, $p<0.0001$, *post hoc* Holm-Sidak's multiple comparisons NonTg males vs. NonTg females, $p>0.05$, Supplemental Fig. 3.3D). Moreover, both males and females swam at the same speed on day 1 (ANOVA, $F_{(3,76)}=17.68$, $p<0.0001$,

post hoc Holm-Sidak's multiple comparisons NonTg males vs. NonTg females, $p>0.05$, Supplemental Fig. 3.3E) and across the entire test period (ANOVA, $F_{(3,76)}=5.197$, $p<0.01$, *post hoc* Holm-Sidak's multiple comparisons NonTg male vs. NonTg female, $p>0.05$, Supplemental Fig. 3.3F). Taken together, these data suggested that learning and memory is comparable regardless of sex in this genetic background but that NonTg females do exhibit an initial anxiety-based delay in the independent discovery of the escape platform.

3.6.4 Learning and memory deficits in Tg mice are sexually dimorphic by 5.5 months of age.

Previous studies have tested learning and memory in the MWM in TgCRND8 males and females either collectively (Chishti et al., 2001; Francis et al., 2012; Janus, 2004; Lovasic et al., 2005) or restricting analyses to a single sex (Adlard et al., 2005; Hyde et al., 2005). To our knowledge, the performances of males and females have yet to be directly compared in the MWM. When we included equal numbers of 5.5 month-old N4 and N5 male and female Tg mice, we found significant deficits in escape latency (Two-way repeated measures ANOVA: Main effect of genotype, $F_{(1,62)}=32.26$, $p<0.0001$) and average time spent in the platform zone ($t=3.992$, $df=62$, $p<0.001$) (Supplemental Fig. 3.4A,B). When compared separately, females exhibited markedly different learning and memory deficits than males (Fig. 3.4A-F, Supplemental Fig. 3.3A-F). MWM acquisition was severely impaired in Tg females (Two-way repeated measures ANOVA: Main effect of genotype, $F_{(1,46)}=23.32$, $p<0.0001$, Fig. 3.4A). Tg females did not show the progressive improvement in escape latencies over the 8 test days seen in NonTg females (Fig. 3.4A).

Figure 3.4 – Tg males and females exhibit different behavioral impairments in the MWM independent of anxiety or motor behaviors. (A) Tg females are significantly impaired compared to their NonTg female littermates at 5.5 months of age. (B) Tg males are only mildly impaired at 5.5 months of age with little to no difference in their rate of MWM acquisition compared to NonTg male littermates. (C) Male Tg mice outperform female Tg mice. In A-C, data represent average escape latencies $\pm$ SEM. Statistics were a two-way repeated measures ANOVA. Main effects of genotype are indicated in the legends, *p<0.05, **p<0.01. Significant genotype x test day interactions were analyzed by post-hoc Holm-Sidak multiple comparison tests comparing mice on each test day as indicated, *<p<0.05 and **p<0.01. (D) Tg males spend significantly more time exploring the escape quadrant than Tg females. (E) Tg males and females exhibit comparable thigmotaxis on test day one. (F) Tg males and females independently obtain the escape platform within comparable numbers of trials. In D-F, statistics were unpaired Student's t-tests, **p<0.01. Data represent n=11 Tg males and n=21 Tg females.

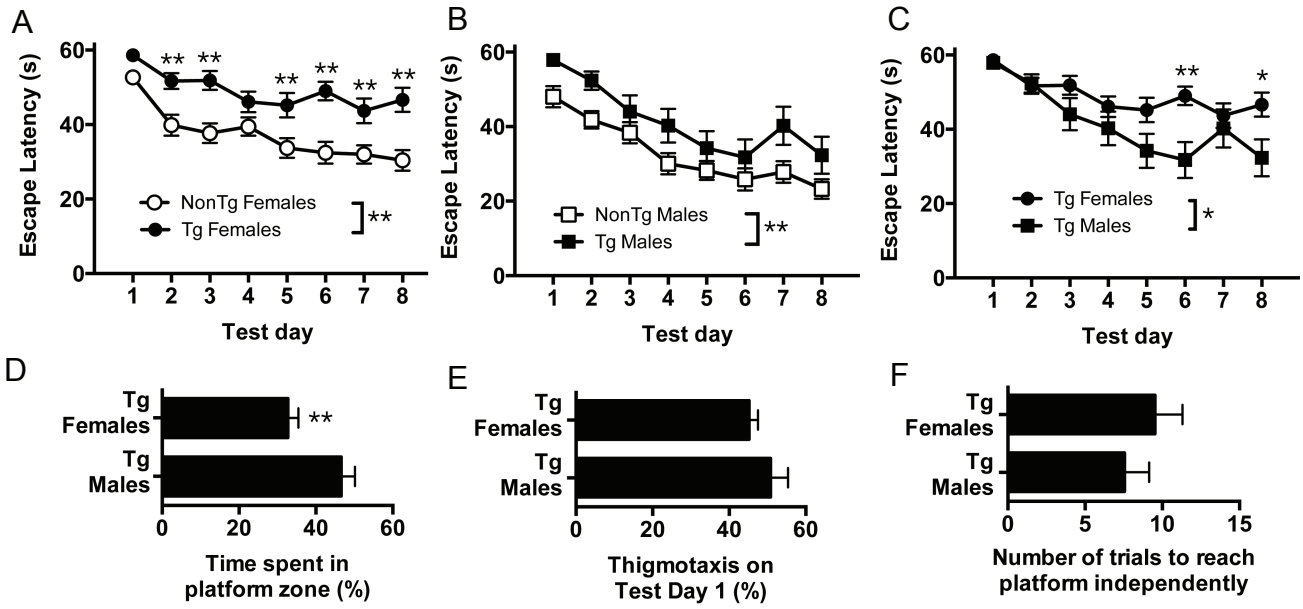
A
Escape Latency (s)
60
40
20
0
1 2 3 4 5 6 7 8
Test day
** ** ** ** ** **
NonTg Females
Tg Females
**
B
Escape Latency (s)
60
40
20
0
1 2 3 4 5 6 7 8
Test day
NonTg Males
Tg Males
**
C
Escape Latency (s)
60
40
20
0
1 2 3 4 5 6 7 8
Test day
** *
Tg Females
Tg Males
*
D
Tg Females
Tg Males
**
0 20 40 60
Time spent in platform zone (%)
E
Tg Females
Tg Males
0 20 40 60
Thigmotaxis on Test Day 1 (%)
F
Tg Females
Tg Males
0 5 10 15
Number of trials to reach platform independently

Figure 3.4

Moreover, Tg females failed to exhibit any spatial bias greater than chance for the escape quadrant during the probe trial (One sample t-test: t=0.552, df=20, p>0.05 Supplemental Fig. 3.3A). These data were not due to an irregular estrus cycle in Tg females. Tg females exhibited comparable cycle lengths to NonTg females (Supplemental Fig. 3.2). By contrast, Tg males exhibited only minor deficits in learning and memory (Fig. 3.4B). Despite higher overall average escape latencies (Two-way repeated measures ANOVA: Main effect of genotype $F(1,30)=8.088$, $p<0.01$), Tg male learning curves were comparable to that of NonTg males (Fig. 3.4B). Tg males were clearly capable of spatial learning as they exhibited significant spatial bias for the escape quadrant during the probe trial ($t=4.174$, $df=10$, $p<0.01$, Supplemental Fig. 3.3A). Furthermore, Tg males consistently outperformed Tg females (Two-way repeated measures ANOVA: Main effect of sex $F_{(1,30)}=5.675$, $p<0.05$; Fig. 3.4C). Tg males spent significantly more time searching the correct quadrant over the 8 test days ($t=3.03$, $df=30$, $p<0.01$; Fig. 3.4D) and exhibited significantly higher spatial bias during the probe trial than Tg females (ANOVA, $F_{(3,76)}=5.05$, $p<0.01$, *post hoc* Holm-Sidak's multiple comparisons, $p<0.01$; Supplemental Fig. 3.3A).

3.6.5 Sexually dimorphic learning and memory deficits in N4 and N5 Tg mice are independent of anxiety, motor impairment, and visual deficits

These sex differences were not due to higher test-related anxiety in Tg females (Fig. 3.4E). Both Tg males and females exhibited comparable thigmotaxic behaviours on the first test day ($t=1.221$, $df=30$, $p>0.05$; Fig. 3.4E) and overall anxiety indices did not differ between male or female Tg or NonTg mice over the entire test period (ANOVA,

main effect of sex: $F_{(1,76)}$=3.355, p>0.05; Main effect of genotype: $F_{(1,76)}$=0.038, p>0.05, Supplemental Fig. 3.3B). The frequency of thigmotaxic behaviours in Tg males and females on Test Day 1 was, however, higher than that observed in NonTg females although this comparison did not reach statistical significance (compare Fig. 3.3F with Fig. 3.4E). Both Tg males and Tg females required more trials than NonTg mice to independently find the escape platform for the first time (compare Fig. 3.3E with Fig. 3.4F); however unlike cognitively intact NonTg mice, Tg males and Tg females were equally impaired (t=0.7238, df=30, p>0.05; Fig. 3.4F). Tg males did not independently obtain the platform faster than Tg females thus had no temporal advantage in their initiation of spatial learning (t=0.7238, df=30, p>0.05; Fig. 3.4F). Motor performance was also comparable between Tg males and females (Supplemental Fig. 3.3C-F). Both sexes swam significantly further (ANOVA, $F_{(3,76)}$=27.67, p<0.0001, *post hoc* Holm-Sidak's multiple comparisons, p<0.01) and faster (i.e., more hyperactive) (ANOVA, $F_{(3,76)}$=5.197, p<0.01, *post hoc* Holm-Sidak's multiple comparison, p<0.01) than their NonTg littermates.

A potential confound in the assessment of learning and memory in AβPP Tg mouse models is the impact of their genetics on vision. Spatial navigation in the MWM requires adequate vision under defined illumination conditions to process intra and extra-maze cues. C57BL/6 mice exhibit no visual impairments (Gil-Pages et al., 2013). C3H/HeJ mice are homozygous for the autosomal recessive retinal degeneration *pde6b*^{rd1} mutation and thus functionally blind (Chang et al., 2002). The F1 TgCRND8 parental line is *pde6b*$^{rd1/+}$ and expected to show increased photosensitivity (Hussain et al., 1992). In our colony, sibling matings produced sighted F2 *pde6b*$^{+/+}$ wild-type mice, photosensitive *pde6b*$^{rd1/+}$ heterozygotes, and blind *pde6b*$^{rd1/rd1}$ homozygotes (Fig. 3.5A). The mice used

Figure 3.5 – N4 Tg mice are photosensitive yet without significant impairment of visual acuity in the MWM. (A) Genotypes of representative progeny derived from sibling mating of the C57Bl/6 x C3H/HeJ TgCRND8 parental line (F2 Tg, left panel), N4 Tg mice (center panel), and N5 Tg mice (right panel) for the A□PP transgene (top panel) and the *pde6b*^{rd1} retinal degeneration mutation (bottom panel). (B) SLAG testing of sighted *pde6b*$^{+/+}$ C57BL/6 mice, functionally blind *pde6b*$^{rd1/rd1}$ C3H/HeNCrl mice, and N4 *pde6b*$^{rd1/+}$ and *pde6b*$^{+/+}$ NonTg and Tg males and females. (C) No sex difference in photosensitivity was detected in N4 NonTg or Tg mice. In (B,C), data represent average percentage of SLAG+ responses ± SEM. Statistics were ANOVA with *post hoc* Dunnett's t-tests comparing each group to the C57BL/6 control, *p<0.05, **p<0.01. (C) SLAG analysis of sex differences within NonTg and Tg genotypes. There are no sex differences in photosensitivity. (D) NonTg and Tg males and females rapidly acquire the MWM when the escape platform is made visible. Data represent average escape latency ± SEM. Data represent n=16 NonTg males, n=9 Tg males, n=6 NonTg females and n=7 Tg females.

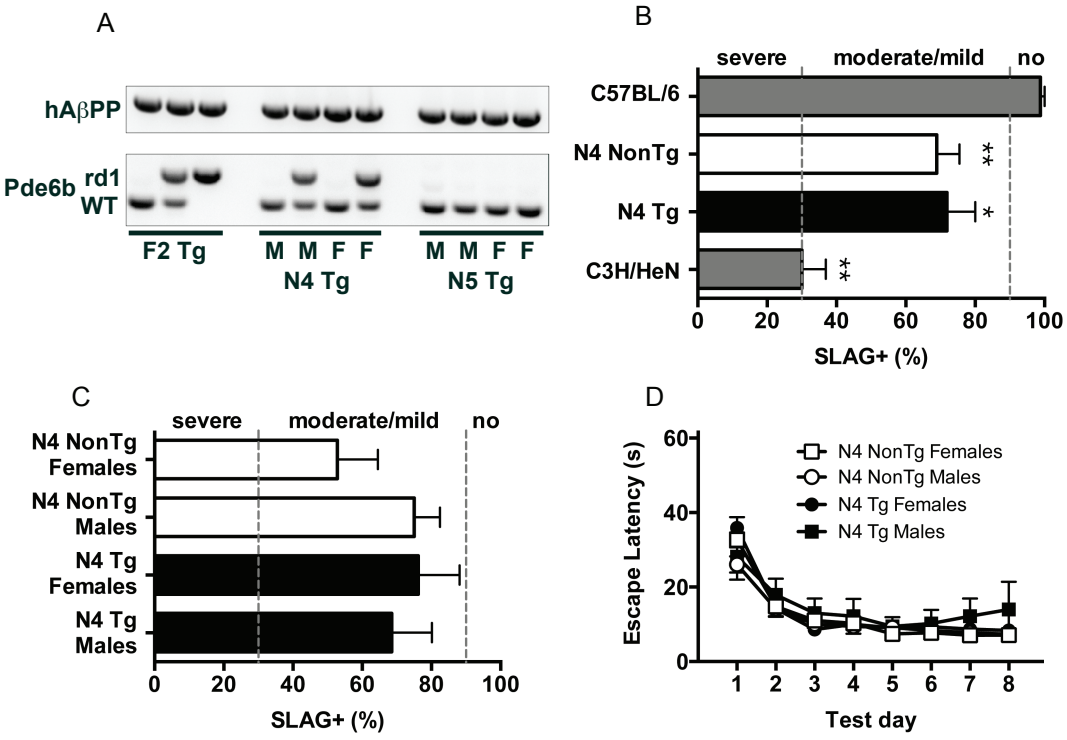
A
hAβPP
Pde6b rd1
WT
F2 Tg
M M F F
N4 Tg
M M F F
N5 Tg
B
severe
moderate/mild
no
C57BL/6
N4 NonTg
N4 Tg
C3H/HeN
**
*
**
0 20 40 60 80 100
SLAG+ (%)
C
severe
moderate/mild
no
N4 NonTg Females
N4 NonTg Males
N4 Tg Females
N4 Tg Males
0 20 40 60 80 100
SLAG+ (%)
D
N4 NonTg Females
N4 NonTg Males
N4 Tg Females
N4 Tg Males
Escape Latency (s)
60
40
20
0
1 2 3 4 5 6 7 8
Test day

Figure 3.5

in this study (both males and females) retained the mutant *pde6b*^{rd1} allele to the N4 generation and were a mix of heterozygotes and wildtype (Fig. 3.5A). This allele was bred out of breeding pairs by the N5 generation (Fig. 3.5A). We verified that our N4 Tg and NonTg *pde6b*$^{rd1/+}$ mice were photosensitive using the SLAG paradigm (Gil-Pages et al., 2013). As expected, C57BL/6 *pde6b*$^{+/+}$ mice showed no visual impairments (Fig. 3.5B). C3H/HeNCrl *pde6b*$^{rd1/rd1}$ mice were severely impaired by 6-9 months of age (Fig. 3.5B). We detected a mild to moderate photosensitivity in N4 Tg and Non Tg mice compared to C57BL/6 controls when tested under 600-700 lux illumination (ANOVA $F_{(3, 58)}$=7.773, p<0.0001; Dunnett's *post hoc* test vs. C57BL/6 mice; Fig. 3.5B). No sex differences were evident (ANOVA $F_{(3, 34)}$=0.842, p>0.05, Fig. 3.5C). We next used the cued MWM to confirm that this photosensitivity did not impair visual acuity required for spatial learning under the 100 lux MWM illumination levels. N4 NonTg and Tg male and female mice rapidly acquired the cued MWM confirming visual status. Performance approached the limit of detection by Ethovision software (approximately 10 s). There were no significant main effects of genotype or sex (Two-way repeated measures ANOVA: genotype: $F_{(1, 29)}$=0.855, p>0.05; sex: $F_{(1, 29)}$=0.007, p>0.05, Fig. 3.5D). Taken together, these data indicate that Tg sex differences in MWM performance are not a consequence of sexual dimorphisms in thigmotaxis (anxiety), visual impairment (photosensitivity), or hyperactivity (swim speed and distance).

3.6.6 Tg mice exhibit sex differences in behavioural indices of cognitive reserve

We asked whether the sex differences observed in MWM performance in N4 and N5 Tg mice reflected sexual dimorphisms in behavioural indices of cognitive reserve,

specifically compensation for Aβ associated behavioural impairments by effectively alternating between navigational search strategies in the Morris Water maze. In humans, cognitive reserve refers to the extent to which an individual can switch between alternative cognitive paradigms to cope with progressive Aβ pathology (Sperling et al., 2011; Stern, 2012). It has been previously established that (a) hyperactivity and (b) an elevated incidence of inefficient looping strategies in both MWM and open field tests are characteristic Aβ-associated behavioural impairments in F1 Tg mice (Janus, 2004; Walker et al., 2011; Walker et al., 2015). Our N4/N5 Tg males and females at 5.5 months of age exhibited these same Aβ-associated impairments manifested as repetitive circular swimming patterns in the MWM (Three-way repeated measures ANOVA, time x sex x genotype interaction: $F_{(7,\ 532)}=3.142$, $p<0.05$, main effect of genotype: $F_{(1,76)}=24.576$, $p<0.001$, Fig. 3.6A,B) with faster swim speeds and longer swim distances (Supplemental Fig. 3.3C-F). While these swim trajectories fall under the overarching MWM looping search strategy (Fig. 3.3B), their repetition are not considered part of the typical MWM acquisition sequence but rather indicative of pathology-associated stereotypy that reduces behavioural flexibility and thereby impedes the initiation of the spatial learning process (Wolfer and Lipp, 2000). Both Tg males and females exhibited significantly higher (yet equivalent) overall incidences of non-productive looping strategies across the entire test period (ANOVA $F_{(3,28)}=37.50$, $p<0.0001$, *post hoc* Holm Sidak's multiple comparisons, $p<0.01$; Fig. 3.6C). To assess whether Tg mice were able overcome this stereotypy by adopting alternative learning strategies, a behavioural index of cognitive reserve, we evaluated how well they were able to adapt to more efficient strategies with repeated MWM exposure. We found that Tg males were capable of switching

Figure 3.6 – Tg male but not female mice exhibit behavioral indices of cognitive reserve. (A) Representative example of the non-productive repetitive circling behavior exhibited by both Tg male and female mice in the MWM. (B) Tg male and female mice exhibit increased incidences of looping search strategies in the MWM compared to NonTg mice. Data represent the percentage of looping search strategies used per day over eight test days (32 trials) ± SEM. Statistics were a three-way repeated measure ANOVA. The significant main effect of genotype is indicated in the legend, **p<0.01. (C) Phenotypic impairments (looping) were comparable between Tg males and females and significantly elevated compared to NonTg sexes. Data represent the percentage of looping search strategies used over the entire test period ± SEM. Statistics were a one-way ANOVA with *post-hoc* Holm-Sidak multiple comparisons, ** p<0.01. (D) Tg males were capable of adopting alternative search strategies, transitioning from predominantly systematic to predominantly spatial navigation strategies on test day 4. (E) Tg females were unable to adopt spatial learning strategies effectively. By the end of the test period, their use of systematic and spatial strategies converged with incidences equivalent to that of non-productive pathological looping. In (D,E), data represent average daily search strategy incidence ± SEM. Statistics were two-way repeated measures ANOVA followed by *post hoc* Holm-Sidak tests examining the significant test day x strategy interactions, *p<0.05, **p<0.01 looping or spatial versus systematic. (F) Overall incidence of spatial strategies was significantly higher in Tg males than females. Data represent average ± SEM. Statistics were unpaired Student t-test, *p<0.05. Data represent n=21 NonTg males, n=11 Tg males, n=27 NonTg females and n=21 Tg females.

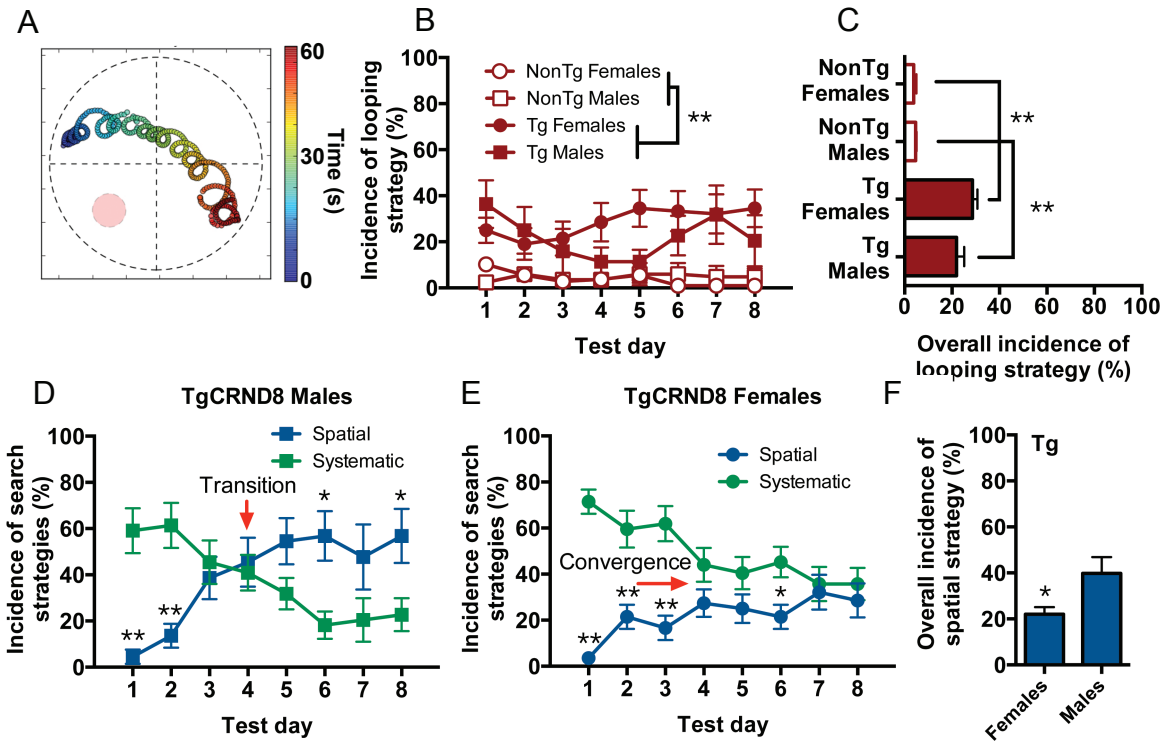
A
60
30
0
Time (s)
B
Incidence of looping strategy (%)
NonTg Females
NonTg Males
Tg Females
Tg Males
**
Test day
C
NonTg Females
NonTg Males
Tg Females
Tg Males
**
**
Overall incidence of looping strategy (%)
D
TgCRND8 Males
Spatial
Systematic
Transition
Incidence of search strategies (%)
Test day
E
TgCRND8 Females
Spatial
Systematic
Convergence
Incidence of search strategies (%)
Test day
F
Tg
Overall incidence of spatial strategy (%)
Females
Males

navigational search strategies more efficiently than females as demonstrated by a progressive increase in the incidence of spatial search strategies (Fig. 3.6D). Tg males transitioned from predominantly systematic to predominantly spatial search strategies by test day 6 (Two-way repeated measures ANOVA, test day x strategy interaction, ($F_{(7,140)}$=9.156, p<0.001; *post hoc* Holm-Sidak multiple comparisons p<0.05, Fig. 3.6D). Tg females were unable to effectively switch between search strategies and thus unable to initiate the spatial learning process (Fig. 3.6E). Tg females maintained a significantly higher incidence of systematic search strategies until test day 6 (two-way repeated measures ANOVA, test day x strategy interaction, $F_{(7,280)}$=9.053, p<0.0001; *post hoc* Holm-Sidak multiple comparisons p<0.05, Fig. 3.6E). They failed to transition to a predominantly spatial learning strategy, rather their use of systematic, spatial, and non-productive looping strategies converged, with females using all three strategies equally by the end of the test period (Fig. 3.6B,E). Males did not exhibit this impairment in behavioural flexibility until approximately 1 year of age thus modeling higher behavioural indices of cognitive reserve (Supplemental Fig. 3.5). As a result, Tg females at 5.5 months of age used significantly fewer spatial strategies than males (t=2.287, df=14, p<0.05; Fig. 3.6F).

3.7 Discussion

Here, we report that, when TgCRND8 mice are placed on an N4/N5 C57BL/6 background, they display sex differences in spatial learning that recapitulate some of the sexual dimorphisms in cognitive reserve associated with the greater risk of earlier AD phenoconversion in women (Barnes et al., 2005; Hua et al., 2010; Li et al., 2015; Lin and

Doraiswamy, 2014; Mielke et al., 2014; Vemuri et al., 2012). Despite equivalent Aβ burden as males, Tg females at 5.5 months fail to overcome Aβ-associated stereotypy (i.e., hyperactive repetitive tight circling behaviours (Ambree et al., 2006; Janus, 2004; Walker et al., 2011; Walker et al., 2015) and disproportionally transition to an AD-like phenotype in the MWM. By contrast, Tg males exhibit robust behavioural indices of cognitive reserve, effectively adopting alternative, increasingly productive search strategies with repeated testing. Phenoconversion and impaired behavioural flexibility is not observed until Tg males are approximately 12 months of age. These sexual dimorphisms in learning and memory are only observed in Tg mice in response to Aβ pathology NonTg male and female littermates show no differences in spatial learning and few dimorphisms in behavioural flexibility beyond a mildly higher level of anxiety when females are first exposed to the MWM. Taken together, these data describe a new phenotype in N4/N5 Tg mice that can be used to model sex differences in cognitive reserve associated with Aβ vulnerability.

To our knowledge, this is the first demonstration of sex differences in learning and memory in an AβPP mouse model wherein both sexes exhibit comparable Aβ load. In other AβPP models, the severity of learning and memory deficits corresponds with greater Aβ pathology in females (Callahan et al., 2001; Clinton et al., 2007; Gallagher et al., 2013; Hirata-Fukae et al., 2008; Schafer et al., 2007; Wang et al., 2003). Here, our N4/N5 Tg model behaviourally recapitulates clinical reports that men exhibit greater cognitive reserves in the face of equivalent (or higher) Aβ challenge than women (Irvine et al., 2012; Lin and Doraiswamy, 2014; Perneczky et al., 2007). It is important to note that we refer exclusively to the capacity to switch between cognitive strategies to cope with progressive

Aβ pathology as the aspect of cognitive reserve experimentally modeled in this study. Interestingly, these mice also model sex differences in lethality associated with Aβ-overexpression (Chishti et al., 2001). In studies of mild cognitive impairment, mortality has been reported to be higher in men than women despite equivalent Aβ load (Contador et al., 2014; Guehne et al., 2007; Vassilaki et al., 2015). We find that Aβ-associated lethality is also higher in N4/N5 Tg males than females between 2 and 6 months of age despite comparable Aβ load in cortex, hippocampus, and entire cerebrum. We have yet to assess whether this genetic background also recapitulates the sexual dimorphisms in age-associated memory impairment that occur independently of Aβ biogenesis. For example, in contrast to individuals with high Aβ load, learning and memory are reported to decline more rapidly in cognitively normal men than women in the absence of significant Aβ pathology (Jack et al., 2015). This decline is hypothesized to contribute to risk of late-life AD phenoconversion rates in males (Jack et al., 2015) also modeled in N4/N5 Tg males by their later life phenoconversion at 12 months of age. However, further research into age-associated cognitive decline in NonTg males will need to be investigated to elicit the degree of phenoconversion found in Tg males at 12 months. These distinctions are critical to therapeutic interventions targeting cognitive reserve in men and women with high and low Aβ load over time and it will be important to follow N4/N5 NonTg and Tg males and females beyond 8 months of age to evaluate whether this model reflects all three phenotypes (i.e., sexually dimorphic vulnerability to Aβ-associated learning and memory impairment, Aβ-associated lethality, age-associated cognitive decline).

Our data indicate that the N4/N5 Tg model can be used to assess inherent sex differences in Aβ vulnerability in males and females raised under identical conditions,

independent of reproductive senescence, alterations in estrous cycle/hormonal status, visual acuity deficits, or motor impairment. Thus, this model is uniquely suited to exploring molecular underpinnings of cognitive reserve and preclinical response to potential therapeutic intervention difficult to study in the clinic. Sociological differences in education level, occupational attainment, leisure activities, exercise, heart disease, and hypertension associated with gender, not sex, are purported to modulate both Aβ-associated mortality and cognitive reserve (Sobral et al., 2015; Vassilaki et al., 2015). Moreover, age-dependent hormonal status likely also contributes to enhanced risk of earlier AD phenoconversion in females than males (Irvine et al., 2012), albeit with controversy (Palm et al., 2012). As a result, it has been difficult to study sex differences in Aβ vulnerability directly without an optimal mouse model. The majority of studies examining cognitive reserve in AβPP transgenics have focused on assessing the effect of diet, environmental enrichment, or strategies designed to enhance neurogenesis on phenoconversion in a single sex to control for differences in Aβ biogenesis (Cracchiolo et al., 2007; Jankowsky et al., 2005; Jankowsky et al., 2003; Valero et al., 2014; Verret et al., 2013). While invaluable, these studies have not been able to address directly why males and females respond differently to Aβ challenge and to these interventions in particular. For example, when females from our parental TgCRND8 line are placed in an enriched environment or given voluntary access to a running wheel hippocampal neurogenesis and plasticity are enhanced (Herring et al., 2009), vascular dysfunction is reduced (Herring et al., 2008), and behavioural indices of learning and memory improve (Adlard et al., 2005). Tg males show a different response. Voluntary wheel running in males reduces Aβ associated stereotypy in males but without significant impact of

learning and memory (Richter et al., 2008). Placed in context with our study, likely amelioration of Aβ-associated behavioural impediments to spatial learning is more effective in females than males given that this stereotypy impair behaviour flexibility and reduce cognitive reserve to a greater extent in Tg females than males.

In summary, this study characterizes an AβPP transgenic model in which females and males exhibit comparable Aβ burden at all ages yet Tg females show enhanced vulnerability to Aβ pathology and Aβ-associated stereotypy, phenocovert in the MWM maze earlier, and exhibit fewer behavioural indices of cognitive reserve than males. We suggest that this line represents a novel preclinical model useful for testing strategies designed to enhance cognitive reserve by targeting the different Aβ vulnerabilities exhibited by males and females.

3.8 Acknowledgements

M.W.G. was supported by Ontario Graduate and the Saroj and Kishori Lal Family Scholarships. M.W.T was supported by a Natural Sciences and Engineering Research Council Canadian Graduate Scholarship-M. M.W.G., M.W.T., and B.F. received support from the Canadian Institutes of Health Research (CIHR) Training Program in Neurodegenerative Lipidomics (CTPNL) and the CIHR Institute of Aging (TGF-96121). This study was funded by NSERC # 5377 and CIHR MOP 311838 to S.A.L.B, and CIHR MOP 114914 to S.A.L.B and P.S.G.H. S.A.L.B. holds a University Research Chair in Neurolipidomics. We thank Graeme Taylor and Mark Akins for their expert technical assistance.

Supplemental Figure 3.1 – No sex-differences in cortical AβPP and CTFβ protein levels are detected at 2, 4, or 6 months of age. Full immunoblots at both exposures depicted in Figure 1 detecting human AβPP and CTFβ are provided to confirm specificity of labeling.

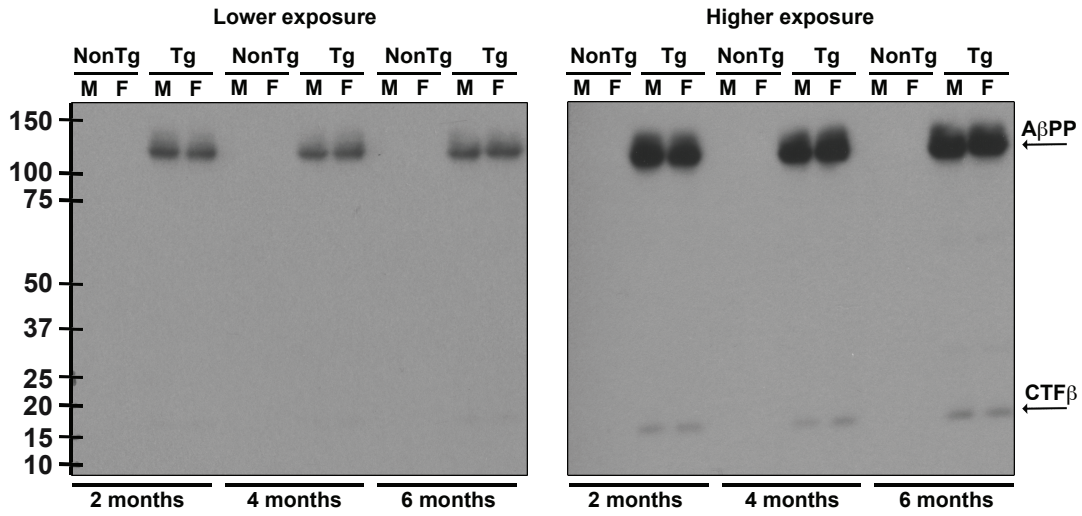
Lower exposure
Higher exposure
NonTg
Tg
M
F
150
100
75
50
37
25
20
15
10
AβPP
CTFβ
2 months
4 months
6 months

Supplemental Figure 3.2 – Tg and NonTg females have comparable estrous cycles. (A) Average estrous cycle length is comparable between NonTg and Tg females. Data represent mean ± SEM. (B) In both genotypes, mice exhibited comparable numbers of 3-4 or 5-6 days cycles. Longer cycles in both genotypes were attributed to extensions the metestrus/diestrus stages. Data represent n=7 NonTg females and n=7 Tg females.

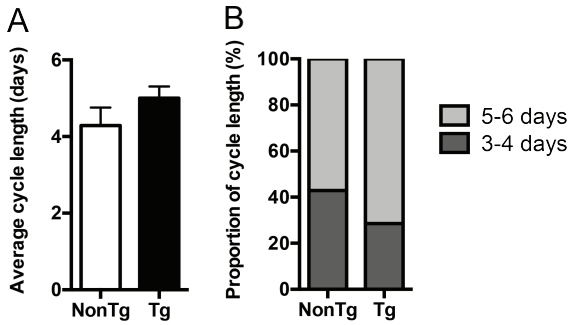

Supplemental Figure 3.2

Supplemental Figure 3.3 – Indices of learning and memory, anxiety, and motor capacity in NonTg and Tg males and females. (A) Spatial bias for the escape quadrant was assessed during the probe trial. Data represent the average amount of time mice spent exploring the correct escape quadrant ± SEM. Statistics were a one-sample t-test comparing each group to a hypothetical value of 25% representing the amount of time a mouse would be expected in the platform quadrant by chance, †p<0.01 ††p<0.001. Between group comparisons were performed by ANOVA and post-hoc Holm-Sidak comparisons, **p<0.01, *p<0.05. (B) Overall percentage of thigmotaxic behaviors across the entire test period ± SEM. (C) Average distance moved on test day one ± SEM. (D) The Average distance moved across all test days ± SEM. (E) Average velocity on test day one ± SEM. (F) Average velocity across the entire test period ± SEM. In (B-F), between group comparisons were performed by ANOVA and post-hoc Holm-Sidak comparisons, **p<0.01, *p<0.05. Data represent n=21 NonTg males, n=11 Tg males, n=27 NonTg females and n=21 Tg females.

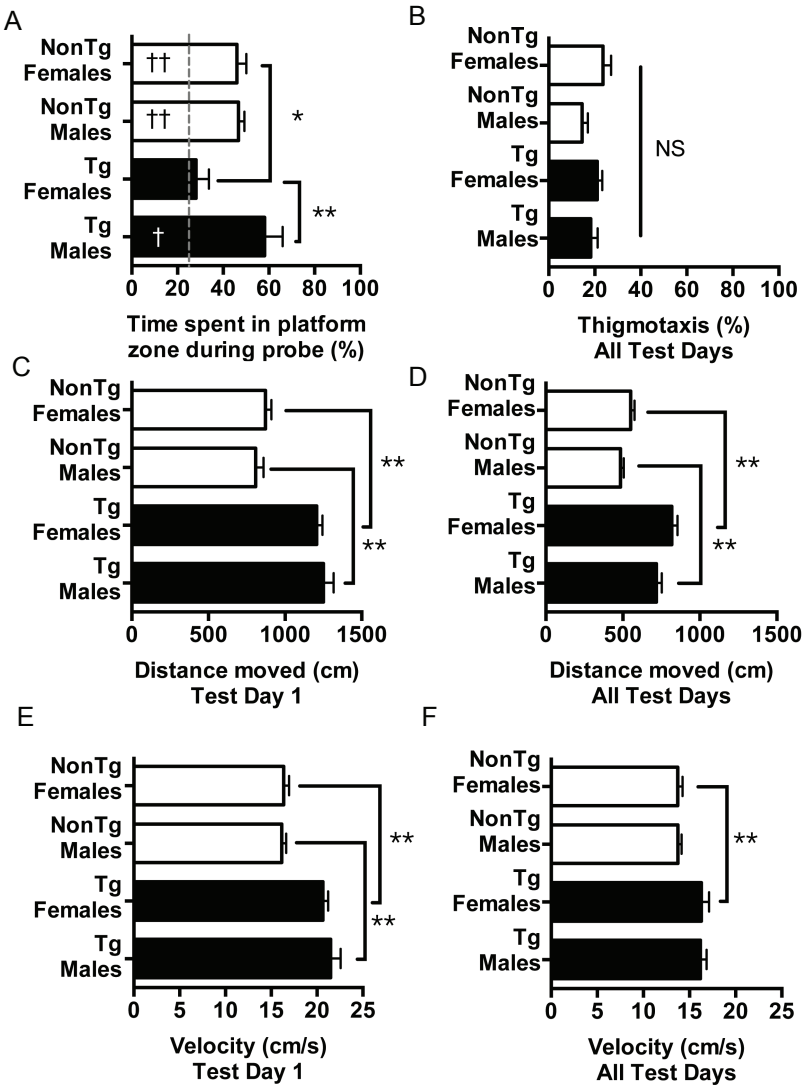
A
NonTg Females
NonTg Males
Tg Females
Tg Males
††
††
†
*
**
0 20 40 60 80 100
Time spent in platform zone during probe (%)
B
NonTg Females
NonTg Males
Tg Females
Tg Males
NS
0 20 40 60 80 100
Thigmotaxis (%) All Test Days
C
NonTg Females
NonTg Males
Tg Females
Tg Males
**
**
0 500 1000 1500
Distance moved (cm) Test Day 1
D
NonTg Females
NonTg Males
Tg Females
Tg Males
**
**
0 500 1000 1500
Distance moved (cm) All Test Days
E
NonTg Females
NonTg Males
Tg Females
Tg Males
**
**
0 5 10 15 20 25
Velocity (cm/s) Test Day 1
F
NonTg Females
NonTg Males
Tg Females
Tg Males
**
0 5 10 15 20 25
Velocity (cm/s) All Test Days

Supplemental Figure 3.4 – Tg mice exhibit learning and memory impairment in the MWM when both sexes are assessed collectively. (A) MWM acquisition in equal numbers of male and female Tg and NonTg mice. Data represent average escape latencies ± SEM. Statistics were two-way repeated measures ANOVA. The main effect of genotype is indicated in the legend, **p<0.01. (B) Tg mice spend less time exploring the correct quadrant across all test days. Data represent mean ± SEM. Statistics were an unpaired Student's t-test, **p<0.01. Data represent n=21 NonTg males, n=21 NonTg females, n=11 Tg males, and n=11 Tg females randomly selected from the entire cohort.

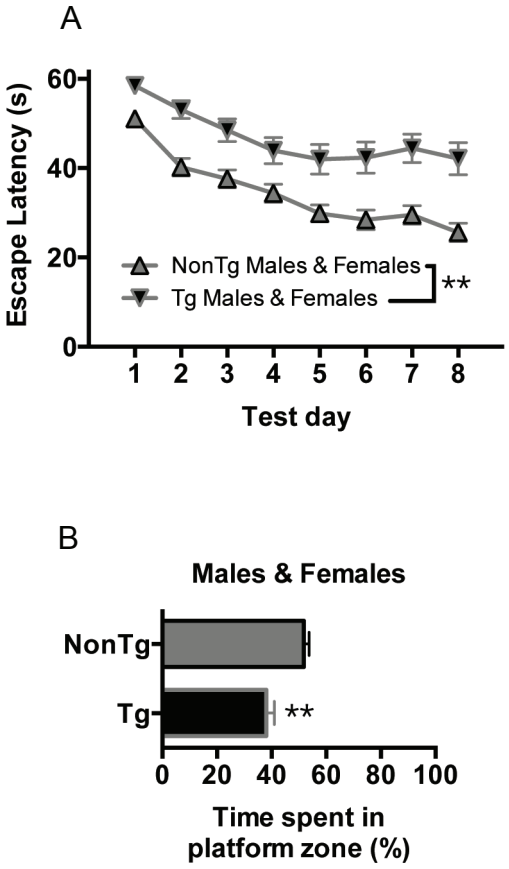
A
Escape Latency (s)
60
40
20
0
1 2 3 4 5 6 7 8
Test day
NonTg Males & Females
Tg Males & Females
**
B
Males & Females
NonTg
Tg
**
0 20 40 60 80 100
Time spent in
platform zone (%)

Supplemental Figure 3.5 – Tg males are unable to achieve a predominant spatial strategy at approximately 12 months age. Impairment in strategy shifting is detected in males by 12 months of age. By the end of the test period, the employment of systematic and spatial strategies converged with Tg males failing to adopt primarily spatial strategies. Data represent average daily search strategy incidence ± SEM. Statistics were two-way repeated measures ANOVA followed by *post hoc* Holm-Sidak tests examining the significant test day x strategy interactions, *p<0.05, **p<0.01 spatial versus systematic.

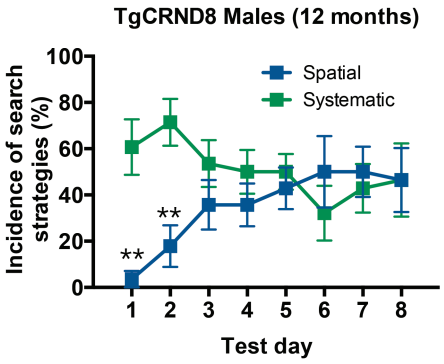

Supplemental Figure 3.5

Supplementary Table 3.1 – Genotyping Protocols

Gene	Reaction Conditions and Amplicon Sizes	Cycling parameters
AβPP	191: 5'GGCCGCGGAGAAATGAAGAAACGCCAAG-CGCCGTGACT-3' 229: 5'-TGTCCAAGATGCAGCAGAACGGCTACGAAAA-3' Final primer concentrations: 0.8 pmol/μL each Volume of DNA: 2 μL Final reaction volume: 12.5 μL (Tg allele = 1000 bp)	94°C 3 m *35 cycles:* 94°C 20 s 68°C 20 s 72°C 90 s 72°C 7 min
Pde6b	RD3: 5'-TGACAATTACTCCTTTTCCCTCAGTCTG-3' RD4: 5'-GTAAACAGCAAGAGGCTTTATTGGGAAC-3' RD6: 5'-TACCCACCCTTCCTAATTTTTCTCACGC-3' Final primer concentrations: 0.5 pmol/μL each Volume of DNA: 1 μL Final reaction volume: 25 μL (Wildtype allele = 550 bp) (Mutant allele = 400 bp)	94°C 2 m *35 cycles:* 94°C 30 s 68°C 30 s 72°C 120 s 72°C 10 min

Chapter 4: Associations between central and peripheral glycerophosphoethanolamine metabolism are linked to spatial learning and memory impairment in a mouse model of Alzheimer's disease

Matthew W. Granger[a], Hongbin Xu[a], Steffany A.L. Bennett[a]

[a]Neural Regeneration Laboratory, Ottawa Institute of Systems Biology, University of Ottawa Brain and Mind Research Institute, Centre for Catalysis Research and Innovation, Department of Biochemistry, Microbiology, and Immunology, University of Ottawa, Ottawa, ON, Canada.

Key words: Alzheimer's disease, glycerophosphocholines, glycerophosphoethanolamines, sexual dimorphism, cognitive reserve, TgCRND8 mice

Chapter 4: Associations between central and peripheral glycerophosphoethanolamine metabolism are linked to spatial learning and memory impairment in a mouse model of Alzheimer's disease.

4.1 Objective of study

Using the mouse model developed and characterized in Chapter 3, the objectives of this study were two-fold: (a) to determine sexually dimorphic differences in gylcerophospholipid metabolism associated with cognitive decline or cognitive reserve, and (b) to identify circulating glycerophospholipid indicators of these central changes.

4.2 Author contributions

MWG and SALB conceived and designed the experiments. MWG performed and analyzed all of the experiments. Tissue dissections and glycerophospholipid extractions were performed by HX and MWG. HPLC-ESI-MS/MS methodology was developed by HX and MWG.

4.3 Abstract

Alzheimer's disease is an insidious, progressive dementia that clinically presents as a progressive loss of cognition beginning with learning and memory ability. Metabolic determinants that contribute to this decline have only begun to be identified. Here, we show while GPC metabolism reflects a state of cognitive reserve, it is GPE metabolism that predicts severity of spatial learning and memory impairment in the N5 TgCRND8 mouse model of AD. Using a targeted lipidomic approach, we profiled GPC and GPE metabolism in plasma, hippocampus and cortex of N5 TgCRND8 mice and their NonTg littermates. We show that LPE(18:0/0:0) levels associate with severity of learning and memory impairment experimentally. Further, these changes and severity of behavioural deficits can be predicted by decreases in circulating abundances of LPE(16:1/0;)0), PE(O-14:1/2:0), and PE(O-18:3/2:0). Taken together, this is the first report that GPE metabolites can be used to predict individual learning and memory decline in an experimental model of AD.

4.4 Introduction

AD is a progressive neurodegenerative disorder characterized by the extracellular deposition of amyloid plaques and intracellular accumulation of hyperphosphorylated tau in the form of neurofibrillary tangles (Kang et al., 2017). Clinically, AD presents as a progressive decline in cognition that can begin with a prodromal form of the disease, aMCI. Further progression to AD dementia results in the loss of patient independence (Petersen et al., 2010a; Petersen et al., 2014). AD pathology and clinical decline, however, progress at different rates; the extent of AD pathology does not predict the onset or degree of AD dementia (Fiandaca et al., 2014; Pietrzak et al., 2015). Thus, individuals presenting with AD pathology but no cognitive impairment are diagnosed with “preclinical AD” (Sperling et al., 2011). This diagnosis can last decades before cognitive symptoms arise, with some patients expiring before any signs of impairment are found (Fiandaca et al., 2014; Pietrzak et al., 2015).

Sexual dimorphisms in AD are evidence of differential cognitive decline with AD pathogenesis. Two-thirds of AD patients are women (Mielke et al., 2014) because men are more resistant to cognitive decline, often requiring more advanced amyloid pathology than women to progress to AD dementia (Barnes et al., 2005; Petersen et al., 2010b). This resistance to cognitive decline has been, in part, attributed to the theory of cognitive reserve (Mielke et al., 2014; Stern, 2002, 2006, 2012). Cognitive reserve is defined as the capacity to adapt to a different cognitive strategies when challenged with AD pathology (Stern, 2006, 2012). Experimentally, behavioural indices of sexually dimorphic cognitive reserve can be modeled in N5 TgCRND8 mice (Granger et al., 2016). In N5 TgCRND8 mice, females are more impaired in a spatial learning and memory tasks than males

despite comparable levels of amyloid pathology. We concluded that this was due to the fact that males have the ability to adopt more efficient search strategies than females (Granger et al., 2016). This model provides the ideal opportunity to identify potential determinants (and biomarkers) that associate with susceptibility and resistance to cognitive decline in AD.

Glycerophospholipid metabolism is disrupted over the course of AD (Wong et al., 2017; Wood, 2012). Changes in regionally specific CNS GPC and GPE levels associate with learning and memory impairments in AD (Ginsberg et al., 1995; Guan et al., 1999; Han et al., 2001; Igarashi et al., 2011; Klein, 2000; Nitsch et al., 1992). Many of these studies were performed approximately 20 years ago and they laid the groundwork linking changes in glycerophospholipid metabolism with AD pathophysiology. Since then, a direct link between cognition and glycerophospholipids has been found, particularly a decrease in total diacyl and plasmalogen GPEs, in the cortical regions and cerebellum of AD patients (Han et al., 2001). It is less clear how these changes are predicted by differences in circulating lipid compositions. However, it is clear that circulating lipids are also linked with cognitive decline in AD with many lipid species identified as potential biomarkers of AD risk (Casanova et al., 2016; Mapstone et al., 2014; Proitsi et al., 2017; Whiley et al., 2014). While successes have certainly been made, questions ultimately remain of whether blood-based lipids are linked to brain-based lipids and if these relationships are predictive of cognitive ability in AD.

To address this question experimentally, we used a targeted lipidomic approach to profile GPC and GPE metabolites and signalling molecules between 450-650 m/z in the N5 TgCRND8 mouse model of AD. We show here that GPC metabolism is enhanced

in both the hippocampus and cortex of male Tg mice, yet the products of GPE catabolism in both the cortex and plasma were more closely associated with individual differences in learning and memory. Taken together, or data demonstrate how glycerophospholipid metabolism in the plasma can reflect regional differences in the brain lipidome associated with behavioural impairment.

4.5 Materials and Methods

4.5.1 Animals

In this study, a total of 20 mice were used to quantify brain and plasma glycerophospholipid metabolites and signalling molecules. Of these, 10 NonTgs and 10 TgCRND8 mice with an equal distribution of males and females were analyzed and compared. We have previously shown that N4 and N5 TgCRND8 mice exhibit sexually dimorphic behaviour through the ability to adapt to spatial strategies in the MWM (Granger et al., 2016). All details of their generation can be found in (Granger et al., 2016). Mice were fed a standard rodent chow (Harlan Teklad, 2018) *ad libitum* and were singly housed from 61 days of age. At 181 days of age (+/- 10 days), mice were sacrificed using 65 mg/mL euthanyl (1EUS001, Bimeda-MTC Animal Health Ins). Blood was collected in heparinized tubes (Eppendorf #022379216) and mice were decapitated. The hippocampus and the collective temporal, parietal, and entorhinal cortical regions were dissected and weighed along with the remainder of the cerebrum. Tissue was then flash-frozen in liquid nitrogen. Plasma was isolated by centrifuging the blood at 1500 x g for 15 minutes at 4^{o}C and removing the supernatant. Brain tissue and plasma were stored at -80^{o}C. All experiments were approved by the Animal Care Committee of the University of

Ottawa and were performed in accordance with the ethical guidelines implemented by the Canadian Council for Animal Care.

4.5.2 MWM and Composite Spatial Score

At 158 +/- 10 days of age, Tg and NonTg mice underwent eight test days followed by a probe day in the MWM as previously described (Granger et al., 2016). The circular MWM pool (ENV-594M-B, Med Associates Inc.) was 134.5 cm in diameter and 53.3 cm deep. The water was kept at 21^{o}C. The platform was 10 cm in diameter and remained 1 cm under the water line for the duration of the test days. To increase contrast for tracking software (Noldus Ethovision XT7 or XT8), non-toxic, white paint (506-BT12801O, Scholar's Choice) was added to enhance opacity of the water. Black visual cues on a white background were in the form of an "X" and a square on adjacent walls. Mice acclimated to the test room for one hour under white noise (70 dB; 2325-0144, San Diego Instruments) prior to the experiment. Each mouse completed four trials per test day with 20 minute intervals between each trial. All mice entered the water at four equally spaced locations around the pool in a different random order each day and their movements tracked for 60 seconds. Failure to find the platform resulted in the experimenter guiding the mouse to the platform for five seconds. The length of time a mouse required to find the platform in a given trial was considered the escape latency. Mean escape latencies were established, collapsing across all eight test days as a measure of spatial learning and memory. Additionally, the average time spent in the platform zone was also calculated across all eight test days as a measure of spatial orientation within the maze. Spatial strategy was defined as a specific, focally directed search with an evident

preference for the platform zone. Spatial strategy criteria were adapted from (Brody and Holtzman, 2006; Janus, 2004) and described in (Granger et al., 2016). Mean spatial strategy was calculated from the average incidence of spatial strategy across all eight test days.

A composite measure of spatial learning and memory impairment incorporating multiple measures of spatial learning and memory was developed by averaging z-scores of (a) mean escape latency, (b) average time spent in the platform zone, and (c) mean spatial strategy. Accommodations for the inverse natures of these variables (i.e. increases in mean escape latency and decreases in mean spatial strategy and average time in the platform zone all indicate impairment) were considered. To ensure consistent directionality, the inverse z-score of mean escape latency was calculated and utilized. Z-scores of each measurement was calculated across all 20 mice. The mean of all three z-scores of each mouse was determined as the composite spatial learning and memory score thus lower values are representative of greater impairment.

4.5.3 Aβ40 and Aβ42 ELISAs

Aβ40 and Aβ42 levels were quantified from the remaining mouse cerebra excluding the hippocampus and temporal, parietal, and entorhinal cortical regions. Tissue was prepared as per ELISA kit instructions (human Aβ40: Invitrogen #KHB3482; human Aβ42: Invitrogen #KHB3442). Briefly, tissue was homogenized in a 5M guanidine hydrochloride, 50 mM Tris hydrochloride solution and then diluted 1:25 in Dulbecco's PBS (0.2 g/L KCl, 0.2 g/L KH_2PO4, 8 g/L NaCl, 1.15 g/L Na_2HPO_4) with 5% BSA (HyClone #SH30574.02), 0.03% Tween (Sigma-Aldrich, P1379), and a 1X protease inhibitor

cocktail (Calbiochem #539131). Aβ42 Samples were further diluted 1/1000 for Aβ42 and 1/500 for Aβ40 to bring within dynamic range of standards. Age-matched NonTg mice were used as negative controls. All samples were run in duplicate and reported as ng of Aβ peptide per g tissue wet weight.

4.5.4 Glycerophospholipid Extractions

Hippocampus, combined cortical regions, and plasma (50 μL) were extracted according to an acidified Bligh and Dyer technique previously described (Bligh and Dyer, 1959; Ryan et al., 2009; Xu et al., 2013). Briefly, brain tissues were homogenized using a tissue tearer (BioSpec 985370) in 4 mL acidified methanol (Fisher A412P-4) containing 2% acetic acid (Fisher 351271-212). Plasma samples were not homogenized. MS-grade lipid standards PC(13:0/0:0) (187.5 ng, Avanti LM-1600), PC(12:0/13:0) (500 ng, Avanti LM-1000), and PE(12:0/13:0) (200 ng, Avanti LM-1100) were added to all samples. Sodium acetate (0.1 M, Sigma S-2889) and chloroform (Fisher Scientific C298-500) were added to each sample for a final ratio of 0.8:1:0.95 sodium acetate/acidified methanol/chloroform. Samples were kept on ice and were vortexed and centrifuged at 600 x g for 2 min at 4^{o}C. The organic bottom phase was retained and the aqueous top phase back-extracted with chloroform three more times. The organic phases were combined and evaporated under nitrogen gas. Final lipid extracts were solubilized in 300 μL of ethanol (Commercial Alcohols P016EAAN) and stored under nitrogen gas at -80 ^{o}C in glass vials (BioLynx C779100AW).

4.5.5 High-performance liquid chromatography electrospray ionization tandem mass spectrometry (LC-ESI-MS/MS)

Lipid extracts (5 μL) were added to microwell plates (Agilent 5042-1385) in an Agilent 1100 autosampler. A standard mixture containing d4-PC(O-16:0/0:0) (2.5 ng, Cayman 360906), d4-PC(O-18:0/0:0) (2.5 ng, Cayman 10010228), d4-PC(O-16:0/2:0) (1.25 ng, Cayman 360900), and d4-PC(O-18:0/2:0) (1.25 ng, Cayman 10010229), suspended in 2.5 μL of ethanol were added to each well along with 16 μL of solvent A (0.1 % formic acid, 10 mM ammonium acetate in MS-grade water). Three microliters of this mixture were injected into a 10 cm x 250 mm (I.D.) column pack with Reprosil-Pur 200 C18 (particle size of 5 mm and pore size of 200 A, Dr. A. Maisch, Ammerbruch, Germany # r25.aq) beads. A gradient elution of mobile solvent A and solvent B (5:2 ratio of acetonitrile/isopropanol with 0.1% formic acid and 10 mM of ammonium acetate) was implemented. For the first 5 min, samples were loaded in 30% B which then increased to 100% B until 36 min when it was reduced to 30% B again until the end of the 45 min run. A blank run of solvent A was included after every sample to minimize inter-sample contamination.

A TurboSpray ion source on a QTRAP-5500 (AB SCIEX) mass spectrometer was used to detect GPC and GPE second messengers and metabolites. Two separate scans running parallel with each other were designed to detect both GPC and GPEs within the same run. GPC detection applied a PIS in positive ion mode to detect the phosphocholine headgroup (184.1 m/z) product ion. Curtain gas was set to 20 uL/min, ion spray voltage to 4500 V and the source gas to 20 uL/min. Collision gas was set to 10 uL/min with an entrance potential of 10 eV, a declustering potential of 100 eV and a collision cell exit

potential of 9 eV. Collision energy for GPCs was 47 eV. GPE detection required a NLS in positive ion mode utilizing the common mass difference of the neutral phosphoethanolamine headgroup (141 m/z) between precursor and product ions. The NLS employed equivalent mass spectrometer parameters as the GPC PIS, except with a collision energy of 30 eV to specifically target fragmentation of the phosphoethanolamine head group. Both PIS and NLS were set to specifically detect GPC and GPE metabolites and seconds messengers ranging from 450-650 m/z. Following the profiling of cortex, hippocampus and plasma, MRM was implemented to select only specific transitions detected in PISs and NLSs thus enhancing the accuracy of quantification. All sample runs were aligned using RT-STAR, an in-house algorithm that standardizes retention times across the lipidome. PIS, NLS, and MRM spectra were analyzed using Analyst 1.6.2 and MultiQuant 3.0.8664.0 (AB SCIEX). Molecular identities were assigned using VaLID v3.0 (Blanchard et al., 2013) and LIPID MAPS structural database (Sud et al., 2007) to elicit the best predicted species. Class-specific internal standards were used to normalize both brain and plasma tissues. Raw peak areas were normalized to either 413.41 pmol of PC(13:0/0:0) for GPC species or 336.83 pmol of PE(12:0/13:0) for GPE species added at time of extraction. Tissue wet weight was also used to normalize data derived from brain regions which is represented as pmol/mg_{tissue}. In plasma, data were normalized to the volume extracted (50 μL) and represented as pmol/mL_{plasma} for plasma.

4.5.6 Lipid nomenclature

We profiled and classified six GPC and five GPE subclasses of metabolites in plasma or brain (hippocampus or temporal parietal entorhinal cortices) between 450-650

m/z. These included GPC subclasses LPCs, LPC(O)s, LPC(P)s, PCs, PC(O)s, PC(P)s, and GPE subclasses LPEs, LPE(O)s, PEs, PE(O)s, and PE(P)s.

Molecular species were defined using the standard lipid nomenclature described by (Fahy et al., 2009). For example, LPE(16:1/0:0) defines a GPE species with a polar head group (PE) at the *sn-3* carbon of the glycerol backbone. At the *sn-1* position, there is an acyl-linked (ester bond, no prefix) hydrocarbon chain with 16 carbons and 1 unsaturation (16:1). At the *sn-2* position, there is only a hydroxyl group (0:0) thus making this species a *lyso*-GPE. For other species, O- represents an alkyl linkage (ether bond) and P- represents an alkenyl linkage (vinyl ether bond). Species with a short chain at the *sn*-2 position are prefaced with either PC or PE for phosphocholine and phosphoethanolamine head groups respectively.

4.5.7 Statistics

Statistical analyses were performed using Prism 7.0 (Graphpad) and Microsoft Excel 2011 (version 14.6.6). All correlative analyses performed were Pearson correlations with linear regressions to assess linear relationships. Multiple t-tests with Welch's correction were corrected for multiple comparisons, setting FDRs to 5% according to (Benjamini and Hochberg, 1995). In all ANOVAs, a Holm-Sidak *post hoc* test was employed to control for family-wise error. A *post hoc* power analysis was performed to establish sample sizes using G*Power 3.1 (Faul et al., 2007) with α set to 0.05. Sample and effect sizes were deemed acceptable at β values of 0.2 or under.

4.6 Results

4.6.1 Tg females but not males exhibit spatial learning and memory impairment in the MWM despite comparable amyloid burden

We have previously reported that N5 TgCRND8 mice at six months of age demonstrate sexually dimorphic learning and memory deficits in the MWM despite comparable amyloid deposition. Tg females fail to adopt efficient spatial navigational search strategies while while Tg males are able to transition from systematic to spatial strategies, a behavioural phenotype of cognitive reserve (Granger et al., 2016). Here, we replicated these findings and developed a composite score of spatial learning and memory that could be used to track individual impairments The mice used in this study exhibited the same sexual dimorphisms in escape latency over the eight test days (n=5/sex/genotype) (Fig. 4.1A) previously reported in (Granger et al., 2016). Mean escape latency (Fig. 4.1B, top row), mean spatial strategy (Fig. 4.1B, middle row), and the amount of time spent in the platform zone across test days (Fig. 4.1B, bottom row) all yielded significant sex-dependent differences in Tgs relative to NonTgs with only females demonstrating a significant impairment. To combine these measures, we calculated a composite spatial learning and memory score (calculations described in Material and Methods) in which a lower score is indicative of greater impairment. Females but not male Tgs had significantly lower composite spatial learning and memory scores compared to their NonTg littermates (Fig. 4.1C). To confirm that these differences were independent of amyloid burden, we assess levels of cerebral $A\beta_{42}$, $A\beta_{40}$ and $A\beta_{42}/A\beta_{40}$ ratios. As we have previously reported (Granger et al., 2016), there was no difference in amyloid load between Tg males and females (Fig. 4.1D).

Figure 4.1 – Spatial learning and memory is sexually dimorphic in TgCRND8 mice despite equivalent Aβ load. (A) Tg males (left panel) show comparable learning curves as NonTg males. Tg females are significantly impaired relative to NonTg females (right panel, n=5/genotype/sex). Statistics were a two-way, repeated measures ANOVA with Holm-Sidak *post hoc* for multiple comparisons (main effect of genotype-males: $F_{(1,8)}$=1.453, df=1, p>0.05; females: $F_{(1,8)}$=9.971, df=1, p<0.05). (B) Overall mean escape latencies over the 8 days of testing were statistically comparable between male Tg and NonTg mice and statistically different between female Tg and NonTg mice (top panels; males: t=1.206, df=8, p>0.05; females: t=3.158, df=8, p<0.05). Utilization of spatial strategies over the 8 test days were statistically reduced in females but not males (middle panel; males: t=1.372, df=8, p>0.05; females: t=3.472, df=8, p<0.01). Average time spent in the platform zone over the eight test days was statistically lower in female but not male Tgs compared to NonTg controls. (bottom panel; males: t=0.09, df=8, p>0.05; females: t=2.78, df=8, p<0.05). (C) Composite z scores of each learning and memory readout corrected for inverse relationships as indicated in Materials and Methods demonstrate that Tg males (left panel; t=0.911, df=8, p>0.05) are unimpaired while females are imparied (right panel; t=3.38, df=8, p<0.01). Statistics were unpaired, two-tailed t-tests Boxes depict the interquartile range; whiskers extend to minimum and maximum points; line depicts median vaues n=5/sex/genotype (**p<0.01, *p<0.05). (D) Cerebrum levels of $A\beta_{42}$ (left panel), $A\beta_{40}$ (middle panel) and $A\beta_{42}/A\beta_{40}$ ratios (right panel) are equivalent between male and female Tg mice. Data are represented as ng per g of tissue wet weight ± SEM of the mean. Statistics were unpaired, two-tailed t-tests, all p-values>0.05.

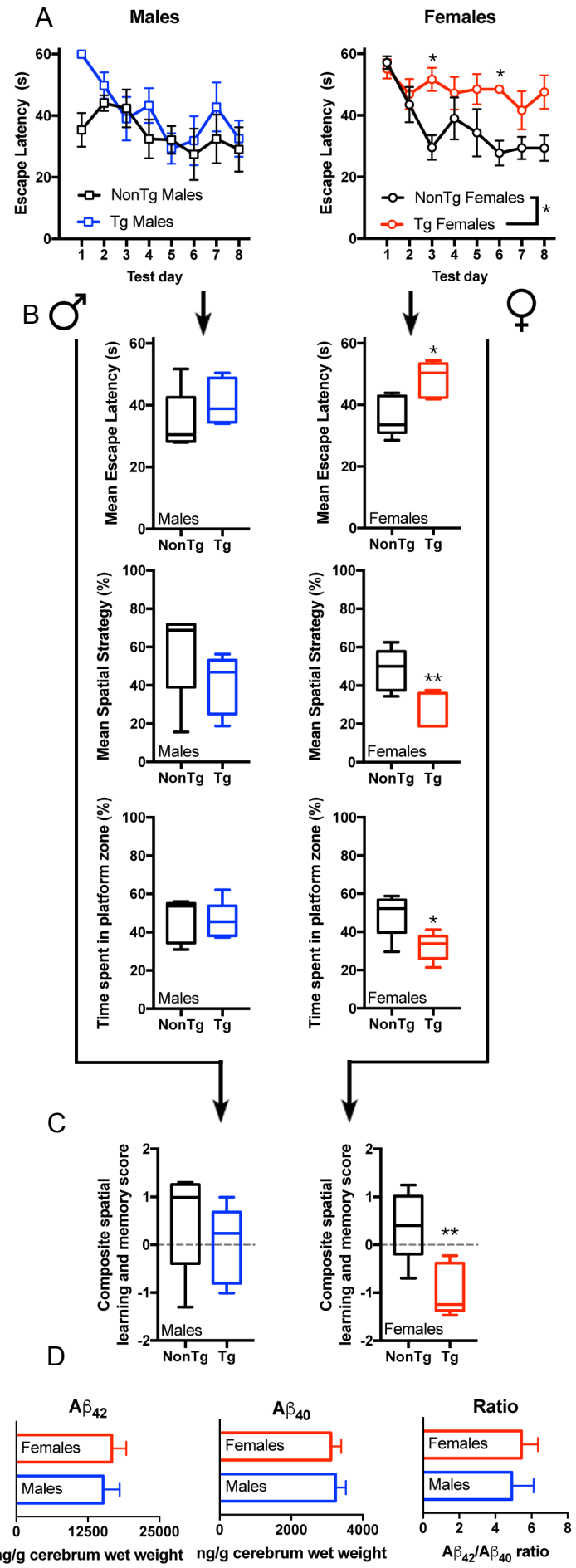
A
Males
Females
Escape Latency (s)
NonTg Males
Tg Males
NonTg Females
Tg Females
Test day
B
Mean Escape Latency (s)
Mean Spatial Strategy (%)
Time spent in platform zone (%)
Males
Females
NonTg
Tg
C
Composite spatial learning and memory score
D
Aβ42
Aβ40
Ratio
ng/g cerebrum wet weight
Aβ42/Aβ40 ratio

Figure 4.1

4.6.2 The GPC and GPE lipidomes are regionally-specific and sexually dimorphic in NonTg mice

To determine whether GPC and GPE are metabolized differently in male and female NonTg mice, we used a targeted lipidomic approach to profile signaling molecules and metabolites (450-650 m/z) generated by catabolism and remodeling of structural glycerophospholipids via the Lands' cycle. We investigated two brain regions involved in learning and memory, the hippocampus and the temporal, parietal, entorhinal cortices (hereafter referred to as cortex). A total of 59 GPC and 33 GPE metabolites and signaling molecules were identified in the hippocampus. Sixty GPC and 33 GPE species were detected in the cortex. Of these, 55 GPC and 32 GPE species were common to both regions. All but five cortical glycerophospholipid species (2 LPC, 2 PC(O), 1 PE(O)) were within dynamic range required for quantification; these five species were excluded from further analysis (Fig. 4.2A).

Subclass levels were calculated using common species between brain regions. Lipid abundances at the subclass level were compared between male and female NonTg mice. The hippocampus yielded no sex differences in total subclass abundances of either GPCs (Fig. 4.2B, top panel) or GPEs (Fig. 4.2B, bottom panel). Cortical GPC and GPE levels were remarkably sexually dimorphic (Fig. 4.2C). Total PC second messengers, PC(O) second messengers, and all *lyso*-GPCs (including LPCs, LPC(O)s, and LPC(P)s) were significantly lower in female mice (Fig. 4.2C, top panel); total *lyso*-GPEs (including LPEs and LPE(O)s) along with PE(P)s and PE(O)s were significantly higher in females (Fig. 4.2C, bottom panel). At the molecular level, abundances of only four LPCs and one PC(O) were significantly higher in NonTg male hippocampus (Fig. 4.2D, top panel). In

Figure 4.2 – GPC and GPE lipid abundances are sexually dimorphic in the cortex but not the hippocampus of NonTg mice. (A) Venn diagrams depicting the distribution of both GPCs (top diagram) and GPEs (bottom diagram). (B) No significant differences in the abundances of GPC (top panel) and GPE (bottom panel) subclasses are detected in hippocampus. (C) Differences in abundances of GPC (top panel) and GPE (bottom panel) subclasses are evident cortex. Select GPC subclasses are significantly higher in males and select GPE subclasses are significantly higher in females. Data are mean pmol per mg of tissue wet weight ± SEM. Statistics were unpaired, two-tailed t-tests, *$p<0.05$. (D) At the molecular level, five GPC species and no GPE species exhibit sex-specific differences in abundance in the hippocampus (top panel). Seventy percent of all detectable GPC and GPE metabolites are sexually different in the cortex (bottom panel). Statistics were multiple t-tests and FDR of 5%; n=10/genotype (*adjusted $p<0.05$).

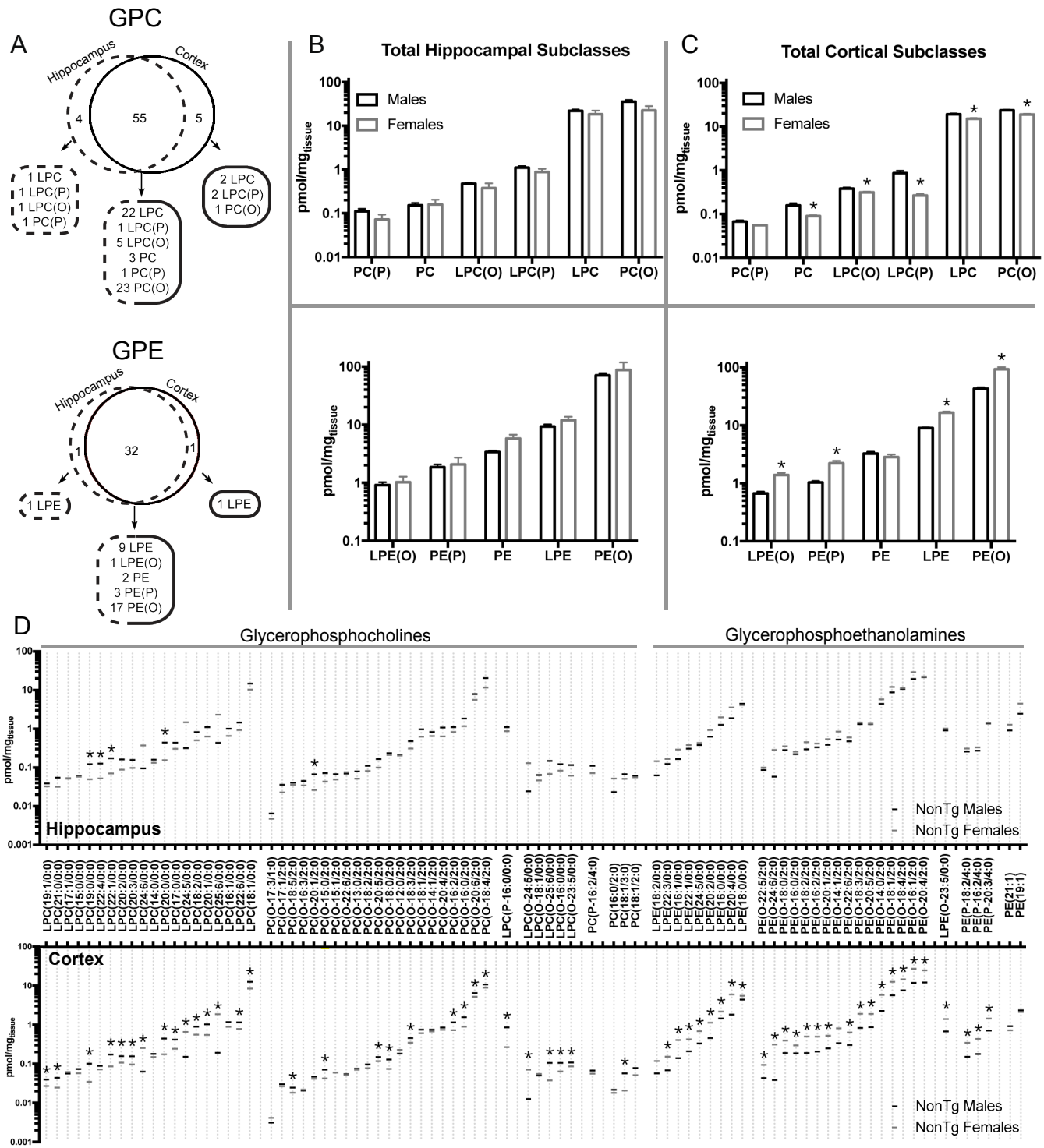
A
GPC
Hippocampus
Cortex
4
55
5
1 LPC
1 LPC(P)
1 LPC(O)
1 PC(P)
22 LPC
1 LPC(P)
5 LPC(O)
3 PC
1 PC(P)
23 PC(O)
2 LPC
2 LPC(P)
1 PC(O)
GPE
Hippocampus
Cortex
32
1
1
1 LPE
1 LPE
9 LPE
1 LPE(O)
2 PE
3 PE(P)
17 PE(O)
B
Total Hippocampal Subclasses
Males
Females
pmol/mg tissue
PC(P)
PC
LPC(O)
LPC(P)
LPC
PC(O)
C
Total Cortical Subclasses
Males
Females
pmol/mg tissue
PC(P)
PC
LPC(O)
LPC(P)
LPC
PC(O)
pmol/mg tissue
LPE(O)
PE(P)
PE
LPE
PE(O)
pmol/mg tissue
LPE(O)
PE(P)
PE
LPE
PE(O)
D
Glycerophosphocholines
Glycerophosphoethanolamines
pmol/mg tissue
Hippocampus
NonTg Males
NonTg Females
LPC(19:1/0:0)
LPC(21:0/0:0)
LPC(17:1/0:0)
LPC(15:0/0:0)
LPC(19:0/0:0)
LPC(22:4/0:0)
LPC(22:1/0:0)
LPC(20:2/0:0)
LPC(20:3/0:0)
LPC(24:6/0:0)
LPC(14:0/0:0)
LPC(20:0/0:0)
LPC(17:0/0:0)
LPC(24:5/0:0)
LPC(18:2/0:0)
LPC(20:1/0:0)
LPC(16:1/0:0)
LPC(25:6/0:0)
LPC(22:6/0:0)
LPC(18:1/0:0)
PC(O-17:3/1:0)
PC(O-17:1/2:0)
PC(O-18:5/2:0)
PC(O-16:3/2:0)
PC(O-20:1/2:0)
PC(O-15:0/2:0)
PC(O-15:1/2:0)
PC(O-22:6/2:0)
PC(O-13:0/2:0)
PC(O-18:2/2:0)
PC(O-20:5/2:0)
PC(O-18:0/2:0)
PC(O-12:0/2:0)
PC(O-18:3/2:0)
PC(O-18:1/2:0)
PC(O-14:1/2:0)
PC(O-20:4/2:0)
PC(O-16:2/2:0)
PC(O-16:0/2:0)
PC(O-20:5/2:0)
PC(O-18:4/2:0)
LPC(P-16:0/0:0)
LPC(O-24:5/0:0)
LPC(O-18:1/0:0)
LPC(O-25:6/0:0)
LPC(O-16:0/0:0)
LPC(O-23:5/0:0)
PC(P-16:2/4:0)
PC(16:0/2:0)
PC(18:1/3:0)
PC(18:1/2:0)
LPE(18:2/0:0)
LPE(22:3/0:0)
LPE(16:1/0:0)
LPE(22:1/0:0)
LPE(24:5/0:0)
LPE(20:2/0:0)
LPE(16:0/0:0)
LPE(20:4/0:0)
LPE(18:0/0:0)
PE(O-22:5/2:0)
PE(O-24:6/2:0)
PE(O-18:0/2:0)
PE(O-16:0/2:0)
PE(O-18:2/2:0)
PE(O-16:2/2:0)
PE(O-20:1/2:0)
PE(O-14:1/2:0)
PE(O-22:6/2:0)
PE(O-18:3/2:0)
PE(O-20:5/2:0)
PE(O-14:0/2:0)
PE(O-18:1/2:0)
PE(O-18:4/2:0)
PE(O-16:1/2:0)
PE(O-20:4/2:0)
LPE(O-23:5/0:0)
PE(P-18:2/4:0)
PE(P-16:2/4:0)
PE(P-20:3/4:0)
PE(21:1)
PE(19:1)
Cortex
pmol/mg tissue
NonTg Males
NonTg Females

Figure 4.2

cortex, abundances of over 70% of GPE and GPC metabolites and signaling molecules were sexually dimorphic (Fig. 4.2D, bottom panel).

4.6.3 Changes to GPC and GPE metabolism in the hippocampus and cortex of Tg mice are sex-specific

We next asked whether metabolism of GPCs and GPEs in the hippocampus and cortex is differentially altered in male and female Tg mice in response to Aβ challenge. In hippocampus of Tg mice, GPC metabolism was clearly sexually dimorphic. Total abundances of five of the six subclasses were significantly higher in Tg males relative to Tg females (Fig. 4.3A). These changes were attributed to an increase in GPC metabolism in Tg males but not Tg females.

At the molecular level, abundances of five individual GPC species were significantly elevated in Tg males relative to NonTg littermates. In Tg females, GPC metabolism was apparently suppressed albeit not statistically significantly. Levels of major individual GPC metabolites and signaling molecules in Tg females were lower than NonTgs although none were significantly different (Fig. 4.3B). In cortex, overall levels of all GPC subclasses were sexually dimorphic (Fig. 4.3C); of these, PC(P), LPC(O), PC(O), and LPC levels were higher in male compared to female Tg mice (Fig. 4.3C). Abundances of 21 GPC species were highere in male Tg mice relative to sex-matched NonTgs (Fig. 4.3C). No changes in GPC metabolism was detected in females (Fig. 4.3D).

There was no change in overall GPE metabolism in response to Aβ comparing male and female Tg and NonTg mice in the hippocampus (Fig. 4.4A,B). In cortex, GPE metabolism was sexually dimorphic in NonTg mice (Fig. 4.4C). When challenged by Aβ,

Figure 4.3 – There is a Tg-specific sex difference in GPC metabolism. (A) In the hippocampus, total PC(P), LPC(O), LPC(P), PC(O), and LPC abundances are significantly higher in Tg males compared to Tg females. Data are represented as total subclass abundance (pmol per mg of tissue wet weight) Boxes depict the interquartile range; whiskers extend to minimum and maximum points; the line represents the median. (B) Heat map comparing $\log_2$ fold change between sex-matched Tgs and NonTgs. Tg males exhibit significantly increased levels of GPC species relative to NonTgs. Females were not significantly different. (C) Cortical GPC metabolism is also sexually dimorphic. Levels of PC(P)s, LPC(O)s, and PC(O)s are higher in Tg males compared to Tg females and NonTg males. (D) At the molecular level, Tg mice exhibit significant increases in GPC metabolite abundances. No statistically signficant change was found in females. Statistics for A and C were a two-way ANOVA with Holm-Sidak *post hoc* for multiple comparisons, n=5/sex/genotype (main effects of sex: **p<0.01, *p<0.05). Statistics for B and D were multiple t-tests with an FDR of 5% between $\log_2$ fold changes of sex-specific NonTg and Tg mice relative to NonTg littermates (*adjusted p<0.05).

Hippocampus

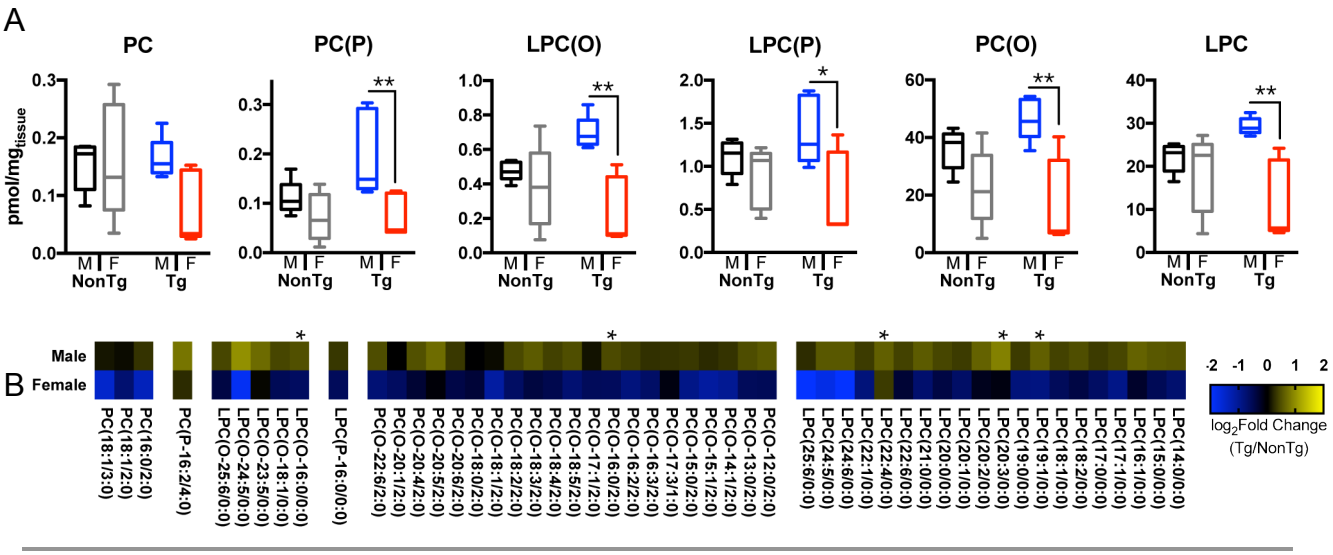

Cortex

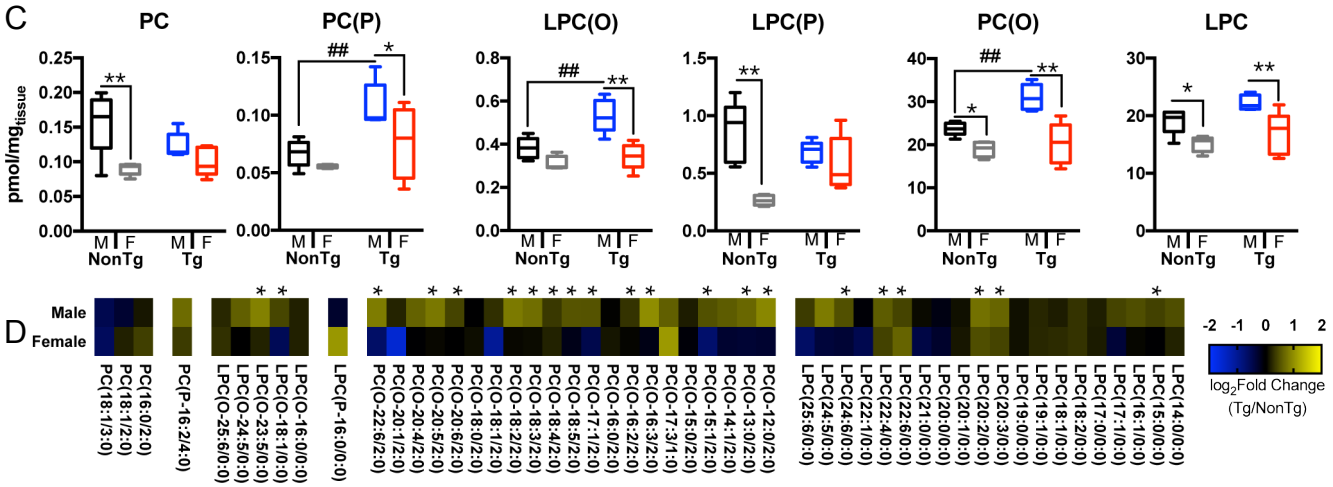

Figure 4.4 – The cortical but not the hippocampal GPE lipidome is sexually dimorphic in Tg mice. (A) No significant difference in GPE subclass abundance is found in hippocampus. Data are represented as total subclass abundance (pmol per mg of tissue wet weight) Boxes depict the interquartile range; whiskers extend to minimum and maximum points; the line represents the median. (B) No significant difference in lipid abundance at the molecular level was detected in Tg males and females. Data are represented as a heat map depicting log_2 fold changes of Tg males and females relative to sex-match NonTg littermates. (C) Cortical levels of total subclass abundances (pmol per mg of tissue wet weight) are sexually dimorphic. PE(P), LPE(O), PE(O) and LPE subclasses were all significantly effected by sex and genotype.. (D) Individual GPE metabolites and signaling molecules are increased in Tg males but decreased in Tg females relative to sex-matched NonTgs. Data are represented as a heat map depicting log_2 fold changes of Tg males and females relative to sex-match NonTg littermates. Statistics for A and C were a two-way ANOVA with Holm-Sidak post hoc for multiple comparisons, n=5/sex/genotype (main effects of sex: **p<0.01, *p<0.05; main effects of genotype: ##p<0.01, #p<0.05). Statistics for B and D were multiple t-tests with a FDR of 5% between log_2 fold changes of sex-specific NonTg and Tg mice relative to NonTg littermates (*adjusted p<0.05).

Hippocampus

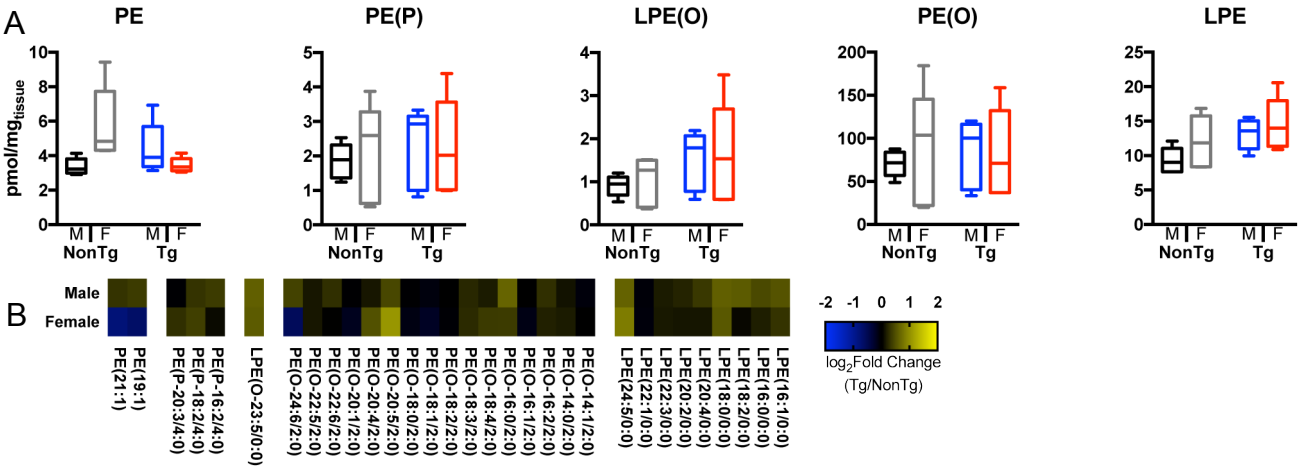

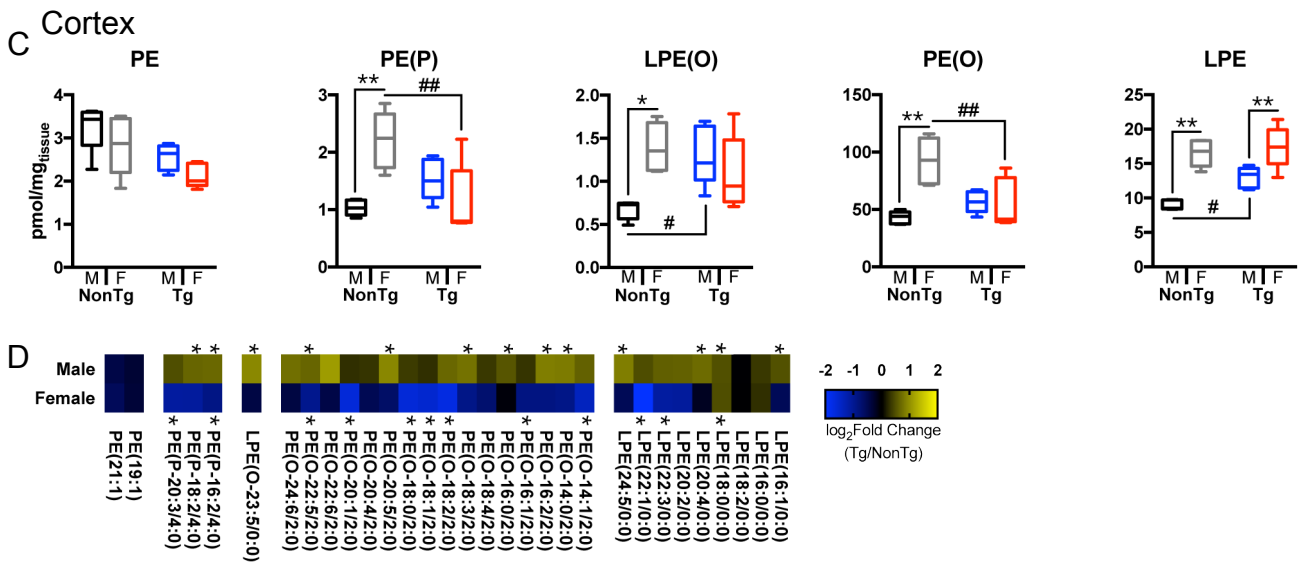

PE(P) and PE(O) metabolism was significantly suppressed in Tg compared to NonTg females (Fig. 4.4C). LPE metabolism was significantly enhanced in Tg compared to NonTg males (Fig. 4.4C,D). Interestingly, Tg females exhibited significantly higher levels of cortical LPEs that Tg males (Fig. 4.4D). Forty-five percent of LPE, PE(O), LPE(O) and PE(P) species were significantly higher in Tg males than NonTgs while 38% of LPE, PE(O) and PE(P) species were significantly lower in Tg females (Fig. 4.4D). Taken to gether, these data suggested that GPC and GPE metabolism is generally suppressed in females and enhanced in males when challenged by Ab pathology. The one common metabolic alteration was an increase in LPE (18:0/0:0) abundance in both sexes.

4.6.4 Changes in LPE(18:0/0:0) abundance in both the hippocampus and cortex associate with behavioural indices of spatial learning and memory impairment

To assess relationships between lipid levels at both the subclass and molecular levels in hippocampus and cortex with learning and memory performance, we correlated lipid abundances with composite spatial learning and memory scores (Table 4.1). Only total hippocampal LPE levels were significantly inversely correlated with performance in the MWM (Fig. 4.5A, left panel). In cortex, this relationship approached signficance ($p=0.06$, Fig. 4.5A, right panel). The most abundance LPE in both regions was LPE(18:0/0:0) (Fig. 4.5B). LPEs in both brain regions had negative relationships with the composite spatial score. We attributed this relationship primarily to the effects of LPE(18:0/0:0) on the total LPE subclass abundance.

LPE(18:0/0:0) was the most abundant LPE species quantified in both the hippocampus and the cortex of our NonTg and TgCRND8 mouse line (Fig. 4.5B). This

Table 4.1. Correlational matrix of hippocampal and cortical GPC and GPE metabolites and signaling molecules with composite spatial scores of learning and memory

	Hippocampus		Cortex	
GPC	Correlation Coefficient r	p-value	Correlation Coefficient r	p-value
LPC(14:0/0:0)	0.125	0.600	-0.143	0.549
LPC(15:0/0:0)	0.032	0.894	0.096	0.686
LPC(16:1/0:0)	0.003	0.989	-0.022	0.928
LPC(17:1/0:0)	0.056	0.815	-0.108	0.660
LPC(17:0/0:0)	0.220	0.352	0.184	0.438
LPC(18:2/0:0)	0.186	0.432	0.101	0.673
LPC(18:1/0:0)	0.119	0.618	0.068	0.775
LPC(19:1/0:0)	0.144	0.546	-0.075	0.760
LPC(19:0/0:0)	0.247	0.294	0.233	0.323
LPC(20:3/0:0)	-0.010	0.966	-0.010	0.967
LPC(20:2/0:0)	0.104	0.661	-0.122	0.610
LPC(20:1/0:0)	0.151	0.526	0.192	0.418
LPC(20:0/0:0)	0.170	0.472	0.293	0.209
LPC(21:0/0:0)	0.097	0.683	0.158	0.507
LPC(22:6/0:0)	0.045	0.852	-0.098	0.680
LPC(22:4/0:0)	0.121	0.611	-0.102	0.670
LPC(22:1/0:0)	0.189	0.425	0.347	0.134
LPC(24:6/0:0)	0.115	0.628	-0.150	0.528
LPC(24:5/0:0)	0.127	0.593	-0.102	0.667
LPC(25:6/0:0)	0.076	0.749	-0.099	0.678
TOTAL LPC	**0.209**	**0.378**	**0.125**	**0.599**
PC(O-12:0/2:0)	-0.044	0.855	-0.129	0.587
PC(O-13:0/2:0)	0.088	0.711	0.007	0.977
PC(O-14:1/2:0)	0.176	0.457	0.117	0.624
PC(O-15:1/2:0)	0.198	0.402	0.177	0.456
PC(O-15:0/2:0)	0.230	0.330	0.248	0.292
PC(O-17:3/1:0)	0.308	0.199	-0.364	0.115
PC(O-16:3/2:0)	0.353	0.127	-0.239	0.309
PC(O-16:2/2:0)	0.252	0.283	0.130	0.584
PC(O-16:0/2:0)	0.112	0.638	0.178	0.452
PC(O-17:1/2:0)	0.317	0.174	0.092	0.708
PC(O-18:5/2:0)	0.079	0.741	-0.090	0.713
PC(O-18:4/2:0)	0.108	0.649	-0.093	0.695
PC(O-18:3/2:0)	0.150	0.527	0.000	1.000
PC(O-18:2/2:0)	0.196	0.408	-0.007	0.977
PC(O-18:1/2:0)	0.239	0.311	0.256	0.276
PC(O-18:0/2:0)	-0.082	0.730	0.189	0.425
PC(O-20:6/2:0)	0.127	0.594	0.036	0.881
PC(O-20:5/2:0)	0.051	0.832	-0.045	0.850
PC(O-20:4/2:0)	0.070	0.771	0.072	0.763
PC(O-20:1/2:0)	0.281	0.231	0.249	0.290
PC(O-22:6/2:0)	0.124	0.601	0.086	0.718
TOTAL PC(O)	**0.209**	**0.377**	**0.034**	**0.887**
LPC(O-16:0/0:0)	0.140	0.555	0.146	0.540
LPC(O-18:1/0:0)	0.032	0.892	0.072	0.764
LPC(O-23:5/0:0)	0.095	0.689	-0.005	0.983
LPC(O-24:5/0:0)	0.154	0.517	-0.225	0.339
LPC(O-25:6/0:0)	0.291	0.227	0.252	0.283
TOTAL LPC(O)	**0.173**	**0.466**	**0.138**	**0.562**
LPC(P-16:0/0:0)	0.116	0.625	0.043	0.857
TOTAL LPC(P)	**0.352**	**0.128**	**0.146**	**0.540**
PC(P-16:2/4:0)	-0.075	0.755	-0.191	0.433
TOTAL PC(P)	**0.147**	**0.537**	**-0.092**	**0.708**
PC(16:0/2:0)	0.054	0.819	-0.054	0.822
PC(18:1/2:0)	0.058	0.808	0.137	0.565
PC(18:1/3:0)	0.420	0.066	0.329	0.156
TOTAL PC	**0.272**	**0.246**	**0.309**	**0.185**

Correlation Coefficient r

1.00
0.66
0.33
0.00
-0.33
-0.66
-1.00

p-value

<0.01
<0.05
>0.05

	Hippocampus		Cortex	
GPE	Correlation Coefficient r	p-value	Correlation Coefficient r	p-value
LPE(16:1/0:0)	-0.099	0.679	-0.165	0.487
LPE(16:0/0:0)	-0.438	0.053	-0.413	0.070
LPE(18:2/0:0)	-0.358	0.121	0.001	0.996
LPE(18:0/0:0)	-0.511	0.021	-0.582	0.007
LPE(20:4/0:0)	-0.309	0.185	-0.239	0.311
LPE(20:2/0:0)	-0.058	0.807	-0.029	0.904
LPE(22:3/0:0)	-0.049	0.838	-0.024	0.921
LPE(22:1/0:0)	0.073	0.760	0.198	0.403
LPE(24:5/0:0)	-0.284	0.225	-0.178	0.452
TOTAL LPE	**-0.482**	**0.031**	**-0.425**	**0.062**
PE(O-14:1/2:0)	0.067	0.780	-0.045	0.850
PE(O-14:0/2:0)	0.051	0.831	-0.093	0.698
PE(O-16:2/2:0)	-0.079	0.742	-0.184	0.436
PE(O-16:1/2:0)	0.021	0.931	-0.037	0.878
PE(O-16:0/2:0)	-0.348	0.132	-0.354	0.125
PE(O-18:4/2:0)	-0.181	0.445	-0.107	0.652
PE(O-18:3/2:0)	0.008	0.974	-0.081	0.733
PE(O-18:2/2:0)	0.077	0.748	0.034	0.887
PE(O-18:1/2:0)	0.042	0.860	0.077	0.745
PE(O-18:0/2:0)	0.105	0.660	0.041	0.864
PE(O-20:5/2:0)	-0.315	0.177	-0.127	0.593
PE(O-20:4/2:0)	-0.057	0.810	-0.122	0.607
PE(O-20:1/2:0)	0.062	0.795	0.083	0.728
PE(O-22:6/2:0)	-0.213	0.367	-0.198	0.402
PE(O-22:5/2:0)	-0.057	0.813	-0.015	0.949
PE(O-24:6/2:0)	-0.018	0.939	-0.166	0.484
TOTAL PE(O)	**-0.260**	**0.269**	**-0.106**	**0.657**
LPE(O-23:5/0:0)	-0.266	0.257	-0.181	0.446
TOTAL LPE(O)	**-0.327**	**0.159**	**-0.166**	**0.485**
PE(P-16:2/4:0)	-0.135	0.582	-0.088	0.713
PE(P-18:2/4:0)	-0.152	0.523	-0.005	0.982
PE(P-20:3/4:0)	-0.083	0.728	0.072	0.762
TOTAL PE(P)	**-0.262**	**0.265**	**0.007**	**0.976**
PE(19:1)	0.167	0.482	0.249	0.289
PE(21:1)	0.229	0.331	0.369	0.109
TOTAL PE	**-0.071**	**0.766**	**0.421**	**0.065**

Figure 4.5 – Hippocampal and cortical LPE(18:0/0:0) levels negatively associate with spatial learning and memory. (A) Correlative analyses of hippocampal (left panel; r=-0.48, p<0.05) and cortical (right; r=-0.43, p=0.06) total LPE abundances with the composite spatial learning and memory scores n=20 NonTg and Tg male and female mice. Data are represented as a scatterplot of composite spatial learning and memory scores (x-axis) against total LPE abundance (pmol per mg tissue wet weight) with a linear regression line-of-best-fit. (B) Total LPE subclass composition as determined by the abundances of individual LPE species. Data are represented as a percent of the total LPE abundance. (C) LPE(18:0/0:0), the most abundant LPE species, is significantly negatively correlated with the composite spatial learning and memory score in both hippocampus (left; r=-0.51, p<0.05) and cortex (right; r=-0.58, p<0.01). (D) Univariate analyses of hippocampal (left; main effect of genotype: $F_{(1,16)}$=31.76, df=1, p<0.01; main effect of sex: $F_{(1,16)}$=1.41, df=1, p>0.05) and cortical (right; main effect of genotype: $F_{(1,16)}$=28.91, df=1, p<0.01; main effect of sex: $F_{(1,16)}$=11.77, df=1, p<0.01) LPE(18:0/0:0). In both regions, LPE(18:0/0:0) levels aer significantly higher in both male and female Tgs relative to NonTgs. Cortical LPE(18:0/0:0) levels are also significantly higher in Tg females than Tg males. Correlational statistics were Pearson correlations. Univariate statistics were a two-way ANOVA, n=5/sex/genotype (main effects of sex: *p<0.05; effects of genotype: ##p<0.01).

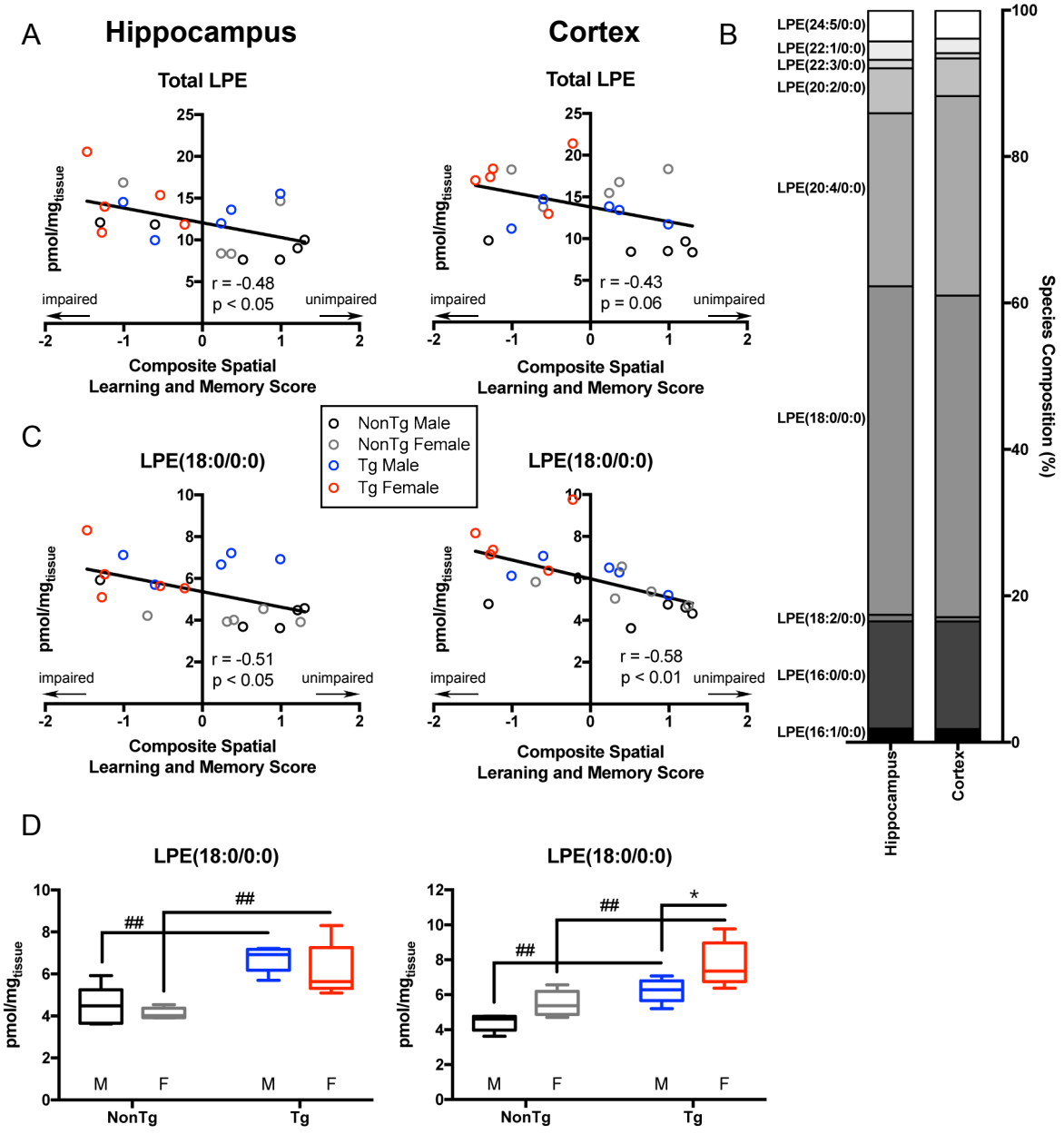
A
Hippocampus
Cortex
Total LPE
pmol/mg tissue
r = -0.48
p < 0.05
r = -0.43
p = 0.06
impaired
unimpaired
Composite Spatial
Learning and Memory Score
B
LPE(24:5/0:0)
LPE(22:1/0:0)
LPE(22:3/0:0)
LPE(20:2/0:0)
LPE(20:4/0:0)
LPE(18:0/0:0)
LPE(18:2/0:0)
LPE(16:0/0:0)
LPE(16:1/0:0)
Species Composition (%)
Hippocampus
Cortex
C
LPE(18:0/0:0)
NonTg Male
NonTg Female
Tg Male
Tg Female
r = -0.51
p < 0.05
r = -0.58
p < 0.01
Composite Spatial
Learning and Memory Score
Composite Spatial
Leraning and Memory Score
D
LPE(18:0/0:0)
##
*
M
F
NonTg
Tg

Figure 4.5

species was the only LPE to exhibit a significant correlation with behavioural indices of spatial learning and memory in both the hippocampus and cortex (Fig. 4.5C, Table 4.1).

To determine whether these differences associated with Ab load, we correlated leavels of LPE(18:0/0:0) with $A\beta_{42}$ and $A\beta_{40}$ abundances as well as the ratio of $A\beta_{42}/A\beta_{40}$. There were no significant associates (Fig. 4.6). Take together, these data demonstrate that higher levels of LPE(18:0/0:0) in both hippocampus and cortex associate with greater learning and memory impairment in Tg male and female mice.

4.6.5 Changes in cortical LPE(18:0/0:0) associated with learning and memory deficits can be predicted by levels of specific GPE species in circulation.

We next asked whether changes in the brain GPE lipidome linked to learning and memory impairment could be predicted by monitoring the plasma GPE lipidome. In the plasma, 24 GPE metabolites were detected with a total of 17 GPE metabolites found in all three biological samples (plasma, hippocampus, and cortex) (Fig. 4.7A). Three GPEs were significantly associated with composite spatial learning and memory scores (Table 4.2). These species, LPE(16:1/0:00, PE(O-14:1/2:0), and PE(O-18:3/2:0), all positively correlated with spatial learning and memory (Table 4.2, Fig 4.7B). Increased abundances correlated with better performance on the MWM. Levels also significantly negatively correlated with LPE(18:0/0:0) levels in cortex but not hippocampus (Fig. 4.7C). LPE(16:1/0:0), PE(O-14:1/2:0), and PE(O-18:3/2:0) plasma levels were not sexually dimorphic in NonTg mice but levels were significantly lower in Tg females compared to Tg males (Fig. 4.7D) corresponding with the severity of their learning and memory

Figure 4.6 – There is no relationship between hippocampal or cortical LPE(18:0/0:0) and amyloid deposition in TgCRND8 mice. Correlative analysis of hippocampal (left column) and cortical (right column) LPE(18:0/0:0) abundances (pmol per mg tissue wet weight) with three measure of amyloid pathology . $A\beta_{42}$ (top row), $A\beta_{40}$ (middle row), and $A\beta_{42}/A\beta_{40}$ ratios were not significantly associated in either brain region. Amyloid abundances represented as ng per g of tissue wet weight. Statistics were Pearson correlations, all p-values>0.05.

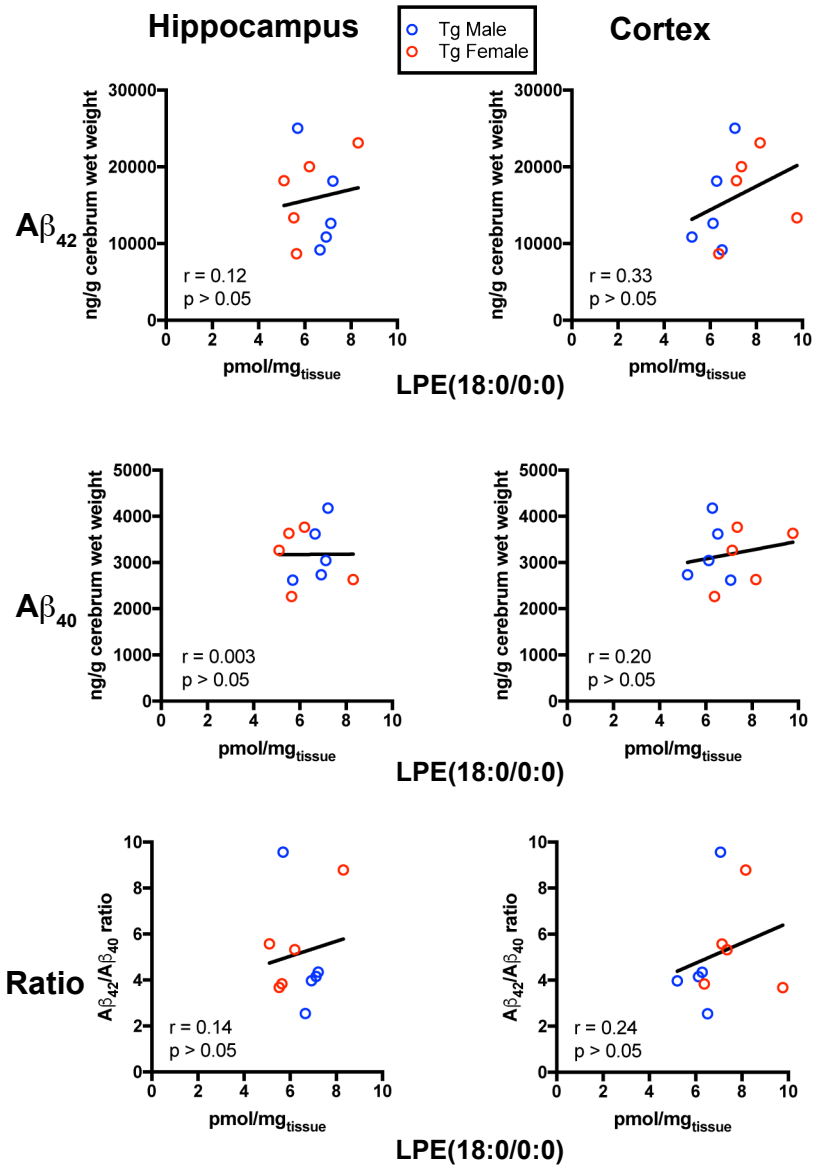
Hippocampus
Cortex
Tg Male
Tg Female
Aβ42
Aβ40
Ratio
ng/g cerebrum wet weight
Aβ42/Aβ40 ratio
pmol/mgtissue
r = 0.12
p > 0.05
r = 0.33
p > 0.05
r = 0.003
p > 0.05
r = 0.20
p > 0.05
r = 0.14
p > 0.05
r = 0.24
p > 0.05
LPE(18:0/0:0)

Figure 4.6

Figure 4.7 – GPE species in the plasma associate with spatial learning and memory and cortical but not hippocampal LPE(18:0/0:0) levels. (A) A Venn diagram depicting the distribution of 39 GPE metabolites and signaling molecules in plasma and brain regions. (B) Correlational scatterplots of the three significantly associated plasma GPE species: LPE(16:1/0:0) (left; $r=0.47$, $p<0.05$), PE(O-14:0/2:0) (middle, $r=0.48$, $p<0.05$), and PE(O-18:3/2:0) (right; $r=0.57$, $p<0.01$) with composite spatial learning and memory scores. GPE abundances are represented as pmol per mg of tissue wet weight. (C) Correlational analyses of both hippocampal (left) and cortical (right) LPE(18:0/0:0) levels with plasma GPE species associating with learning and memory. Hippocampal LPE(18:0/0:0) levels are not significantly associated with plasma GPE predicators (all $p>0.05$). Cortical LPE(18:0/0:0) levels are significantly negatively correlated with all three plasma predictors. (D) Univariate analysis of LPE(16:1/0:0) (left; main effect of sex: $F_{(1,16)}=11.12$, df=1, $p<0.01$), PE(O-14:1/2:0) (middle; main effect of sex: $F_{(1,16)}=4.58$, df=1, $p<0.05$), and PE(O-18:3/2:0) (right; main effect of sex: $F_{(1,16)}=11.2$, df=1, $p<0.01$) levels. Levels of all three lipids are significantly lower in Tg females compared Tg males. Plasma lipid abundances are represented as pmol per mL plasma. Brain lipid abundances are represented as pmol per mg tissue wet weight. Correlational statistics for B and C were Pearson correlations. Statistics for D were two-way ANOVAs with a Holm-Sidak *post-hoc* for multiple comparisons between sexes within genotypes (*$p<0.05$).

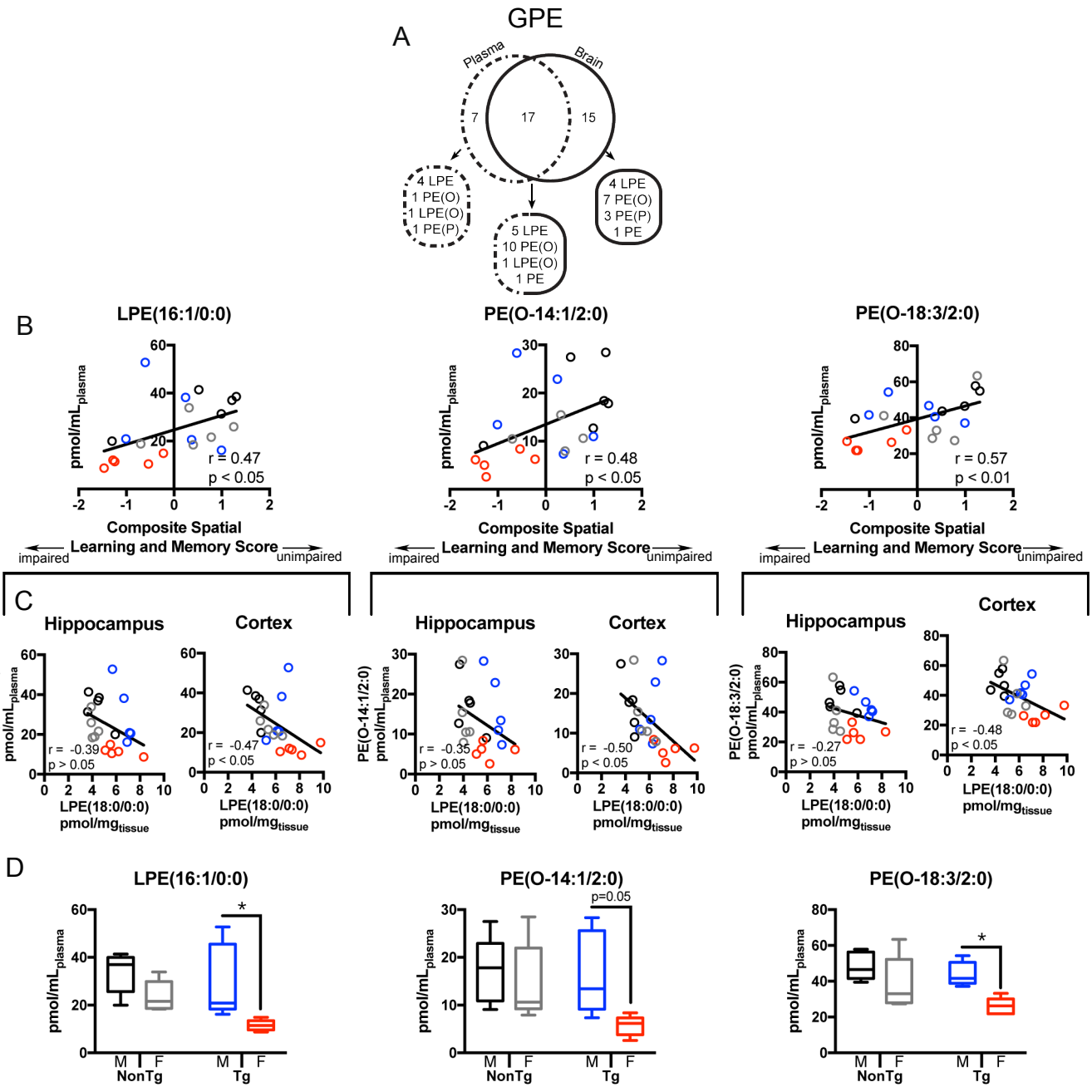
A
GPE
Plasma
Brain
7
17
15
4 LPE
1 PE(O)
1 LPE(O)
1 PE(P)
5 LPE
10 PE(O)
1 LPE(O)
1 PE
4 LPE
7 PE(O)
3 PE(P)
1 PE
B
LPE(16:1/0:0)
PE(O-14:1/2:0)
PE(O-18:3/2:0)
pmol/mL plasma
r = 0.47
p < 0.05
r = 0.48
p < 0.05
r = 0.57
p < 0.01
Composite Spatial
Learning and Memory Score
impaired
unimpaired
C
Hippocampus
Cortex
LPE(16:1/0:0) pmol/mL plasma
r = -0.39
p > 0.05
r = -0.47
p < 0.05
PE(O-14:1/2:0) pmol/mL plasma
r = -0.35
p > 0.05
r = -0.50
p < 0.05
PE(O-18:3/2:0) pmol/mL plasma
r = -0.27
p > 0.05
r = -0.48
p < 0.05
LPE(18:0/0:0) pmol/mg tissue
D
LPE(16:1/0:0)
PE(O-14:1/2:0)
PE(O-18:3/2:0)
pmol/mL plasma
*
p=0.05
M F M F
NonTg
Tg

Figure 4.7

Table 4.2. Correlational matrix of plasma GPE metabolites and signaling molecules with composite spatial scores of learning and memory

	Plasma	
GPE	**Correlation Coefficient r**	**p-value**
LPE(16:1/0:0)	0.471	0.036
LPE(16:0/0:0)	0.085	0.723
LPE(18:2/0:0)	-0.106	0.655
LPE(18:0/0:0)	-0.301	0.198
LPE(20:4/0:0)	-0.066	0.781
TOTAL LPE	**-0.073**	**0.758**
PE(O-14:1/2:0)	0.477	0.034
PE(O-14:0/2:0)	-0.052	0.826
PE(O-16:2/2:0)	0.169	0.477
PE(O-16:1/2:0)	0.188	0.427
PE(O-16:0/2:0)	-0.383	0.096
PE(O-18:4/2:0)	0.313	0.179
PE(O-18:3/2:0)	0.567	0.009
PE(O-18:1/2:0)	0.234	0.321
PE(O-20:5/2:0)	0.212	0.369
PE(O-20:4/2:0)	0.275	0.254
TOTAL PE(O)	**0.210**	**0.374**
LPE(O-23:5/0:0)	0.110	0.643
TOTAL LPE(O)	**0.110**	**0.643**
PE(19:1)	0.087	0.714
TOTAL PE	**0.087**	**0.714**

Correlation Coefficient r

1.00
0.66
0.33
0.00
-0.33
-0.66
-1.00

p-value

<0.01
<0.05
>0.05

impairment in the MWM (Fig. 4.1). In fact, of these three critical species, both LPE(16:1/0:0) and PE(O-18:3/2:0) demonstrate a clear distinction between Tg males and females with no overlapping data between the two groups. Taken together these data suggest that in animals with pre-existing amyloid pathology, plasma levels of LPE(16:1/0:0) and PE(O-18:3/2:0) represent potential biomarkers of spatial learning and memory impairment.

4.7 Discussion

Here, we report that alterations in GPE metabolism in the brain and circulation are associated with spatial learning and memory impairment in N5 TgCRND8 hAβPP mice. Specifically, we identify increases in cortical abundance of LPC(18:0/0:0) as a critical correlate of learning and memory deficits in both male and female mice. Moreover, we find that this metabolic change and severity of learning and memory impairment can be predicted by decreases in circulating LPE(16:1/0:0), PE(O-14:1/2:0), and PE(O-18:3/2:0) levels. These changes associate with learning and memory performance in N5 TgCRND8 mice suggesting that they reflect a critical metabolic response to accumulating Aβ linked to behavioural indices of cognitive decline.

Our intent in performing this study was to identify a lipidomic signature of cognitive reserve. We did not detect a robust signature. Male Tg mice exhibited increases in cortical GPC and GPE metabolites suggesting an upregulation of enzymatic activity involved in the catabolism of glycerophospholipids, likely $cPLA_2$, as reported in our previous study (Chapter 2). We further show that as levels of LPE(18:0/0:0) increase, behavioural indices of spatial learning and memory decline. Interestingly, we previously demonstrated that

LPC levels are reduced at phenoconversion but rise over the course of symptomatic progression. This finding is consistent with evidence that $cPLA_2$ activity is lower during the initial phases of cognitive decline (Schaeffer et al., 2009; Sun et al., 2010) and suggest a difference in GPC and GPE metabolism that may be useful in predicting phenoconversion in preclinical AD patients. In fact, lithium treatment enhances the activity of specific PLA_2 groups, including $sPLA_2$ and $iPLA_2$ which in turn improves memory in rats (Mury et al., 2016). It is tempting to speculate that increased glycerophospholipid metabolism represents a lipidomic signature of cognitive reserve given the sexually dimorphic metabolic response shown in this study that segregates impaired Tg females from non-impaired Tg males; however we show here that while this response is clearly sexually dimorphic, it is not robustly correlated with learning and memory performance.

The primary finding of this paper is that levels of cortical LPE(18:0/0:0) associated with severity of learning and memory impairment can be predicted by changes in circulating GPE metabolites and second messengers in plasma. The sexual dimorphisms evident in both learning and memory performance and glycerophospholipid metabolism in N5 TgCRND8 mice under comparable Aβ load provide a new model to discriminate between sex-specific metabolic responses to Aβ challenge and capacity for individual learning and memory preservation by offering a spectrum of impaired and unimpaired individuals. Our primary findings associate individual murine learning abilities with lipid metabolic responses rather than the group as a whole. This is reflected in human AD patients whereby some individuals are more impaired than other regardless of the current biomarkers of AD pathology. While Tg females were certainly impaired relative to Tg males as groups, impairment in both sexes correlated with LPE(18:0/0:0) levels in the

brain. These effects could be the result of increased LPEAT2 activity, a lysophospholipid acyltransferase predominantly expressed in the murine brain that preferentially transfers stearoyl-CoA (C18:0) to GPEs (Cao et al., 2008; Shindou et al., 2009). This corresponds with previous work finding a reduction in cortical stearic acid in AD brains (Fraser et al., 2010), suggesting that increased activity of LPEAT2 causes the integration of stearic acyls into GPE molecules. While little is currently known about the role of LPEAT2 in AD pathogenesis, our data do point to a novel metabolic determinant contributing to AD decline. As such, this is the first report of a predictive role for GPE metabolism in tracking the progression of spatial learning and memory decline.

4.8 Acknowledgements

M.W.G. was supported by the Ontario Graduate and the Saroj and Kishori Lal Family Scholarships. M.W.G. and H.X. were supported by CTPNL and the CIHR Institute of Aging (TGF-96121). This study was funded by NSERC # 5377 and CIHR MOP 311838 to S.A.L.B.

Chapter 5 – General Discussion

In this thesis, I combine lipidomic and behavioural experiments to determine how glycerophospholipid metabolism is affected in models of AD over the course of spatial learning and memory impairment as assessed in the MWM. I found that, at the onset of learning and memory impairment, $cPLA_2$ activity declines along with generation of LPCs in the cortices of $A\beta PP^{Swe}/PS1^{dE9}$ and N5 TgCRND8 mice. I identified decreases in LPC(18:0/0:0), LPC(16:0/0:0), LPC(24:6/0:0), LPC(25:6/0:0), LPC(O-18:0/0:0), and PC(O-22:6/2:0) as critical metabolic indicators of phenoconversion. I further demonstrated that these same metabolic changes occur in younger $A\beta PP^{Swe}/PS1^{dE9}$ animals following treatment with chronic intermittent hypoxia, an environmental risk actor that accelerates onset of learning and memory deficits. I next tracked changes in GPC metabolism over disease progression in N5 Tg female mice. I found that once Tg females are fully impaired, $cPLA_2$ activity rises; LPC and LPC(O) levels increase; PC(O-18:1/2:0) PAF accumulates in cortex but not hippocampus. I attributed this increase to an age-dependent shift in the expression of the PAFAH1b α1 and α2 catalytic subunits predicts to reduce the rate of PAF hydrolysis. Next, I asked whether these changes were sexually dimorphic given the higher prevalence of AD in females than males.

I developed a model of cognitive reserve reflective of the sexually dimorphic nature of AD by back-crossing F1 C57Bl/6 x C3H/HeJ TgCRND8 mice to a C57Bl/6 lineage. I found that N5 Tg males and females exhibited equivalent Aβ pathologies a 2, 4, 6, and 8 months of age yet females displayed learning and memory deficits earlier than males. I further ensured that this N5 line did not carry the autosomal recessive *pde6b*^{rd1} mutation that leads to retinal degeneration. Finally, I profiled GPC and GPE metabolism in both the

brain and plasma of N5 Tg mice and their NonTg littermates. I demonstrated that GPE metabolites are directly correlated with spatial learning and memory ability in the cortex. Moreover, I show that central lipidomic changes can be predicted by assessment of the circulating lipidome. Taken together, these data provide a strong link between behavioural indices of cognitive impairment and glycerophospholipid metabolism in multiple AD experimental models.

I will discuss in this chapter the varying lipid profiles within the brain, as well as the different roles glycerophospholipid metabolism may play in modulating cognitive reserve and impairment in males and females. This general discussion will place the findings of this thesis into context with the existing literature of AD, cognition, and glycerophospholipid metabolism.

5.1 Lipidomic contributions to the links between chronic intermittent hypoxia and phenoconversion in a model of AD

This thesis is the first study to demonstrate that chronic intermittent hypoxia alters GPC metabolism associated with AD learning and memory impairment. I hypothesize that hypoxia likely enhances the aging process in AβPP^{Swe}/PS1^{dE9} mice thus advancing both phenoconversion and the GPC profile.

Interestingly, I found this to exclusively take place in AβPP^{Swe}/PS1^{dE9} mice and not in WT mice thus indicating a role for amyloid pathology in the alteration of GPC metabolism over time. Our colleagues have found that hypoxia indeed elevates amyloid levels and accelerates the aberrant rise of Aβ in these same mice (Liu et al., 2016). Therefore it may be that amyloid load plays a role in initiating aberrant

glycerophospholipid metabolism associated with transition from pre-symptomatic to a symptomatic state in experimental models of AD in the “preclinical” state of cognitive decline (Fig. 5.1).

The most predictive changes of phenoconversion were decreases in *lyso*-GPCs, specifically LPC(18:0/0:0), LPC(16:0/0:0), LPC(24:6/0:0), LPC(25:6/0:0) as well as LPC(O-18:0/0:0), indicative of altered glycerophospholipid catabolism. These changes could be accelerated by chronic intermittent hypoxia and were attributed to a suppression of $cPLA_2$ activity upon transition from pre-symptomatic to a symptomatic state. Previous work by Yakovlev and colleagues has demonstrated the effects of differential exposures to hypoxic conditions on glycerophospholipids. Longer exposure to hypoxia elicits a progressive decrease in LPCs in liver tissue (Yakovlev et al., 2013). Chronic intermittent hypoxia, however, may impact on the activity of the various PLA_2 families differentially (Micova et al., 2017). Micova and colleagues have found that Wistar rats exposed to a chronic hypoxia regimen representing 7000 m altitude for eight hours/day for five weeks (a more intensive paradigm than used in Chapter 2) elicited family-specific effects on PLA_2 expression in the heart. GIV $cPLA_2$ expression increases, $iPLA_2$ and $sPLA_2$ expressions decrease. While this contrasts with the transient decrease in cortical $cPLA_2$ activity I detect in Chapter 2, this may be due to the longer paradigm and more intensive hypobaric environment used by Micova and colleagues.

Certainly, differential PLA_2 activity has been reported in AD patients (Schaeffer et al., 2010). $cPLA_2$ activity has been proposed to decrease in early-stage AD (Ross et al., 1998) followed by an increase in late-stage AD (Schaeffer et al., 2009; Sun et al., 2010) consistent with this thesis. Increased expression of $sPLA_2$ GIIA in astrocytes is found to

Figure 5.1 – Proposed model of normoxic aging and hypoxic exposure on the Lands' cycle in mouse models of hAβPP mice. Both age and hypoxic exposure elevate Aβ levels in hAβPP mice resulting in symptomatic onset followed by full impairment. Lands' cycle $cPLA_2$ activity exhibits biphasic activity characterized by transiently suppressed activity upon symptomatic onset and progressive activation during full impairment. $iPLA_2$ activity is reduced in hAβPP while PAFAH activity decreases upon full impairment as a result of age-dependent changes in subunit-expression increasing PC(O)-PAF/LPC(O) ratios. Red text describes increased levels and teal text denotes a decrease.

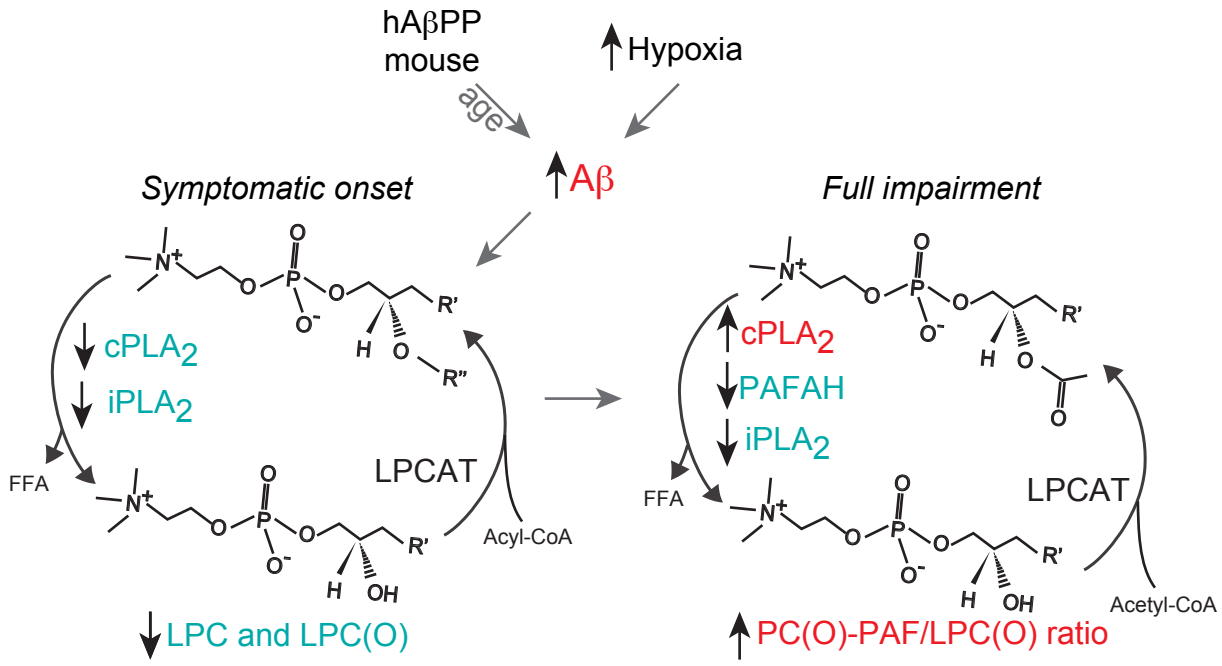
hAβPP
mouse
age
Hypoxia
Aβ
Symptomatic onset
Full impairment
cPLA2
iPLA2
FFA
LPCAT
Acyl-CoA
LPC and LPC(O)
cPLA2
PAFAH
iPLA2
FFA
LPCAT
Acetyl-CoA
PC(O)-PAF/LPC(O) ratio

Figure 5.1

be associated with amyloid plaques in the inferior temporal gyrus (Moses et al., 2006) while decreased iPLA$_2$ activity is common to both hypoxic insult and AD (Micova et al., 2017; Ross et al., 1998; Smesny et al., 2008). Taken together, it is possible that it is not only a decrease in cPLA$_2$ activity but also decreases in iPLA$_2$ activity that contributes to both the hypoxia and age/Aβ-associated GPC metabolic disruptions observed in this thesis. An exciting topic for future investigation includes the temporal analysis of activity in all PLA$_2$ families to clarify the family-specific responses to amyloid pathology in AD.

5.2 Sex-specific differences in glycerophospholipid metabolism in a sexually dimorphic AD mouse model of cognitive reserve

In Chapter 3 I developed and characterized a hAβPP mouse model that recapitulates the sexually dimorphic nature of AD, according to the theory of cognitive reserve (Mielke et al., 2014; Stern, 2006). I show that this N5 TgCRND8 mouse line exhibits a unique sexually dimorphic phenotype that behaviourally models cognitive reserve found in the human condition. What distinguishes this model from other sexually dimorphic hAβPP mouse models is that while female Tg mice are significantly more impaired than males, they present with comparable amyloid pathology. In Chapter 4, I further confirm that there is a prominent sex-specific change in the glycerophospholipid metabolome in the presence of AD pathology.

5.2.1 Measuring cognitive reserve in the context of amyloid pathology

Prior to this thesis work, the theory of cognitive reserve was introduced by Yaakov Stern describing the maintenance of cognitive function despite pathological insults (i.e.

amyloid plaques) through the use of alternative neural networks to adapt new cognitive strategies (Stern, 2002, 2006). In Chapter 3, I was the first to quantify cognitive reserve in rodents using MWM. I utilized the path trajectories employed by each individual mouse and assigned it a strategy, adopting previously set standards (Brody and Holtzman, 2006; Janus, 2004). Because mice that are successful at the MWM are capable of transitioning from a predominantly systematic strategy to a more efficient spatial strategy, I was able to use the strategy shifting in male and female Tg mice to evaluate sexual dimorphisms in the behavioural indices of learning and memory from the perspective of cognitive reserve. I found that males exhibited common characteristics to unimpaired animals thus reflecting the principals of cognitive reserve (Mielke et al., 2014). To my knowledge, no other experimental methods of measuring murine cognitive reserve have been established.

In humans, recent work has presented a novel measure of cognitive reserve that implicates differential functional activation of alternative cortical regions in the presence of amyloid pathology. This work utilized neuroimaging techniques including structural MRI to establish cognitive reserve using correlations between grey matter volumes in both whole brain or temporoparietal regions and composite cognitive scores in patients with AD pathology (van Loenhoud et al., 2017). Subjects with high cognitive reserve likely need to employ different neural networks to compensate for AD pathology and maintain cognitive ability. Indeed, this compensation has been documented using functional magnetic resonance imaging (fMRI) during tasks of increasing difficulty (Oh et al., 2018). In the presence of Aβ pathology, there is a clear change in regional activation in the brain using fMRI during intellectual activity (Oh et al., 2018). In the absence of Aβ pathology,

there was a negative relationship with brain activation in the lateral and medial parietal cortices. Yet when Aβ is present, there is a positive relationship in the lateral temporoparietal cortex, medial frontal cortex, and posterior cingulate and retrosplenial cortices (Oh et al., 2018). These studies offer insight into the adaptability necessary in employing different cortical regions to successfully accomplish a task and the ability to now potentially measure it in humans in vivo. I suggest that my N5 TgCRND8 mouse model of cognitive reserve further provides a viable medium to explore biological mechanisms of cognitive reserve and to test possible interventions.

5.2.2 Sex-specific differences in glycerophospholipid metabolism.

In Chapter 4, I describe regionally-specific sex differences in the cortex of NonTg mice whereby females had greater levels of GPE metabolites and lower levels of GPC metabolites. Sexually dimorphic profiles have been established in a variety of tissues. In brown adipose tissue, the fatty acid composition of structural GPEs, GPCs and GPSs are different between male and female C57Bl/6N mice (Hoene et al., 2014). Moreover, in the plasma of young adults, men have a greater abundance of both LPC and LPC(O) species than women (Rauschert et al., 2017). My research confirms these differences in cortex and, to a lesser extent the hippocampus of NonTg mice. PLA_2 activity is, in part, responsible for the regulation of *lyso*-glycerophosphocholines, including LPCs, LPC(O)s, and LPC(P)s. Limited research has been done to distinguish the effect of sex on PLA_2 regulation and activity in the brain. However, some sex differences do exist in PLA_2 regulation whereby lipoprotein-associated PLA_2 activity in the blood has been found to be higher in males thus supporting a higher level of *lyso*-glycerophospholipids (Jia et al.,

2013). It would be very interesting to further investigate how the role of sex affects tissue-specific expression and activity of the many isoforms of PLA_2 enzymes.

While my work has focused primarily on the Lands' cycle, a second hypothesis, not directly tested in this thesis, is that differences in GPC and GPE metabolite levels between males and females are due to a change in lysophospholipase D (LPLD) activity (Fig. 5.2).

LPLD cleaves the head group moiety from a *lyso*-glycerophospholipid to generate lysophosphatidic acid (LPA) (Fig. 5.2). This enzyme (also called autotaxin) is secreted into the extracellular matrix and has equal specificity for both choline and ethanolamine head groups (Aoki et al., 2002; Yung et al., 2015). However, substrate specificity of LPLD is dependent on the level of saturation, length, and linkage of the single hydrocarbon chain (Tokumura et al., 1999). LPLD shows higher affinity for unsaturated, acyl-linked lysophospholipids but can still act on alkyl-linked lysophospholipids and saturated lysophospholipids (Tokumura et al., 1999).

LPLD expression is not only sexually dichotomous, but is also affected in AD patients. LPLD expression is increased in the CSF and cortex of AD patients (McLimans et al., 2017; Umemura et al., 2006). Interestingly, healthy women exhibit higher serum activity of LPLD than men (Nakamura et al., 2007; Reeves et al., 2015). It may be, that in the presence of AD pathology, the sexually dimorphic expression of LPLD is accentuated therefore contributing to the sexually dimorphic lysophospholipid profiles seen in this thesis. Lower levels of LPLD in males would result in higher levels of precursor molecules such as LPCs, LPC(O)s, LPEs, and LPE(O)s, consistent with the results generated in Chapter 4 (proposed mechanism Fig. 5.3). It has yet to be investigated whether there are

Figure 5.2 –LPLD hydrolyzes the head group from the phosphate of *lyso*-glycerophosphospholipids. A structural representation of the reaction catalyzed by LPLD .

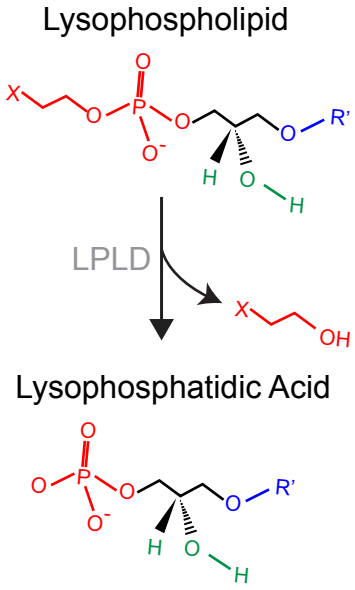
Lysophospholipid
X
O
P
O
O-
O
R'
H
O
H
LPLD
X
OH
Lysophosphatidic Acid
O
P
O
O-
O
R'
H
O
H

Figure 5.2

sex-specific changes in LPLD activity in patients with AD pathology. Enhanced levels in patients already exhibiting signs of AD symptomology suggests that impaired individuals likely have higher levels of LPLD (Umemura et al., 2006). Considering the pre-existing sex difference in LPLD, I propose that males with preclinical AD maintain low levels of LPLD activity thus enhancing precursors such as LPC, LPC(O), LPE, and LPE(O).

5.2.3 Evidence for the role of LPA signaling in spatial learning and memory

It is tempting, therefore, to speculate that the synthesis of LPAs via the actions of LPLD would enhance extracellular LPA signaling which is primarily initiated by binding to G protein-coupled LPA receptors (LPARs). In this thesis, LPAs were not profiled and should be a future target. There are six LPAR subtypes ($LPAR_{1-6}$) expressed in the adult CNS with cell-specific expression. Mature neurons only express $LPAR_{1-3}$ and LPA_5 although glial expression is varied. $LPAR_1$ and $LPAR_3$ are expressed in microglia whereas $LPAR_{1-5}$ are in astrocytes yet only $LPAR_1$ is found in oligodendrocytes and only $LPAR_6$ is found in ependymal cells (reviewed in (Yung et al., 2015)). LPARs couple to one of four $G\alpha$ proteins ($G_{12/13}$, $G_{q/11}$, $G_{i/o}$, and G_s) to initiate a plethora of downstream signaling cascades (reviewed in (Choi and Chun, 2013)). The myriad of cellular processes affected by LPA signaling lead to many varied outcomes, one of which are the effects on learning and memory behaviour.

The impact of LPA signaling on learning and memory likely requires the combined signaling of specific LPAR subtypes. For example, in a $LPAR_1$ null-mutant mouse, *malpa*$_1^{-/-}$ mice exhibit differences in spatial learning and memory in the MWM (Santin et al., 2009). While not significant, these mice exhibit mildly improved escape latencies compared to

WT mice but have significantly impaired reference memory in the probe task (Santin et al., 2009). These conflicting results indicate a role for $LPAR_1$ in learning and memory that may be compensated for by other subtypes of LPAR. Indeed, $LPAR_5$ null (*lpa*$_5^{-/-}$) mice exhibit mild improvements in escape latency as well, likely due through a significantly higher utilization of spatial search strategies (Callaerts-Vegh et al., 2012). No overt phenotypes have been observed in *lpa*$_2^{-/-}$ mice even when coupled with *malpar*$_1^{-/-}$ although no behavioural tests were conducted (Contos et al., 2002). *Lpa*$_4$-/- mice have been produced but no behavioural tests have been performed. (Sumida et al., 2010; Yung et al., 2014). $LPAR_6$ as the most recently discovered LPAR has also not been linked to any behavioural abnormalities (Yung et al., 2014). Thus while these data do not provide direct evidence for a role of LPAs in learning and memory, clearly more concise investigations must be performed in the context of LPA signaling in learning and memory.

This need is highlighted by one highly interesting outcome of behavioural studies involving LPA signaling, namely the effect of LPAR subclasses on spatial search strategy (Callaerts-Vegh et al., 2012; Santin et al., 2009). *malpar*$_1^{-/-}$ mice exhibit a reduction in spatial strategy compared to WT mice in the MWM using comparable strategy as used in Chapter 3 (Brody and Holtzman, 2006; Granger et al., 2016). However, authors noted that this may be a result of enhanced thigmotaxis during MWM thus indicating that the reduced spatial strategy was a result of increased anxiety and not a *bona fide* impairment in spatial navigation from the lack of LPA signaling (Santin et al., 2009). This suggests that the absence of $LPAR_1$ signalling could enhance spatial strategy although anxiety plays a confounding role in this observation. Additionally, conflicting results arise in *lpa*$_5^{-/-}$ mice that exhibit enhanced spatial strategy in the MWM (Callaerts-Vegh et al., 2012).

Unlike *malpar*$_1^{-/-}$ mice, *lpa*$_5^{-/-}$ mice have reduced anxiety thus providing an unadulterated assessment of spatial navigation ability (Callaerts-Vegh et al., 2012). While more investigations are required to fully understand the roll of LPA signaling in spatial navigation, current findings support evidence that the impact of LPA signaling on behaviour may be subclass-dependent. Currently it seems that $LPAR_5$ signaling is involved in impairing spatial navigation, particularly in the MWM. In relation to this thesis, I propose that elevations in *lyso*-GPCs and *lyso*-GPEs in Tg males are representative of lower LPLD activity thus contributing to lower LPA synthesis and $LPAR_5$ activation. Lower LPAR activation, particularly at $LPAR_5$, may contribute to the improved spatial learning and memory exhibited by this model (Proposed model, Fig. 5.3).

5.2.4 LPLD activity exhibits lower activity on LPE(18:0/0:0), a brain-derived indicator of spatial learning and memory ability

One caveat to this alternative "non-Lands' cycle" model is the common increase in LPE(18:0/0:0) in both male and female Tg mice. In the brain, I show elevations in this species is a critical indicators of spatial learning and memory impairment. LPE(18:0/0:0) is the most abundant LPE within detectable range quantified in the brains of these mice. The proposed effects of LPLD activity would influence LPE(18:0/0:0) levels the least since LPLD has lower activity on saturated species (Tokumura et al., 1999). This is supported by the fact that all other significantly changing LPEs have at least one unsaturation and are consistently decreasing in females and increasing in males. In Chapter 2, I show that in 6 month Tg females, there is a mild but significant increase in $cPLA_2$ activity following symptomatic onset. It is possible that varied changes in the Lands' cycle enzymes may

Figure 5.3 Proposed mechanism of non-Lands' cycle mediated effects on sexually dimorphic glycerophospholipid metabolism and spatial navigation. N5 TgCRND8 mice at six-months of age exhibit sexually dimorphic lysophospholipid levels whereby males exhibit a significant increase and females show no change relative to sex- and age-matched NonTg littermates. I suggest that this reflects a difference in lysophospholipid catabolism into lysophosphatidic acid via the actions of LPLD combined with increased in $cPLA_2$ activity in the synthesis of lysophospholipids. Females exhibit higher baseline levels of LPLD than men, and this can be further accentuated by Aβ causing further increases in activity. In male Tgs, an increase in $cPLA_2$ activity due to Aβ, coupled with decreased LPLD activity relative to females may lead to enhanced lysophospholipid levels. In female Tgs, higher activity of LPLD counteracts the high $cPLA_2$ activity thus effecting no change in lysophospholipids. I postulate that this would lead to enhanced LPA levels causing activation of $LPAR_5$ and subsequent impairment in spatial navigation.

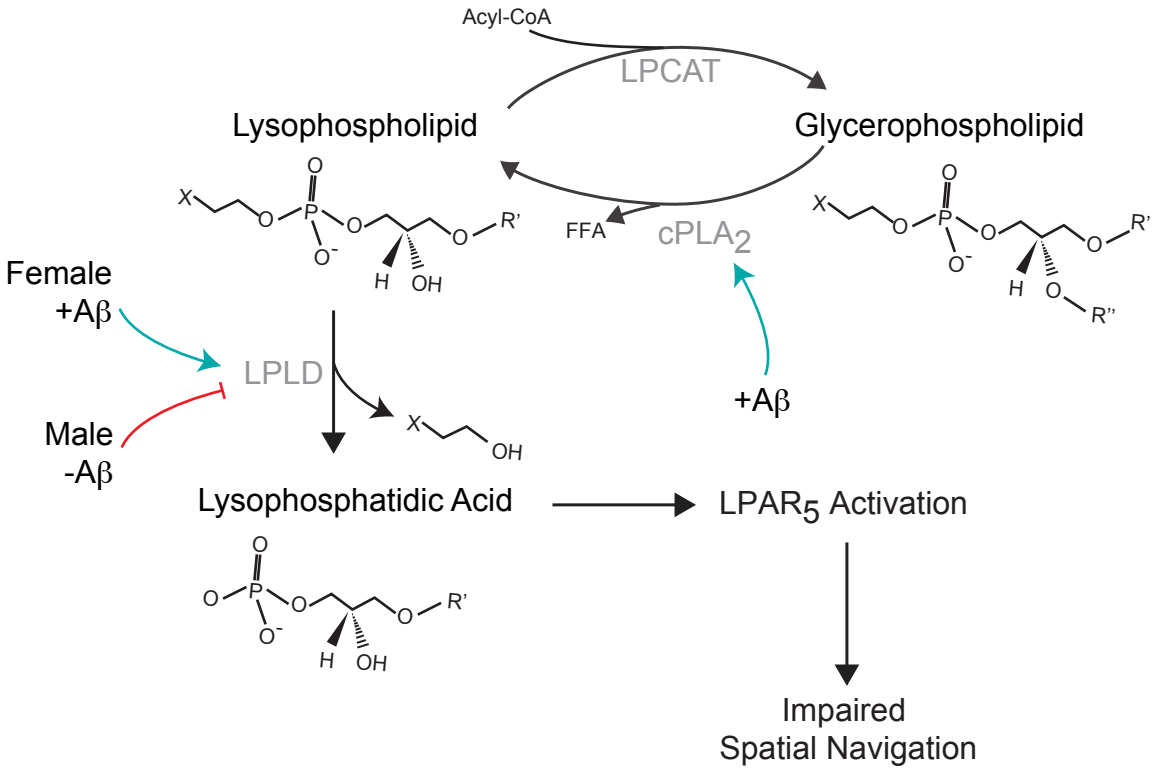
Acyl-CoA
LPCAT
Lysophospholipid
Glycerophospholipid
FFA
cPLA2
Female
+Aβ
Male
-Aβ
LPLD
+Aβ
Lysophosphatidic Acid
LPAR5 Activation
Impaired
Spatial Navigation

Figure 5.3

impact LPE(18:0/0:0). These results are supported by an increase in LPE(18:0/0:0) in AD patients relative to healthy controls (Olazaran et al., 2015). However, while Tg males are unimpaired relative to Tg females as a group, they (as all mouse groups do) exhibit individual variances in composite spatial score, as described in Chapter 4. These individual variances elicit a distinction between (a) the discovery of markers that distinguish an entire group based on the presence of risk factors and behavioural impairment, and (b) determining markers that distinguish individuals based on the specific outcome that the individuals are capable of. In other words, finding predictors of behavioural ability from the perspective of individuals and not their conditions.

5.2.5 Investigations linking individual glycerophospholipidome profiles with spatial learning and memory in AD require an association between central and peripheral lipidomes

In this thesis I have profiled individual differences in the glycerophospholipidome in N5 NonTg and Tg mice. Links between GPE metabolites were found to be predictive of spatial learning and memory ability in both central and circulating lipidomes. Researchers have previously found many relationships between the varying lipidomes of healthy controls, patients with MCI, and full AD dementia patients in either blood (Mapstone et al., 2014; Oresic et al., 2011; Proitsi et al., 2017; Toledo et al., 2017; Whiley et al., 2014) or brain (Wood et al., 2015; Wood et al., 2016) lipidomes. Many of these studies found lower levels of specific structural glycerophospholipids in the blood (Proitsi et al., 2017; Whiley et al., 2014) and brain in AD (Han et al., 2001; Wood et al., 2015; Wood et al., 2016). Upon the beginning of this thesis, no studies existed linking both

central and circulating lipidomes to learning and memory in the same subjects. In Chapter 4, I was able to find significant relationships between levels of specific LPEs and PE(O)s in the plasma with LPE(18:0/0:0) in the brain all of which are significantly associated with spatial learning and memory abilities in the N5 Tg mouse line.

These data complement recent publications (Varma et al., 2018). GPCs were the exclusive glycerophospholipid class investigated in this study. Using limited brain samples, decreases in LPC(18:0/0:0) and structural PC(O) and PC species were significantly associated with disease progression in the brain yet only LPC(18:0/0:0) showed a significantly positive relationship in the serum (Varma et al., 2018). While this suggests negative relationship between blood and brain-based lipids, one limitation to this study is the absence of any direct associations between central and circulating lipidomes. Brain and serum samples were unbalanced and associations did not reflect the same sample cohorts (Varma et al., 2018). An important focus of investigation in lipidomics is the association between blood and brain-based lipidomes. While research is limited in this area, one study has recently found links between glycerophospholipids in the brain the plasma (Giles et al., 2016). Interestingly, negative relationships between the many structural GPEs investigated have been found between brain and plasma lipidomes (Giles et al., 2016). While this study did not investigate the metabolites of GPE catabolism, I confirm this theme of a negative relationship between specific GPE metabolites in the plasma and brain.

5.3 Summary

In this thesis, I have combined multiple techniques incorporating spatial learning and memory measures with glycerophospholipid profiling and signaling pathways. I have elucidated the glycerophospholipid profiles in the context of two prominent, yet distinct risk factors of AD in two separate mouse models of hAβPP. My working mechanistic model is summarized in Fig. 5.4. I have determined that biphasic activity of $cPLA_2$ results in age-dependent changes in GPC profiles in the presence of Aβ pathology representing metabolites and second messengers of GPC catabolism and remodelling. These changes can be accelerated when mice are exposed to chronic intermittent hypoxia. This data helps to resolve conflicting results about $cPLA_2$ activity in AD progression and confirms the presence of a biphasic shift in activity corresponding with cognitive decline. I further show, in an experimental model of sex differences in cognitive reserve that cortical LPE(18:0/0:0) levels are a critical indicator of spatial learning and memory impairment and that metabolic changes can be predicted by alterations in other circulating LPE lipids. This corresponds with previous work linking either brain or plasma glycerophospholipids with cognitive scores although this was the first work to describe the additional link between brain and plasma glycerophospholipids. Bringing both central and peripheral lipidomic signatures together with a common relationship to spatial learning and memory is crucial in determining not only predictors of cognitive impairment but also in offering therapeutic targets and potential biomarkers in the blood that infer lipid levels in the brain. Taken together, this thesis supports further investigations into how the negative cognitive effects of risk factors may be ameliorated through therapies targeting glycerophospholipid metabolism.

Figure 5.4 Combined risk factors of AD and the effects on glycerophospholipid metabolism and spatial learning and memory. The effects of hypoxia and sex can be collapsed into one combined model incorporating pathways introduced in Fig. 5.1 and 5.3. Hypoxia can additionally enhance LPLD activity thus contributing to the decreased *lyso*-GPCs found in Chapter 2.

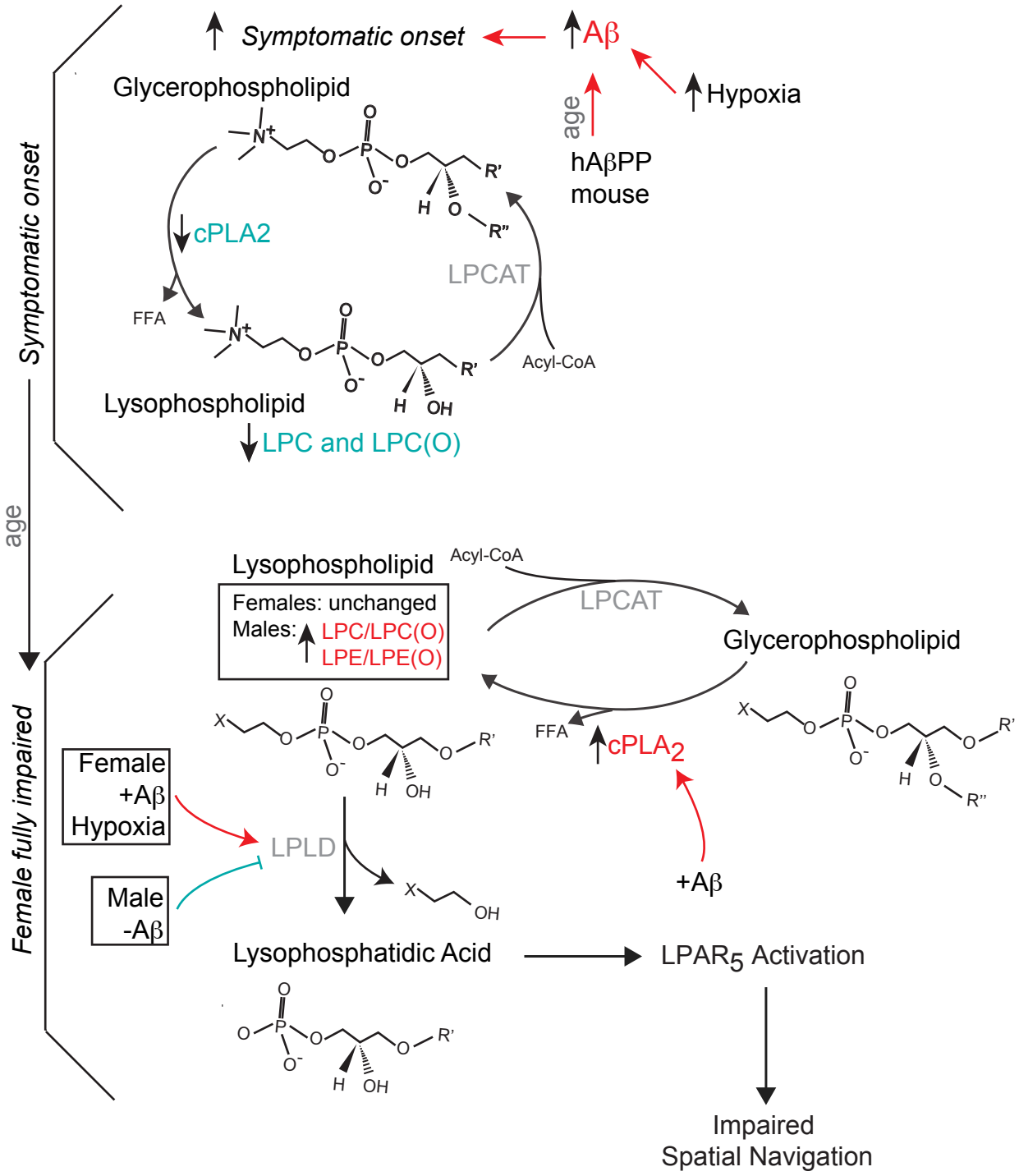
Symptomatic onset
Aβ
Hypoxia
age
hAβPP
mouse
Glycerophospholipid
cPLA2
LPCAT
FFA
Acyl-CoA
Lysophospholipid
LPC and LPC(O)
Symptomatic onset
age
Female fully impaired
Lysophospholipid
Acyl-CoA
Females: unchanged
Males: LPC/LPC(O)
LPE/LPE(O)
LPCAT
Glycerophospholipid
FFA
cPLA2
Female
+Aβ
Hypoxia
Male
-Aβ
LPLD
+Aβ
Lysophosphatidic Acid
LPAR5 Activation
Impaired
Spatial Navigation

Figure 5.4

Chapter 1 - References

Abe, A., and Shayman, J.A. (1998). Purification and characterization of 1-O-acylceramide synthase, a novel phospholipase A2 with transacylase activity. J Biol Chem *273*, 8467-8474.

Alzheimer, A., Stelzmann, R.A., Schnitzlein, H.N., and Murtagh, F.R. (1995). An English translation of Alzheimer's 1907 paper, "Uber eine eigenartige Erkankung der Hirnrinde". Clin Anat *8*, 429-431.

Andrews, S.J., Das, D., Anstey, K.J., and Easteal, S. (2017). Late Onset Alzheimer's Disease Risk Variants in Cognitive Decline: The PATH Through Life Study. J Alzheimers Dis *57*, 423-436.

Apostolova, L.G. (2017). Alzheimer disease: A quantitative trait approach to GWAS pays dividends. Nat Rev Neurol.

Bai, F., Zhang, Z., Watson, D.R., Yu, H., Shi, Y., Zhu, W., Wang, L., Yuan, Y., and Qian, Y. (2009). Absent gender differences of hippocampal atrophy in amnestic type mild cognitive impairment. Neurosci Lett *450*, 85-89.

Banerjee, S., and Mazumdar, S. (2012). Electrospray ionization mass spectrometry: a technique to access the information beyond the molecular weight of the analyte. Int J Anal Chem *2012*, 282574.

Barnes, L.L., Wilson, R.S., Bienias, J.L., Schneider, J.A., Evans, D.A., and Bennett, D.A. (2005). Sex differences in the clinical manifestations of Alzheimer disease pathology. Arch Gen Psychiatry *62*, 685-691.

Bartus, R.T., Dean, R.L., 3rd, Beer, B., and Lippa, A.S. (1982). The cholinergic hypothesis of geriatric memory dysfunction. Science *217*, 408-414.

Bateman, R.J., Xiong, C., Benzinger, T.L., Fagan, A.M., Goate, A., Fox, N.C., Marcus, D.S., Cairns, N.J., Xie, X., Blazey, T.M.*, et al.* (2012). Clinical and biomarker changes in dominantly inherited Alzheimer's disease. N Engl J Med *367*, 795-804.

Bauckneht, M., Chincarini, A., Piva, R., Arnaldi, D., Girtler, N., Massa, F., Pardini, M., Grazzini, M., Efeturk, H., Pagani, M.*, et al.* (2018). Metabolic correlates of reserve and resilience in MCI due to Alzheimer's Disease (AD). Alzheimers Res Ther *10*, 35.

Benilova, I., Karran, E., and De Strooper, B. (2012). The toxic Abeta oligomer and Alzheimer's disease: an emperor in need of clothes. Nat Neurosci *15*, 349-357.

Bennett, S.A., Valenzuela, N., Xu, H., Franko, B., Fai, S., and Figeys, D. (2013). Using neurolipidomics to identify phospholipid mediators of synaptic (dys)function in Alzheimer's Disease. Front Physiol *4*, 168.

Bligh, E.G., and Dyer, W.J. (1959). A rapid method of total lipid extraction and purification. Can J Biochem Physiol *37*, 911-917.

Bochkov, V.N., Oskolkova, O.V., Birukov, K.G., Levonen, A.L., Binder, C.J., and Stockl, J. (2010). Generation and biological activities of oxidized phospholipids. Antioxid Redox Signal *12*, 1009-1059.

Bou Khalil, M., Hou, W., Zhou, H., Elisma, F., Swayne, L.A., Blanchard, A.P., Yao, Z., Bennett, S.A.L., and Figeys, D. (2010). Lipidomics era: Accomplishments and challenges. Mass Spectrom Rev *29*, 877-929.

Bozek, K., Wei, Y., Yan, Z., Liu, X., Xiong, J., Sugimoto, M., Tomita, M., Paabo, S., Sherwood, C.C., Hof, P.R.*, et al.* (2015). Organization and evolution of brain lipidome revealed by large-scale analysis of human, chimpanzee, macaque, and mouse tissues. Neuron *85*, 695-702.

Bozlu, G., Atici, A., Turhan, A.H., Polat, A., Nayci, A., Okuyaz, C., and Taskinlar, H. (2007). Platelet-activating factor antagonist (ABT-491) decreases neuronal apoptosis in neonatal rat model of hypoxic ischemic brain injury. Brain Res *1143*, 193-198.

Braak, H., Alafuzoff, I., Arzberger, T., Kretzschmar, H., and Del Tredici, K. (2006). Staging of Alzheimer disease-associated neurofibrillary pathology using paraffin sections and immunocytochemistry. Acta Neuropathol *112*, 389-404.

Braak, H., and Braak, E. (1991). Neuropathological stageing of Alzheimer-related changes. Acta Neuropathol *82*, 239-259.

Braak, H., and Braak, E. (1995). Staging of Alzheimer's disease-related neurofibrillary changes. Neurobiol Aging *16*, 271-278; discussion 278-284.

Braverman, N.E., and Moser, A.B. (2012). Functions of plasmalogen lipids in health and disease. Biochim Biophys Acta *1822*, 1442-1452.

Broniec, A., Klosinski, R., Pawlak, A., Wrona-Krol, M., Thompson, D., and Sarna, T. (2011). Interactions of plasmalogens and their diacyl analogs with singlet oxygen in selected model systems. Free Radic Biol Med *50*, 892-898.

Brown, H.A., and Murphy, R.C. (2009). Working towards an exegesis for lipids in biology. Nat Chem Biol *5*, 602-606.

Bruins, A.P. (1998). Mechanistic aspects of electrospray ionization. J Chromatogr A *794*, 345-357.

Brundtland, G.H. (2002). From the World Health Organization. Reducing risks to health, promoting healthy life. JAMA *288*, 1974.

Bu, G. (2009). Apolipoprotein E and its receptors in Alzheimer's disease: pathways, pathogenesis and therapy. Nat Rev Neurosci *10*, 333-344.

Burke, J.E., and Dennis, E.A. (2009). Phospholipase A2 structure/function, mechanism, and signaling. J Lipid Res *50 Suppl*, S237-242.

Cao, J., Shan, D., Revett, T., Li, D., Wu, L., Liu, W., Tobin, J.F., and Gimeno, R.E. (2008). Molecular identification of a novel mammalian brain isoform of acyl-CoA:lysophospholipid acyltransferase with prominent ethanolamine lysophospholipid acylating activity, LPEAT2. J Biol Chem *283*, 19049-19057.

Chen, X., Hyatt, B.A., Mucenski, M.L., Mason, R.J., and Shannon, J.M. (2006). Identification and characterization of a lysophosphatidylcholine acyltransferase in alveolar type II cells. Proc Natl Acad Sci U S A *103*, 11724-11729.

Chen, X., Zhang, W., Laird, J., Hazen, S.L., and Salomon, R.G. (2008). Polyunsaturated phospholipids promote the oxidation and fragmentation of gamma-hydroxyalkenals: formation and reactions of oxidatively truncated ether phospholipids. J Lipid Res *49*, 832-846.

Clark, J.D., Lin, L.L., Kriz, R.W., Ramesha, C.S., Sultzman, L.A., Lin, A.Y., Milona, N., and Knopf, J.L. (1991). A novel arachidonic acid-selective cytosolic PLA2 contains a Ca(2+)-dependent translocation domain with homology to PKC and GAP. Cell *65*, 1043-1051.

Cone, E.J., Buchwald, W.F., and Darwin, W.D. (1982). Analytical controls in drug metabolic studies. II. Artifact formation during chloroform extraction of drugs and metabolites with amine substituents. Drug Metab Dispos *10*, 561-567.

Corder, E.H., Saunders, A.M., Strittmatter, W.J., Schmechel, D.E., Gaskell, P.C., Small, G.W., Roses, A.D., Haines, J.L., and Pericak-Vance, M.A. (1993). Gene dose of

apolipoprotein E type 4 allele and the risk of Alzheimer's disease in late onset families. Science *261*, 921-923.

Cosentino, F.I., Bosco, P., Drago, V., Prestianni, G., Lanuzza, B., Iero, I., Tripodi, M., Spada, R.S., Toscano, G., Caraci, F.*, et al.* (2008). The APOE epsilon4 allele increases the risk of impaired spatial working memory in obstructive sleep apnea. Sleep Med *9*, 831-839.

Dass, C. (2000). Principles and Practice of Biological Mass Spectrometry (Wiley).

Davidson, Y., Gibbons, L., Pritchard, A., Hardicre, J., Wren, J., Stopford, C., Julien, C., Thompson, J., Payton, A., Pickering-Brown, S.M.*, et al.* (2007). Apolipoprotein E epsilon4 allele frequency and age at onset of Alzheimer's disease. Dement Geriatr Cogn Disord *23*, 60-66.

Davis, D.G., Schmitt, F.A., Wekstein, D.R., and Markesbery, W.R. (1999). Alzheimer neuropathologic alterations in aged cognitively normal subjects. J Neuropathol Exp Neurol *58*, 376-388.

Delaere, P., He, Y., Fayet, G., Duyckaerts, C., and Hauw, J.J. (1993). Beta A4 deposits are constant in the brain of the oldest old: an immunocytochemical study of 20 French centenarians. Neurobiol Aging *14*, 191-194.

Di Girolamo, F., Lante, I., Muraca, M., and Putignani, L. (2013). The Role of Mass Spectrometry in the "Omics" Era. Curr Org Chem *17*, 2891-2905.

Douchamps, V., and Mathis, C. (2017). A second wind for the cholinergic system in Alzheimer's therapy. Behav Pharmacol *28*, 112-123.

Duan, Y., Dong, S., Gu, F., Hu, Y., and Zhao, Z. (2012). Advances in the pathogenesis of Alzheimer's disease: focusing on tau-mediated neurodegeneration. Transl Neurodegener *1*, 24.

Dubois, B., Hampel, H., Feldman, H.H., Scheltens, P., Aisen, P., Andrieu, S., Bakardjian, H., Benali, H., Bertram, L., Blennow, K.*, et al.* (2016). Preclinical Alzheimer's disease: Definition, natural history, and diagnostic criteria. Alzheimers Dement *12*, 292-323.

Erez, E., Fass, D., and Bibi, E. (2009). How intramembrane proteases bury hydrolytic reactions in the membrane. Nature *459*, 371-378.

Evans, D.A., Funkenstein, H.H., Albert, M.S., Scherr, P.A., Cook, N.R., Chown, M.J., Hebert, L.E., Hennekens, C.H., and Taylor, J.O. (1989). Prevalence of Alzheimer's disease in a community population of older persons. Higher than previously reported. JAMA *262*, 2551-2556.

Fahy, E., Subramaniam, S., Brown, H.A., Glass, C.K., Merrill, A.H., Jr., Murphy, R.C., Raetz, C.R., Russell, D.W., Seyama, Y., Shaw, W.*, et al.* (2005). A comprehensive classification system for lipids. J Lipid Res *46*, 839-861.

Fahy, E., Subramaniam, S., Murphy, R.C., Nishijima, M., Raetz, C.R., Shimizu, T., Spener, F., van Meer, G., Wakelam, M.J., and Dennis, E.A. (2009). Update of the LIPID MAPS comprehensive classification system for lipids. J Lipid Res *50 Suppl*, S9-14.

Farlow, M., Anand, R., Messina, J., Jr., Hartman, R., and Veach, J. (2000). A 52-week study of the efficacy of rivastigmine in patients with mild to moderately severe Alzheimer's disease. Eur Neurol *44*, 236-241.

Farooqui, A.A., Horrocks, L.A., and Farooqui, T. (2000). Glycerophospholipids in brain: their metabolism, incorporation into membranes, functions, and involvement in neurological disorders. Chem Phys Lipids *106*, 1-29.

Farrer, L.A., Cupples, L.A., Haines, J.L., Hyman, B., Kukull, W.A., Mayeux, R., Myers, R.H., Pericak-Vance, M.A., Risch, N., and van Duijn, C.M. (1997). Effects of age, sex, and ethnicity on the association between apolipoprotein E genotype and Alzheimer disease. A meta-analysis. APOE and Alzheimer Disease Meta Analysis Consortium. JAMA *278*, 1349-1356.

Ferri, C.P., Prince, M., Brayne, C., Brodaty, H., Fratiglioni, L., Ganguli, M., Hall, K., Hasegawa, K., Hendrie, H., Huang, Y.*, et al.* (2005). Global prevalence of dementia: a Delphi consensus study. Lancet *366*, 2112-2117.

Fiandaca, M.S., Mapstone, M.E., Cheema, A.K., and Federoff, H.J. (2014). The critical need for defining preclinical biomarkers in Alzheimer's disease. Alzheimers Dement *10*, S196-212.

Folch, J., Lees, M., and Sloane Stanley, G.H. (1957). A simple method for the isolation and purification of total lipides from animal tissues. J Biol Chem *226*, 497-509.

Frisardi, V., Panza, F., Seripa, D., Farooqui, T., and Farooqui, A.A. (2011). Glycerophospholipids and glycerophospholipid-derived lipid mediators: a complex meshwork in Alzheimer's disease pathology. Prog Lipid Res *50*, 313-330.

Furse, S., Egmond, M.R., and Killian, J.A. (2015). Isolation of lipids from biological samples. Mol Membr Biol *32*, 55-64.

Gazos-Lopes, F., Oliveira, M.M., Hoelz, L.V., Vieira, D.P., Marques, A.F., Nakayasu, E.S., Gomes, M.T., Salloum, N.G., Pascutti, P.G., Souto-Padron, T.*, et al.* (2014). Structural

and functional analysis of a platelet-activating lysophosphatidylcholine of Trypanosoma cruzi. PLoS Negl Trop Dis *8*, e3077.

Gibellini, F., and Smith, T.K. (2010). The Kennedy pathway--De novo synthesis of phosphatidylethanolamine and phosphatidylcholine. IUBMB Life *62*, 414-428.

Ginsberg, L., Rafique, S., Xuereb, J.H., Rapoport, S.I., and Gershfeld, N.L. (1995). Disease and anatomic specificity of ethanolamine plasmalogen deficiency in Alzheimer's disease brain. Brain Res *698*, 223-226.

Giri, M., Zhang, M., and Lu, Y. (2016). Genes associated with Alzheimer's disease: an overview and current status. Clin Interv Aging *11*, 665-681.

Gong, C.X., and Iqbal, K. (2008). Hyperphosphorylation of microtubule-associated protein tau: a promising therapeutic target for Alzheimer disease. Curr Med Chem *15*, 2321-2328.

Gottlieb, D.J., DeStefano, A.L., Foley, D.J., Mignot, E., Redline, S., Givelber, R.J., and Young, T. (2004). APOE epsilon4 is associated with obstructive sleep apnea/hypopnea: the Sleep Heart Health Study. Neurology *63*, 664-668.

Guan, Z., Wang, Y., Cairns, N.J., Lantos, P.L., Dallner, G., and Sindelar, P.J. (1999a). Decrease and structural modifications of phosphatidylethanolamine plasmalogen in the brain with Alzheimer disease. J Neuropathol Exp Neurol *58*, 740-747.

Guan, Z.Z., Wang, Y.N., Xiao, K.Q., Hu, P.S., and Liu, J.L. (1999b). Activity of phosphatidylethanolamine-N-methyltransferase in brain affected by Alzheimer's disease. Neurochem Int *34*, 41-47.

Haass, C., Kaether, C., Thinakaran, G., and Sisodia, S. (2012). Trafficking and proteolytic processing of APP. Cold Spring Harb Perspect Med *2*, a006270.

Han, X. (2016). Lipidomics for studying metabolism. Nat Rev Endocrinol *12*, 668-679.

Han, X., Holtzman, D.M., and McKeel, D.W., Jr. (2001). Plasmalogen deficiency in early Alzheimer's disease subjects and in animal models: molecular characterization using electrospray ionization mass spectrometry. J Neurochem *77*, 1168-1180.

Harayama, T., Shindou, H., Ogasawara, R., Suwabe, A., and Shimizu, T. (2008). Identification of a novel noninflammatory biosynthetic pathway of platelet-activating factor. J Biol Chem *283*, 11097-11106.

Hardy, J., and Selkoe, D.J. (2002). The amyloid hypothesis of Alzheimer's disease: progress and problems on the road to therapeutics. Science *297*, 353-356.

Hauser, P.S., Narayanaswami, V., and Ryan, R.O. (2011). Apolipoprotein E: from lipid transport to neurobiology. Prog Lipid Res *50*, 62-74.

Herrup, K. (2010). Reimagining Alzheimer's disease--an age-based hypothesis. J Neurosci *30*, 16755-16762.

Hippius, H., and Neundorfer, G. (2003). The discovery of Alzheimer's disease. Dialogues Clin Neurosci *5*, 101-108.

Hishikawa, D., Shindou, H., Kobayashi, S., Nakanishi, H., Taguchi, R., and Shimizu, T. (2008). Discovery of a lysophospholipid acyltransferase family essential for membrane asymmetry and diversity. Proc Natl Acad Sci U S A *105*, 2830-2835.

Ho, C.S., Lam, C.W., Chan, M.H., Cheung, R.C., Law, L.K., Lit, L.C., Ng, K.F., Suen, M.W., and Tai, H.L. (2003). Electrospray ionisation mass spectrometry: principles and clinical applications. Clin Biochem Rev *24*, 3-12.

Hossain, M.S., Ifuku, M., Take, S., Kawamura, J., Miake, K., and Katafuchi, T. (2013). Plasmalogens rescue neuronal cell death through an activation of AKT and ERK survival signaling. PLoS One *8*, e83508.

Hossain, M.S., Mineno, K., and Katafuchi, T. (2016). Neuronal Orphan G-Protein Coupled Receptor Proteins Mediate Plasmalogens-Induced Activation of ERK and Akt Signaling. PLoS One *11*, e0150846.

Hostettler, M.E., and Carlson, S.L. (2002). PAF antagonist treatment reduces pro-inflammatory cytokine mRNA after spinal cord injury. Neuroreport *13*, 21-24.

Huang, Y., and Mahley, R.W. (2014). Apolipoprotein E: structure and function in lipid metabolism, neurobiology, and Alzheimer's diseases. Neurobiol Dis *72 Pt A*, 3-12.

Igarashi, M., Ma, K., Gao, F., Kim, H.W., Rapoport, S.I., and Rao, J.S. (2011). Disturbed choline plasmalogen and phospholipid fatty acid concentrations in Alzheimer's disease prefrontal cortex. J Alzheimers Dis *24*, 507-517.

Igbavboa, U., Hamilton, J., Kim, H.Y., Sun, G.Y., and Wood, W.G. (2002). A new role for apolipoprotein E: modulating transport of polyunsaturated phospholipid molecular species in synaptic plasma membranes. J Neurochem *80*, 255-261.

Imae, R., Inoue, T., Kimura, M., Kanamori, T., Tomioka, N.H., Kage-Nakadai, E., Mitani, S., and Arai, H. (2010). Intracellular phospholipase A1 and acyltransferase, which are involved in Caenorhabditis elegans stem cell divisions, determine the sn-1 fatty acyl chain of phosphatidylinositol. Mol Biol Cell *21*, 3114-3124.

Izquierdo, I., Fin, C., Schmitz, P.K., Da Silva, R.C., Jerusalinsky, D., Quillfeldt, J.A., Ferreira, M.B., Medina, J.H., and Bazan, N.G. (1995). Memory enhancement by intrahippocampal, intraamygdala, or intraentorhinal infusion of platelet-activating factor measured in an inhibitory avoidance task. Proc Natl Acad Sci U S A *92*, 5047-5051.

Jack, C.R., Jr., Albert, M.S., Knopman, D.S., McKhann, G.M., Sperling, R.A., Carrillo, M.C., Thies, B., and Phelps, C.H. (2011). Introduction to the recommendations from the

National Institute on Aging-Alzheimer's Association workgroups on diagnostic guidelines for Alzheimer's disease. Alzheimers Dement *7*, 257-262.

Jack, C.R., Jr., Knopman, D.S., Jagust, W.J., Petersen, R.C., Weiner, M.W., Aisen, P.S., Shaw, L.M., Vemuri, P., Wiste, H.J., Weigand, S.D.*, et al.* (2013). Tracking pathophysiological processes in Alzheimer's disease: an updated hypothetical model of dynamic biomarkers. Lancet Neurol *12*, 207-216.

Jack, C.R., Jr., Knopman, D.S., Jagust, W.J., Shaw, L.M., Aisen, P.S., Weiner, M.W., Petersen, R.C., and Trojanowski, J.Q. (2010). Hypothetical model of dynamic biomarkers of the Alzheimer's pathological cascade. Lancet Neurol *9*, 119-128.

Jicha, G.A., and Rentz, D.M. (2013). Cognitive and brain reserve and the diagnosis and treatment of preclinical Alzheimer disease. Neurology *80*, 1180-1181.

Jonsson, T., Atwal, J.K., Steinberg, S., Snaedal, J., Jonsson, P.V., Bjornsson, S., Stefansson, H., Sulem, P., Gudbjartsson, D., Maloney, J.*, et al.* (2012). A mutation in APP protects against Alzheimer's disease and age-related cognitive decline. Nature *488*, 96-99.

Kang, S., Lee, Y.H., and Lee, J.E. (2017). Metabolism-Centric Overview of the Pathogenesis of Alzheimer's Disease. Yonsei Med J *58*, 479-488.

Kato, K., Clark, G.D., Bazan, N.G., and Zorumski, C.F. (1994). Platelet-activating factor as a potential retrograde messenger in CA1 hippocampal long-term potentiation. Nature *367*, 175-179.

Katzman, R., Terry, R., DeTeresa, R., Brown, T., Davies, P., Fuld, P., Renbing, X., and Peck, A. (1988). Clinical, pathological, and neurochemical changes in dementia: a

subgroup with preserved mental status and numerous neocortical plaques. Ann Neurol *23*, 138-144.

Kennedy, E.P., and Weiss, S.B. (1956). The function of cytidine coenzymes in the biosynthesis of phospholipides. J Biol Chem *222*, 193-214.

Kent, C. (1995). Eukaryotic phospholipid biosynthesis. Annu Rev Biochem *64*, 315-343.

Kheirandish, L., Row, B.W., Li, R.C., Brittian, K.R., and Gozal, D. (2005). Apolipoprotein E-deficient mice exhibit increased vulnerability to intermittent hypoxia-induced spatial learning deficits. Sleep *28*, 1412-1417.

Kim, J., Yoon, H., Basak, J., and Kim, J. (2014). Apolipoprotein E in synaptic plasticity and Alzheimer's disease: potential cellular and molecular mechanisms. Mol Cells *37*, 767-776.

Klein, J. (2000). Membrane breakdown in acute and chronic neurodegeneration: focus on choline-containing phospholipids. Journal of neural transmission *107*, 1027-1063.

Knopman, D.S., Parisi, J.E., Salviati, A., Floriach-Robert, M., Boeve, B.F., Ivnik, R.J., Smith, G.E., Dickson, D.W., Johnson, K.A., Petersen, L.E.*, et al.* (2003). Neuropathology of cognitively normal elderly. J Neuropathol Exp Neurol *62*, 1087-1095.

Koedam, E.L., Lauffer, V., van der Vlies, A.E., van der Flier, W.M., Scheltens, P., and Pijnenburg, Y.A. (2010). Early-versus late-onset Alzheimer's disease: more than age alone. J Alzheimers Dis *19*, 1401-1408.

Kofeler, H.C., Fauland, A., Rechberger, G.N., and Trotzmuller, M. (2012). Mass spectrometry based lipidomics: an overview of technological platforms. Metabolites *2*, 19-38.

Lam, S.M., and Shui, G. (2013). Lipidomics as a principal tool for advancing biomedical research. J Genet Genomics *40*, 375-390.

Lane-Donovan, C., Philips, G.T., and Herz, J. (2014). More than cholesterol transporters: lipoprotein receptors in CNS function and neurodegeneration. Neuron *83*, 771-787.

Larson, E.B., Shadlen, M.F., Wang, L., McCormick, W.C., Bowen, J.D., Teri, L., and Kukull, W.A. (2004). Survival after initial diagnosis of Alzheimer disease. Ann Intern Med *140*, 501-509.

Lauwers, E., Goodchild, R., and Verstreken, P. (2016). Membrane Lipids in Presynaptic Function and Disease. Neuron *90*, 11-25.

Laws, K.R., Irvine, K., and Gale, T.M. (2016). Sex differences in cognitive impairment in Alzheimer's disease. World J Psychiatry *6*, 54-65.

Lehninger, A.L. (1968). The neuronal membrane. Proc Natl Acad Sci U S A *60*, 1069-1080.

Li, L., Han, J., Wang, Z., Liu, J., Wei, J., Xiong, S., and Zhao, Z. (2014). Mass spectrometry methodology in lipid analysis. Int J Mol Sci *15*, 10492-10507.

Lin, K.A., and Doraiswamy, P.M. (2014). When Mars Versus Venus is Not a Cliche: Gender Differences in the Neurobiology of Alzheimer's Disease. Front Neurol *5*, 288.

Lipton, S.A. (2005). The molecular basis of memantine action in Alzheimer's disease and other neurologic disorders: low-affinity, uncompetitive antagonism. Curr Alzheimer Res *2*, 155-165.

Liu, C.C., Liu, C.C., Kanekiyo, T., Xu, H., and Bu, G. (2013). Apolipoprotein E and Alzheimer disease: risk, mechanisms and therapy. Nat Rev Neurol *9*, 106-118.

Liu, Y., Shields, L.B., Gao, Z., Wang, Y., Zhang, Y.P., Chu, T., Zhu, Q., Shields, C.B., and Cai, J. (2016). Current Understanding of Platelet-Activating Factor Signaling in Central Nervous System Diseases. Mol Neurobiol.

Lofgren, L., Forsberg, G.B., and Stahlman, M. (2016). The BUME method: a new rapid and simple chloroform-free method for total lipid extraction of animal tissue. Sci Rep *6*, 27688.

Lomnitski, L., Oron, L., Sklan, D., and Michaelson, D.M. (1999). Distinct alterations in phospholipid metabolism in brains of apolipoprotein E-deficient mice. J Neurosci Res *58*, 586-592.

Luy, M., and Minagawa, Y. (2014). Gender gaps--Life expectancy and proportion of life in poor health. Health Rep *25*, 12-19.

Manya, H., Aoki, J., Kato, H., Ishii, J., Hino, S., Arai, H., and Inoue, K. (1999). Biochemical characterization of various catalytic complexes of the brain platelet-activating factor acetylhydrolase. J Biol Chem *274*, 31827-31832.

Marathe, G.K., Zimmerman, G.A., Prescott, S.M., and McIntyre, T.M. (2002). Activation of vascular cells by PAF-like lipids in oxidized LDL. Vascul Pharmacol *38*, 193-200.

Matsui, T., Ingelsson, M., Fukumoto, H., Ramasamy, K., Kowa, H., Frosch, M.P., Irizarry, M.C., and Hyman, B.T. (2007). Expression of APP pathway mRNAs and proteins in Alzheimer's disease. Brain Res *1161*, 116-123.

Mayeux, R., and Stern, Y. (2012). Epidemiology of Alzheimer disease. Cold Spring Harb Perspect Med *2*.

McDonald, J.G., Cummins, C.L., Barkley, R.M., Thompson, B.M., and Lincoln, H.A. (2008). Identification and quantitation of sorbitol-based nuclear clarifying agents extracted

from common laboratory and consumer plasticware made of polypropylene. Anal Chem *80*, 5532-5541.

McIntyre, T.M. (2012). Bioactive oxidatively truncated phospholipids in inflammation and apoptosis: formation, targets, and inactivation. Biochim Biophys Acta *1818*, 2456-2464.

McKhann, G., Drachman, D., Folstein, M., Katzman, R., Price, D., and Stadlan, E.M. (1984). Clinical diagnosis of Alzheimer's disease: report of the NINCDS-ADRDA Work Group under the auspices of Department of Health and Human Services Task Force on Alzheimer's Disease. Neurology *34*, 939-944.

McKhann, G.M., Knopman, D.S., Chertkow, H., Hyman, B.T., Jack, C.R., Jr., Kawas, C.H., Klunk, W.E., Koroshetz, W.J., Manly, J.J., Mayeux, R.*, et al.* (2011). The diagnosis of dementia due to Alzheimer's disease: recommendations from the National Institute on Aging-Alzheimer's Association workgroups on diagnostic guidelines for Alzheimer's disease. Alzheimers Dement *7*, 263-269.

Mielke, M.M., Vemuri, P., and Rocca, W.A. (2014). Clinical epidemiology of Alzheimer's disease: assessing sex and gender differences. Clin Epidemiol *6*, 37-48.

Moessinger, C., Klizaite, K., Steinhagen, A., Philippou-Massier, J., Shevchenko, A., Hoch, M., Ejsing, C.S., and Thiele, C. (2014). Two different pathways of phosphatidylcholine synthesis, the Kennedy Pathway and the Lands Cycle, differentially regulate cellular triacylglycerol storage. BMC Cell Biol *15*, 43.

Morris, J.C., Storandt, M., McKeel, D.W., Jr., Rubin, E.H., Price, J.L., Grant, E.A., and Berg, L. (1996). Cerebral amyloid deposition and diffuse plaques in "normal" aging: Evidence for presymptomatic and very mild Alzheimer's disease. Neurology *46*, 707-719.

Mouchlis, V.D., Chen, Y., McCammon, J.A., and Dennis, E.A. (2018). Membrane Allostery and Unique Hydrophobic Sites Promote Enzyme Substrate Specificity. J Am Chem Soc *140*, 3285-3291.

Mulder, C., Wahlund, L.O., Teerlink, T., Blomberg, M., Veerhuis, R., van Kamp, G.J., Scheltens, P., and Scheffer, P.G. (2003). Decreased lysophosphatidylcholine/phosphatidylcholine ratio in cerebrospinal fluid in Alzheimer's disease. J Neural Transm (Vienna) *110*, 949-955.

Murakami, M., Sato, H., Miki, Y., Yamamoto, K., and Taketomi, Y. (2015). A new era of secreted phospholipase A(2). J Lipid Res *56*, 1248-1261.

Nakanishi, H., Shindou, H., Hishikawa, D., Harayama, T., Ogasawara, R., Suwabe, A., Taguchi, R., and Shimizu, T. (2006). Cloning and characterization of mouse lung-type acyl-CoA:lysophosphatidylcholine acyltransferase 1 (LPCAT1). Expression in alveolar type II cells and possible involvement in surfactant production. J Biol Chem *281*, 20140-20147.

Nalivaeva, N.N., and Turner, A.J. (2013). The amyloid precursor protein: a biochemical enigma in brain development, function and disease. FEBS Lett *587*, 2046-2054.

Nalivaevaa, N.N., Fisk, L., Kochkina, E.G., Plesneva, S.A., Zhuravin, I.A., Babusikova, E., Dobrota, D., and Turner, A.J. (2004). Effect of hypoxia/ischemia and hypoxic preconditioning/reperfusion on expression of some amyloid-degrading enzymes. Ann N Y Acad Sci *1035*, 21-33.

Nelson, P.T., Braak, H., and Markesbery, W.R. (2009). Neuropathology and cognitive impairment in Alzheimer disease: a complex but coherent relationship. J Neuropathol Exp Neurol *68*, 1-14.

Nitsch, R.M., Blusztajn, J.K., Pittas, A.G., Slack, B.E., Growdon, J.H., and Wurtman, R.J. (1992). Evidence for a membrane defect in Alzheimer disease brain. Proc Natl Acad Sci U S A *89*, 1671-1675.

O'Flaherty, J.T., Tessner, T., Greene, D., Redman, J.R., and Wykle, R.L. (1994). Comparison of 1-O-alkyl-, 1-O-alk-1'-enyl-, and 1-O-acyl-2-acetyl-sn-glycero-3-phosphoethanolamines and -3-phosphocholines as agonists of the platelet-activating factor family. Biochim Biophys Acta *1210*, 209-216.

Ohto, T., Uozumi, N., Hirabayashi, T., and Shimizu, T. (2005). Identification of novel cytosolic phospholipase A(2)s, murine cPLA(2){delta}, {epsilon}, and {zeta}, which form a gene cluster with cPLA(2){beta}. J Biol Chem *280*, 24576-24583.

Okonkwo, O.C., and Vemuri, P. (2017). Stemming the Alzheimer tsunami: introduction to the special issue on reserve and resilience in Alzheimer's disease. Brain Imaging Behav *11*, 301-303.

Oresic, M., Hyotylainen, T., Herukka, S.K., Sysi-Aho, M., Mattila, I., Seppanan-Laakso, T., Julkunen, V., Gopalacharyulu, P.V., Hallikainen, M., Koikkalainen, J.*, et al.* (2011). Metabolome in progression to Alzheimer's disease. Transl Psychiatry *1*, e57.

Packard, M.G., Teather, L.A., and Bazan, N.G. (1996). Effects of intrastriatal injections of platelet-activating factor and the PAF antagonist BN 52021 on memory. Neurobiol Learn Mem *66*, 176-182.

Pajak, B., Kania, E., and Orzechowski, A. (2016). Killing Me Softly: Connotations to Unfolded Protein Response and Oxidative Stress in Alzheimer's Disease. Oxid Med Cell Longev *2016*, 1805304.

Panegyres, P.K. (1997). The amyloid precursor protein gene: a neuropeptide gene with diverse functions in the central nervous system. Neuropeptides *31*, 523-535.

Perneczky, R., Drzezga, A., Diehl-Schmid, J., Li, Y., and Kurz, A. (2007). Gender differences in brain reserve : an (18)F-FDG PET study in Alzheimer's disease. J Neurol *254*, 1395-1400.

Petersen, R.C. (2004). Mild cognitive impairment as a diagnostic entity. J Intern Med *256*, 183-194.

Petersen, R.C. (2011). Clinical practice. Mild cognitive impairment. N Engl J Med *364*, 2227-2234.

Petersen, R.C., Aisen, P., Boeve, B.F., Geda, Y.E., Ivnik, R.J., Knopman, D.S., Mielke, M., Pankratz, V.S., Roberts, R., Rocca, W.A.*, et al.* (2013). Mild cognitive impairment due to Alzheimer disease in the community. Ann Neurol *74*, 199-208.

Petersen, R.C., Aisen, P.S., Beckett, L.A., Donohue, M.C., Gamst, A.C., Harvey, D.J., Jack, C.R., Jr., Jagust, W.J., Shaw, L.M., Toga, A.W.*, et al.* (2010a). Alzheimer's Disease Neuroimaging Initiative (ADNI): clinical characterization. Neurology *74*, 201-209.

Petersen, R.C., Roberts, R.O., Knopman, D.S., Geda, Y.E., Cha, R.H., Pankratz, V.S., Boeve, B.F., Tangalos, E.G., Ivnik, R.J., and Rocca, W.A. (2010b). Prevalence of mild cognitive impairment is higher in men. The Mayo Clinic Study of Aging. Neurology *75*, 889-897.

Pietrzak, R.H., Lim, Y.Y., Ames, D., Harrington, K., Restrepo, C., Martins, R.N., Rembach, A., Laws, S.M., Masters, C.L., Villemagne, V.L.*, et al.* (2015). Trajectories of memory decline in preclinical Alzheimer's disease: results from the Australian Imaging, Biomarkers and Lifestyle Flagship Study of ageing. Neurobiol Aging *36*, 1231-1238.

Piomelli, D., Astarita, G., and Rapaka, R. (2007). A neuroscientist's guide to lipidomics. Nat Rev Neurosci *8*, 743-754.

Plassman, B.L., Langa, K.M., Fisher, G.G., Heeringa, S.G., Weir, D.R., Ofstedal, M.B., Burke, J.R., Hurd, M.D., Potter, G.G., Rodgers, W.L.*, et al.* (2007). Prevalence of dementia in the United States: the aging, demographics, and memory study. Neuroepidemiology *29*, 125-132.

Price, J.L., and Morris, J.C. (1999). Tangles and plaques in nondemented aging and "preclinical" Alzheimer's disease. Ann Neurol *45*, 358-368.

Pruzanski, W., Lambeau, L., Lazdunsky, M., Cho, W., Kopilov, J., and Kuksis, A. (2005). Differential hydrolysis of molecular species of lipoprotein phosphatidylcholine by groups IIA, V and X secretory phospholipases A2. Biochim Biophys Acta *1736*, 38-50.

Pugh, E.L., Kates, M., and Hanahan, D.J. (1977). Characterization of the alkyl ether species of phosphatidylcholine in bovine heart. J Lipid Res *18*, 710-716.

Puzzo, D., Gulisano, W., Arancio, O., and Palmeri, A. (2015). The keystone of Alzheimer pathogenesis might be sought in Abeta physiology. Neuroscience.

Qiu, C., Kivipelto, M., and von Strauss, E. (2009). Epidemiology of Alzheimer's disease: occurrence, determinants, and strategies toward intervention. Dialogues Clin Neurosci *11*, 111-128.

Qiu, T., Liu, Q., Chen, Y.X., Zhao, Y.F., and Li, Y.M. (2015). Abeta42 and Abeta40: similarities and differences. J Pept Sci *21*, 522-529.

Rademakers, R., Cruts, M., and Van Broeckhoven, C. (2003). Genetics of early-onset Alzheimer dementia. ScientificWorldJournal *3*, 497-519.

Rapoport, S.I. (2014). Lithium and the other mood stabilizers effective in bipolar disorder target the rat brain arachidonic acid cascade. ACS Chem Neurosci *5*, 459-467.

Reis, A., Rudnitskaya, A., Blackburn, G.J., Mohd Fauzi, N., Pitt, A.R., and Spickett, C.M. (2013). A comparison of five lipid extraction solvent systems for lipidomic studies of human LDL. J Lipid Res *54*, 1812-1824.

Reis, A., and Spickett, C.M. (2012). Chemistry of phospholipid oxidation. Biochim Biophys Acta *1818*, 2374-2387.

Reitz, C., Brayne, C., and Mayeux, R. (2011). Epidemiology of Alzheimer disease. Nat Rev Neurol *7*, 137-152.

Reitz, C., and Mayeux, R. (2014). Alzheimer disease: epidemiology, diagnostic criteria, risk factors and biomarkers. Biochem Pharmacol *88*, 640-651.

Richmond, G.S., and Smith, T.K. (2011). Phospholipases A(1). Int J Mol Sci *12*, 588-612.

Rizzi, L., Rosset, I., and Roriz-Cruz, M. (2014). Global epidemiology of dementia: Alzheimer's and vascular types. Biomed Res Int *2014*, 908915.

Rodriguez-Rodriguez, E., Mateo, I., Llorca, J., Sanchez-Quintana, C., Infante, J., Garcia-Gorostiaga, I., Sanchez-Juan, P., Berciano, J., and Combarros, O. (2007). Association of genetic variants of ABCA1 with Alzheimer's disease risk. Am J Med Genet B Neuropsychiatr Genet *144B*, 964-968.

Rogawski, M.A., and Wenk, G.L. (2003). The neuropharmacological basis for the use of memantine in the treatment of Alzheimer's disease. CNS Drug Rev *9*, 275-308.

Rountree, S.D., Waring, S.C., Chan, W.C., Lupo, P.J., Darby, E.J., and Doody, R.S. (2007). Importance of subtle amnestic and nonamnestic deficits in mild cognitive

impairment: prognosis and conversion to dementia. Dement Geriatr Cogn Disord *24*, 476-482.

Row, B.W., Kheirandish, L., Li, R.C., Guo, S.Z., Brittian, K.R., Hardy, M., Bazan, N.G., and Gozal, D. (2004). Platelet-activating factor receptor-deficient mice are protected from experimental sleep apnea-induced learning deficits. J Neurochem *89*, 189-196.

Ryan, S.D., Harris, C.S., Carswell, C.L., Baenziger, J.E., and Bennett, S.A. (2008). Heterogeneity in the sn-1 carbon chain of platelet-activating factor glycerophospholipids determines pro- or anti-apoptotic signaling in primary neurons. J Lipid Res *49*, 2250-2258.

Ryan, S.D., Whitehead, S.N., Swayne, L.A., Moffat, T.C., Hou, W., Ethier, M., Bourgeois, A.J., Rashidian, J., Blanchard, A.P., Fraser, P.E.*, et al.* (2009). Amyloid-beta42 signals tau hyperphosphorylation and compromises neuronal viability by disrupting alkylacylglycerophosphocholine metabolism. Proc Natl Acad Sci U S A *106*, 20936-20941.

Sastry, P.S. (1985). Lipids of nervous tissue: composition and metabolism. Prog Lipid Res *24*, 69-176.

Schaloske, R.H., and Dennis, E.A. (2006). The phospholipase A2 superfamily and its group numbering system. Biochim Biophys Acta *1761*, 1246-1259.

Scholl, M., Lockhart, S.N., Schonhaut, D.R., O'Neil, J.P., Janabi, M., Ossenkoppele, R., Baker, S.L., Vogel, J.W., Faria, J., Schwimmer, H.D.*, et al.* (2016). PET Imaging of Tau Deposition in the Aging Human Brain. Neuron *89*, 971-982.

Selkoe, D.J., and Hardy, J. (2016). The amyloid hypothesis of Alzheimer's disease at 25 years. EMBO Mol Med *8*, 595-608.

Sengupta, A., Kabat, J., Novak, M., Wu, Q., Grundke-Iqbal, I., and Iqbal, K. (1998). Phosphorylation of tau at both Thr 231 and Ser 262 is required for maximal inhibition of its binding to microtubules. Arch Biochem Biophys *357*, 299-309.

Seshadri, S., Wolf, P.A., Beiser, A., Au, R., McNulty, K., White, R., and D'Agostino, R.B. (1997). Lifetime risk of dementia and Alzheimer's disease. The impact of mortality on risk estimates in the Framingham Study. Neurology *49*, 1498-1504.

Sethi, S., and Brietzke, E. (2017). Recent advances in lipidomics: Analytical and clinical perspectives. Prostaglandins Other Lipid Mediat *128-129*, 8-16.

Shaw, P., Ahn, K., and Rapoport, J.L. (2017). Good News for Screening for Adult Attention-Deficit/Hyperactivity Disorder. JAMA Psychiatry *74*, 527.

Shindou, H., Hishikawa, D., Harayama, T., Yuki, K., and Shimizu, T. (2009). Recent progress on acyl CoA: lysophospholipid acyltransferase research. J Lipid Res *50 Suppl*, S46-51.

Sinforiani, E., Citterio, A., Zucchella, C., Bono, G., Corbetta, S., Merlo, P., and Mauri, M. (2010). Impact of gender differences on the outcome of Alzheimer's disease. Dement Geriatr Cogn Disord *30*, 147-154.

Smiley, P.L., Stremler, K.E., Prescott, S.M., Zimmerman, G.A., and McIntyre, T.M. (1991). Oxidatively fragmented phosphatidylcholines activate human neutrophils through the receptor for platelet-activating factor. J Biol Chem *266*, 11104-11110.

Snowdon, D.A., and Nun, S. (2003). Healthy aging and dementia: findings from the Nun Study. Ann Intern Med *139*, 450-454.

Sole-Padulles, C., Bartres-Faz, D., Junque, C., Vendrell, P., Rami, L., Clemente, I.C., Bosch, B., Villar, A., Bargallo, N., Jurado, M.A.*, et al.* (2009). Brain structure and function

related to cognitive reserve variables in normal aging, mild cognitive impairment and Alzheimer's disease. Neurobiol Aging *30*, 1114-1124.

Solis-Calero, C., Ortega-Castro, J., Frau, J., and Munoz, F. (2015). Nonenzymatic Reactions above Phospholipid Surfaces of Biological Membranes: Reactivity of Phospholipids and Their Oxidation Derivatives. Oxid Med Cell Longev *2015*, 319505.

Sperling, R.A., Aisen, P.S., Beckett, L.A., Bennett, D.A., Craft, S., Fagan, A.M., Iwatsubo, T., Jack, C.R., Jr., Kaye, J., Montine, T.J.*, et al.* (2011). Toward defining the preclinical stages of Alzheimer's disease: recommendations from the National Institute on Aging-Alzheimer's Association workgroups on diagnostic guidelines for Alzheimer's disease. Alzheimers Dement *7*, 280-292.

Spickett, C.M., and Pitt, A.R. (2015). Oxidative lipidomics coming of age: advances in analysis of oxidized phospholipids in physiology and pathology. Antioxid Redox Signal *22*, 1646-1666.

Stern, Y. (2002). What is cognitive reserve? Theory and research application of the reserve concept. J Int Neuropsychol Soc *8*, 448-460.

Stern, Y. (2006). Cognitive reserve and Alzheimer disease. Alzheimer Dis Assoc Disord *20*, S69-74.

Stern, Y. (2012). Cognitive reserve in ageing and Alzheimer's disease. Lancet Neurol *11*, 1006-1012.

Tanzi, R.E., Gusella, J.F., Watkins, P.C., Bruns, G.A., St George-Hyslop, P., Van Keuren, M.L., Patterson, D., Pagan, S., Kurnit, D.M., and Neve, R.L. (1987). Amyloid beta protein gene: cDNA, mRNA distribution, and genetic linkage near the Alzheimer locus. Science *235*, 880-884.

Tian, H., Bai, J., An, Z., Chen, Y., Zhang, R., He, J., Bi, X., Song, Y., and Abliz, Z. (2013). Plasma metabolome analysis by integrated ionization rapid-resolution liquid chromatography/tandem mass spectrometry. Rapid Commun Mass Spectrom *27*, 2071-2080.

Underwood, K.W., Song, C., Kriz, R.W., Chang, X.J., Knopf, J.L., and Lin, L.L. (1998). A novel calcium-independent phospholipase A2, cPLA2-gamma, that is prenylated and contains homology to cPLA2. J Biol Chem *273*, 21926-21932.

Valentin, E., Ghomashchi, F., Gelb, M.H., Lazdunski, M., and Lambeau, G. (2000). Novel human secreted phospholipase A(2) with homology to the group III bee venom enzyme. J Biol Chem *275*, 7492-7496.

Valentin, E., and Lambeau, G. (2000). Increasing molecular diversity of secreted phospholipases A(2) and their receptors and binding proteins. Biochim Biophys Acta *1488*, 59-70.

van Harten, A.C., Kester, M.I., Visser, P.J., Blankenstein, M.A., Pijnenburg, Y.A., van der Flier, W.M., and Scheltens, P. (2011). Tau and p-tau as CSF biomarkers in dementia: a meta-analysis. Clin Chem Lab Med *49*, 353-366.

Wahrle, S.E., Jiang, H., Parsadanian, M., Legleiter, J., Han, X., Fryer, J.D., Kowalewski, T., and Holtzman, D.M. (2004). ABCA1 is required for normal central nervous system ApoE levels and for lipidation of astrocyte-secreted apoE. J Biol Chem *279*, 40987-40993.

Walter, A., Korth, U., Hilgert, M., Hartmann, J., Weichel, O., Hilgert, M., Fassbender, K., Schmitt, A., and Klein, J. (2004). Glycerophosphocholine is elevated in cerebrospinal fluid of Alzheimer patients. Neurobiol Aging *25*, 1299-1303.

Ward, A., Tardiff, S., Dye, C., and Arrighi, H.M. (2013). Rate of conversion from prodromal Alzheimer's disease to Alzheimer's dementia: a systematic review of the literature. Dement Geriatr Cogn Dis Extra *3*, 320-332.

Webster, S.J., Bachstetter, A.D., Nelson, P.T., Schmitt, F.A., and Van Eldik, L.J. (2014). Using mice to model Alzheimer's dementia: an overview of the clinical disease and the preclinical behavioral changes in 10 mouse models. Front Genet *5*, 88.

Welch, E.J., Naikawadi, R.P., Li, Z., Lin, P., Ishii, S., Shimizu, T., Tiruppathi, C., Du, X., Subbaiah, P.V., and Ye, R.D. (2009). Opposing effects of platelet-activating factor and lyso-platelet-activating factor on neutrophil and platelet activation. Mol Pharmacol *75*, 227-234.

Whiley, L., Sen, A., Heaton, J., Proitsi, P., Garcia-Gomez, D., Leung, R., Smith, N., Thambisetty, M., Kloszewska, I., Mecocci, P.*, et al.* (2014). Evidence of altered phosphatidylcholine metabolism in Alzheimer's disease. Neurobiol Aging *35*, 271-278.

Wilkins, H.M., and Swerdlow, R.H. (2016). Amyloid precursor protein processing and bioenergetics. Brain Res Bull.

Witzke, N.M., and Bittman, R. (1986). Convenient synthesis of racemic mixed-chain ether glycerophosphocholines from fatty alkyl allyl ethers: useful analogs for biophysical studies. J Lipid Res *27*, 344-351.

Wood, P.L. (2012). Lipidomics of Alzheimer's disease: current status. Alzheimers Res Ther *4*, 5.

Wood, P.L., Locke, V.A., Herling, P., Passaro, A., Vigna, G.B., Volpato, S., Valacchi, G., Cervellati, C., and Zuliani, G. (2016). Targeted lipidomics distinguishes patient subgroups

in mild cognitive impairment (MCI) and late onset Alzheimer's disease (LOAD). BBA Clin *5*, 25-28.

Wynalda, K.M., and Murphy, R.C. (2010). Low-concentration ozone reacts with plasmalogen glycerophosphoethanolamine lipids in lung surfactant. Chem Res Toxicol *23*, 108-117.

Xiang, Y., Lam, S.M., and Shui, G. (2015). What can lipidomics tell us about the pathogenesis of Alzheimer disease? Biol Chem *396*, 1281-1291.

Xu, H., Valenzuela, N., Fai, S., Figeys, D., and Bennett, S.A.L. (2013). Targeted lipidomics - advances in profiling lysophosphocholine and platelet-activating factor second messengers. FEBS J *280*, 5652-5667

Yamashita, S., Kiko, T., Fujiwara, H., Hashimoto, M., Nakagawa, K., Kinoshita, M., Furukawa, K., Arai, H., and Miyazawa, T. (2016). Alterations in the Levels of Amyloid-beta, Phospholipid Hydroperoxide, and Plasmalogen in the Blood of Patients with Alzheimer's Disease: Possible Interactions between Amyloid-beta and These Lipids. J Alzheimers Dis *50*, 527-537.

Yang, K., and Han, X. (2016). Lipidomics: Techniques, Applications, and Outcomes Related to Biomedical Sciences. Trends Biochem Sci *41*, 954-969.

Yiannopoulou, K.G., and Papageorgiou, S.G. (2013). Current and future treatments for Alzheimer's disease. Ther Adv Neurol Disord *6*, 19-33.

Zhang, X., Li, Y., Xu, H., and Zhang, Y.W. (2014). The gamma-secretase complex: from structure to function. Front Cell Neurosci *8*, 427.

Zhang, Y.W., Thompson, R., Zhang, H., and Xu, H. (2011). APP processing in Alzheimer's disease. Mol Brain *4*, 3.

Zhao, Y.Y., Cheng, X.L., Lin, R.C., and Wei, F. (2015). Lipidomics applications for disease biomarker discovery in mammal models. Biomark Med *9*, 153-168.

Zhu, L., Zhong, M., Elder, G.A., Sano, M., Holtzman, D.M., Gandy, S., Cardozo, C., Haroutunian, V., Robakis, N.K., and Cai, D. (2015). Phospholipid dysregulation contributes to ApoE4-associated cognitive deficits in Alzheimer's disease pathogenesis. Proc Natl Acad Sci U S A *112*, 11965-11970.

Chapter 2 – References

Bateman, R.J., Xiong, C., Benzinger, T.L., Fagan, A.M., Goate, A., Fox, N.C., Marcus, D.S., Cairns, N.J., Xie, X., Blazey, T.M.*, et al.* (2012). Clinical and biomarker changes in dominantly inherited Alzheimer's disease. N Engl J Med *367*, 795-804.

Benjamini, Y., Kreiger, A., and Yekutieli, D. (2006). Adaptive linear step-up procedures that control the false discovery rate. Biometrika *93*.

Bennett, S.A.L., Valenzuela, N., Xu, H., Franko, B., Fai, S., and Figeys, D. (2013). Using neurolipidomics to identify phospholipid mediators of synaptic (dys)function in Alzheimer's Disease. Frontiers in physiology *4*, 168.

Bierer, L.M., Hof, P.R., Purohit, D.P., Carlin, L., Schmeidler, J., Davis, K.L., and Perl, D.P. (1995). Neocortical neurofibrillary tangles correlate with dementia severity in Alzheimer's disease. Arch Neurol *52*, 81-88.

Blanchard, A.P., McDowell, G.S., Valenzuela, N., Xu, H., Gelbard, S., Bertrand, M., Slater, G.W., Figeys, D., Fai, S., and Bennett, S.A.L. (2013). Visualization and Phospholipid Identification (VaLID): online integrated search engine capable of identifying and visualizing glycerophospholipids with given mass. Bioinformatics *29*, 284-285.

Bligh, E.C., and Dyer, W.J. (1959). A rapid method of lipid extraction and purification. Can J Biochem *37*, 911-917.

Bonin, F., Ryan, S.D., Migahed, L., Mo, F., Lallier, J., Franks, D.J., Arai, H., and Bennett, S.A.L. (2004). Anti-apoptotic actions of the platelet activating factor acetylhydrolase I alpha 2 catalytic subunit. J Biol Chem *279*, 52425-52436.

Buchhave, P., Minthon, L., Zetterberg, H., Wallin, A.K., Blennow, K., and Hansson, O. (2012). Cerebrospinal fluid levels of beta-amyloid 1-42, but not of tau, are fully changed already 5 to 10 years before the onset of Alzheimer dementia. Arch Gen Psychiatry *69*, 98-106.

Burke, J.E., and Dennis, E.A. (2009). Phospholipase A2 Biochemistry. Cardiovasc Drugs Ther *23*, 49-59.

Chalbot, S., Zetterberg, H., Blennow, K., Fladby, T., Grundke-Iqbal, I., and Iqbal, K. (2009). Cerebrospinal fluid secretory Ca2+-dependent phospholipase A2 activity is increased in Alzheimer disease. Clin Chem *55*, 2171-2179.

Chang, B., Hawes, N.L., Hurd, R.E., Davisson, M.T., Nusinowitz, S., and Heckenlively, J.R. (2002). Retinal degeneration mutants in the mouse. Vision Res *42*, 517-525.

Chishti, M.A., Yang, D.S., Janus, C., Phinney, A.L., Horne, P., Pearson, J., Strome, R., Zuker, N., Loukides, J., French, J.*, et al.* (2001). Early-onset amyloid deposition and cognitive deficits in transgenic mice expressing a double mutant form of amyloid precursor protein 695. J Biol Chem *276*, 21562-21570.

Daulatzai, M.A. (2013). Death by a thousand cuts in Alzheimer's disease: hypoxia--the prodrome. Neurotoxicity research *24*, 216-243.

de Hoon, M.J., Imoto, S., Nolan, J., and Miyano, S. (2004). Open source clustering software. Bioinformatics *20*, 1453-1454.

de Leeuw, F.A., Peeters, C.F.W., Kester, M.I., Harms, A.C., Struys, E.A., Hankemeier, T., van Vlijmen, H.W.T., van der Lee, S.J., van Duijn, C.M., Scheltens, P.*, et al.* (2017). Blood-based metabolic signatures in Alzheimer's disease. Alzheimer's & dementia (Amsterdam, Netherlands) *8*, 196-207.

Diez, E., Louis-Flamberg, P., Hall, R.H., and Mayer, R.J. (1992). Substrate specificities and properties of human phospholipases A2 in a mixed vesicle model. J Biol Chem *267*, 18342-18348.

Doody, R.S., Demirovic, J., Ballantyne, C.M., Chan, W., Barber, R., Powell, S., and Pavlik, V. (2015). Lipoprotein-associated phospholipase A2, homocysteine, and Alzheimer's disease. Alzheimer's & dementia (Amsterdam, Netherlands) *1*, 464-471.

Dubois, B., Hampel, H., Feldman, H.H., Scheltens, P., Aisen, P., Andrieu, S., Bakardjian, H., Benali, H., Bertram, L., Blennow, K.*, et al.* (2016). Preclinical Alzheimer's disease: Definition, natural history, and diagnostic criteria. Alzheimers Dement *12*, 292-323.

Fagan, A.M., Xiong, C., Jasielec, M.S., Bateman, R.J., Goate, A.M., Benzinger, T.L., Ghetti, B., Martins, R.N., Masters, C.L., Mayeux, R.*, et al.* (2014). Longitudinal change in CSF biomarkers in autosomal-dominant Alzheimer's disease. Sci Transl Med *6*, 226ra230.

Fahy, E., Cotter, D., Sud, M., and Subramaniam, S. (2011). Lipid classification, structures and tools. Biochim Biophys Acta *1811*, 637-647.

Farooqui, A.A., and Horrocks, L.A. (2006). Phospholipase A2-generated lipid mediators in the brain: the good, the bad, and the ugly. Neuroscientist *12*, 245-260.

Faul, F., Erdfelder, E., Lang, A.G., and Buchner, A. (2007). G*Power 3: a flexible statistical power analysis program for the social, behavioral, and biomedical sciences. Behav Res Methods *39*, 175-191.

Fjell, A.M., McEvoy, L., Holland, D., Dale, A.M., Walhovd, K.B., and Alzheimer's Disease Neuroimaging, I. (2014). What is normal in normal aging? Effects of aging, amyloid and

Alzheimer's disease on the cerebral cortex and the hippocampus. Prog Neurobiol *117*, 20-40.

Gao, L., Tian, S., Gao, H., and Xu, Y. (2013). Hypoxia increases Abeta-induced tau phosphorylation by calpain and promotes behavioral consequences in AD transgenic mice. J Mol Neurosci *51*, 138-147.

Garcia-Alloza, M., Robbins, E.M., Zhang-Nunes, S.X., Purcell, S.M., Betensky, R.A., Raju, S., Prada, C., Greenberg, S.M., Bacskai, B.J., and Frosch, M.P. (2006). Characterization of amyloid deposition in the APPswe/PS1dE9 mouse model of Alzheimer disease. Neurobiol Dis *24*, 516-524.

Gattaz, W.F., Cairns, N.J., Levy, R., Forstl, H., Braus, D.F., and Maras, A. (1996). Decreased phospholipase A2 activity in the brain and in platelets of patients with Alzheimer's disease. Eur Arch Psychiatry Clin Neurosci *246*, 129-131.

Gattaz, W.F., Forlenza, O.V., Talib, L.L., Barbosa, N.R., and Bottino, C.M. (2004). Platelet phospholipase A(2) activity in Alzheimer's disease and mild cognitive impairment. J Neural Transm *111*, 591-601.

Gattaz, W.F., Talib, L.L., Schaeffer, E.L., Diniz, B.S., and Forlenza, O.V. (2014). Low platelet iPLA(2) activity predicts conversion from mild cognitive impairment to Alzheimer's disease: a 4-year follow-up study. Journal of neural transmission (Vienna, Austria : 1996) *121*, 193-200.

Gelbard, H.A., Nottet, H.S.L.M., Swindells, S., Jett, M., Dzenko, K.A., Genis, P., White, R., Wang, L., Choi, Y.-B., Zhang, D.*, et al.* (1994). Platelet-activating factor: a candidate human immunodeficiency virus type 1-induced neurotoxin. JVirol *68*, 4628-4635.

Granger, M.W., Franko, B., Taylor, M.W., Messier, C., George-Hyslop, P.S., and Bennett, S.A.L. (2016). A TgCRND8 Mouse Model of Alzheimer's Disease Exhibits Sexual Dimorphisms in Behavioral Indices of Cognitive Reserve. J Alzheimers Dis *51*, 757-773.

Haass, C., and Selkoe, D.J. (2007). Soluble protein oligomers in neurodegeneration: lessons from the Alzheimer's amyloid beta-peptide. Nat Rev Mol Cell Biol *8*, 101-112.

Herrup, K. (2010). Reimagining Alzheimer's disease--an age-based hypothesis. J Neurosci *30*, 16755-16762.

Kawas, C., Gray, S., Brookmeyer, R., Fozard, J., and Zonderman, A. (2000). Age-specific incidence rates of Alzheimer's disease: the Baltimore Longitudinal Study of Aging. Neurology *54*, 2072-2077.

Kelesidis, T., Papakonstantinou, V., Detopoulou, P., Fragopoulou, E., Chini, M., Lazanas, M.C., and Antonopoulou, S. (2015). The Role of Platelet-Activating Factor in Chronic Inflammation, Immune Activation, and Comorbidities Associated with HIV Infection. AIDS reviews *17*, 191-201.

Li, L., Zhang, X., Yang, D., Luo, G., Chen, S., and Le, W. (2009). Hypoxia increases Abeta generation by altering beta- and gamma-cleavage of APP. Neurobiology of aging *30*, 1091-1098.

Liu, H., Qiu, H., Yang, J., Ni, J., and Le, W. (2016). Chronic hypoxia facilitates Alzheimer's disease through demethylation of gamma-secretase by downregulating DNA methyltransferase 3b. Alzheimers Dement *12*, 130-143.

Manya, H., Aoki, J., Kato, H., Ishii, J., Hino, S., Arai, H., and Inoue, K. (1999). Biochemical characterization of various catalytic complexes of the brain platelet-activating factor acetylhydrolase. J Biol Chem *274*, 31827-31832.

Mapstone, M., Cheema, A.K., Fiandaca, M.S., Zhong, X., Mhyre, T.R., MacArthur, L.H., Hall, W.J., Fisher, S.G., Peterson, D.R., Haley, J.M.*, et al.* (2014). Plasma phospholipids identify antecedent memory impairment in older adults. Nat Med *20*, 415-418.

McHale-Owen, H., and Bate, C. (2018). Cholesterol ester hydrolase inhibitors reduce the production of synaptotoxic amyloid-beta oligomers. Biochim Biophys Acta *1864*, 649-659.

Montine, T.J., Markesbery, W.R., Zackert, W., Sanchez, S.C., Roberts, L.J., 2nd, and Morrow, J.D. (1999). The magnitude of brain lipid peroxidation correlates with the extent of degeneration but not with density of neuritic plaques or neurofibrillary tangles or with APOE genotype in Alzheimer's disease patients. Am J Pathol *155*, 863-868.

Mulder, C., Wahlund, L.O., Teerlink, T., Blomberg, M., Veerhuis, R., van Kamp, G.J., Scheltens, P., and Scheffer, P.G. (2003). Decreased lysophosphatidylcholine/phosphatidylcholine ratio in cerebrospinal fluid in Alzheimer's disease. J Neural Transm (Vienna) *110*, 949-955.

Nakanishi, H., Shindou, H., Hishikawa, D., Harayama, T., Ogasawara, R., Suwabe, A., Taguchi, R., and Shimizu, T. (2006). Cloning and characterization of mouse lung-type acyl-CoA:lysophosphatidylcholine acyltransferase 1 (LPCAT1). Expression in alveolar type II cells and possible involvement in surfactant production. J Biol Chem *281*, 20140-20147.

Prescott, S.M., Zimmerman, G.A., Stafforini, D.M., and McIntyre, T.M. (2000). Platelet activating factor and related lipid mediators. Annu Rev Biochem *69*, 419-445.

Proitsi, P., Kim, M., Whiley, L., Simmons, A., Sattlecker, M., Velayudhan, L., Lupton, M.K., Soininen, H., Kloszewska, I., Mecocci, P.*, et al.* (2017). Association of blood lipids with

Alzheimer's disease: A comprehensive lipidomics analysis. Alzheimers Dement *13*, 140-151.

Reiserer, R.S., Harrison, F.E., Syverud, D.C., and McDonald, M.P. (2007). Impaired spatial learning in the APPSwe + PSEN1DeltaE9 bigenic mouse model of Alzheimer's disease. Genes, brain, and behavior *6*, 54-65.

Ross, B.M., Moszczynska, A., Erlich, J., and Kish, S.J. (1998). Phospholipid-metabolizing enzymes in Alzheimer's disease: increased lysophospholipid acyltransferase activity and decreased phospholipase A2 activity. J Neurochem *70*, 786-793.

Ryan, S.D., Whitehead, S.N., Swayne, L.A., Moffat, T.C., Hou, W., Ethier, M., Bourgeois, A.J.G., Rashidian, J., P Blanchard, A., Fraser, P.E.*, et al.* (2009). Amyloid-β42 signals tau hyperphosphorylation and compromises neuronal viability by disrupting alkylacylglycerophosphocholine metabolism. Proc Natl Acad Sci U S A *106*, 20936-20941.

Saldanha, A.J. (2004). Java Treeview--extensible visualization of microarray data. Bioinformatics *20*, 3246-3248.

Shindou, H., and Shimizu, T. (2009). Acyl-CoA: lysophospholipid acyltransferases. J Biol Chem *284*, 1-5.

Simmons, C., Ingham, V., Williams, A., and Bate, C. (2014). Platelet-activating factor antagonists enhance intracellular degradation of amyloid-beta42 in neurons via regulation of cholesterol ester hydrolases. Alzheimer's research & therapy *6*, 15.

Smesny, S., Stein, S., Willhardt, I., Lasch, J., and Sauer, H. (2008). Decreased phospholipase A2 activity in cerebrospinal fluid of patients with dementia. J Neural Transm (Vienna) *115*, 1173-1179.

Sud, M., Fahy, E., Cotter, D., Brown, A., Dennis, E.A., Glass, C.K., Merrill, A.H., Jr., Murphy, R.C., Raetz, C.R., Russell, D.W.*, et al.* (2007). LMSD: LIPID MAPS structure database. Nucleic Acids Res *35*, D527-532.

Sun, X., He, G., Qing, H., Zhou, W., Dobie, F., Cai, F., Staufenbiel, M., Huang, L.E., and Song, W. (2006). Hypoxia facilitates Alzheimer's disease pathogenesis by up-regulating BACE1 gene expression. Proc Natl Acad Sci U S A *103*, 18727-18732.

Sweet, R.A., Panchalingam, K., Pettegrew, J.W., McClure, R.J., Hamilton, R.L., Lopez, O.L., Kaufer, D.I., DeKosky, S.T., and Klunk, W.E. (2002). Psychosis in Alzheimer disease: postmortem magnetic resonance spectroscopy evidence of excess neuronal and membrane phospholipid pathology. Neurobiol Aging *23*, 547-553.

Toledo, J.B., Arnold, M., Kastenmuller, G., Chang, R., Baillie, R.A., Han, X., Thambisetty, M., Tenenbaum, J.D., Suhre, K., Thompson, J.W.*, et al.* (2017). Metabolic network failures in Alzheimer's disease-A biochemical road map. Alzheimers Dement.

Toye, A.A., Lippiat, J.D., Proks, P., Shimomura, K., Bentley, L., Hugill, A., Mijat, V., Goldsworthy, M., Moir, L., Haynes, A.*, et al.* (2005). A genetic and physiological study of impaired glucose homeostasis control in C57BL/6J mice. Diabetologia *48*, 675-686.

Wang, F., Blanchard, A.P., Elisma, F., Granger, M., Xu, H., Bennett, S.A.L., Figeys, D., and Zou, H. (2013). Phosphoproteome analysis of an early onset mouse model (TgCRND8) of Alzheimer's disease reveals temporal changes in neuronal and glia signaling pathways. Proteomics *13*, 1292-1305.

Xia, J., Sinelnikov, I.V., Han, B., and Wishart, D.S. (2015). MetaboAnalyst 3.0--making metabolomics more meaningful. Nucleic acids research *43*, W251-257.

Xu, H., Valenzuela, N., Fai, S., Figeys, D., and Bennett, S.A.L. (2013). Targeted lipidomics - advances in profiling lysophosphocholine and platelet-activating factor second messengers. The FEBS journal *280*, 5652-5667

Yang, R.Y., Zhao, G., Wang, D.M., Pang, X.C., Wang, S.B., Fang, J.S., Li, C., Liu, A.L., Wu, S., and Du, G.H. (2015). DL0410 can reverse cognitive impairment, synaptic loss and reduce plaque load in APP/PS1 transgenic mice. Pharmacol Biochem Behav *139*, 15-26.

Zhang, X., Li, L., Zhang, X., Xie, W., Li, L., Yang, D., Heng, X., Du, Y., Doody, R.S., and Le, W. (2013). Prenatal hypoxia may aggravate the cognitive impairment and Alzheimer's disease neuropathology in APPSwe/PS1A246E transgenic mice. Neurobiology of aging *34*, 663-678.

Chapter 3 - References

Adlard, P.A., Perreau, V.M., Pop, V., and Cotman, C.W. (2005). Voluntary exercise decreases amyloid load in a transgenic model of Alzheimer's disease. The Journal of neuroscience : the official journal of the Society for Neuroscience *25*, 4217-4221.

Ambree, O., Touma, C., Gortz, N., Keyvani, K., Paulus, W., Palme, R., and Sachser, N. (2006). Activity changes and marked stereotypic behavior precede Abeta pathology in TgCRND8 Alzheimer mice. Neurobiol Aging *27*, 955-964.

Barnes, L.L., Wilson, R.S., Bienias, J.L., Schneider, J.A., Evans, D.A., and Bennett, D.A. (2005). Sex differences in the clinical manifestations of Alzheimer disease pathology. Arch Gen Psychiatry *62*, 685-691.

Barron, A.M., Rosario, E.R., Elteriefi, R., and Pike, C.J. (2013). Sex-specific effects of high fat diet on indices of metabolic syndrome in 3xTg-AD mice: implications for Alzheimer's disease. PLoS One *8*, e78554.

Benilova, I., Karran, E., and De Strooper, B. (2012). The toxic Abeta oligomer and Alzheimer's disease: an emperor in need of clothes. Nat Neurosci *15*, 349-357.

Bories, C., Guitton, M.J., Julien, C., Tremblay, C., Vandal, M., Msaid, M., De Koninck, Y., and Calon, F. (2012). Sex-dependent alterations in social behaviour and cortical synaptic activity coincide at different ages in a model of Alzheimer's disease. PloS one *7*, e46111.

Brody, D.L., and Holtzman, D.M. (2006). Morris water maze search strategy analysis in PDAPP mice before and after experimental traumatic brain injury. Exp Neurol *197*, 330-340.

Callahan, M.J., Lipinski, W.J., Bian, F., Durham, R.A., Pack, A., and Walker, L.C. (2001). Augmented senile plaque load in aged female beta-amyloid precursor protein-transgenic mice. The American journal of pathology *158*, 1173-1177.

Carroll, J.C., Rosario, E.R., Kreimer, S., Villamagna, A., Gentzschein, E., Stanczyk, F.Z., and Pike, C.J. (2010). Sex differences in beta-amyloid accumulation in 3xTg-AD mice: role of neonatal sex steroid hormone exposure. Brain research *1366*, 233-245.

Chang, B., Hawes, N.L., Hurd, R.E., Davisson, M.T., Nusinowitz, S., and Heckenlively, J.R. (2002). Retinal degeneration mutants in the mouse. Vision research *42*, 517-525.

Chishti, M.A., Yang, D.S., Janus, C., Phinney, A.L., Horne, P., Pearson, J., Strome, R., Zuker, N., Loukides, J., French, J.*, et al.* (2001). Early-onset amyloid deposition and cognitive deficits in transgenic mice expressing a double mutant form of amyloid precursor protein 695. The Journal of biological chemistry *276*, 21562-21570.

Clinton, L.K., Billings, L.M., Green, K.N., Caccamo, A., Ngo, J., Oddo, S., McGaugh, J.L., and LaFerla, F.M. (2007). Age-dependent sexual dimorphism in cognition and stress response in the 3xTg-AD mice. Neurobiol Dis *28*, 76-82.

Contador, I., Bermejo-Pareja, F., Mitchell, A.J., Trincado, R., Villarejo, A., Sanchez-Ferro, A., and Benito-Leon, J. (2014). Cause of death in mild cognitive impairment: a prospective study (NEDICES). Eur J Neurol *21*, 253-e259.

Cracchiolo, J.R., Mori, T., Nazian, S.J., Tan, J., Potter, H., and Arendash, G.W. (2007). Enhanced cognitive activity--over and above social or physical activity--is required to protect Alzheimer's mice against cognitive impairment, reduce Abeta deposition, and increase synaptic immunoreactivity. Neurobiol Learn Mem *88*, 277-294.

Dong, H.W., Swanson, L.W., Chen, L., Fanselow, M.S., and Toga, A.W. (2009). Genomic-anatomic evidence for distinct functional domains in hippocampal field CA1. Proc Natl Acad Sci U S A *106*, 11794-11799.

Fjell, A.M., Walhovd, K.B., Fennema-Notestine, C., McEvoy, L.K., Hagler, D.J., Holland, D., Blennow, K., Brewer, J.B., Dale, A.M., and Alzheimer's Disease Neuroimaging, I. (2010). Brain atrophy in healthy aging is related to CSF levels of Abeta1-42. Cereb Cortex *20*, 2069-2079.

Francis, B.M., Kim, J., Barakat, M.E., Fraenkl, S., Yucel, Y.H., Peng, S., Michalski, B., Fahnestock, M., McLaurin, J., and Mount, H.T. (2012). Object recognition memory and BDNF expression are reduced in young TgCRND8 mice. Neurobiology of aging *33*, 555-563.

Franklin, K.B.J., and Paxinos, G.T. (2007). The Mouse Brain in Stereotaxic Coordinates, 3 edn (New York: Elesvier Academic Press).

Gallagher, J.J., Minogue, A.M., and Lynch, M.A. (2013). Impaired performance of female APP/PS1 mice in the Morris water maze is coupled with increased Abeta accumulation and microglial activation. Neuro-degenerative diseases *11*, 33-41.

Gil-Pages, M., Stiles, R.J., Parks, C.A., Neier, S.C., Radulovic, M., Oliveros, A., Ferrer, A., Reed, B.K., Wilton, K.M., and Schrum, A.G. (2013). Slow angled-descent forepaw grasping (SLAG): an innate behavioral task for identification of individual experimental mice possessing functional vision. Behavioral and brain functions : BBF *9*, 35.

Gimenez, E., and Montoliu, L. (2001). A simple polymerase chain reaction assay for genotyping the retinal degeneration mutation (Pdeb(rd1)) in FVB/N-derived transgenic mice. Laboratory animals *35*, 153-156.

Guehne, U., Luck, T., Busse, A., Angermeyer, M.C., and Riedel-Heller, S.G. (2007). Mortality in individuals with mild cognitive impairment. Results of the Leipzig Longitudinal Study of the Aged (LEILA75+). Neuroepidemiology *29*, 226-234.

Hardy, J., and Selkoe, D.J. (2002). The amyloid hypothesis of Alzheimer's disease: progress and problems on the road to therapeutics. Science *297*, 353-356.

Hebert, L.E., Weuve, J., Scherr, P.A., and Evans, D.A. (2013). Alzheimer disease in the United States (2010-2050) estimated using the 2010 census. Neurology *80*, 1778-1783.

Herring, A., Ambree, O., Tomm, M., Habermann, H., Sachser, N., Paulus, W., and Keyvani, K. (2009). Environmental enrichment enhances cellular plasticity in transgenic mice with Alzheimer-like pathology. Experimental neurology *216*, 184-192.

Herring, A., Yasin, H., Ambree, O., Sachser, N., Paulus, W., and Keyvani, K. (2008). Environmental enrichment counteracts Alzheimer's neurovascular dysfunction in TgCRND8 mice. Brain pathology *18*, 32-39.

Hirata-Fukae, C., Li, H.F., Hoe, H.S., Gray, A.J., Minami, S.S., Hamada, K., Niikura, T., Hua, F., Tsukagoshi-Nagai, H., Horikoshi-Sakuraba, Y.*, et al.* (2008). Females exhibit more extensive amyloid, but not tau, pathology in an Alzheimer transgenic model. Brain research *1216*, 92-103.

Hochgrafe, K., Sydow, A., and Mandelkow, E.M. (2013). Regulatable transgenic mouse models of Alzheimer disease: onset, reversibility and spreading of Tau pathology. The FEBS journal *280*, 4371-4381.

Hof, P.Y., Bloom, F.E., Belichenko, P.V., and Celio, M.R. (2001). Comparative Cytoarchitectonic Atlas of the C57Bl/6 and 129/Sv Mouse Brains. (London, UK: Elsevier Science).

Hooijmans, C.R., Van der Zee, C.E., Dederen, P.J., Brouwer, K.M., Reijmer, Y.D., van Groen, T., Broersen, L.M., Lutjohann, D., Heerschap, A., and Kiliaan, A.J. (2009). DHA and cholesterol containing diets influence Alzheimer-like pathology, cognition and cerebral vasculature in APPswe/PS1dE9 mice. Neurobiol Dis *33*, 482-498.

Hua, X., Hibar, D.P., Lee, S., Toga, A.W., Jack, C.R., Jr., Weiner, M.W., Thompson, P.M., and Alzheimer's Disease Neuroimaging, I. (2010). Sex and age differences in atrophic rates: an ADNI study with n=1368 MRI scans. Neurobiology of aging *31*, 1463-1480.

Hussain, A.A., Willmott, N.J., and Voaden, M.J. (1992). Cyclic GMP, calcium and photoreceptor sensitivity in mice heterozygous for the rod dysplasia gene designated "rd". Vision research *32*, 29-36.

Hyde, L.A., Kazdoba, T.M., Grilli, M., Lozza, G., Brusa, R., Zhang, Q., Wong, G.T., McCool, M.F., Zhang, L., Parker, E.M.*, et al.* (2005). Age-progressing cognitive impairments and neuropathology in transgenic CRND8 mice. Behavioural brain research *160*, 344-355.

Irvine, K., Laws, K.R., Gale, T.M., and Kondel, T.K. (2012). Greater cognitive deterioration in women than men with Alzheimer's disease: a meta analysis. J Clin Exp Neuropsychol *34*, 989-998.

Jack, C.R., Jr., Wiste, H.J., Weigand, S.D., Knopman, D.S., Vemuri, P., Mielke, M.M., Lowe, V., Senjem, M.L., Gunter, J.L., Machulda, M.M.*, et al.* (2015). Age, Sex, and APOE epsilon4 Effects on Memory, Brain Structure, and beta-Amyloid Across the Adult Life Span. JAMA Neurol *72*, 511-519.

Jankowsky, J.L., Melnikova, T., Fadale, D.J., Xu, G.M., Slunt, H.H., Gonzales, V., Younkin, L.H., Younkin, S.G., Borchelt, D.R., and Savonenko, A.V. (2005). Environmental

enrichment mitigates cognitive deficits in a mouse model of Alzheimer's disease. J Neurosci *25*, 5217-5224.

Jankowsky, J.L., Xu, G., Fromholt, D., Gonzales, V., and Borchelt, D.R. (2003). Environmental enrichment exacerbates amyloid plaque formation in a transgenic mouse model of Alzheimer disease. J Neuropathol Exp Neurol *62*, 1220-1227.

Janus, C. (2004). Search strategies used by APP transgenic mice during navigation in the Morris water maze. Learn Mem *11*, 337-346.

Li, J.Q., Tan, L., Wang, H.F., Tan, M.S., Tan, L., Xu, W., Zhao, Q.F., Wang, J., Jiang, T., and Yu, J.T. (2015). Risk factors for predicting progression from mild cognitive impairment to Alzheimer's disease: a systematic review and meta-analysis of cohort studies. Journal of neurology, neurosurgery, and psychiatry *doi:10.1136/jnnp-2014-310095*.

Lin, K.A., and Doraiswamy, P.M. (2014). When Mars Versus Venus is Not a Cliche: Gender Differences in the Neurobiology of Alzheimer's Disease. Front Neurol *5*, 288.

Lovasic, L., Bauschke, H., and Janus, C. (2005). Working memory impairment in a transgenic amyloid precursor protein TgCRND8 mouse model of Alzheimer's disease. Genes, brain, and behavior *4*, 197-208.

McLean, A.C., Valenzuela, N., Fai, S., and Bennett, S.A. (2012). Performing vaginal lavage, crystal violet staining, and vaginal cytological evaluation for mouse estrous cycle staging identification. Journal of visualized experiments : JoVE, e4389.

Mielke, M.M., Vemuri, P., and Rocca, W.A. (2014). Clinical epidemiology of Alzheimer's disease: assessing sex and gender differences. Clin Epidemiol *6*, 37-48.

Oddo, S., Caccamo, A., Shepherd, J.D., Murphy, M.P., Golde, T.E., Kayed, R., Metherate, R., Mattson, M.P., Akbari, Y., and LaFerla, F.M. (2003). Triple-transgenic

model of Alzheimer's disease with plaques and tangles: intracellular Abeta and synaptic dysfunction. Neuron *39*, 409-421.

Palm, R., Ayala-Fontanez, N., Garcia, Y., Lee, H.G., Smith, M.A., and Casadesus, G. (2012). Neuroendocrinology-based therapy for Alzheimer's disease. Biofactors *38*, 123-132.

Palop, J.J., and Mucke, L. (2010). Amyloid-beta-induced neuronal dysfunction in Alzheimer's disease: from synapses toward neural networks. Nat Neurosci *13*, 812-818.

Perneczky, R., Drzezga, A., Diehl-Schmid, J., Li, Y., and Kurz, A. (2007). Gender differences in brain reserve : an (18)F-FDG PET study in Alzheimer's disease. J Neurol *254*, 1395-1400.

Pettit, A.S., Desroches, R., and Bennett, S.A. (2012). The opiate analgesic buprenorphine decreases proliferation of adult hippocampal neuroblasts and increases survival of their progeny. Neuroscience *200*, 211-222.

Placanica, L., Zhu, L., and Li, Y.M. (2009). Gender- and age-dependent gamma-secretase activity in mouse brain and its implication in sporadic Alzheimer disease. PloS one *4*, e5088.

Richter, H., Ambree, O., Lewejohann, L., Herring, A., Keyvani, K., Paulus, W., Palme, R., Touma, C., Schabitz, W.R., and Sachser, N. (2008). Wheel-running in a transgenic mouse model of Alzheimer's disease: protection or symptom? Behavioural brain research *190*, 74-84.

Savonenko, A., Xu, G.M., Melnikova, T., Morton, J.L., Gonzales, V., Wong, M.P., Price, D.L., Tang, F., Markowska, A.L., and Borchelt, D.R. (2005). Episodic-like memory deficits

in the APPswe/PS1dE9 mouse model of Alzheimer's disease: relationships to beta-amyloid deposition and neurotransmitter abnormalities. Neurobiol Dis *18*, 602-617.

Schafer, S., Wirths, O., Multhaup, G., and Bayer, T.A. (2007). Gender dependent APP processing in a transgenic mouse model of Alzheimer's disease. Journal of neural transmission *114*, 387-394.

Snowdon, D.A. (2003). Healthy aging and dementia: findings from the Nun Study. Ann Intern Med *139*, 450-454.

Sobral, M., Pestana, M.H., and Paul, C. (2015). Cognitive reserve and the severity of Alzheimer's disease. Arq Neuropsiquiatr *73*, 480-486.

Sperling, R.A., Aisen, P.S., Beckett, L.A., Bennett, D.A., Craft, S., Fagan, A.M., Iwatsubo, T., Jack, C.R., Jr., Kaye, J., Montine, T.J.*, et al.* (2011). Toward defining the preclinical stages of Alzheimer's disease: recommendations from the National Institute on Aging-Alzheimer's Association workgroups on diagnostic guidelines for Alzheimer's disease. Alzheimers Dement *7*, 280-292.

Stern, Y. (2012). Cognitive reserve in ageing and Alzheimer's disease. Lancet Neurol *11*, 1006-1012.

Thies, W., Bleiler, L., and Alzheimer's, A. (2013). 2013 Alzheimer's disease facts and figures. Alzheimer's & dementia : the journal of the Alzheimer's Association *9*, 208-245.

Valero, J., Mastrella, G., Neiva, I., Sanchez, S., and Malva, J.O. (2014). Long-term effects of an acute and systemic administration of LPS on adult neurogenesis and spatial memory. Front Neurosci *8*, 83.

Vassilaki, M., Cha, R.H., Geda, Y.E., Mielke, M.M., Knopman, D.S., Petersen, R.C., and Roberts, R.O. (2015). Mortality in mild cognitive impairment varies by subtype, sex, and lifestyle factors: the mayo clinic study of aging. J Alzheimers Dis *45*, 1237-1245.

Vemuri, P., Lesnick, T.G., Przybelski, S.A., Knopman, D.S., Roberts, R.O., Lowe, V.J., Kantarci, K., Senjem, M.L., Gunter, J.L., Boeve, B.F.*, et al.* (2012). Effect of lifestyle activities on Alzheimer disease biomarkers and cognition. Annals of neurology *72*, 730-738.

Verret, L., Krezymon, A., Halley, H., Trouche, S., Zerwas, M., Lazouret, M., Lassalle, J.M., and Rampon, C. (2013). Transient enriched housing before amyloidosis onset sustains cognitive improvement in Tg2576 mice. Neurobiol Aging *34*, 211-225.

Walker, J.M., Fowler, S.W., Miller, D.K., Sun, A.Y., Weisman, G.A., Wood, W.G., Sun, G.Y., Simonyi, A., and Schachtman, T.R. (2011). Spatial learning and memory impairment and increased locomotion in a transgenic amyloid precursor protein mouse model of Alzheimer's disease. Behavioural brain research *222*, 169-175.

Walker, J.M., Klakotskaia, D., Ajit, D., Weisman, G.A., Wood, W.G., Sun, G.Y., Serfozo, P., Simonyi, A., and Schachtman, T.R. (2015). Beneficial effects of dietary EGCG and voluntary exercise on behavior in an Alzheimer's disease mouse model. Journal of Alzheimer's disease : JAD *44*, 561-572.

Wang, F., Blanchard, A.P., Elisma, F., Granger, M., Xu, H., Bennett, S.A.L., Figeys, D., and Zou, H. (2013). Phosphoproteome analysis of an early onset mouse model (TgCRND8) of Alzheimer's disease reveals temporal changes in neuronal and glia signaling pathways. Proteomics *13*, 1292-1305.

Wang, J., Tanila, H., Puolivali, J., Kadish, I., and van Groen, T. (2003). Gender differences in the amount and deposition of amyloidbeta in APPswe and PS1 double transgenic mice. Neurobiol Dis *14*, 318-327.

Webster, S.J., Bachstetter, A.D., Nelson, P.T., Schmitt, F.A., and Van Eldik, L.J. (2014). Using mice to model Alzheimer's dementia: an overview of the clinical disease and the preclinical behavioral changes in 10 mouse models. Front Genet *5*, 88.

Wolfer, D.P., and Lipp, H.P. (2000). Dissecting the behaviour of transgenic mice: is it the mutation, the genetic background, or the environment? Experimental physiology *85*, 627-634.

Zahs, K.R., and Ashe, K.H. (2010). 'Too much good news' - are Alzheimer mouse models trying to tell us how to prevent, not cure, Alzheimer's disease? Trends in neurosciences *33*, 381-389.

Zhang, W., Hao, J., Liu, R., Zhang, Z., Lei, G., Su, C., Miao, J., and Li, Z. (2011). Soluble Abeta levels correlate with cognitive deficits in the 12-month-old APPswe/PS1dE9 mouse model of Alzheimer's disease. Behav Brain Res *222*, 342-350.

Chapter 4 - References

Barnes, L.L., Wilson, R.S., Bienias, J.L., Schneider, J.A., Evans, D.A., and Bennett, D.A. (2005). Sex differences in the clinical manifestations of Alzheimer disease pathology. Arch Gen Psychiatry *62*, 685-691.

Benjamini, Y., and Hochberg, Y. (1995). Controlling the False Discovery Rate - a Practical and Powerful Approach to Multiple Testing. J Roy Stat Soc B Met *57*, 289-300.

Blanchard, A.P., McDowell, G.S., Valenzuela, N., Xu, H., Gelbard, S., Bertrand, M., Slater, G.W., Figeys, D., Fai, S., and Bennett, S.A. (2013). Visualization and Phospholipid Identification (VaLID): online integrated search engine capable of identifying and visualizing glycerophospholipids with given mass. Bioinformatics *29*, 284-285.

Bligh, E.G., and Dyer, W.J. (1959). A rapid method of total lipid extraction and purification. Can J Biochem Physiol *37*, 911-917.

Brody, D.L., and Holtzman, D.M. (2006). Morris water maze search strategy analysis in PDAPP mice before and after experimental traumatic brain injury. Exp Neurol *197*, 330-340.

Cao, J., Shan, D., Revett, T., Li, D., Wu, L., Liu, W., Tobin, J.F., and Gimeno, R.E. (2008). Molecular identification of a novel mammalian brain isoform of acyl-CoA:lysophospholipid acyltransferase with prominent ethanolamine lysophospholipid acylating activity, LPEAT2. J Biol Chem *283*, 19049-19057.

Casanova, R., Varma, S., Simpson, B., Kim, M., An, Y., Saldana, S., Riveros, C., Moscato, P., Griswold, M., Sonntag, D.*, et al.* (2016). Blood metabolite markers of preclinical Alzheimer's disease in two longitudinally followed cohorts of older individuals. Alzheimers Dement *12*, 815-822.

Fahy, E., Subramaniam, S., Murphy, R.C., Nishijima, M., Raetz, C.R., Shimizu, T., Spener, F., van Meer, G., Wakelam, M.J., and Dennis, E.A. (2009). Update of the LIPID MAPS comprehensive classification system for lipids. J Lipid Res *50 Suppl*, S9-14.

Faul, F., Erdfelder, E., Lang, A.G., and Buchner, A. (2007). G*Power 3: a flexible statistical power analysis program for the social, behavioral, and biomedical sciences. Behav Res Methods *39*, 175-191.

Fiandaca, M.S., Mapstone, M.E., Cheema, A.K., and Federoff, H.J. (2014). The critical need for defining preclinical biomarkers in Alzheimer's disease. Alzheimers Dement *10*, S196-212.

Fraser, T., Tayler, H., and Love, S. (2010). Fatty acid composition of frontal, temporal and parietal neocortex in the normal human brain and in Alzheimer's disease. Neurochem Res *35*, 503-513.

Ginsberg, L., Rafique, S., Xuereb, J.H., Rapoport, S.I., and Gershfeld, N.L. (1995). Disease and anatomic specificity of ethanolamine plasmalogen deficiency in Alzheimer's disease brain. Brain Res *698*, 223-226.

Granger, M.W., Franko, B., Taylor, M.W., Messier, C., George-Hyslop, P.S., and Bennett, S.A. (2016). A TgCRND8 Mouse Model of Alzheimer's Disease Exhibits Sexual Dimorphisms in Behavioral Indices of Cognitive Reserve. J Alzheimers Dis *51*, 757-773.

Guan, Z., Wang, Y., Cairns, N.J., Lantos, P.L., Dallner, G., and Sindelar, P.J. (1999). Decrease and structural modifications of phosphatidylethanolamine plasmalogen in the brain with Alzheimer disease. J Neuropathol Exp Neurol *58*, 740-747.

Han, X., Holtzman, D.M., and McKeel, D.W., Jr. (2001). Plasmalogen deficiency in early Alzheimer's disease subjects and in animal models: molecular characterization using electrospray ionization mass spectrometry. J Neurochem *77*, 1168-1180.

Igarashi, M., Ma, K., Gao, F., Kim, H.W., Rapoport, S.I., and Rao, J.S. (2011). Disturbed choline plasmalogen and phospholipid fatty acid concentrations in Alzheimer's disease prefrontal cortex. J Alzheimers Dis *24*, 507-517.

Janus, C. (2004). Search strategies used by APP transgenic mice during navigation in the Morris water maze. Learn Mem *11*, 337-346.

Kang, S., Lee, Y.H., and Lee, J.E. (2017). Metabolism-Centric Overview of the Pathogenesis of Alzheimer's Disease. Yonsei Med J *58*, 479-488.

Klein, J. (2000). Membrane breakdown in acute and chronic neurodegeneration: focus on choline-containing phospholipids. J Neural Transm (Vienna) *107*, 1027-1063.

Mapstone, M., Cheema, A.K., Fiandaca, M.S., Zhong, X., Mhyre, T.R., MacArthur, L.H., Hall, W.J., Fisher, S.G., Peterson, D.R., Haley, J.M.*, et al.* (2014). Plasma phospholipids identify antecedent memory impairment in older adults. Nat Med *20*, 415-418.

Mielke, M.M., Vemuri, P., and Rocca, W.A. (2014). Clinical epidemiology of Alzheimer's disease: assessing sex and gender differences. Clin Epidemiol *6*, 37-48.

Mury, F.B., da Silva, W.C., Barbosa, N.R., Mendes, C.T., Bonini, J.S., Sarkis, J.E., Cammarota, M., Izquierdo, I., Gattaz, W.F., and Dias-Neto, E. (2016). Lithium activates brain phospholipase A2 and improves memory in rats: implications for Alzheimer's disease. Eur Arch Psychiatry Clin Neurosci *266*, 607-618.

Nitsch, R.M., Blusztajn, J.K., Pittas, A.G., Slack, B.E., Growdon, J.H., and Wurtman, R.J. (1992). Evidence for a membrane defect in Alzheimer disease brain. Proc Natl Acad Sci U S A *89*, 1671-1675.

Petersen, R.C., Aisen, P.S., Beckett, L.A., Donohue, M.C., Gamst, A.C., Harvey, D.J., Jack, C.R., Jr., Jagust, W.J., Shaw, L.M., Toga, A.W.*, et al.* (2010a). Alzheimer's Disease Neuroimaging Initiative (ADNI): clinical characterization. Neurology *74*, 201-209.

Petersen, R.C., Caracciolo, B., Brayne, C., Gauthier, S., Jelic, V., and Fratiglioni, L. (2014). Mild cognitive impairment: a concept in evolution. J Intern Med *275*, 214-228.

Petersen, R.C., Roberts, R.O., Knopman, D.S., Geda, Y.E., Cha, R.H., Pankratz, V.S., Boeve, B.F., Tangalos, E.G., Ivnik, R.J., and Rocca, W.A. (2010b). Prevalence of mild cognitive impairment is higher in men. The Mayo Clinic Study of Aging. Neurology *75*, 889-897.

Pietrzak, R.H., Lim, Y.Y., Ames, D., Harrington, K., Restrepo, C., Martins, R.N., Rembach, A., Laws, S.M., Masters, C.L., Villemagne, V.L.*, et al.* (2015). Trajectories of memory decline in preclinical Alzheimer's disease: results from the Australian Imaging, Biomarkers and Lifestyle Flagship Study of ageing. Neurobiol Aging *36*, 1231-1238.

Proitsi, P., Kim, M., Whiley, L., Simmons, A., Sattlecker, M., Velayudhan, L., Lupton, M.K., Soininen, H., Kloszewska, I., Mecocci, P.*, et al.* (2017). Association of blood lipids with Alzheimer's disease: A comprehensive lipidomics analysis. Alzheimers Dement *13*, 140-151.

Ryan, S.D., Whitehead, S.N., Swayne, L.A., Moffat, T.C., Hou, W., Ethier, M., Bourgeois, A.J., Rashidian, J., Blanchard, A.P., Fraser, P.E.*, et al.* (2009). Amyloid-beta42 signals tau hyperphosphorylation and compromises neuronal viability by disrupting

alkylacylglycerophosphocholine metabolism. Proc Natl Acad Sci U S A *106*, 20936-20941.

Schaeffer, E.L., Forlenza, O.V., and Gattaz, W.F. (2009). Phospholipase A2 activation as a therapeutic approach for cognitive enhancement in early-stage Alzheimer disease. Psychopharmacology (Berl) *202*, 37-51.

Shindou, H., Hishikawa, D., Harayama, T., Yuki, K., and Shimizu, T. (2009). Recent progress on acyl CoA: lysophospholipid acyltransferase research. J Lipid Res *50 Suppl*, S46-51.

Sperling, R.A., Aisen, P.S., Beckett, L.A., Bennett, D.A., Craft, S., Fagan, A.M., Iwatsubo, T., Jack, C.R., Jr., Kaye, J., Montine, T.J.*, et al.* (2011). Toward defining the preclinical stages of Alzheimer's disease: recommendations from the National Institute on Aging-Alzheimer's Association workgroups on diagnostic guidelines for Alzheimer's disease. Alzheimers Dement *7*, 280-292.

Stern, Y. (2002). What is cognitive reserve? Theory and research application of the reserve concept. J Int Neuropsychol Soc *8*, 448-460.

Stern, Y. (2006). Cognitive reserve and Alzheimer disease. Alzheimer Dis Assoc Disord *20*, S69-74.

Stern, Y. (2012). Cognitive reserve in ageing and Alzheimer's disease. Lancet Neurol *11*, 1006-1012.

Sud, M., Fahy, E., Cotter, D., Brown, A., Dennis, E.A., Glass, C.K., Merrill, A.H., Jr., Murphy, R.C., Raetz, C.R., Russell, D.W.*, et al.* (2007). LMSD: LIPID MAPS structure database. Nucleic Acids Res *35*, D527-532.

Sun, G.Y., Shelat, P.B., Jensen, M.B., He, Y., Sun, A.Y., and Simonyi, A. (2010). Phospholipases A2 and inflammatory responses in the central nervous system. Neuromolecular Med *12*, 133-148.

Whiley, L., Sen, A., Heaton, J., Proitsi, P., Garcia-Gomez, D., Leung, R., Smith, N., Thambisetty, M., Kloszewska, I., Mecocci, P.*, et al.* (2014). Evidence of altered phosphatidylcholine metabolism in Alzheimer's disease. Neurobiol Aging *35*, 271-278.

Wong, M.W., Braidy, N., Poljak, A., Pickford, R., Thambisetty, M., and Sachdev, P.S. (2017). Dysregulation of lipids in Alzheimer's disease and their role as potential biomarkers. Alzheimers Dement *13*, 810-827.

Wood, P.L. (2012). Lipidomics of Alzheimer's disease: current status. Alzheimers Res Ther *4*, 5.

Xu, H., Valenzuela, N., Fai, S., Figeys, D., and Bennett, S.A. (2013). Targeted lipidomics - advances in profiling lysophosphocholine and platelet-activating factor second messengers. FEBS J *280*, 5652-5667.

Chapter 5 - References

Aoki, J., Taira, A., Takanezawa, Y., Kishi, Y., Hama, K., Kishimoto, T., Mizuno, K., Saku, K., Taguchi, R., and Arai, H. (2002). Serum lysophosphatidic acid is produced through diverse phospholipase pathways. J Biol Chem *277*, 48737-48744.

Brody, D.L., and Holtzman, D.M. (2006). Morris water maze search strategy analysis in PDAPP mice before and after experimental traumatic brain injury. Exp Neurol *197*, 330-340.

Callaerts-Vegh, Z., Leo, S., Vermaercke, B., Meert, T., and D'Hooge, R. (2012). LPA5 receptor plays a role in pain sensitivity, emotional exploration and reversal learning. Genes Brain Behav *11*, 1009-1019.

Choi, J.W., and Chun, J. (2013). Lysophospholipids and their receptors in the central nervous system. Biochim Biophys Acta *1831*, 20-32.

Contos, J.J., Ishii, I., Fukushima, N., Kingsbury, M.A., Ye, X., Kawamura, S., Brown, J.H., and Chun, J. (2002). Characterization of lpa(2) (Edg4) and lpa(1)/lpa(2) (Edg2/Edg4) lysophosphatidic acid receptor knockout mice: signaling deficits without obvious phenotypic abnormality attributable to lpa(2). Mol Cell Biol *22*, 6921-6929.

Giles, C., Takechi, R., Mellett, N.A., Meikle, P.J., Dhaliwal, S., and Mamo, J.C. (2016). The Effects of Long-Term Saturated Fat Enriched Diets on the Brain Lipidome. PLoS One *11*, e0166964.

Granger, M.W., Franko, B., Taylor, M.W., Messier, C., George-Hyslop, P.S., and Bennett, S.A. (2016). A TgCRND8 Mouse Model of Alzheimer's Disease Exhibits Sexual Dimorphisms in Behavioral Indices of Cognitive Reserve. J Alzheimers Dis *51*, 757-773.

Han, X., Holtzman, D.M., and McKeel, D.W., Jr. (2001). Plasmalogen deficiency in early Alzheimer's disease subjects and in animal models: molecular characterization using electrospray ionization mass spectrometry. J Neurochem *77*, 1168-1180.

Hoene, M., Li, J., Haring, H.U., Weigert, C., Xu, G., and Lehmann, R. (2014). The lipid profile of brown adipose tissue is sex-specific in mice. Biochim Biophys Acta *1842*, 1563-1570.

Janus, C. (2004). Search strategies used by APP transgenic mice during navigation in the Morris water maze. Learn Mem *11*, 337-346.

Jia, Z.R., Zhao, D., Qi, Y., Wang, W., Wang, M., Sun, J.Y., Qin, L.P., and Liu, J. (2013). [Impact of gender on lipoprotein-associated phospholipase A2 activity and association with known cardiovascularrisk factors]. Zhonghua Xin Xue Guan Bing Za Zhi *41*, 962-967.

Liu, H., Qiu, H., Yang, J., Ni, J., and Le, W. (2016). Chronic hypoxia facilitates Alzheimer's disease through demethylation of gamma-secretase by downregulating DNA methyltransferase 3b. Alzheimers Dement *12*, 130-143.

Mapstone, M., Cheema, A.K., Fiandaca, M.S., Zhong, X., Mhyre, T.R., MacArthur, L.H., Hall, W.J., Fisher, S.G., Peterson, D.R., Haley, J.M.*, et al.* (2014). Plasma phospholipids identify antecedent memory impairment in older adults. Nat Med *20*, 415-418.

McLimans, K.E., Willette, A.A., and Alzheimer's Disease Neuroimaging, I. (2017). Autotaxin is Related to Metabolic Dysfunction and Predicts Alzheimer's Disease Outcomes. J Alzheimers Dis *56*, 403-413.

Micova, P., Klevstig, M., Holzerova, K., Vecka, M., Zurmanova, J., Neckar, J., Kolar, F., Novakova, O., Novotny, J., and Hlavackova, M. (2017). Antioxidant tempol suppresses

heart cytosolic phospholipase A2alpha stimulated by chronic intermittent hypoxia. Can J Physiol Pharmacol *95*, 920-927.

Mielke, M.M., Vemuri, P., and Rocca, W.A. (2014). Clinical epidemiology of Alzheimer's disease: assessing sex and gender differences. Clin Epidemiol *6*, 37-48.

Moses, G.S., Jensen, M.D., Lue, L.F., Walker, D.G., Sun, A.Y., Simonyi, A., and Sun, G.Y. (2006). Secretory PLA2-IIA: a new inflammatory factor for Alzheimer's disease. J Neuroinflammation *3*, 28.

Nakamura, K., Ohkawa, R., Okubo, S., Tozuka, M., Okada, M., Aoki, S., Aoki, J., Arai, H., Ikeda, H., and Yatomi, Y. (2007). Measurement of lysophospholipase D/autotaxin activity in human serum samples. Clin Biochem *40*, 274-277.

Oh, H., Razlighi, Q.R., and Stern, Y. (2018). Multiple pathways of reserve simultaneously present in cognitively normal older adults. Neurology *90*, e197-e205.

Olazaran, J., Gil-de-Gomez, L., Rodriguez-Martin, A., Valenti-Soler, M., Frades-Payo, B., Marin-Munoz, J., Antunez, C., Frank-Garcia, A., Acedo-Jimenez, C., Morlan-Gracia, L.*, et al.* (2015). A blood-based, 7-metabolite signature for the early diagnosis of Alzheimer's disease. J Alzheimers Dis *45*, 1157-1173.

Oresic, M., Hyotylainen, T., Herukka, S.K., Sysi-Aho, M., Mattila, I., Seppanan-Laakso, T., Julkunen, V., Gopalacharyulu, P.V., Hallikainen, M., Koikkalainen, J.*, et al.* (2011). Metabolome in progression to Alzheimer's disease. Transl Psychiatry *1*, e57.

Proitsi, P., Kim, M., Whiley, L., Simmons, A., Sattlecker, M., Velayudhan, L., Lupton, M.K., Soininen, H., Kloszewska, I., Mecocci, P.*, et al.* (2017). Association of blood lipids with Alzheimer's disease: A comprehensive lipidomics analysis. Alzheimers Dement *13*, 140-151.

Rauschert, S., Uhl, O., Koletzko, B., Mori, T.A., Beilin, L.J., Oddy, W.H., and Hellmuth, C. (2017). Sex differences in the association of phospholipids with components of the metabolic syndrome in young adults. Biol Sex Differ *8*, 10.

Reeves, V.L., Trybula, J.S., Wills, R.C., Goodpaster, B.H., Dube, J.J., Kienesberger, P.C., and Kershaw, E.E. (2015). Serum Autotaxin/ENPP2 correlates with insulin resistance in older humans with obesity. Obesity (Silver Spring) *23*, 2371-2376.

Ross, B.M., Moszczynska, A., Erlich, J., and Kish, S.J. (1998). Phospholipid-metabolizing enzymes in Alzheimer's disease: increased lysophospholipid acyltransferase activity and decreased phospholipase A2 activity. J Neurochem *70*, 786-793.

Santin, L.J., Bilbao, A., Pedraza, C., Matas-Rico, E., Lopez-Barroso, D., Castilla-Ortega, E., Sanchez-Lopez, J., Riquelme, R., Varela-Nieto, I., de la Villa, P.*, et al.* (2009). Behavioral phenotype of maLPA1-null mice: increased anxiety-like behavior and spatial memory deficits. Genes Brain Behav *8*, 772-784.

Schaeffer, E.L., da Silva, E.R., Novaes Bde, A., Skaf, H.D., and Gattaz, W.F. (2010). Differential roles of phospholipases A2 in neuronal death and neurogenesis: implications for Alzheimer disease. Prog Neuropsychopharmacol Biol Psychiatry *34*, 1381-1389.

Schaeffer, E.L., Forlenza, O.V., and Gattaz, W.F. (2009). Phospholipase A2 activation as a therapeutic approach for cognitive enhancement in early-stage Alzheimer disease. Psychopharmacology (Berl) *202*, 37-51.

Smesny, S., Stein, S., Willhardt, I., Lasch, J., and Sauer, H. (2008). Decreased phospholipase A2 activity in cerebrospinal fluid of patients with dementia. J Neural Transm (Vienna) *115*, 1173-1179.

Stern, Y. (2002). What is cognitive reserve? Theory and research application of the reserve concept. J Int Neuropsychol Soc *8*, 448-460.

Stern, Y. (2006). Cognitive reserve and Alzheimer disease. Alzheimer Dis Assoc Disord *20*, S69-74.

Sumida, H., Noguchi, K., Kihara, Y., Abe, M., Yanagida, K., Hamano, F., Sato, S., Tamaki, K., Morishita, Y., Kano, M.R.*, et al.* (2010). LPA4 regulates blood and lymphatic vessel formation during mouse embryogenesis. Blood *116*, 5060-5070.

Sun, G.Y., Shelat, P.B., Jensen, M.B., He, Y., Sun, A.Y., and Simonyi, A. (2010). Phospholipases A2 and inflammatory responses in the central nervous system. Neuromolecular Med *12*, 133-148.

Tokumura, A., Nishioka, Y., Yoshimoto, O., Shinomiya, J., and Fukuzawa, K. (1999). Substrate specificity of lysophospholipase D which produces bioactive lysophosphatidic acids in rat plasma. Biochim Biophys Acta *1437*, 235-245.

Toledo, J.B., Arnold, M., Kastenmuller, G., Chang, R., Baillie, R.A., Han, X., Thambisetty, M., Tenenbaum, J.D., Suhre, K., Thompson, J.W.*, et al.* (2017). Metabolic network failures in Alzheimer's disease: A biochemical road map. Alzheimers Dement *13*, 965-984.

Umemura, K., Yamashita, N., Yu, X., Arima, K., Asada, T., Makifuchi, T., Murayama, S., Saito, Y., Kanamaru, K., Goto, Y.*, et al.* (2006). Autotaxin expression is enhanced in frontal cortex of Alzheimer-type dementia patients. Neurosci Lett *400*, 97-100.

van Loenhoud, A.C., Wink, A.M., Groot, C., Verfaillie, S.C.J., Twisk, J., Barkhof, F., van Berckel, B., Scheltens, P., van der Flier, W.M., and Ossenkoppele, R. (2017). A

neuroimaging approach to capture cognitive reserve: Application to Alzheimer's disease. Hum Brain Mapp *38*, 4703-4715.

Varma, V.R., Oommen, A.M., Varma, S., Casanova, R., An, Y., Andrews, R.M., O'Brien, R., Pletnikova, O., Troncoso, J.C., Toledo, J.*, et al.* (2018). Brain and blood metabolite signatures of pathology and progression in Alzheimer disease: A targeted metabolomics study. PLoS Med *15*, e1002482.

Whiley, L., Sen, A., Heaton, J., Proitsi, P., Garcia-Gomez, D., Leung, R., Smith, N., Thambisetty, M., Kloszewska, I., Mecocci, P.*, et al.* (2014). Evidence of altered phosphatidylcholine metabolism in Alzheimer's disease. Neurobiol Aging *35*, 271-278.

Wood, P.L., Barnette, B.L., Kaye, J.A., Quinn, J.F., and Woltjer, R.L. (2015). Non-targeted lipidomics of CSF and frontal cortex grey and white matter in control, mild cognitive impairment, and Alzheimer's disease subjects. Acta Neuropsychiatr *27*, 270-278.

Wood, P.L., Locke, V.A., Herling, P., Passaro, A., Vigna, G.B., Volpato, S., Valacchi, G., Cervellati, C., and Zuliani, G. (2016). Targeted lipidomics distinguishes patient subgroups in mild cognitive impairment (MCI) and late onset Alzheimer's disease (LOAD). BBA Clin *5*, 25-28.

Yakovlev, V.M., Vishnevskii, A.A., and Shanazarov, A.S. (2013). Tissue and Cell Membrane Lipid Composition in Rats on Adaptation to Highland Conditions. Neuroscience and Behavioral Physiology *43*, 918-923.

Yung, Y.C., Stoddard, N.C., and Chun, J. (2014). LPA receptor signaling: pharmacology, physiology, and pathophysiology. J Lipid Res *55*, 1192-1214.

Yung, Y.C., Stoddard, N.C., Mirendil, H., and Chun, J. (2015). Lysophosphatidic Acid signaling in the nervous system. Neuron *85*, 669-682.